

# Controlling ultracold gases on the quantum level

Habilitationsschrift

von

**Johannes Hecker Denschlag**

Institut für Experimentalphysik  
Universität Innsbruck

Innsbruck, Juni 2005



# Abstract

In this habilitation-thesis a collection of 14 experiments is presented. In these experiments we have developed and used novel techniques to control ultracold gases on the quantum level.

In brief, Bose-Einstein condensates (BEC) and degenerate Fermi gases of laser-cooled alkali atoms are subjected to specially designed optical and magnetic fields. The fields influence in a coherent way the behavior, properties and dynamics of the gases. On this basis we developed tools to prepare, coherently manipulate, and analyze pre-defined quantum states. With this high level of control, it was possible to investigate interesting physics phenomena, and we were able to achieve several breakthroughs in the field of ultracold atoms.

Highlights of our experimental results include the demonstration of phase engineering of a BEC wavefunction where we created solitons in a BEC and studied their propagation. In another experiment we constructed a spatially resolved matter wave interferometer with which we mapped out the phase distribution on a condensate. Illuminating the BEC with a periodic pattern, i.e. an optical lattice, allowed us to study solid states physics phenomena. In a second set of experiments we demonstrated optically tuning of the interaction between atoms with optical Feshbach resonances. Employing either magnetically tunable Feshbach resonances or laser radiation, we were able to produce ground state molecules in well defined quantum states. This led to the production of the first molecular BEC. By tuning the coupling of atom pairs in a Fermi gas of atoms, we could for the first time investigate the so-called BEC-BCS crossover which describes the continuous change from a BEC superfluid to a Bardeen-Cooper Schrieffer (BCS) superfluid.

Due to the excellent control on the quantum level, the developed cold atom techniques open up intriguing prospects for future applications and experiments. They represent a general tool box to investigate fundamental physical phenomena in a pure and undisturbed environment. In the future, cold atoms might serve as a testing ground for fundamental theories or as quantum simulators for complex systems.



# Contents

<b>1</b>	<b>Introduction</b>	<b>1</b>
<b>2</b>	<b>Ultracold degenerate quantum gases</b>	<b>5</b>
2.1	Bosons and Fermions . . . . .	5
2.1.1	Interaction of ultracold particles . . . . .	6
2.1.2	Dilute Bose-Einstein condensates . . . . .	8
2.1.3	The Fermi sea . . . . .	10
2.2	Key experimental methods . . . . .	13
2.2.1	Magneto-optical trap . . . . .	13
2.2.2	Conservative traps . . . . .	14
2.2.3	Evaporative cooling . . . . .	15
2.2.4	Detection of atoms . . . . .	17
<b>3</b>	<b>Controlling matter waves with potentials made of light</b>	<b>19</b>
3.1	Diffracting atoms off optical lattices . . . . .	20
3.2	Phase engineering with light . . . . .	22
3.3	Solid state physics in optical lattice . . . . .	24
3.3.1	Bloch states in optical lattices . . . . .	24
3.3.2	The Mott insulator . . . . .	26
3.4	“Generating Solitons by Phase Engineering of a Bose-Einstein Condensate” . . . . .	29
3.5	“Imaging the Phase of an evolving Bose-Einstein Condensate Wave Function” . . . . .	35
3.6	“A Bose-Einstein Condensate in an optical lattice” . . . . .	41
<b>4</b>	<b>Controlling the interaction between atoms with Feshbach resonances</b>	<b>59</b>
4.1	Magnetically tunable Feshbach resonance in ${}^6\text{Li}$ . . . . .	60
4.2	Optical tuning of the scattering length . . . . .	62

4.3	“Magnetic Field Control of Elastic Scattering in a Cold Gas of Fermionic Lithium Atoms” . . . . .	65
4.4	“Precise determination of ${}^6\text{Li}$ cold collision parameters by radiofrequency spectroscopy on weakly bound molecules” . . . .	71
4.5	“Tuning the scattering length with an optically induced Feshbach resonance” . . . . .	77
4.6	“Inducing an optically induced Feshbach resonance via stimulated Raman coupling” . . . . .	83
<b>5</b>	<b>Converting atoms into ultracold molecules</b>	<b>93</b>
5.1	Photoassociation . . . . .	94
5.2	Producing molecules with Feshbach resonances . . . . .	97
5.3	“Photoassociation of Sodium in a Bose-Einstein Condensate” .	101
5.4	“Atom-molecule dark states in a Bose-Einstein condensate” . .	107
5.5	“Pure Gas of Optically Trapped Molecules Created from Fermionic Atoms” . . . . .	113
<b>6</b>	<b>Bose-Einstein condensation of molecules and the BEC-BCS crossover</b>	<b>119</b>
6.1	Bose-Einstein condensation of Fermi pairs: molecules and Cooper pairs . . . . .	122
6.2	Probing the BEC-BCS crossover . . . . .	124
6.3	“Bose-Einstein Condensation of Molecules” . . . . .	129
6.4	“Observation of the pairing gap in a strongly interacting Fermi gas” . . . . .	133
6.5	“Crossover from a Molecular Bose-Einstein Condensate to a Degenerate Fermi Gas” . . . . .	137
6.6	“Collective excitations of a degenerate gas at the BEC-BCS crossover” . . . . .	143
<b>7</b>	<b>Summary and Outlook</b>	<b>149</b>
	<b>Bibliography</b>	<b>151</b>
	<b>Acknowledgements</b>	<b>169</b>

# Chapter 1

## Introduction

When laser cooling of neutral atoms was first demonstrated in the early 1980's, the handful of researchers at that time could not have possibly imagined the size to which their field would grow within a few years. Initially proposed as a tool for high precision spectroscopy and as a means to build a new generation of atomic clocks, laser cooling has also led to new developments and research well beyond the field of atomic, molecular and optical physics. The importance of these developments has been widely accredited. In 1997 Steven Chu, Claude Cohen-Tannoudji, and William D. Phillips were awarded the Nobel prize for laser cooling. In 2001 Eric Cornell, Wolfgang Ketterle and Carl Wieman shared the Nobel prize for Bose-Einstein condensation of dilute atomic gases.

Ultracold atoms are now being used as a key technology to investigate such diverse fields as condensed matter physics, plasma physics, physics of chaos and quantum information. Highlights of condensed matter experiments with ultracold atoms include Bose-Einstein condensation (BEC) [And95, Bra95, Dav95], Bloch oscillations [Dah96, Mor01, Den02], quantized vortices [Mad00, Abo01, Ino01], quantum phase transitions [Jak02, Gre02] and low dimensional states of matter, e.g. the Tonks-Girardeau gas [Par04, Kin04]. Non-linear phenomena such as four-wave-mixing for matter waves in a BEC can be studied [Deng99b]. Ultracold neutral atoms can be used to study entanglement [Jak99, Man03], and proposals for quantum information processing schemes look encouraging (e.g. [Bri00, Cal03]). It has been even suggested that BEC could be used to simulate astro-physical processes connected to black holes and the expansion of the universe [Fed03, Che05]. Employing ultracold atoms has not only led to the construction of the most precise clocks (e.g. [Gib93, Kat03]) but also to very sensitive detectors for rotation and gravitation which are based on matter wave interferometry [Gus97, Sna98]. By ionizing ultracold atomic gases, it is also possible to

produce plasmas in the strongly coupled regime [Kil99]. Finally, the recent achievement to produce ultracold molecules out of degenerate atomic gases opens new avenues for quantum chemistry (e.g. [Don02, Her03, Reg03]).

The success of the ultracold gases is largely based on the very high degree of control we have gained over the atoms in recent years. We have learned how to manipulate the internal and external degrees of freedom of the atoms on the quantum level using light fields, radio frequency and magnetic fields. We can prepare the atoms in a single quantum state and trap them, so that they are well isolated from the outside world. This leads to long coherence times and allows for studying the coherent dynamics of the atomic ensemble in a pure environment. Finally, with the help of Feshbach resonances we have also recently learned to control the interaction between atoms.

Together with my collaborators I have contributed to a number of these developments in recent years. This habilitation thesis is a compilation of original research papers describing experimental research work which was carried out within the last 6 years in Prof. William D. Phillip's group at the National Institute for Standards and Technology (NIST), Gaithersburg (Maryland) and in Prof. Rudolf Grimm's group at the Institut für Experimentalphysik, Universität Innsbruck. The experiments at NIST were performed with a sodium BEC during a two-year postdoc. My work in Innsbruck can be grouped into two projects: an experiment with an ultracold fermionic lithium gas and a rubidium BEC experiment which was set up from scratch. One unifying theme of our research is the development of control and analysis tools in order to manipulate atomic and molecular quantum degenerate gases on the quantum level. By applying these methods in experiments, novel and fundamental physics phenomena can be studied and observed in a very direct manner.

The thesis is organized as follows. In chapter 2, a brief overview of the basic concepts of ultracold degenerate quantum gases is given. Also, the key experimental methods to produce and work with ultracold gases are described. This chapter has tutorial character and is intended for the general reader.

Chapter 3 demonstrates methods for controlling and manipulating the wavefunction of a BEC with specially designed light fields. Pulsed optical lattices can be used to build coherent matter wave beam-splitters and spatially resolved matter wave interferometers. We have used these interferometers to study a temporal Talbot Effect for matter waves [Den99], and to measure the distribution and the dynamical evolution of the quantum mechanical phase of a BEC wavefunction [Den00, Sim00]. With spatially designed light fields we demonstrated phase engineering of the BEC wavefunction and generated dark soliton waves in a condensate [Den00]. Optical lattices represent an ex-

cellent environment to study solid state physics. In [Den02] we have prepared specific Bloch eigenstates of the lattice and investigated their coherent evolution after inducing coherent excitations. A BEC accelerator and a coherent multi-photon beamsplitter was constructed [Den02]. In a 3D optical lattice we have observed the Mott insulator phase transition which is an important starting point for future experiments.

Chapter 4 discusses various methods to control the interactions between the particles of the degenerate gas. These methods are based on the use of magnetically or optically tunable Feshbach resonances. Such a scattering resonance appears when a state of two colliding particles is resonantly coupled to a molecular bound state. In [Joc02] we observe such a Feshbach resonance for  ${}^6\text{Li}$  as previously predicted by [Hou98]. By changing the magnetic field we can continuously tune and control the interaction between the lithium atoms. In two following articles [The04, Tha04] we demonstrate for the first time a novel optical scheme to tune the inter-particle interaction. This so-called optical Feshbach resonance is based on laser light coupling the colliding atoms to a molecular state. The atomic interaction can be tuned by changing the power and detuning of the laser.

In Chapter 5 we discuss experiments which are linked to the production of ultracold dimer molecules out of an ultracold gas of atoms. We apply two methods. One method uses photoassociation, where laser light ‘fuses’ two atoms into one molecule [McK02, Win05]. The appearance of a novel atom-molecule dark state indicates the formation of a BEC-like molecular quantum gas [Win05]. Our second method to produce ultracold molecules is based on three-body recombination close to a Feshbach resonance. In an inelastic collision of three atoms, two atoms combine to form a ground state molecule and the third atom takes care of energy and momentum conservation. The formation rate can be controlled via a magnetically tunable Feshbach resonance [Joc03b].

The topic of Chapter 6 is the BCS-BEC crossover where we study a superfluid gas of paired fermionic atoms in various coupling regimes. In the two limiting cases of strong and weak coupling, atom pairs correspond to molecular dimers and Cooper pairs, respectively. Starting out in the strong coupling limit, we have produced the world’s first molecular Bose-Einstein condensate [Joc03a] simultaneously with that from [Gre03]. In a next step, we have converted this molecular condensate into a degenerate gas of paired fermions [Chi04a]. The paired fermions are similar to Cooper pairs in superconductors as described by the Bardeen-Cooper-Schrieffer (BCS) theory. In [Chi04a] we have been able to measure the binding energy of the Fermi pairs using radio frequency. Using a Feshbach resonance it is possible to continuously tune from the BEC to the BCS regime. This is called the

BEC-BCS crossover. We have employed several methods to investigate this crossover: studying the cloud size [Bar04c], collective oscillations [Bar04b] and measuring the pair binding energy [Chi04a]. These measurements provide interesting information about the state of the gas, e.g. whether it is superfluid or thermal.

Finally, chapter 7 gives a short summary of the work presented here and an outlook for future directions.

The reprinted research papers of each chapter are preceded by an introduction to the theoretical concepts and experimental methods. We also discuss how our work relates to the research of other groups worldwide.

# Chapter 2

## Ultracold degenerate quantum gases

This chapter is a brief review for the general reader on the properties of ultracold degenerate bosonic and fermionic gases and how to actually produce them in the laboratory. In addition to some historic background information, these tutorials present the essentials in order to understand the following research articles.

### 2.1 Bosons and Fermions

Since the early days of quantum mechanics, it has been known that particles can be classified depending on their collective properties in two groups: fermions and bosons. Fermions and bosons are characterized by half integer and integer spins, respectively. In the experiments described here we worked with the alkali atoms  $^{87}\text{Rb}$ ,  $^{23}\text{Na}$  and  $^6\text{Li}$ , where  $^{87}\text{Rb}$  and  $^{23}\text{Na}$  are bosons and  $^6\text{Li}$  is a fermion. As a consequence of the indistinguishability of identical particles and the symmetry of their wavefunctions, the quantum statistic behavior of bosons and fermions is quite different. The antisymmetry of the fermion wavefunction under particle exchange gives rise to the Pauli exclusion principle: two identical fermions can not exist in the same quantum state. This is not true for bosons. Putting two identical bosons into the same quantum state is even ‘Bose enhanced’, leading ultimately to Bose-Einstein condensation. A Fermi gas, however, can at best form a Fermi sea where all the lowest quantum states are filled up to the Fermi energy (see Fig. 2.1). Quantum statistical effects of Fermi and Bose gases become visible, when the wave packets of the individual particles start to overlap, i.e. the phase space

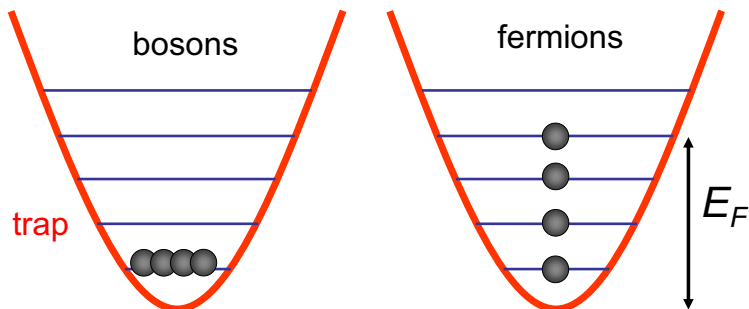


Figure 2.1: (left) At zero temperature bosons are fully condensed in a single macroscopic matterwave, the Bose-Einstein condensate. (right) Fermions, on the other hand, form a Fermi sea filling the trap potential up to the Fermi energy  $E_F$ .

density becomes sizeable,

$$\lambda_{\text{dB}}^3 n \geq 1. \quad (2.1)$$

Here  $\lambda_{\text{dB}} = \sqrt{2\pi\hbar^2/mk_{\text{B}}T}$  is the thermal de Broglie wavelength,  $n$  is the density of the gas,  $T$  is its temperature, and  $k_{\text{B}}$  is the Boltzmann factor. Experimentally we reach these high phase space densities by confining the atoms in a trap and using various procedures to cool the ensemble down below  $\mu\text{K}$  temperatures.

There is an extensive literature covering degenerate gases and quantum statistics. For an in depth introduction I recommend the textbooks by Pitaevski and Stringari [Pit03], Pethick and Smith [Pet02] and Huang [Hua63].

### 2.1.1 Interaction of ultracold particles

In our experiments the effective interactions between particles are mediated through collisions. These collisions are described by scattering theory of which here only a few main results are summarized. For a thorough treatment the reader has to be referred to the literature, e.g. [Jul92, Dal99b, Wei99].

Collisions and interactions between the atoms are of central importance for our research. As we will show later, by controlling the interaction between the particles we can create molecules, molecular condensates, and investigate strongly coupled Fermi pairs. The interactions give rise to various collective phenomena of the quantum gases which we study. On a practical side, we use elastic collisions for evaporative cooling of our atomic and molecular

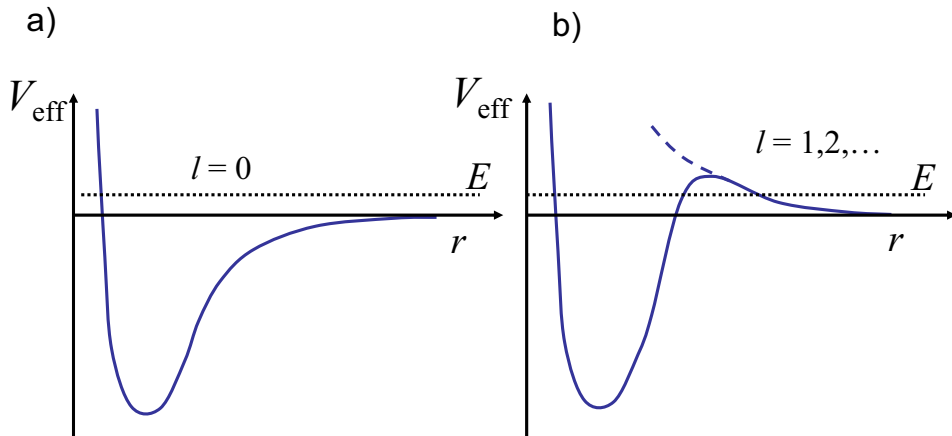


Figure 2.2: Schematic of the effective potential of the 1D radial Schrödinger equation. a) The situation for s-wave scattering. b) For  $l > 0$  a centrifugal barrier  $\hbar^2 l(l+1)/2m_r r^2$  is added. If the collision energy  $E$  is much lower than this barrier, collisions are suppressed.

gases. At the same time, inelastic collisions leading to trap loss have to be minimized.

We consider the collision of two particles with a spherically symmetric interaction potential  $V(r)$ . Angular momentum is then a conserved quantity and we can diagonalize the scattering problem into partial waves, i.e. states with well defined angular momentum  $l$ . These partial waves  $\psi_l$  are described by a one-dimensional (1D) Schrödinger equation

$$\left[ \frac{\partial^2}{\partial r^2} + k^2 + \frac{2m_r}{\hbar^2} V(r) + \frac{l(l+1)}{r^2} \right] \psi_l(r) = 0, \quad (2.2)$$

where  $r$  is the interparticle distance,  $m_r$  is the reduced mass of the collision partners and  $\hbar k$  is the collision momentum. As can be seen from Eq. 2.2, the higher partial waves experience an effective potential which includes a repulsive centrifugal barrier  $V_{\text{eff}} = V(r) + \hbar^2 l(l+1)/(2m_r r^2)$ . An illustration of this is shown in Fig. 2.2. If the collision energy is much lower than this barrier, particles with angular momentum  $l > 0$  cannot reach the inner part of potential  $V(r)$  and as a consequence do not interact. As an example, lithium has a  $l = 1$  centrifugal barrier of  $k_B \times 7\text{mK}$  [Jul92]. *Thus in general for typical experimental temperatures in the  $\mu\text{K}$  regime only  $l = 0$  partial waves (s-waves) contribute to scattering.*

One can show [Jul92, Dal99b, Wei99] that in this low temperature limit the scattering process is described by a *single* number: the scattering length

a. Typical s-wave scattering lengths for alkali atoms are on the order of 10 - 100  $a_0$  (1  $a_0 = 1$  Bohr =  $0.529 \times 10^{-10}$  m.). From the scattering length we can calculate the scattering cross section  $\sigma$ ,

$$\lim_{k \rightarrow 0} \sigma = 4\pi a^2. \quad (2.3)$$

This relation can be extended to higher collision energies through  $\sigma = 4\pi a^2 / (1 + k^2 a^2)$ . If  $k^2 a^2 \ll 1$ , we recover the zero-energy limit in Eq. 2.3, whereas the limit  $k^2 a^2 \gg 1$  yields the so-called unitarity limit  $\sigma(k) = 4\pi/k^2$ , which is the maximum possible cross section for s-wave collisions. For the above considerations we assumed that the two colliding particles were distinguishable, which is not the case if one considers identical particles. In this case, two scattering amplitudes interfere (see [Dal99b]). This leads to an extinction of the scattering cross section for the symmetric even partial waves in the case of fermions and of the symmetric odd partial waves in the case of bosons. The cross sections for the remaining partial waves are doubled. Thus the cross section for identical bosons reads  $\sigma = 8\pi a^2$ .

## Mean field interaction

We now consider a particle in a dilute, weakly interacting gas ( $a^3 n \ll 1$ ) at sufficiently cold temperatures so that only s-waves contribute to scattering. The interaction through the collisions gives rise to a mean interaction energy which can be considerably larger than the thermal energy of the system. Applying the Born approximation, one can derive a simple expression for this effective mean field potential  $V_{mf}$  [Pit03],

$$V_{mf} = \frac{4\pi\hbar^2 a}{m} n. \quad (2.4)$$

If we deal with identical, noncondensed particles, this mean field interaction has to be multiplied by a factor of two due to exchange symmetry [Gri96]. Expression (2.4) is of central importance for all following chapters.

### 2.1.2 Dilute Bose-Einstein condensates

The theoretical prediction of Bose-Einstein condensation dates back 80 years. Following the work of Bose on the statistics of photons [Bos24], Einstein considered a gas of non-interacting, massive bosons. He concluded, that below a certain temperature a certain fraction of the total number of particles would occupy the the lowest-energy single-particle state [Ein25]. Bose-Einstein condensation is a quantum statistical effect which takes place even in the absence

of interparticle interactions. In this case the occupation number  $N_i$  of the quantum states with energy  $\epsilon_i$  is determined by

$$N_i = \frac{1}{\exp [(\epsilon_i - \mu)/k_B T] - 1}, \quad (2.5)$$

where  $\mu$  is the chemical potential [Pit03]. Since Fritz London in 1938, it is known that superfluid liquid  $^4\text{He}$  is a Bose-Einstein condensate. However, the strong interaction between the  $^4\text{He}$  atoms depletes the condensate which can be problematic for certain applications and investigations. This led to the search for BEC in weakly-interacting Bose gases which was finally achieved in 1995 with dilute gases of alkali atoms in the groups of E. Cornell, C. Wiemann, W. Ketterle and R. Hulet [And95, Dav95, Bra95]. Stemming from this discovery, a new branch of cold atom physics grew very fast and this compilation gives account of some of these developments.

We will now list a few facts about BEC which are important for the following chapters. A full account can be found in the following books and review article, respectively [Pit03, Pet02, Dal99a]. Bose-Einstein condensation sets in when the phase space density  $\lambda_{\text{dB}}^3 n$  of a gas which is held in a harmonic trap reaches  $\approx 1.2$ . For a pure condensate all atoms are in the same quantum state  $\psi$  and the overall wavefunction  $\Psi$  is a product state

$$\Psi = \psi(r_N, t) \psi(r_{N-1}, t) \dots \psi(r_2, t) \psi(r_1, t). \quad (2.6)$$

Within the mean field approximation the wavefunction  $\psi$  is a solution of a non-linear Schrödinger equation, the so-called Gross-Pitaevskii equation,

$$i\hbar \frac{\partial}{\partial t} \psi(r, t) = \left( -\frac{\hbar^2}{2m} \Delta + V(r) + g |\psi(r, t)|^2 \right) \psi(r, t) \quad (2.7)$$

which for a time independent case reads

$$\mu \psi(r, t) = \left( -\frac{\hbar^2}{2m} \Delta + V(r) + g |\psi(r, t)|^2 \right) \psi(r, t). \quad (2.8)$$

Here  $\mu$  is the chemical potential and  $g = 4\pi\hbar^2 a/m$ , as discussed before in Eq. 2.4. It is conventional to normalize  $\psi$  to  $\int d^3r |\psi|^2 = N$ , the number of atoms in the condensate.

Often the kinetic energy in the condensate is completely negligible compared to the interaction energy. In this so called Thomas-Fermi regime, one can rewrite Eq. 2.8 as

$$\mu = V(r) + g n(r) \quad (2.9)$$

We can solve Eq. (2.9) for  $n(r)$  and find that it has the inverted shape of the trapping potential. In the case of a harmonic trap, the BEC density distribution looks like an inverted parabola. Eq. (2.9) can further be conveniently used to calculate various quantities, as for example the chemical potential  $\mu$ . Using  $N = \int d^3r n(r)$  we obtain for a harmonic potential  $V(r) = 1/2m\omega^2r^2$

$$\mu = \frac{\hbar\omega}{2} \left( \frac{15^2 N^2 a^2 m\omega}{\hbar} \right)^{1/5}. \quad (2.10)$$

### 2.1.3 The Fermi sea

The distribution of non-interacting fermions is described by the Fermi function

$$N_i = \frac{1}{\exp[(\epsilon_i - \mu)/k_B T] + 1}, \quad (2.11)$$

similar to Eq. 2.5 for bosons [Hua63, Pet02, Joc04]. At zero temperature, the ensemble of fermions forms a so-called Fermi sea where each quantum state is filled up to the Fermi energy  $E_F = \mu = k_B T_F$ .  $T_F$  is called the Fermi temperature. For an isotropic harmonic trap with trapping frequency  $\omega$  and  $N$  fermions one finds

$$E_F = \hbar\omega(6N)^{1/3}. \quad (2.12)$$

As an example,  $10^5$  identical fermions harmonically trapped with a trapping frequency  $\omega = 2\pi \times 100$  Hz correspond to a Fermi energy of about 400nK. It is useful to define a Fermi wavenumber  $k_F = \sqrt{2mE_F}/\hbar$ . This wavenumber can be expressed in terms of the density  $n$ ,

$$k_F = (6\pi^2 n)^{1/3}. \quad (2.13)$$

This shows that apart from a constant factor, the Fermi wave number corresponds to the mean inverse particle separation. In a local density approximation we can write

$$\frac{\hbar^2 k_F^2(r)}{2m} + V(r) = \mu. \quad (2.14)$$

From Eqs. (2.13) and (2.14) we can then solve for the density distribution  $n(r)$ , similar as in the Thomas Fermi approximation for the Bose gas in Eq. (2.9).

The Fermi temperature  $T_F$  is a convenient temperature scale. If the gas temperature exceeds  $T_F$ , we essentially recover the behavior of a classical Boltzmann gas. At  $T = T_F$  the phase space density approaches unity and quantum statistic effects begin to play a role. It is interesting to note, that the physics of degenerate Fermi gases play an important role in our everyday lives

even at ambient temperatures: not only does it determine the properties of electric conductors. The Fermi pressure, due to the Pauli exclusion principle, stabilizes neutron stars as well as all material objects around us against collapse.

Still, it took until 1999, 4 years after BEC had been demonstrated, before the onset of quantum degeneracy of a dilute Fermi gas could first be observed by Deborah Jin's group at JILA [DeM99b]. Subsequently other groups at Rice, Paris and MIT, Florence, Duke, Innsbruck, Zurich and Hamburg have also produced degenerate Fermi gases, and the field has seen a tremendous development and success these last years. So far only the fermionic elements  ${}^6\text{Li}$  und  ${}^{40}\text{K}$  have been brought to degeneracy. One reason for this is that fermionic atoms are less abundant than bosonic atoms, which can be traced back to the odd-even effect in the pairing of nucleons in nuclei. A second reason is that cooling fermions to coldest temperatures is more difficult than for bosons due to Pauli blocking. As we have shown in chapter 2.1.1 at very low temperatures identical fermions do not collide and therefore the standard procedure of evaporative cooling does not work. The absence of s-wave scattering in an ultracold Fermi gas was observed at JILA for a cold gas of  ${}^{40}\text{K}$  [DeM99a]. The group was also able to measure how p-wave collisions are frozen out according to  $\sigma_p \propto E^2$ .

In order to get around the reduction in evaporative cooling, one uses mixtures of non-identical atoms, e.g. atoms in different spin states. S-wave collisions between the non-identical atoms are allowed and lead to the necessary thermalization of the atomic ensemble. For  ${}^6\text{Li}$  we use a 50-50 mix of the two lowest spin states which, at low magnetic fields, correlate to  $F = 1/2, m_F = \pm 1/2$ . We employ evaporative cooling in a scheme similar to the one demonstrated at the group of J. Thomas [Gra02]. Another successful method for cooling is to sympathetically cool fermions with bosons, which can be cooled to BEC temperatures [Tru01, Sch01, Had02, Roa02].

## Cooper pairing and superfluidity

The properties of the degenerate Fermi gas become really interesting when interactions between the fermions are taken into account. For attractive effective interactions between the fermions and low enough temperatures, fermions can pair up to form a superfluid phase. This is in analogy to Bardeen, Cooper and Schrieffer's (BCS) theory of superconductivity where electrons in metals form bosonic Cooper pairs [Bar57]. The BCS theory successfully describes Fermi systems with weak interactions, for which the mean distance between paired atoms is much larger than the mean interparticle spacing in the gas. Cooper pairing goes along with the formation of an en-

ergy gap  $\Delta_0$  in the single particle excitation spectrum which corresponds to the binding energy of the Cooper pairs.  $\Delta_0$  is given by [Pit03, Tin96]

$$\Delta_0 = \frac{1}{2} \left(\frac{2}{e}\right)^{7/3} E_F \exp\left(-\frac{\pi}{2k_F|a|}\right), \quad (2.15)$$

where  $a$  is the scattering length. The critical temperature  $T_{BCS}$  for the transition to the BCS state is proportional to the gap energy at zero temperature [Pit03],

$$T_{BCS} = 0.57 \Delta_0/k_B. \quad (2.16)$$

In the weak coupling (BCS) limit, when  $k_F|a| \ll 1$ , we can see from Eqs. (2.15) and (2.16) that  $T_{BCS}$  is a very small fraction of  $T_F$ . High temperature superconductivity, of which the theory still is not fully understood, corresponds to a relatively strongly interacting Fermi system. Therefore this strong coupling regime is currently of high interest to the superconductivity community. As it is now possible to experimentally control the scattering length  $a$  via Feshbach resonances, experiments in atomic quantum gases can contribute to this research. Using ultracold atoms we can, for the first time, explore pairing of fermions and superfluidity in the strong interacting limit, a regime which has been called resonance superfluidity [Hol01, Oha02]. In this limit, where  $-k_F a \gg 1$ , the critical temperature can be quite high,  $\approx 0.2 T_F$ . Since such temperatures can be routinely achieved in current experiments with fermionic atomic gases, resonance superfluidity should be experimentally observable.

### Universal regime

The regime of resonance superfluidity where  $k_F|a| \gg 1$ , is also interesting for another reason. Here the interactions are unitarity limited by the Fermi momentum  $1/k_F$ . In this so-called universal regime the properties of the gas become independent of any particularities of the atomic interaction properties [Hei01, Car03, Ho04] and interesting scaling laws appear. First investigations of the universal regime were performed at Duke university [Har02a]. In chapter 6 we will discuss our own experiments.

### BCS-BEC cross over

Coming from the weakly coupling BCS limit, the initially large Cooper-pairs become increasingly localized and tightly bound as the interaction is increased. Finally, for strong enough coupling, bosonic molecular dimers are formed. The gas of fermions can then be treated as a gas of elementary bosons

which can undergo Bose-Einstein condensation. In the zero-temperature limit one can thus continuously go from a BCS superfluid of atoms to a superfluid BEC of molecules by controlling the coupling between the particles. This so called BCS-BEC cross over has already been in the focus of theorists for several decades [Eag69, Leg80, Noz85, Che04]. It can now, for the first time, be investigated in our experiments (see chapter 6).

## 2.2 Key experimental methods

In this section we will briefly introduce the main experimental methods that were used in all our experiments to create and observe the bosonic condensates or the fermionic degenerate quantum gases. Because of lack of space, only a short overview will be given. For more background information the interested reader is referred to the excellent book by H. Metcalf and P. van der Straten [Met99]. Details about the laser systems and vacuum chambers of the Innsbruck experiments can be found in the PhD theses by Selim Jochim [Joc04], Markus Bartenstein [Bar04a] and Matthias Theis [The05].

### 2.2.1 Magneto-optical trap

The magneto-optical trap (MOT) has become *the* ‘workhorse’ in basically every cold atom lab around the globe. Conceived by J. Dalibard, it was first demonstrated in 1987 by E. Raab and collaborators [Raa87]. The MOT robustly laser cools thermal, room-temperature atoms down below mK temperatures and traps them. It consists of three red-detuned counter-propagating pairs of laser beams along the orthogonal x, y, z directions in space and a magnetic quadrupole field (gradient  $\approx 10$  G/cm).

Laser cooling uses Doppler-shift tuned radiation pressure from spontaneously scattered laser photons in a closed excitation scheme. It was first proposed by Hänsch and Schawlow in 1975 [Hän75] and then applied for neutral atoms in the beginning of the 80’s. For a review see [JOSA, Chu98, Coh98, Phi98]. Typical MOTs can capture up to  $10^{11}$  atoms in a mm-sized cloud at densities of about  $10^{11}\text{cm}^{-3}$ . The lowest reachable temperatures are in general bound by the Doppler limit,

$$T_D = \frac{\hbar\gamma}{2k_B}, \quad (2.17)$$

where  $\gamma$  is the linewidth (typ.  $\gamma \approx 2\pi \times 6\text{MHz}$ ) of the excited atomic level. Correspondingly, the achievable phase space densities reach only  $10^{-6}$  which

is still far away from degeneracy! In order to reach quantum degeneracy, cooling and trapping schemes without spontaneous light scattering are necessary which are described in the following.

## 2.2.2 Conservative traps

There are mainly two types of conservative traps for cold atoms: magnetic and optical dipole traps. These traps are typically only 1mK deep and thus can only trap atoms which have been previously laser cooled, e.g. in a MOT.

### Magnetic traps

An atom with a magnetic moment  $\vec{\mu}$  feels a force  $\vec{F}$  in an inhomogeneous magnetic field  $\vec{B}$  as demonstrated in 1924 in the Stern-Gerlach experiment.

$$\vec{F} = \vec{\nabla}(\vec{\mu} \cdot \vec{B}) = g_F \mu_B m_F \vec{\nabla} B, \quad (2.18)$$

where  $g_F$  is the g factor,  $\mu_B$  is the Bohr magneton and  $m_F$  is the magnetic quantum number of the atom. For  $g_F m_F < 0$  the atom is a ‘low field seeker’, being attracted to magnetic field strength minima. Various such magnetic fields with local minima exist and the corresponding traps carry different names. In our experiments we have used magnetic quadrupole traps [Ber87], a Ioffe trap [Ber87] in the QUIC configuration [Ess98] and the TOP trap [Pet95]. Ioffe and TOP traps exhibit a non-zero magnetic field minimum, which is essential to prevent the so-called Majorana losses of atoms through spin flips. Close to this field minimum their trapping potential  $V(r)$  is approximately harmonic

$$V(r) = V(x, y, z) = \frac{m}{2} (\omega_x^2 x^2 + \omega_y^2 y^2 + \omega_z^2 z^2). \quad (2.19)$$

Typical trapping frequencies  $\omega_i$  range between  $2\pi \times 10 \dots 200$  Hz.

### Optical dipole traps

Optical dipole traps are versatile tools to confine ultracold atomic and molecular gases independent of their spin state [Gri00]. They rely on the electric polarizability of the particles in the light field, not on spontaneous scattering of photons. If the laser frequency is tuned below the atomic resonance frequency, the induced atomic dipole oscillates in phase with the laser field and the resulting potential is attractive. Conversely, for blue detuning the atomic dipole oscillates  $180^\circ$  out of phase and the potential is repulsive. This

phenomenon is known as AC-Stark shift or light shift. The potential depth is approximately given by [Gri00],

$$V_{\text{dip}}(r) = -\frac{3\pi c^2}{2\omega_0^3} \left( \frac{\gamma}{\omega_0 - \omega} + \frac{\gamma}{\omega_0 + \omega} \right) I(r), \quad (2.20)$$

where  $\omega_0$  denotes the atomic resonance frequency,  $\omega$  is the laser frequency,  $I(r)$  is the laser intensity and  $\gamma$  is the excited state linewidth (typically  $2\pi \times 6\text{MHz}$ ). The associated spontaneous photon scattering rate is

$$\Gamma_{\text{dip}}(r) = -\frac{3\pi c^3}{2\hbar\omega_0^3} \left( \frac{\omega}{\omega_0} \right)^3 \left( \frac{\gamma}{\omega_0 - \omega} + \frac{\gamma}{\omega_0 + \omega} \right)^2 I(r). \quad (2.21)$$

Note that the photon scattering rate is suppressed stronger than the trapping potential as the laser frequency is tuned away from the atomic resonance. Therefore, it is advantageous to work at very large detuning, if a low photon scattering rate is desired.

Optical dipole traps were introduced by A. Ashkin in 1970 to hold dielectric objects [Ash70] and were first applied to trap atoms in 1986 [Chu86]. Optical dipole traps are now ubiquitous in atomic physics as well as in optical tweezer applications in biology [Dho02]. A simple dipole trap consists of a focussed gaussian laser beam whose intensity varies as

$$I(r) = I_0 \left( \frac{w_0}{w(z)} \right)^2 \exp \left( \frac{-2(x^2 + y^2)}{w^2(z)} \right) \quad \text{with } w(z)^2 = w_0^2 \left( 1 + (z/z_0)^2 \right), \quad (2.22)$$

where  $w_0$  is the waist at the focus and  $z_0$  is the Rayleigh range. Around its focus the resulting trap is again approximated by a harmonic potential. As an example, we use a 10 W Yb-YAG laser in our Li experiment. Focussing the beam to a about 20 microns, we achieve trapping frequencies in the kHz range while keeping the spontaneous scattering rate at the Hz level [Joc04].

### 2.2.3 Evaporative cooling

Evaporative cooling can in principle produce arbitrarily low temperatures. It is well known in our every day life as it cools our cup of coffee in the morning and is used by our body when we sweat during sports. Evaporative cooling was proposed by H. Hess in 1985 [Hes85, Hes86] as an efficient way to cool trapped hydrogen atoms. After adapting it for alkali atoms in 1994, evaporative cooling quickly led to Bose-Einstein condensation [And95, Bra95, Dav95]. For a detailed review we refer the reader to [Ket96]. The main idea behind evaporative cooling is to remove the high energy particles in the tail of

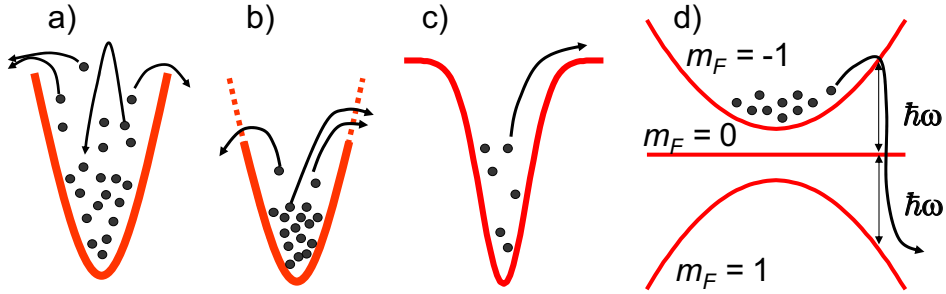


Figure 2.3: a) Evaporative cooling. The hottest particles escape from the trap. b) Forced evaporation. In order to keep the evaporation going the potential ‘rim’ is lowered. c) Optical dipole trap based on a focussed gaussian laser beam (transverse direction). d) Evaporative cooling in a magnetic trap with radio-frequency.

the Maxwell-Boltzmann distribution in a thermal gas. Since the evaporating particles carry away more than their share of thermal energy, the temperature of the system decreases after re-thermalization through collisions. In the experiments this is realized by holding the atoms in a trap of finite depth, so that particles with higher energy than the trap depth escape (see Fig. 2.3 a).

In order to prevent the slow down of the evaporation process as the temperature decreases, one uses ‘forced evaporation’ by lowering the potential rim of the trap (Fig. 2.3 b). For an optical dipole trap this potential depth is controlled via the light intensity (Fig. 2.3 c). For magnetic traps the depth is set by radio frequency (rf) which induces resonant transitions to non-trapped spin states (Fig. 2.3 d).

Evaporation can be made very efficient by choosing a large potential depth, so that a few lost particles carry away a lot of energy. However, there is a trade-off since increasing the depth slows down the evaporation. This can be compensated by high collision rates in tight traps. A useful theoretical model to understand the evaporation dynamics and efficiency is given in [Lui96, Har01].

In our experiments with rf-evaporative cooling we typically lose 99% of all magnetically trapped thermal atoms before we achieve degeneracy [Den00, Tha04]. In contrast, in our fermionic lithium experiment where we use a tight optical dipole trap, we achieve degeneracy after losing only about 80% of the trapped atoms [Joc04]. The highly efficient evaporative cooling to degeneracy with optical dipole traps was first realized by M. Chapman’s group for the creation of a Rb BEC [Bar01] and by the group of J. Thomas

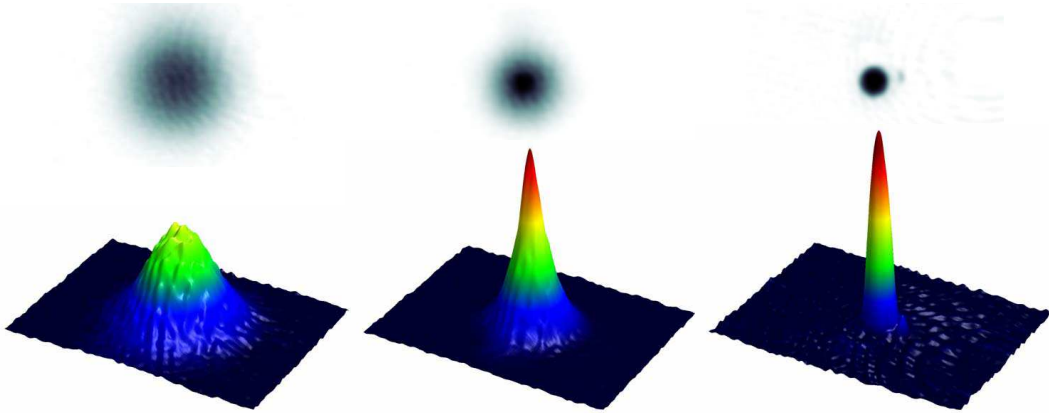


Figure 2.4: Typical absorption imaging pictures of a  $^{87}\text{Rb}$  gas undergoing the phase transition to Bose-Einstein condensation. Above: Raw images showing the shadow cast by the atomic gas. Below: 3D and false color rendering of the corresponding density distribution.

for the creation of a degenerate Fermi gas [Gra02].

## 2.2.4 Detection of atoms

Almost all our experiments end with a measurement of the atomic density distribution  $n(r)$  which can be used to determine the number of atoms and the temperature of the gas. In the case of a BEC,  $n(r)$  maps out the quantum mechanical wavefunction in position or, after time of flight, momentum space. We image the atoms with the well established absorption imaging technique [Ket99]. The atoms are irradiated by a homogenous laser beam in  $z$ -direction. They cast a shadow according to the column density  $\tilde{n} = \int n \, dz$ . According to Beer's law, the transmission of the light is given by  $I = I_0 \exp(-\tilde{n}\sigma)$ . Here,  $\sigma$  is the absorption cross section which is a function of the wavelength and the laser detuning. Absorption imaging can be sensitive enough to discriminate between different spin states. It is, however, destructive and after each image, a "fresh" condensate for further measurements has to be prepared. There exists also a non-destructive imaging method [And96] based on phase contrast imaging. This method was only used once in our experiments when it was important to compare atom numbers in a BEC before and after exposure to photoassociation light [McK02]. A typical resolution for absorption imaging is on the order of  $5 \, \mu\text{m}$ . We worked with exposure times as short as  $10 \, \mu\text{s}$  in order to prevent blurring of subtle patterns in the

atomic density distribution.

## Chapter 3

# Controlling matter waves with potentials made of light

Far-detuned optical light fields are an excellent means to coherently manipulate and analyze states of degenerate quantum gases. When located in a light field, the atoms of the gas experience a potential which is proportional to the local light intensity (see Eq. (2.20) in chapter 2.2.2). Detuning far from resonance suppresses spontaneous scattering of photons, which otherwise would lead to decoherence. By shaping these light fields in time and space, almost any arbitrary potential can be created. The spatial resolution of the light pattern is essentially diffraction limited. The light field potentials can form interesting environments within which matter-wave dynamics can be studied. Optical lattices, for example, allow for novel solid state physics experiments. Furthermore, applying optical light fields in a *pulsed* manner provides a powerful set of tools to control and manipulate the atomic wavefunctions. A lot of these applications have already been used with non-degenerate gases in the early days of laser cooling (for an overview see [Met99, Ber97, Ada94]), i.e. before the advent of BEC. However, in combination with BEC their full potential for coherent manipulation has become clear.

In the following three sections, various applications of light fields are described: diffraction of atoms with pulsed light fields, phase engineering, and emulation of solid state physics in optical lattices. With these methods specific quantum states of matter are prepared and interesting physics can be investigated. The corresponding original research papers are attached at the end of the chapter.

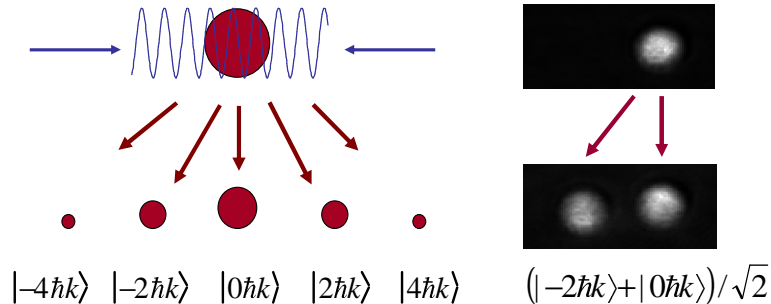


Figure 3.1: Diffracting atoms off an optical lattice. (left) The lattice imparts momentum in multiples of the lattice vector to the atoms, which can be observed after time of flight. (right) A moving lattice can resonantly couple two momentum states. This so-called Bragg scattering can be used to build a coherent beam splitter for atoms.

### 3.1 Diffracting atoms off optical lattices

We consider here the important case where a BEC is subjected to an optical lattice for a *short* interaction time. Such an optical lattice can be constructed simply by superimposing to counter-propagating laser beams, which results in a standing light wave. The atoms experience a sinusoidal potential which imparts momenta in multiples of the inverse lattice constant to the atoms. This results in a diffraction of atoms by this optical lattice (see Fig. 3.1). Bragg scattering is a special form of diffraction where (in general) a moving lattice resonantly couples two momentum states. Bragg scattering is the basis for several very useful tools in atom optics, e.g. coherent beam splitters for matter waves and matter wave interferometers (see Fig. 3.2).

Historically, the first diffraction experiments with optical lattices were performed in D. Pritchard's lab at MIT (e.g. [Gou86, Mar88]) where a collimated beam of thermal sodium atoms impinged on a standing laser light field. Since then extensive studies were carried out with thermal collimated atom beams (for a review see [Ber00, Sen95]), laser cooled atoms [Kun97], and BEC which was first diffracted in 1999 [Koz99]. A further development lead to Bragg spectroscopy [Ste99] to measure the momentum distribution in a condensate. As we will show in chapter 4, Bragg spectroscopy can also be used as a fast method to measure the scattering length in a condensate [The04]. Furthermore, Bragg diffraction was used to collide atomic matter waves with well defined momentum. This lead to beautiful experiments demonstrating for example 4-wave mixing of matter waves [Deng99b] and

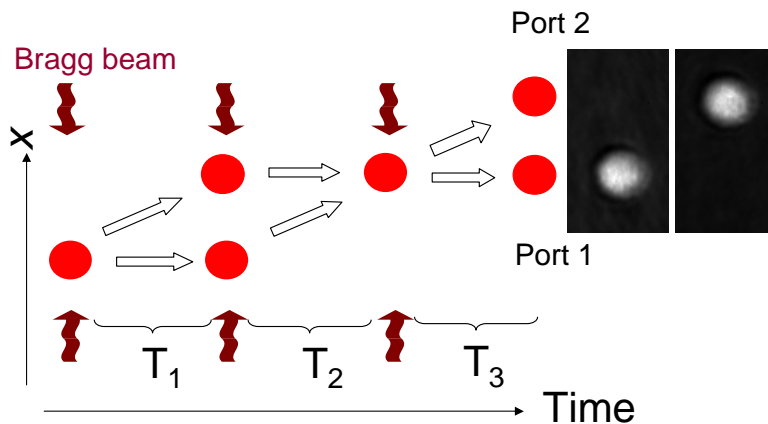


Figure 3.2: Mach-Zehnder interferometer for atoms. By combining two Bragg diffraction beam splitters (at time  $t = 0$  and  $t = T_1 + T_2$ ) and a Bragg diffraction  $\pi$ -pulse which swaps the momenta of the wave packets, a matter wave interferometer can be constructed. Depending on the relative phase of the two interferometer arms, atoms leave the interferometer in port 1 or 2. Since we can spatially resolve the condensate wave packets, also phase distributions across the condensate can be measured.

matter wave amplification [Ino99].

During my postdoc at NIST, we employed optical lattices to diffract a sodium BEC in several experiments. In a first experiment [Den99], we demonstrated a temporal analog of the well-known Talbot effect. Using a pair of short exposures of an optical lattice onto a condensate, interferometric diffraction patterns were created which showed temporal periodic recurrences. In another set of experiments we combined two matter wave beam splitters based on Bragg diffraction to build a Mach-Zehnder type interferometer for matter waves (see Fig. 3.2). The specialty of the interferometer was that it could spatially resolve the condensate wave function. In this way we were able to interferometrically measure the phase distribution on a condensate wave packet [Den00]. In a further development we mapped out the evolution of the phase of a condensate wave packet [Sim00]. Here an interferometric autocorrelation measurement on the BEC was performed. This scheme is analog to the “FROG” technique [Tre97] which is used to measure the complete electric field of ultrafast laser pulses. We found that a released, free evolving condensate in the Thomas-Fermi regime develops spatially a quadratic phase distribution across its wave packet.

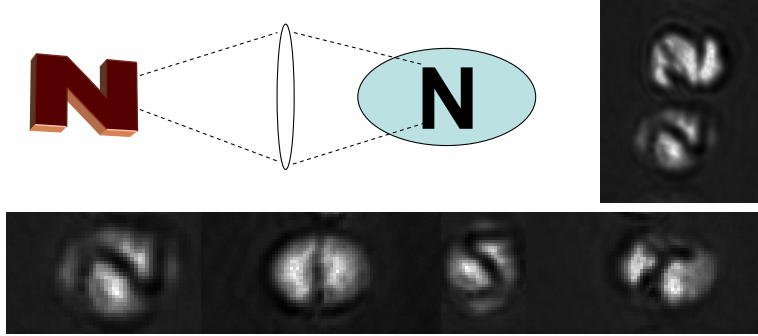


Figure 3.3: Phase imprinting. By exposing a BEC wave function to an off-resonant light field, phase patterns can be written onto the BEC. These phase distributions can be read out via matter wave interferometry. Here we spelled the word “NIST” on a sequence of condensates. On the upper right the two ports of the interferometer are shown. The density distributions of the two ports are complementary. The typical size of the condensate in the images is about  $60 \mu\text{m}$ .

## 3.2 Phase engineering with light

Using far off resonant light we can control the phase distribution of a BEC wavefunction. The idea is to expose the BEC to pulsed off-resonant laser light field pattern  $I(\vec{r})$ . The condensate experiences a spatially varying light shift potential (see also Eq. (2.20))

$$U(\vec{r}) \propto I(\vec{r}).$$

After a time  $t$  the BEC acquires a corresponding phase shift

$$\phi(\vec{r}) = -U(\vec{r})t/\hbar.$$

This modifies the condensate wave function accordingly

$$\Psi \longrightarrow \Psi \exp[i\phi(\vec{r})].$$

It is important that the pulse duration  $t$  is short enough that atomic motion in the condensate is negligible during the pulse. In this limit the effect of the pulse can be expressed as a sudden phase imprint. In principle, phase imprinting can produce arbitrary phase distributions as determined by the light field pattern. Ultimately the resolution of the light field patterned is diffraction limited and is on the order of the laser wavelength. Figure 3.3

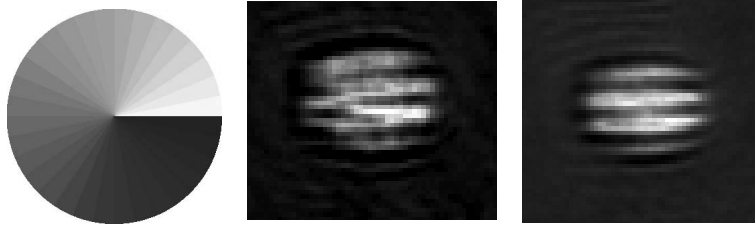


Figure 3.4: Imprinting a azimuthally varying phase pattern (left) can be used to create vortices. We have imprinted such phase patterns on a condensate. After matter wave interferometry we obtained the characteristic fork patterns for vortices (center). (right) The interference pattern without phase imprint.

shows a BEC onto which we phase imprinted letters from the alphabet. Using an interferometer similar to the one shown in Fig. 3.2 we converted this “secret” phase-ink into a density distribution which can be read out with absorption imaging. Phase imprinting allowed to excite dark solitons for the first time in a BEC, as demonstrated by our group at NIST and the group of W. Ertmer in Hannover [Den00, Bur99]. Dark solitons feature a characteristic phase jump across their wave packet. By imprinting such a phase jump onto a BEC, we could create such a soliton. Bright solitons also exist, which, however, do not feature a phase jump. Such bright solitons were created in 2002 with a different method where the interaction between the condensate atoms was tuned with the help of a Feshbach resonance [Kha02, Str02]. Phase imprinting can also excite other interesting quantum mechanical states. For example an azimuthally varying phase pattern could create quantized vortices<sup>1</sup> [Dob99, Den00]. We have imprinted such phase patterns (see Fig. 3.4) at NIST and after consecutive interferometry we obtained the characteristic fork patterns for vortices. However, the search for vortex holes via direct imaging of the condensate was not successful since the density distribution of the condensate was too agitated and turbulent. These experiments are unpublished. Vortex phase singularities were reported in 2001 by the Ketterle group [Ino01].

---

<sup>1</sup>Vortices have been already successfully produced in atomic BECs, e.g. by stirring [Mad00].

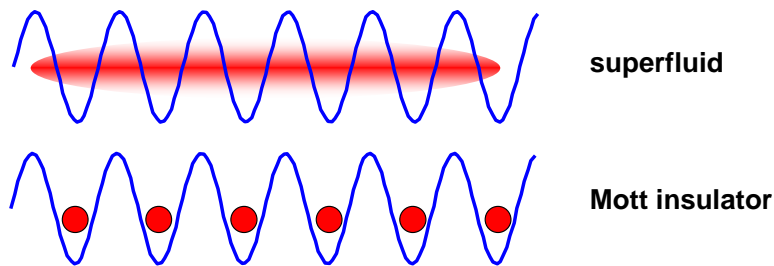


Figure 3.5: Two different regimes for quantum mechanical ground states in the lattice. The delocalized superfluid state can be attributed a phase and exhibits coherence. The Mott insulator state has a well defined atom number per lattice site and there is no phase relation between the different sites.

### 3.3 Solid state physics in optical lattice

Studying ultracold atoms in optical lattices has evolved into an incredibly active and successful research field which investigates solid state physics. In comparison to ordinary solid state systems like metals and crystals, optical lattices are essentially free of defects, are fully controllable, and can be dynamically changed. Over the last 15 years, many research groups have contributed to this research and as a consequence it will be impossible here to give an overview of their achievements. Already before the advent of BEC many fascinating effects like Bloch oscillations and the quantized lattice band structure could be studied with laser-cooled atomic gases (for an overview see [Jes96]). With BEC and degenerate Fermi gases at hand, the interest in optical lattices has grown even more and many new groups have joined the field.

Despite the multitude of experiments dealing with bosons, fermions or mixtures in lattice systems with various dimensions, one can group the recent experiments roughly into two categories. In the first category atoms are coherently delocalized over many lattice sites, and the quantum states are well described in a Bloch state basis. The second category corresponds to the Mott insulator regime where atoms are localized at individual lattice sites (see Fig. 3.5) and coherences between neighboring lattices are suppressed.

#### 3.3.1 Bloch states in optical lattices

Bloch states are the single-particle eigenstates in a periodic environment. In the band structure theory these eigenstates  $|n, q\rangle$  are characterized by their quasi-momentum  $q$  and the band index  $n$  and they can be expanded in a

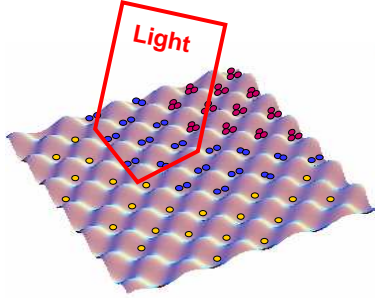


Figure 3.6: The Mott insulator state is a promising tool to create stable ground state molecules via photoassociation and to perform quantum information processing.

discrete plane wave basis

$$|n, q\rangle = \sum_{m=-\infty}^{\infty} a(m) |m2\hbar k + q\rangle, \quad (3.1)$$

where  $2k$  is the lattice vector and  $a(m)$  are the coefficients. These Bloch states are delocalized over the lattice. Their wavefunction shows a well defined phase relation between the lattice sites which is determined by the quasi-momentum. When a BEC is loaded into an optical lattice, the mean-field self-interaction of the condensate atoms will give rise to non-linear effects. This can strongly affect the dynamics of the wave function and has generated a lot of interest. The list of topics which were recently investigated in the superfluid regime include experiments on Bloch oscillations [Dah96, And98, Mor01, Den02, Pez04], gap solitons [Eie04], self-trapping [Ank05], collective excitations [Mor03, For03, Sch04], patterned loading [Pei03], dynamical instabilities [Fal04, Cri04, Sco04], Landau-Zener tunnelling [Den02, Jon03] and Josephson junctions [Cat04].

In our work at NIST [Den02] we have studied in detail different loading regimes of a BEC into an optical lattice in order to create specific Bloch states. Various schemes were used to analyze these states in terms of momentum composition and band population. We showed how Bloch states can be coherently transferred to other Bloch states in different bands and quasi-momenta. For example, interband transitions can be excited via generation of appropriate side bands of the lattice lasers frequencies. We used these interband transfers to investigate the band structure spectroscopically, i.e. measure the energy gap between the lattice bands as a function of the quasi-momentum. Finally using these techniques we built a BEC accelerator

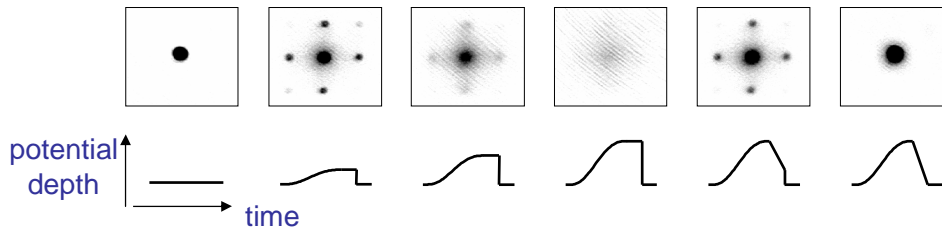


Figure 3.7: Quantum phase transition into the Mott insulator state. For high enough lattice depths ( $\approx 15\times$  photon recoil energy) the diffraction pattern disappears, a signature for the localization of the atoms. The coherence reappears by ramping down the lattice within a few ms (last two images). Shown are experimental data from our experiment in Innsbruck. The lattice was based on laser light at a wavelength of 830nm, far detuned from atomic resonance of  $^{87}\text{Rb}$ .

and a novel, coherent, large-momentum-transfer beam-splitter. These experiments were performed in the limit of negligible mean-field interaction of the condensate.

### 3.3.2 The Mott insulator

The Mott insulator phase transition for ultracold atoms in optical lattices was predicted in 1998 by Jaksch *et al.* [Jak98] in Innsbruck and was first demonstrated by Greiner *et al.* [Gre02] in Munich. In a deep optical lattice where tunnelling between the lattice sites is hampered and the atoms experience a strong repulsive inter-particle potential, the quantum mechanical ground state of the system is highly correlated and beyond the usual mean-field description of BEC. This Mott insulator state exhibits a well defined number of particles per lattice site which locally corresponds to Fock states. Due to a gap in the excitation spectrum the insulator is insensitive to perturbations below a certain threshold. Quite a large number of proposals exist to use the Mott insulator to, e.g. study new quantum phases, realize quantum information processing, entangle atoms, create stable ultracold molecules and study disordered systems (see Fig. 3.6).

In December 2004 we have achieved such a Mott insulator phase transition in our lab in Innsbruck starting from a  $^{87}\text{Rb}$  condensate ( $4 \times 10^5$  atoms) in an optical lattice, see Fig. 3.7. We want to use the Mott insulator for two lines of research. One goal is to create stable molecules in deeply bound vibrational states and possibly the vibrational ground state. If these molecules are stable enough against inelastic collisions, then it should be possible to

create a BEC of such deeply bound molecules by melting the Mott insulator [Jak02]. Our second goal is to realize quantum information processing schemes. The interesting proposal [Cal03] by Calarco *et al.* involves superlattices, marker atoms, q-bit atoms and Feshbach resonances. Modulating the superlattice moves the marker atoms which carry the quantum information through the optical lattice. The quantum gates involve controlled collisions of marker and q-bit atoms via Feshbach resonances. First promising steps in the direction of quantum information processing with optical lattices have been recently demonstrated by the group around I. Bloch and T. Hänsch (Munich, Mainz) demonstrating coherent transport [Man03a] and entanglement of atoms [Man03].



### 3.4 “Generating Solitons by Phase Engineering of a Bose-Einstein Condensate”

J. Denschlag, J. E. Simsarian, D. L. Feder, C. W. Clark, L. A. Collins, J. Cubizolles, L. Deng, E. W. Hagley, K. Helmer-son, W. P. Reinhardt, S. L. Rolston, B. I. Schneider, and W. D. Phillips

Science **287**, 97-101 (2000)

## RESEARCH ARTICLES

- visualized on 15% denaturing polyacrylamide gels using tricine buffer. All stable fragments larger than 2 kD were identified through NH<sub>2</sub>-terminal sequencing and mass spectrometric analyses.
- Mutant constructs were generated using standard polymerase chain reaction-based cloning strategy, and the identities of individual clones were verified through double-strand plasmid sequencing. The Smad-binding fragment from SARA (residues 665–721) was overexpressed in *Escherichia coli* strain BL21(DE3) as a glutathione S-transferase (GST)-fusion protein using a pGEX-2T vector (Pharmacia) and was purified by a glutathione sepharose 4B affinity column. The MH2 domain from Smad2 (residues 241–467) was overexpressed in a pET3d vector (Novagen). The soluble fraction of Smad2 MH2 in the *E. coli* lysate was purified by cation-exchange chromatography (SP-sepharose; Pharmacia) and gel-filtration chromatography (Superdex-75 column; Pharmacia). Equimolar amounts of GST-SARA SBD and Smad2 MH2 domain were mixed and incubated in 25 mM NaMES (pH 6.0), 50 mM NaCl, and 2 mM dithiothreitol (DTT). The complex was then passed through a cation-exchange column (SP-sepharose; Pharmacia), to which Smad2 MH2 domain binds avidly. GST-SARA SBD in isolation does not bind this column. Smad2 binding to the column has no effect on interaction with SARA. The bound complex was eluted from this column with 1 M NaCl and visualized on 15% SDS-polyacrylamide gel electrophoresis.
  - Proteins of the Smad2 MH2 domain and SARA SBD were individually purified and mixed in a 1:1 molar ratio. The final complex was concentrated and purified through gel-filtration chromatography (Superdex-75 column; Pharmacia). The concentration of the complex is ~20 mg/ml. Heavily twinned crystal clusters were grown at 4°C by the hanging-drop vapor-diffusion method by mixing the SARA-Smad2 protein complex with an equal volume of reservoir solution containing 100 mM Tris buffer (pH 8.5), 10% Dioxane (v/v), 2.0 M ammonium sulfate, and 10 mM DTT. Streak-seeding followed by three rounds of macro-seeding eventually generated crystals suitable for x-ray diffraction. The crystals, with a typical size of 0.1 mm by 0.1 mm by 0.4 mm, are in the trigonal space group P3121, with unit cell dimensions  $a = b = 138.5 \text{ \AA}$ ,  $c = 55.9 \text{ \AA}$ ,  $\alpha = \beta = 90^\circ$ ,  $\gamma = 120^\circ$ , and contain two complexes in the asymmetric unit. Initial diffraction data were collected using an R-AxisIIIC imaging plate detector mounted on a Rigaku 200HB generator. High-resolution data sets were collected at beamline X25 at the National Synchrotron Light Source (NSLS), Brookhaven National Laboratory. All data sets were collected under freezing conditions; crystals were equilibrated in a cryoprotectant buffer containing 100 mM Tris buffer (pH 8.5), 10% Dioxane (v/v), 2.0 M ammonium sulfate, and 20% glycerol, and were flash frozen under a  $-170^\circ\text{C}$  nitrogen stream. The structure was primarily determined by molecular replacement using the software AMoRe [J. Navaza, *J. Acta Crystallogr. A* **50**, 157 (1994)]. The atomic coordinates of Smad4 MH2 were used for a rotational search against a 15–3.5 Å data set. The top 50 solutions from the rotational search were individually used for a subsequent translational search, which yielded one solution with a correlation factor of 20.8 and an *R*-factor of 52.4%. This solution was used to locate the second complex in the crystals. Together, these two solutions gave a combined correlation factor of 33.5 and an *R*-factor of 44%. This model was examined with the program O [T. A. Jones *et al.*, *Acta Crystallogr. A* **47**, 110 (1991)], and the Smad4 side chains were replaced with those of Smad2. Refinement by simulated annealing with the program X-PLOR (A. T. Brünger, Yale University), against a 3.0 Å native data set decreased the *R* factor and *R* free to 35% and 42%, respectively. Refinement against 2.2 Å resolution data allowed progressive identification of the SARA fragment. The final refined model contains two complexes of Smad2 (residues 263–456) and SARA (residues 669–709), and 243 water molecules. The NH<sub>2</sub>- and COOH-terminal residues in Smad2 have no electron density, and we presume that these regions are disordered in the crystals. The two complexes

in one asymmetric unit are similar with a rmsd of 0.79 Å for all aligned C $\alpha$  atoms. We only report here one representative complex.

- Miyaki *et al.*, *Oncogene* **18**, 3098 (1999).
- Immunofluorescence was performed as described (9). Rhodamine-conjugated goat anti-mouse and fluorescein isothiocyanate (FITC)-conjugated goat anti-rabbit antibodies were purchased from Jackson ImmunoResearch Laboratories.
- X. Chen, M. J. Rubock, M. Whitman, *Nature* **383**, 691 (1996).
- Using a calcium phosphate-DNA precipitation method, HepG2 cells were transfected with the *Mix.2* ARE-luciferase reporter (16), FAST-2 [F. Liu *et al.*, *Mol. Cell. Biol.* **19**, 424 (1999)], with or without SARA and Smad2 constructs. Cells were treated with TGF $\beta$ 2 for 20 hours, and luciferase activity was determined.
- X.-H. Feng and R. Derynck, *EMBO J.* **16**, 3912 (1997).
- M. Huse, Y.-G. Chen, J. Massagué, J. Kuriyan, *Cell* **96**, 425 (1999).
- R. Wieser, J. L. Wrana, J. Massagué, *EMBO J.* **14**, 2199 (1995).

- Willis, C. M. Zimmerman, L. Li, L. S. Mathews, *Mol. Endocrinol.* **10**, 367 (1996).
- X.-H. Feng, E. H. Filvaroff, R. Derynck, *J. Biol. Chem.* **270**, 24237 (1995).
- A. A. Russo, P. D. Jeffrey, A. K. Patten, J. Massagué, N. P. Pavletich, *Nature* **382**, 325 (1996).
- P. J. Klaulis, *J. Appl. Crystallogr.* **24**, 946 (1991).
- A. Nicholls, K. A. Sharp, B. Honig, *Proteins Struct. Funct. Genet.* **11**, 281 (1991).
- We thank H. Lewis for help with the X25 beamline at NSLS, S. Kyin for peptide sequencing and mass spectroscopic analysis, F. Hughson for critically reading the manuscript, L.-A. Swaby for technical support, M. Taga for help in early stages of this project, and E. Steckman for secretarial assistance. Supported by NIH grant CA85171 (Y.S.), Howard Hughes Medical Institutes (J.M.), Medical Research Council of Canada (J.L.W.), the Searle Foundation and the Rita Allen Foundation (Y.S.). Coordinates have been deposited with the Protein Data Bank (accession number 1DEV).

19 October 1999; accepted 19 November 1999

# Generating Solitons by Phase Engineering of a Bose-Einstein Condensate

J. Denschlag,<sup>1</sup> J. E. Simsarian,<sup>1</sup> D. L. Feder,<sup>1,2</sup> Charles W. Clark,<sup>1</sup> L. A. Collins,<sup>3</sup> J. Cubizolles,<sup>1,4</sup> L. Deng,<sup>1</sup> E. W. Hagley,<sup>1</sup> K. Helmerson,<sup>1</sup> W. P. Reinhardt,<sup>1,5</sup> S. L. Rolston,<sup>1</sup> B. I. Schneider,<sup>6</sup> W. D. Phillips<sup>1</sup>

Quantum phase engineering is demonstrated with two techniques that allow the spatial phase distribution of a Bose-Einstein condensate (BEC) to be written and read out. A quantum state was designed and produced by optically imprinting a phase pattern onto a BEC of sodium atoms, and matter-wave interferometry with spatially resolved imaging was used to analyze the resultant phase distribution. An appropriate phase imprint created solitons, the first experimental realization of this nonlinear phenomenon in a BEC. The subsequent evolution of these excitations was investigated both experimentally and theoretically.

Ultimate control over a physical system can be achieved by precisely manipulating its quantum mechanical wave function, which fully characterizes its state. A BEC of a dilute gas (*I*) is particularly well suited for such manipulations because of its directly observable wave function: It has many identical atoms in the same quantum state, and it is large enough to be optically imaged.

We demonstrate two optical techniques to prepare and measure the phase of a BEC wave function. A chosen pattern of laser light

imaged onto a condensate shapes its phase almost arbitrarily in two dimensions (2–4). Matter-wave interferometry (5) using optically induced Bragg diffraction (6, 7) is then used to analyze the spatial phase distribution by direct imaging (8). These methods are applied in experimental studies of a phenomenon in nonlinear atom optics (9), the propagation of solitons [solitary waves (10)] in a BEC. Three-dimensional (3D) numerical calculations agree well with and substantiate the experimental observations of soliton generation and propagation. Both reveal the rich dynamics of this nonlinear system, such as the formation of multiple solitons.

**Theoretical background.** Solitons are stable, localized waves that propagate in a nonlinear medium without spreading. They appear in diverse contexts of science and engineering, such as the dynamics of waves in shallow water (11), transport along DNA and other macromolecules (12), and fiber

<sup>1</sup>National Institute of Standards and Technology (NIST), Gaithersburg, MD 20899, USA. <sup>2</sup>University of Oxford, Parks Road, Oxford OX1 3PU, UK. <sup>3</sup>Theoretical Division, Mail Stop B212, Los Alamos National Laboratory, Los Alamos, NM 87545, USA. <sup>4</sup>Ecole Normale Supérieure, 24 rue Lhomond, 75231 Paris, France. <sup>5</sup>Department of Chemistry, University of Washington, Seattle, WA 98195, USA. <sup>6</sup>Physics Division, National Science Foundation, Arlington, VA 22230, USA.

optic communications (13). Solitons may be either bright or dark, depending on the details of the governing nonlinear wave equation. A bright soliton is a peak in the amplitude; a dark soliton is a notch with a characteristic phase step across it.

A weakly interacting BEC obeys a nonlinear wave equation that supports solitons, as shown by recent theoretical studies (14–17). At zero temperature, this wave equation is known as the Gross-Pitaevskii equation (18),

$$i\hbar(\partial/\partial t)\psi = [-(\hbar^2/2M)\nabla^2 + V + g|\psi|^2]\psi \quad (1)$$

where  $\psi$  is the condensate wave function normalized to the number of atoms,  $V$  is the trapping potential,  $M$  is the atomic mass,  $\hbar$  is the Planck constant divided by  $2\pi$  and  $g$  describes the strength of the atom-atom interaction (19). Solitons propagate without spreading (dispersing) because the nonlinearity balances the dispersion; for Eq. 1, the corresponding terms are the nonlinear interaction  $g|\psi|^2$  and the kinetic energy  $-(\hbar^2/2M)\nabla^2$ , respectively. Our sodium condensate only supports dark solitons because the atom-atom interactions are repulsive ( $g > 0$ ).

A distinguishing characteristic of a dark soliton is that its speed is less than the Bogoliubov speed of sound,  $v_0 = (gn/M)^{1/2}$  (18, 20), where  $n = |\psi_0|^2$  is the unperturbed condensate density. The soliton speed  $v_s$  can be expressed in terms of either the phase step  $\delta$  ( $0 < \delta \leq \pi$ ) or the soliton “depth”  $n_d$ , which is the difference between  $n$  and the density at the bottom of the notch (14, 15):

$$v_s/v_0 = \cos(\delta/2) = [1 - (n_d/n)]^{1/2} \quad (2)$$

For  $\delta = \pi$ , the soliton has zero velocity, zero

density at its center, a width on the order of the healing length  $\xi = (2nMg/\hbar^2)^{-1/2}$  (15), and a discontinuous phase step. As  $\delta$  decreases, the speed increases and approaches the speed of sound. The solitons become shallower and wider and have a more gradual phase step (15). They travel opposite to the direction of the phase gradient. Because a soliton has a characteristic phase step, optically imprinting a phase step on the BEC wave function should be a way to create a soliton.

**Phase imprinting.** We performed our experiments with a condensate having  $\sim 2 \times 10^6$  sodium atoms in the  $3S_{1/2}$ ,  $F = 1$ ,  $m_F = -1$  state, with no discernible thermal fraction (7). The condensate was held in a magnetic trap with trapping frequencies  $\omega_x = \sqrt{2}\omega_y = 2\omega_z = 2\pi \times 28$  Hz. The Thomas-Fermi diameters (18) were 45, 64, and 90  $\mu\text{m}$ , respectively. Initially the BEC, described by the ground-state solution of Eq. 1, had a uniform phase (21, 22).

We modified the phase distribution of the BEC by exposing it to pulsed, off-resonant laser light with an intensity pattern  $I(x, y)$  (Fig. 1). In this process, the atoms experience a spatially varying light-shift potential  $U(x, y) = (\hbar\Gamma^2/8\Delta)[I(x, y)/I_0]$  and acquire a corresponding phase  $\phi(x, y) = -U(x, y)T/\hbar$ . Here  $\Gamma$  is the transition line width,  $I_0$  is the saturation intensity,  $\Delta$  is the detuning of the laser from the atomic resonance, and  $T$  is the laser pulse duration (23). We chose  $T$  to be short enough so that the atomic motion was negligible during the pulse (Raman-Nath regime). In this limit, the effect of the pulse can be expressed as a sudden phase imprint, which modifies the initial wave function:  $\psi \rightarrow \psi \exp[i\phi(x, y)]$  (24).

**Interferometry.** We measured the imprint-

ed phase distribution of the condensate wave function with a Mach-Zehnder matter-wave interferometer that makes use of optically induced Bragg diffraction (25, 26). Our Bragg interferometer differs from previous ones in that we can independently manipulate atoms in the two arms (because of their large separation) and can resolve the output ports to reveal the spatial distribution of the condensate phase. In our interferometer, a Bragg pulse splits the initial condensate into two states,  $|A\rangle$  and  $|B\rangle$ , differing only in their momenta (Fig. 2). After they spatially separate, the phase step (Fig. 1A) is imprinted on  $|A\rangle$ , while  $|B\rangle$  is unaffected and serves as a phase reference. When recombined, they interfere according to their local phase difference. Where this phase difference is 0, atoms appear in port 1, and where it is  $\pi$  atoms appear in port 2. Imaging the density distributions of ports 1 and 2 displays the spatially varying phase (27). The image in Fig. 2 shows the output of the interferometer when a phase of  $\pi$  was imprinted on the upper half of  $|A\rangle$  (28). The high-contrast “half moons” are direct evidence that we can control the condensate spatial phase distribution and, in particular, imprint the phase step appropriate for a soliton (29).

**Soliton propagation.** To observe soliton propagation, we did not use interferometry (30) but instead measured BEC density distributions with absorption imaging (1, 27) after imprinting a phase step (31). Figure 3, A to E, shows the evolution of the condensate after the top half was phase-imprinted with  $\phi_0 \approx 1.5\pi$ , a phase for which we observed a single deep soliton (the reason for imprinting a phase step larger than  $\pi$  is discussed below). Immediately after the phase imprint, there is a steep phase gradient across the middle of the condensate such that this por-

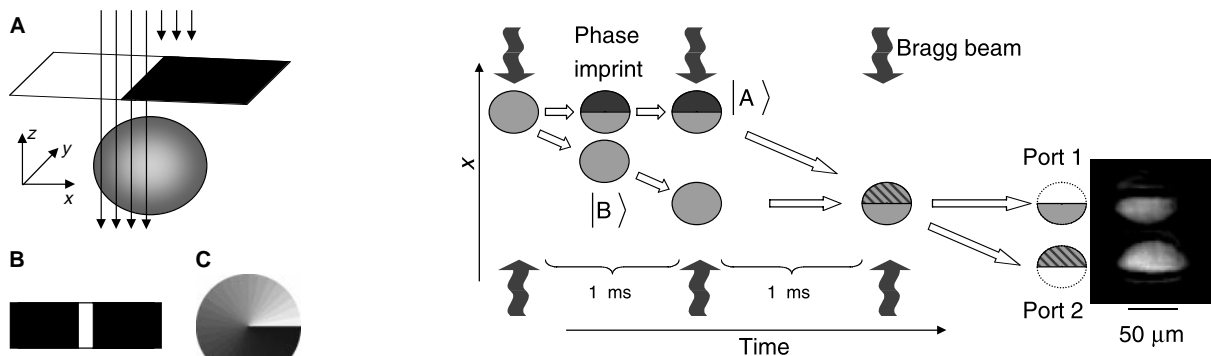


**Fig. 1.** (A) Writing a phase step onto the condensate. A far-detuned uniform light pulse projects a mask (a razor blade) onto the condensate. Because of the light shift, this imprints a phase distribution that is proportional to the light intensity distribution. A lens (not shown) is used to image the razor blade onto the condensate. The mask in (B) writes a phase stripe onto the condensate. The mask in (C) imprints an azimuthally varying phase pattern that can be used to create vortices.

**Fig. 2.** Space-time diagram of the matter-wave interferometer used to measure the spatial phase distribution imprinted on the BEC. Three optically induced Bragg diffraction pulses (7) formed the interferometer. Each pulse consisted of two counterpropagating laser beams detuned by  $-2$  GHz from atomic resonance (so that spontaneous emission is negligible), with their frequencies differing by 100 kHz. The first Bragg pulse had a duration of 8  $\mu\text{s}$  and coherently split the condensate into two components  $|A\rangle$  and  $|B\rangle$  with equal numbers of atoms;  $|A\rangle$  remained at rest and  $|B\rangle$  received two photon recoils of momentum. When they were completely separated, we applied the 500-ns phase imprint pulse to the top half of  $|A\rangle$ , which changed the phase distribution of  $|A\rangle$  while  $|B\rangle$  served as a phase reference. A second Bragg pulse (duration 16  $\mu\text{s}$ ), 1 ms after the first pulse, brought  $|B\rangle$  to rest and imparted two photon momenta to  $|A\rangle$ . When they overlapped again, 1 ms later, a third pulse (duration 8  $\mu\text{s}$ ) converted their phase differences into density distributions at ports 1 and 2. The image shows the output ports 1 and 2 as seen when we imprinted a phase step of  $\pi$  (29).

## RESEARCH ARTICLES

tion has a large velocity in the  $+x$  direction. This velocity, which can be understood as arising from the impulse imparted by the optical dipole force, results in a positive density disturbance that travels at or above the speed of sound. A dark notch is left behind; this is a soliton moving slowly in the  $-x$  direction (opposite to the direction of the applied force).

We have numerically solved Eq. 1 in three dimensions through the application of real-space product formulas (32) and by using a discrete variable representation of the wave function (33) based on Gauss-Chebyshev quadrature with 50 to 400 spatial grid points in each dimension; in the latter approach, the time dependence of the solution was obtained by Runge-Kutta integration. Figure 3, F to J, shows the results of the simulations where the experimental phase imprint is approximated as  $\phi(x, y) = (\phi_0/2)[1 + \tanh(x/l)]$ , where  $\phi_0 = 1.5\pi$ , and  $l = 2 \mu\text{m}$  corresponds to an imprinting resolution of  $\sim 4.4 \mu\text{m}$  (27, 34). The calculated and experimental images are in very good agreement.

A striking feature of the images is the curvature of the soliton. This curvature arises from the 3D geometry of the trapped condensate and occurs for two reasons. First, the speed of sound  $v_0$  is largest at the trap center, where the density is greatest, and decreases toward the condensate edge. Second, as the soliton moves into regions of lower condensate density, we find numerically that the density at its center ( $n - n_d$ ) approaches zero,  $\delta$  approaches  $\pi$ , and  $v_s$  decreases to zero before reaching the edge. The soliton stops because its depth  $n_d$ , rather than its phase offset  $\delta$ , appears to be a conserved quantity in a nonuniform medium.

**Soliton speed.** The subsonic propagation speed of the notches seen in Fig. 3 shows that they are solitons and not simply sound waves. To determine this speed, we measured the distance after propagation between the notch and the position of the imprinted phase step along the direction indicated in Fig. 3H. Because the position of our condensate varied randomly from one shot to the next (presumably because of stray, time-varying fields), we could not always apply the phase step at the center. A marker for the location of the initial phase step is the intersection of the soliton with the condensate edge, because at this point the soliton has zero velocity. By using images taken 5 ms after the imprint, at which time the soliton had not traveled far from the BEC center, we obtained a mean soliton speed of  $1.8 \pm 0.4 \text{ mm/s}$  (35). This value is significantly less than the mean Bogoliubov speed of sound,  $v_0 = 2.8 \pm 0.1 \text{ mm/s}$ . From the propagation of the notch in the numerical simulations (Fig. 3, F to J), we obtained a mean soliton speed,  $v_s = 1.6 \text{ mm/s}$ , in agreement with the experimental

value. The experimental uncertainty is mainly due to the difficulty in determining the position of the initial phase step.

We can also compare the results of the numerical 3D solutions of Eq. 1 to the analytical predictions of Eq. 2, which describes a traditional dark soliton in a homogeneous, 1D geometry. We calculated the soliton speed using a local density approximation in Eq. 2 [ $n = |\pi_0(r)|^2$ , where  $\pi_0(r)$  is the ground-state solution of Eq. 1] from either the phase or depth of the solitons obtained in the 3D simulations. In every case examined, this speed is in excellent agreement with the results of 3D numerical simulations.

Figure 4 shows the theoretical density and phase profile along the  $x$  axis through the center of the condensate 5 ms after the  $\phi_0 = 1.5\pi$  phase imprint (Fig. 3H). The dark soliton notch and its phase step are centered at  $x = -8 \mu\text{m}$ . This phase step,  $\delta = 0.58\pi$  is less than the imprinted phase of  $1.5\pi$ . The difference is caused by the mismatch between the phase imprint and the phase and depth of the soliton solution of Eq. 1: Our imprinting resolution (27) is larger than the soliton width, which is on the order of the healing length ( $\xi \approx 0.7 \mu\text{m}$ ), and we do not control the amplitude of the wave function. The mismatch produces features in addition to the deep soliton, such as a shallow dark soliton at  $x = -14 \mu\text{m}$  moving to the left

and other excitations near  $x = 20 \mu\text{m}$  moving rapidly to the right. Most of these features are not well resolved in the experimental images (Fig. 3, A to E). We observed both experimentally and theoretically that when the imprinted phase step is increased, the weak soliton on the left becomes deeper; when the phase step is lowered, both solitons become shallower and propagate faster.

We could avoid the uncertainty in the position of the initial phase step and improve our measurement of the soliton speed by replacing the step mask (Fig. 1A) with a thin slit (Fig. 1B). The thin slit produced a stripe of light with a Gaussian profile ( $1/e^2$  full width  $\approx 15 \mu\text{m}$ ). With this stripe in the center of the condensate, numerical simulations predict the generation of solitons that propagate symmetrically outward. We selected experimental images with solitons symmetrically located about the middle of the condensate and measured the distance between them. Figure 5A shows the separation of the pair of solitons as a function of time. For a small phase imprint of  $\phi_0 \approx 0.5\pi$  at Gaussian maximum, we observed solitons moving at the Bogoliubov speed of sound within experimental uncertainty. For a larger phase imprint of  $\phi_0 \approx 1.5\pi$ , we observed a much slower soliton propagation, in agreement with numerical simulations. An even larger phase imprint

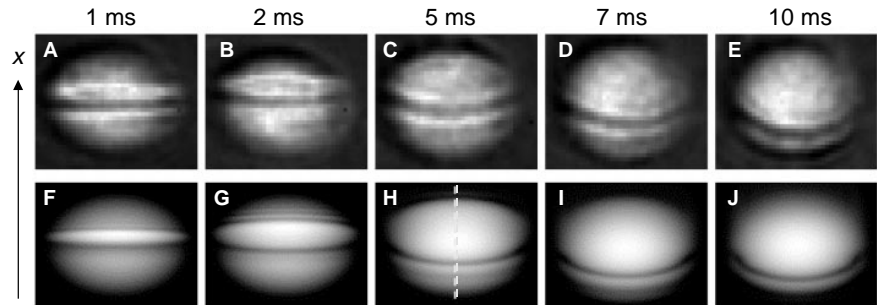


**Fig. 3.** Experimental (A to E) and theoretical (F to J) images of the integrated BEC density for various times after we imprinted a phase step of  $\sim 1.5\pi$  on the top half of the condensate with a  $1\text{-}\mu\text{s}$  pulse. The measured number of atoms in the condensate was  $1.7 (\pm 0.3) \times 10^6$ , and this value was used in the calculations. A positive density disturbance moved rapidly in the  $+x$  direction, and a dark soliton moved oppositely at significantly less than the speed of sound. Because the imaging pulse (27) is destructive, each image shows a different BEC. The width of each frame is  $70 \mu\text{m}$ .

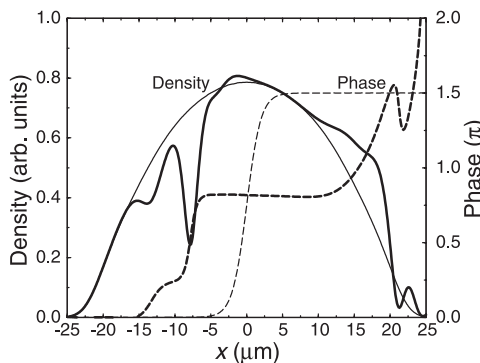
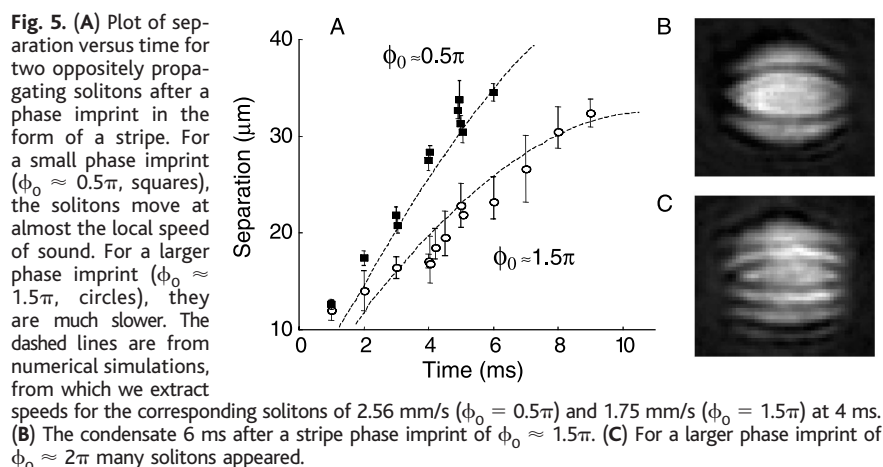


**Fig. 4.** Calculated density and phase along the  $x$  axis (dashed line in Fig. 3H) at 0 ms (thin lines) and at 5 ms (thick lines) after applying a phase step imprint of  $1.5\pi$ . The soliton located at  $x = -8 \mu\text{m}$  has a phase step of  $0.58\pi$  and a speed of  $1.61 \text{ mm/s}$ , which is much less than that of sound.



generates many solitons (Fig. 5C).

The lower theoretical curve in Fig. 5A shows that the speed of the corresponding solitons (the slope of the curve) approaches zero at a separation of  $\sim 33 \mu\text{m}$  before they reach the edge of the condensate (whose Thomas-Fermi diameter is  $45 \mu\text{m}$ ). This result follows directly from Eq. 2. Assuming a constant soliton depth  $n_d$  and working in the Thomas-Fermi limit, the derivative of  $v_s$  with respect to time yields the equation of motion  $dv_s/dt \equiv d^2x_s/dt^2 = -\omega^2 x_s/2$ . Thus, the soliton in a 1D trap should oscillate harmonically with a frequency  $\omega_s = \omega/\sqrt{2}$ , smaller than the trap frequency  $\omega$ . Previous calculations have also found this behavior (17). In our system, therefore, the soliton should stop after one-quarter of the oscillation time,  $(\pi/2)(\sqrt{2}/\omega_x)$  ms, which is in agreement with our 3D simulations. The 3D calculations, however, indicate that the soliton does not oscillate back after stopping, but instead breaks up, forming vortices that migrate to the BEC surface and disappear.

**Future directions.** The optical phase imprinting and matter-wave interferometry techniques presented here are new control and analysis tools for wave function engineering of Bose-Einstein condensates. For example, the interferometer might also be used to study randomness in the evolution of the condensate phase (phase diffusion). Our optical imprinting techniques could be extended to the control of wave function amplitude, with the use of near-resonant laser frequencies to induce absorption. The probability of removing atoms from the condensate would then be proportional to the local intensity of the laser beam, allowing us to tailor the density distribution of the BEC in addition to its phase.

Future avenues for research include studies of soliton stabilities and the interactions between solitons, as well as other nonlinear dynamics of condensates. Another possibility is the use of optical phase imprinting to create quantized vortices in a BEC (2). The  $2\pi$

phase winding of the vortex wave function around its core can be imprinted by imaging an intensity pattern with a linear azimuthal dependence (Fig. 1C). Quantized vortices in a BEC are a manifestation of superfluidity and have recently been observed in a two-component condensate (4) and a condensate in a rotating trap (36). We note that a group in Hannover, Germany, has independently studied solitons in a BEC using optical phase imprinting (37).

#### References and Notes

- M. H. Anderson, J. R. Ensher, M. R. Matthews, C. E. Wieman, E. A. Cornell, *Science* **269**, 198 (1995); K. B. Davis *et al.*, *Phys. Rev. Lett.* **75**, 3969 (1995); C. C. Bradley, C. A. Sackett, R. G. Hulet, *Phys. Rev. Lett.* **78**, 985 (1997); see also C. C. Bradley, C. A. Sackett, J. J. Tollett, R. G. Hulet, *Phys. Rev. Lett.* **75**, 985 (1995).
- The optical phase imprinting technique has been independently proposed by L. Dobrek *et al.* [*Phys. Rev. A* **60**, R3381 (1999)].
- A different phase-engineering scheme using a two-component BEC was recently developed [M. R. Matthews *et al.*, *Phys. Rev. Lett.* **83**, 3358 (1999); J. Williams and M. Holland, *Nature* **401**, 568 (1999); see also (4)].
- M. R. Matthews *et al.*, *Phys. Rev. Lett.* **83**, 2498 (1999).
- P. R. Berman, Ed., *Atom Interferometry* (Academic Press, Cambridge, 1997); C. S. Adams, M. Sigel, J. Mlynek, *Phys. Rep.* **240**, 143 (1994).
- P. J. Martin, B. G. Oldaker, A. H. Miklich, D. E. Pritchard, *Phys. Rev. Lett.* **60**, 515 (1988).
- M. Kozuma *et al.*, *Phys. Rev. Lett.* **82**, 871 (1999).
- Recent experiments also demonstrated spatial phase measurements by direct imaging using interferometry with two different internal states (4).
- G. Lens, P. Meystre, E. W. Wright, *Phys. Rev. Lett.* **71**, 3271 (1993); L. Deng *et al.*, *Nature* **398**, 218 (1999).
- In this article, we do not distinguish between the terms "soliton" and "solitary wave" because we do not investigate their collisional properties (13).
- R. K. Bullough, in *Solitons*, M. Lakshmanan, Ed. (Springer-Verlag, Berlin, 1988), pp. 150–281.
- M. Peyrard, Ed., *Molecular Excitations in Biomolecules* (Springer-Verlag, New York, 1995).
- A. Hasegawa, *Optical Solitons in Fibers* (Springer-Verlag, Berlin, ed. 2, 1990); J. K. Taylor, Ed., *Optical Solitons Theory & Experiment* (Cambridge Univ. Press, New York, 1992).
- W. P. Reinhardt and C. W. Clark, *J. Phys. B* **30**, L785 (1997); W. P. Reinhardt, in *Tunneling in Complex Systems*, S. Tomsovic, Ed. (World Scientific, Singapore, 1998), pp. 277–326.
- A. D. Jackson, G. M. Kavoulakis, C. J. Pethick, *Phys. Rev. A* **58**, 2417 (1998).
- R. Dum, J. I. Cirac, M. Lewenstein, P. Zoller, *Phys. Rev. Lett.* **80**, 2972 (1998); V. M. Pérez-García, H. Michinel, H. Herrero, *Phys. Rev. A* **57**, 3837 (1998); O. Zobay, S. Pötting, P. Meystre, E. M. Wright, *Phys. Rev. A* **59**, 643 (1999); P. O. Fedichev, A. E. Muryshev, G. V. Shlyapnikov, *Phys. Rev. A* **60**, 3220 (1999).
- A. E. Muryshev, H. B. van Linden van den Heuvell, G. V. Shlyapnikov, *Phys. Rev. A* **60**, R2665 (1999); T. Busch and J. Anglin, Los Alamos National Laboratory e-print cond-mat/9809408 (1998).
- F. Dalfonso, S. Giorgini, L. P. Pitaevskii, S. Stringari, *Rev. Mod. Phys.* **71**, 463 (1999).
- The coupling constant  $g$  is given by  $g = 4\pi\hbar^2 a/M$ , where  $a = 2.75 \text{ nm}$  [E. Tiesinga *et al.*, *J. Res. Natl. Inst. Stand. Technol.* **101**, 505 (1996)] is the scattering length of sodium for the  $F = 1$ ,  $m_F = -1$  state.
- M. R. Andrews *et al.*, *Phys. Rev. Lett.* **79**, 553 (1997).
- E. W. Hagley *et al.*, *Phys. Rev. Lett.* **83**, 3112 (1999).
- J. Stenger *et al.*, *Phys. Rev. Lett.* **82**, 4569 (1999).
- For the  $3S_{1/2}$ ,  $F = 1 \rightarrow 3P_{3/2}$  sodium transition at 589 nm,  $\Gamma/2\pi = 10 \text{ MHz}$ , and  $I_0 = 9.3 \text{ mW/cm}^2$  is the effective saturation intensity for linearly polarized light detuned far from resonance compared with the relevant upper-state hyperfine splitting (50 MHz). In our case,  $\Delta/2\pi = -0.6 \text{ GHz}$  and  $T \sim 1 \mu\text{s}$ . The probability of spontaneous emission during the pulse is small.
- Diffraction with an optical standing wave can also be interpreted as a sinusoidal phase imprint.
- Y. Torii *et al.*, Los Alamos National Laboratory e-print cond-mat/9908160 (1999).
- D. M. Giltner, R. W. McGowan, S. A. Lee, *Phys. Rev. Lett.* **75**, 2638 (1995).
- The condensate was imaged with a probe along the direction of the phase imprinting beam. We used absorption imaging with a  $5\text{-}\mu\text{s}$  light pulse (intensity  $\sim 170 \text{ mW/cm}^2$ ) detuned 15 MHz from resonance (7). This produced high-contrast images that made use of nearly the full dynamic range of the charge-coupled device camera. The images gave a reliable measurement of the soliton location. We measured a combined resolution of the phase imprinting and the imaging optics to be  $7 \mu\text{m}$ , whereas the diffraction limit of the phase imprinting optics is  $2.5 \mu\text{m}$ . We define the resolution as the distance in which the light intensity falls from 90% to 10% of its full value.
- For Fig. 2, we released the BEC from the magnetic trap  $500 \mu\text{s}$  after the first interferometer pulse.
- Because of mirror vibrations, our interferometer experiences random phase variations between the interferometer arms from one shot to the next. Despite this limitation, we can still unambiguously identify phase step imprints of  $\pi$  because only then can high-contrast "half moon" images be obtained. In that case we can choose an image for which the random phase is zero, as in Fig. 2. By mechanically stabilizing the interferometer, the global random phase can be controlled and the interferometer could then be used more quantitatively.
- The asymmetric nature of our interferometer does not lend itself to measuring the phase of a trapped condensate after long propagation times. The differential velocity between the interferometer arms, which results from the action of the trapping potential, leads to fringes at the output.
- The condensate was released from the magnetic trap 1 ms before being imaged. Expansion of the released BEC during that time was negligible.
- L. A. Collins, J. D. Kress, R. B. Walker, *Comput. Phys. Commun.* **114**, 15 (1998).
- B. I. Schneider and D. L. Feder, *Phys. Rev. A* **59**, 2232 (1999).
- The  $4.4\text{-}\mu\text{m}$  resolution (27) is centered within the range of the  $2.5\text{-}\mu\text{m}$  diffraction limit and the measured  $7\text{-}\mu\text{m}$  upper limit. Simulations with a phase-imprinting resolution of  $7 \mu\text{m}$  yielded results that are qualitatively similar to those with the  $4.4\text{-}\mu\text{m}$  calculation but do not agree as well with the experimental observations.
- All uncertainties reported in this article are 1 standard deviation combined statistical and systematic uncertainties.

36. K. W. Madison *et al.*, preprint available at <http://xxx.lanl.gov/abs/cond-mat/9912015>.

37. S. Burger *et al.*, preprint available at <http://xxx.lanl.gov/abs/cond-mat/9910487>.

38. We thank K. Burnett, M. A. Edwards, and K. Jones for discussions. Supported in part by the U.S. Office of Naval Research and NASA. J.D., J.E.S., and W.P.R. acknowledge support from the Alexander von Hum-

boldt Foundation, a NIST–National Research Council fellowship, and NSF, respectively.

15 October 1999; accepted 2 December 1999

## REPORTS

# Equilibrium Regained: From Nonequilibrium Chaos to Statistical Mechanics

David A. Egolf

Far-from-equilibrium, spatially extended chaotic systems have generally eluded analytical solution, leading researchers to consider theories based on a statistical rather than a detailed knowledge of the microscopic length scales. Building on the recent discovery of a separation of length scales between macroscopic behavior and microscopic chaos, a simple far-from-equilibrium spatially extended chaotic system has been studied computationally at intermediate, coarse-grained scales. Equilibrium properties such as Gibbs distributions and detailed balance are recovered at these scales, which suggests that the macroscopic behavior of some far-from-equilibrium systems might be understood in terms of equilibrium statistical mechanics.

Statistical mechanics describes the macroscopic physical properties of matter through a probabilistic, rather than a detailed, knowledge of the microscopic dynamics and has been applied successfully to a wide variety of equilibrium systems, from simple molecular gases to white dwarf stars. It has provided a theoretical understanding of the phases of matter, the transitions between phases, and the deep property of universality that unifies the descriptions of continuous transitions in systems that are physically quite distinct (for example, magnets and gases). In nature, however, many systems are not in equilibrium, including, for example, large-scale flows in the atmosphere, the evolution of ecological systems, and the transport of energy in cells. None of these situations can be understood with equilibrium statistical mechanics.

Although theory has been developed to extend equilibrium statistical mechanics to systems only slightly perturbed away from equilibrium (for which the evolution of the system is well-approximated with only linear terms), in deterministic systems driven far from equilibrium (where nonlinearities are important) theoretical progress has been limited to “simple” situations, such as the onset of symmetry breaking, the stability of perfect patterns, and the motions of single topological defects in perfect patterns (1). Theorists have not yet developed an understanding of the intriguing phenomenon of “spatiotemporal chaos” (or spatially extended chaos)

that is typically characterized by disordered arrays of defects, patches of uncorrelated regions, and a chaotic dynamics that persists indefinitely (2). This remarkable behavior has been found in large, deterministic, far-from-equilibrium systems as varied as convecting horizontal fluid layers (3), chemical reaction-diffusion systems (4), colonies of microorganisms (5), and fibrillating heart tissue (6). These disparate systems often display strikingly similar macroscopic features (such as locally ordered striped or hexagonal patterns and dislocation, spiral, and target defects) and behavior (for example, dramatic qualitative changes in response to modifications of experimental parameters reminiscent of phase transitions in equilibrium systems). Such behavior within a system and the similarities between different systems beg the question of whether one can construct a statistical, predictive theory of phases and transitions in these chaotic, far-from-equilibrium systems.

At first glance, far-from-equilibrium, strongly dissipative, deterministic systems may appear to have little in common with equilibrium systems; for example, at the detailed level, these systems do not have the benefit of tending toward the minimum of a free-energy functional, do not have a Gibbsian distribution of states, and do not allow the calculational technique of averages over noise terms. However, several experimental and computational studies have explored the similarities in the behaviors of these systems and the behaviors of equilibrium systems. A particular focus has been the possibility of phase transition–like behavior in these systems (4, 7–11). The data reported here uncover a deeper level of similarity and suggest the possibility of salvaging much of the frame-

work of equilibrium statistical mechanics. In particular, large-scale computational studies of a simple, large, chaotic, far-from-equilibrium system demonstrate that several cornerstones of equilibrium statistical mechanics—ergodicity, detailed balance, Gibbs distributions, partition functions, and renormalization group flows of coupling constants—are recovered at a coarse-grained scale.

In analogy to the simple explorations of equilibrium statistical mechanics with the Ising model, one of the simplest spatially extended chaotic systems was used as a test bed (12). This system, a coupled map lattice (CML) first studied by Miller and Huse (8), consists of a set of scalar variables  $u_{\vec{x}}^t$  at integer time  $t$  on a square two-dimensional spatially periodic  $L \times L$  grid with positions indicated by  $\vec{x} = a\hat{x} + b\hat{y}$ , where  $a$  and  $b$  are integers and  $\hat{x}$  and  $\hat{y}$  are the unit vectors of the two-dimensional lattice. The rule for updating the variables from time  $t$  to  $t + 1$  is

$$u_{\vec{x}}^{t+1} = \phi(u_{\vec{x}}^t) + g \sum_{\vec{y}(\vec{x})} [\phi(u_{\vec{y}}^t) - \phi(u_{\vec{x}}^t)] \quad (1a)$$

where  $g$  indicates the strength of the spatial coupling, and  $\vec{y}(\vec{x})$  denotes nearest neighbors of site  $\vec{x}$ . The chaotic local map  $\phi(u)$  is given by

$$\phi(u) = \begin{cases} -3u - 2 & -1 \leq u \leq -\frac{1}{3} \\ 3u & -\frac{1}{3} < u < \frac{1}{3} \\ -3u + 2 & \frac{1}{3} \leq u \leq 1 \end{cases} \quad (1b)$$

This CML exhibits chaotic, spatially disordered dynamics for values of  $g$  at least within the range  $[0, 0.25]$ . Miller and Huse (8) reported that at  $g_c \approx 0.2054$ , this system undergoes a paramagnetic-to-ferromagnetic transition exhibiting a number of features in common with the equilibrium transition in the Ising ferromagnet (13).

To study the statistical bulk properties of spatially extended chaotic states [“extensive chaos” (1, 14)], the “thermodynamic limit” of systems approaching infinite size was taken. O’Hern *et al.* (15) demonstrated that the behavior of Eq. 1 can be considered extensive for system sizes as small as  $L \approx 9$ . Results reported here were obtained for system sizes ranging from  $1 \times 1$  to  $1024 \times 1024$  over times as large as  $10^{10}$  iterations (after typically  $10^6$  iterations of transient), often averaged over ensembles of up to 256 systems with identical parameters but differing initial conditions [with each site  $u_{\vec{x}}^{t=0}$  initialized to a

Center for Nonlinear Studies (MS B258), Theoretical Division and Condensed Matter and Thermal Physics, Los Alamos National Laboratory, Los Alamos, NM 87545, USA. E-mail: egolf@cns.lanl.gov

### 3.5 “Imaging the Phase of an evolving Bose-Einstein Condensate Wave Function”

J. E. Simsarian, J. Denschlag, C. W. Clark, L. Deng,  
M. A. Edwards, E. W. Hagley, K. Helmerson, S. L. Rolston,  
and W. D. Phillips

Phys. Rev. Lett **85**, 2040-2043 (2000)



## Imaging the Phase of an Evolving Bose-Einstein Condensate Wave Function

J. E. Simsarian,<sup>1</sup> J. Denschlag,<sup>1</sup> Mark Edwards,<sup>1,2</sup> Charles W. Clark,<sup>1</sup> L. Deng,<sup>1</sup>  
E. W. Hagley,<sup>1</sup> K. Helmerson,<sup>1</sup> S. L. Rolston,<sup>1</sup> and W. D. Phillips<sup>1</sup>

<sup>1</sup>National Institute of Standards and Technology, Gaithersburg, Maryland 20899

<sup>2</sup>Georgia Southern University, Statesboro, Georgia 30460-8031

(Received 28 April 2000)

We demonstrate a spatially resolved autocorrelation measurement with a Bose-Einstein condensate and measure the evolution of the spatial profile of its quantum mechanical phase. Upon release of the condensate from the magnetic trap, its phase develops a form that we measure to be quadratic in the spatial coordinate. Our experiments also reveal the effects of the repulsive interaction between two overlapping condensate wave packets and we measure the small momentum they impart to each other.

PACS numbers: 03.75.Fi, 32.80.Qk, 39.20.+q

A trapped Bose-Einstein condensate (BEC) [1] has unique value as a source for atom lasers [2] and matter-wave interferometry [3] because its atoms occupy the same quantum state, with uniform spatial phase. However, when released from the trapping potential, a BEC with repulsive atom-atom interactions expands, developing a nonuniform phase profile. Understanding this phase evolution will be important for applications of coherent matter waves. We have developed a new interferometric technique using spatially resolved autocorrelation to measure the functional form and time evolution of the phase of a BEC wave packet expanding under the influence of its mean-field repulsion.

In 1997, the coherence of weakly interacting BECs was demonstrated by releasing two spatially separated condensates and observing their interference [4]. Subsequent experiments have further investigated condensate coherence properties. One [5] used velocity-resolved Bragg diffraction [6] to probe the momentum spectrum of trapped and released BECs. A complementary experiment [7] that used matter-wave interferometry can be interpreted as a measurement of the spatial correlation function, whose Fourier transform is the momentum spectrum. These experiments showed that a trapped condensate has a uniform phase, and a released condensate develops a nonuniform phase profile. (Recently the influence of nonzero temperature on coherence properties was also investigated [8].) The experiments reported in this Letter combine spatial resolution and interferometry to measure the functional form of the time-dependent phase profile of a released condensate. We also make the first measurement of the velocity imparted to two equal BEC wave packets from their mutual mean-field repulsion [9].

We perform our experiments with a condensate of  $1.8(4) \times 10^6$  [10] sodium atoms in the  $3S_{1/2}$ ,  $F = 1$ ,  $m_F = -1$  state. The sample has no discernible non-condensed (i.e., thermal) component. The condensate is prepared following the method of Ref. [6] and is held in a magnetic trap with trapping frequencies  $\omega_x = \sqrt{2}\omega_y = 2\omega_z = 2\pi \times 27$  Hz. Using a scattering length of  $a =$

2.8 nm, the calculated Thomas-Fermi diameters [11] are 47, 66, and 94  $\mu\text{m}$ , respectively.

We release the BEC from the magnetic trap and it expands, driven mostly by the mean-field repulsion of the atoms. This expansion implies the development of a non-uniform spatial phase profile (recall that the velocity field is proportional to the gradient of the quantum phase). After an expansion time  $T_0$ , we probe the phase profile with matter-wave Bragg interferometry [12–14]. Our interferometer splits the BEC into two wave packets and recombines them with a chosen overlap, producing interference fringes, which we measure with absorption imaging [15]. From the dependence of the fringe spacing on the overlap, we extract the phase profile of the wave packets.

Our atom interferometer [14] consists of three optically induced Bragg-diffraction pulses applied successively in time (Fig. 1). Each pulse consists of two counterpropagating laser beams whose frequencies differ by 100 kHz. They are detuned by about  $-2$  GHz from atomic resonance ( $\lambda = 2\pi/k = 589$  nm) so that spontaneous emission is negligible. The first pulse has a duration of 6  $\mu\text{s}$

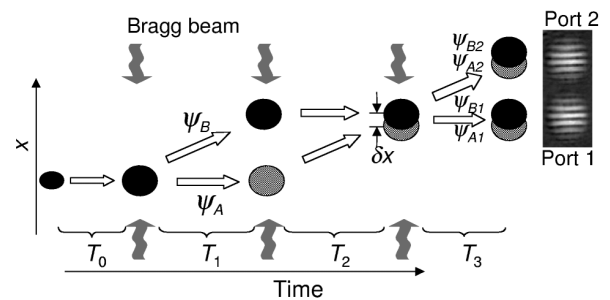


FIG. 1. Space-time diagram of the experiment. Three optically induced Bragg-diffraction pulses form the interferometer. The condensate is released for a time  $T_0$  before the first Bragg pulse. The centers of  $\psi_A$  and  $\psi_B$  are separated by  $\delta x$  at the time of the third Bragg pulse, which splits them into  $\psi_{A1}$ ,  $\psi_{B1}$ , and  $\psi_{A2}$ ,  $\psi_{B2}$ . Before imaging the atoms, we allow the output ports to separate for a time  $T_3 \approx 2$  ms. The image shows the output ports when  $T_0 = 3$  ms,  $T_1 = 1$  ms, and  $T_2 = 1.3$  ms.

and intensity sufficient to provide a  $\pi/2$  pulse, which coherently splits the BEC into two wave packets,  $\psi_A$  and  $\psi_B$ . The wave packets have about the same number of atoms and differ only in their momenta:  $p = 0$  and  $p = 2\hbar k$ . At a time  $T_1 = 1$  ms after the first Bragg pulse, the two wave packets are completely separated and a second Bragg pulse (a  $\pi$  pulse) of 12  $\mu\text{s}$  duration transfers  $\psi_B$  to a state with  $p \approx 0$  and  $\psi_A$  to  $p \approx 2\hbar k$  [16]. After a variable time  $T_2$  the wave packets partially overlap again and we apply a third pulse, of 6  $\mu\text{s}$  duration (a  $\pi/2$  pulse). This last pulse splits each wave packet into the two momentum states. The interference of the overlapping wave packets in each of the two momentum states allows the determination of the local phase difference between them. By changing the time  $T_2$  we vary  $\delta x = x_A - x_B$ , the separation of  $\psi_A$  and  $\psi_B$  at the time of the final Bragg pulse. The set of data at different  $\delta x$  constitutes a new type of spatial autocorrelation measurement that is similar to the ‘‘FROG’’ technique [17] used to measure the complete electric field of ultrafast laser pulses. From these measurements we obtain the phase profile of the wave packets in the  $x$  direction.

Figures 2a–2e shows one interferometer output port for different  $\delta x$  (different  $T_2$ ) after an expansion time  $T_0 = 4$  ms. In general, we observe straight, evenly spaced fringes (although for small  $T_0$  and  $T_2$  the fringes may be somewhat curved). There is a value of  $\delta x = x_0 \neq 0$  where we observe no fringes (Fig. 2c) and the fringe spacing decreases as  $|\delta x - x_0|$  increases. Figure 2f, a cut through Fig. 2d, shows the high-contrast fringes [18]. Our data analysis uses the average fringe period  $d$ , obtained from plots like Fig. 2f.

The fringes come from two different effects: the interference of two wave packets with quadratic phase profile, and a relative velocity between the wave packets’ centers. The data can be understood by calculating the fringe spacing along  $x$  at output port 1 [19]. We assume that the phase  $\phi$  of the wave function  $f e^{i\phi}$  can be written as  $\phi = \frac{\alpha}{2}x^2 + \beta x$ . The equal spacing of the fringes im-

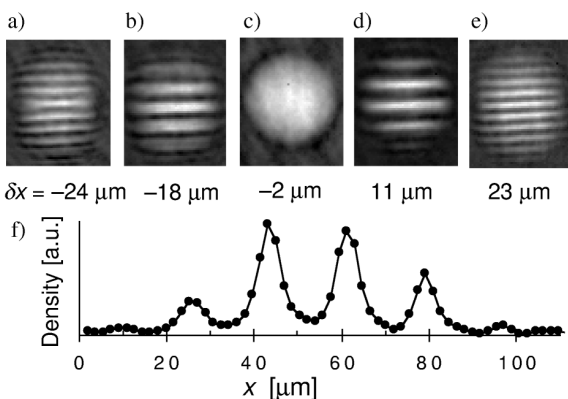


FIG. 2. (a)–(e) One of the two output ports of the interferometer with  $T_0 = 4$  ms and  $\delta x$  as indicated. (f) A plot of the density along the  $x$  direction of (d).

plies, as predicted in the Thomas-Fermi limit [20], that  $\phi$  has no significant higher-order terms [21]. The curvature coefficient  $\alpha$  describes the mean-field expansion of the wave packets and  $\beta$  describes a relative repulsion velocity. The velocity arises because the wave packets experience a repulsive push as they first separate and again as they recombine. The density at port 1 (see Fig. 1) just after the final interferometer pulse is the interference pattern  $|\psi_{A1} + \psi_{B1}|^2$  of the wave packets  $\psi_{A1}$  and  $\psi_{B1}$ :

$$|f(x - \delta x)e^{i[(\alpha/2)(x - \delta x)^2 - \beta(x - \delta x)]} + f(x)e^{i[(\alpha/2)x^2 + \beta x]}|^2, \quad (1)$$

where we assume that the amplitudes and curvatures of the wave packets are equal and their velocities have equal magnitude and opposite direction. The cross term of (1) is

$$2f(x - \delta x)f(x) \cos\left[\left(\alpha \delta x + \frac{M \delta v}{\hbar}\right)x + C\right], \quad (2)$$

where  $M$  is the sodium mass,  $M \delta v / \hbar \equiv 2\beta$ , and  $C$  is independent of  $x$  [22].  $\delta v = v_B - v_A$  is the relative repulsion velocity between the wave packets  $\psi_{A1}$  and  $\psi_{B1}$ . Expression (2) predicts fringes with spatial frequency,

$$\kappa = \alpha \delta x + \frac{M \delta v}{\hbar}, \quad (3)$$

where  $|\kappa| = 2\pi/d$ . When there are no fringes,  $\kappa = 0$  and the wave packet separation  $\delta x = x_0 \equiv -M \delta v / \alpha \hbar$ .

Figure 3 plots the measured  $\kappa$  vs  $\delta x$  [23] for  $T_0 = 1$  and 4 ms. The data are well fit by a straight line as expected from Eq. (3) in the approximation that  $\alpha$  and  $\delta v$  are independent of  $\delta x$ . The slopes of the lines are the phase curvatures  $\alpha$ , and the  $\kappa$  intercepts give the relative velocities  $\delta v$ .

We checked the validity of the data analysis procedure by analyzing data simulated with a 1D Gross-Pitaevskii (GP) treatment. Despite variations of  $\delta v$  and  $\alpha$  with  $\delta x$  (due to their continued evolution during the variable time  $T_2$ ), we find that  $\kappa$  is still linear in  $\delta x$ . The slopes and intercepts in general are averages over the range of  $\delta x$  used in the experiment.

The interference fringes used to determine  $\alpha$  and  $\delta v$  are created at the time of the final interferometer pulse. Because the two outputs overlap at that moment, we wait a time  $T_3$  for them to separate before imaging. During

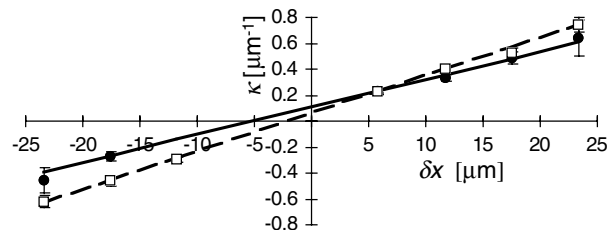


FIG. 3. Plot of the spatial fringe frequency  $\kappa$  versus  $\delta x$  for  $T_0 = 1$  ms (filled circles) and 4 ms (open squares). The solid and dashed lines are linear fits to the data.

this time, the wave packets continue to expand. The 1D simulations show that the fringe spacings and the wave packets expand in the same proportion. We correct  $\kappa$  (by typically 15%) for this, using the calculated expansion from a 3D solution of the GP equation described below.

The different slopes and intercepts of the two lines in Fig. 3 show that the curvature  $\alpha$  and relative velocity  $\delta v$  of the wave packets depend on the release time  $T_0$  before the first interferometer pulse. Figure 4 plots the dependence of  $\alpha$  and  $\delta v$  on various release times  $T_0$ . The condensate initially has a uniform phase so that immediately after its release from the trap  $\alpha = 0$ . We nevertheless measure a nonzero  $\alpha$  for  $T_0 = 0$  ms because the BEC expands during  $T_1$  and  $T_2$ . As a function of time,  $\alpha$  behaves as  $\dot{D}/D$  where  $D$  is the wave packet diameter and  $\dot{D}$  is its rate of change [20]. At early times when the mean-field energy is being converted to kinetic energy,  $\dot{D}$  increases rapidly, increasing  $\alpha$ . At late times, after the mean-field energy has been converted,  $D$  increases while  $\dot{D}$  is nearly constant, decreasing  $\alpha$ .

We predict the time evolution of  $\alpha$  using the Lagrangian variational method (LVM) [24]. The LVM uses trial wave functions with time-dependent parameters to provide approximate solutions of the 3D time-dependent GP equation. In the model, the effect of the interferometer pulses is to replace the original wave packet with a superposition of wave packets having different momenta; e.g., the action of our first interferometer pulse is  $\psi_0 \rightarrow (\psi_0 + e^{i2kx}\psi_0)/\sqrt{2}$ . We use Gaussian trial wave functions in the LVM to calculate the phase curvature  $\alpha$  at the time of the last interferometer pulse. For simplicity, the interaction between the wave packets is neglected. This result, with  $T_1 = T_2$ , is the solid line of Fig. 4a.

We use energy conservation to calculate the relative repulsion velocity  $\delta v$  between  $\psi_{A1}$  and  $\psi_{B1}$  because we neglect wave packet interactions in the LVM. In the Thomas-Fermi approximation, we can calculate the amount of energy available for repulsion when  $T_0 = 0$ . A trapped condensate has  $\frac{5}{7}\mu$  average total energy per particle,

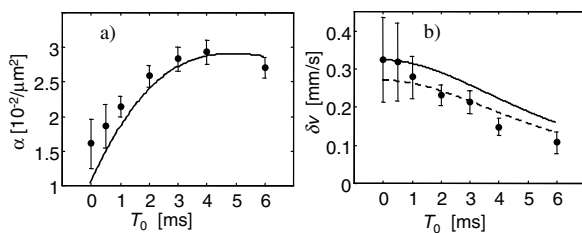


FIG. 4. (a) Plot of the phase curvature  $\alpha$  versus the initial expansion time  $T_0$  showing the phase evolution from mean-field expansion. The solid line is a calculation using the Lagrangian variational method (LVM). (b) Plot of the relative repulsion velocity  $\delta v$  versus  $T_0$ . The solid curve is the calculated maximum repulsion velocity (when  $\delta x = 0$ ) and the dashed curve is the repulsion velocity averaged over the range of  $\delta x$  used in the experiment.

where  $\mu$  is the chemical potential [11]. After release from the trap, it has  $\frac{2}{7}\mu$  average mean-field energy per particle. Applying a  $\pi/2$  Bragg pulse to the BEC causes a density corrugation, which increases the mean-field energy to  $\frac{3}{7}\mu$  per particle. In the approximation that the wave packets do not deform as they separate and recombine, one can show that  $\frac{1}{3}$  of the total mean-field energy goes into expansion of the wave packets, and  $\frac{2}{3}$  is available for kinetic energy of center-of-mass motion. Therefore  $\frac{2}{7}\mu$  of mean-field energy per particle is available for repulsion. The corresponding repulsion velocity is only about  $10^{-2}$  of a photon recoil velocity. The repulsion energy and  $\delta v$  decrease for larger  $T_0$  because both are inversely proportional to the condensate volume, which we calculate with the LVM. The two curves shown in Fig. 4b are the calculated  $\delta v$  when  $\delta x = 0$  (solid curve) and  $\delta v$  averaged over the different  $\delta x$  used in the experiment (dashed curve). The 1D GP simulations suggest that for small  $T_0$ , the results of the experiment should be closer to the solid curve, and for large  $T_0$ , closer to the dashed curve. The data are consistent with this trend.

In a related set of experiments we performed interferometry in the trap. This differs from the experiments on a released BEC because there is no expansion before the first interferometer pulse [25] and the magnetic trap changes the relative velocity of the wave packets between the interferometer pulses (Fig. 5a). To better reveal the velocity differences, we choose  $T_1 = T_2 = T$  to suppress fringes arising from the phase curvature. As with the released BEC measurements, we observe equally spaced fringes at the output of the interferometer, although the fringes are almost entirely due to a relative velocity  $v$  between the wave packets  $\psi_{A1}$  and  $\psi_{B1}$  at the time of the third interferometer pulse. We obtain  $v$  from the fringe periodicity after a small correction for residual phase curvature [26].

Two effects contribute to  $v$ : the mutual repulsion between the wave packets  $\psi_A$  and  $\psi_B$  and the different action of the trapping potential on the two wave packets in the interferometer. The latter effect occurs because after the first Bragg pulse,  $\psi_A$  remains at the minimum of the magnetic potential while  $\psi_B$  is displaced. Wave packet  $\psi_B$  therefore

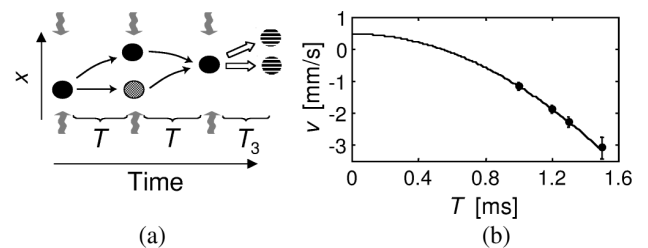


FIG. 5. (a) Schematic representation of the interferometer in the trap, with the principle difference from Fig. 1 being the curved arrows indicating the acceleration of the wave packets. (b) The relative velocity  $v$  between the two trapped wave packets versus the interferometer time  $T$ . The solid line is a fit.

spends more time away from the center of the trap and experiences more acceleration than  $\psi_A$ .

Following the last Bragg pulse,  $\psi_{A1}$  and  $\psi_{B1}$  have a velocity difference which for our parameters can be approximated by  $v \approx -\frac{2\hbar k}{M} \sin^2(\omega_x T) + \delta v$  [27]. Figure 5b plots  $v$  versus  $T$ , and the curve is a fit to the above expression. We obtain the trap frequency  $\omega_x/2\pi = 26.7(15)$  Hz, in excellent agreement with an independent measurement. We also obtain the relative velocity from the mean-field repulsion  $\delta v = 0.49(12)$  mm/s, which we expect to be somewhat larger than for the released measurements because the wave packets contract, producing a larger mean field.

In conclusion, we demonstrate an autocorrelating matter-wave interferometer and use it to study the evolution of a BEC phase profile by analyzing spatial images of interference patterns. We study how the phase curvature of the condensate develops in time and measure the repulsion velocity between two BEC wave packets. Our interferometric method should be useful for characterizing other interesting condensate phase profiles. For example, it can be applied to detect excitations of a BEC with characteristic phase patterns, such as vortices and solitons [14,28–31]. The method should be useful for further studies of the interaction of coherent wave packets and to study the coherence of atom lasers.

We thank T. Busch, D. Feder, and L. Collins for helpful discussions. This work was supported in part by the U.S. Office of Naval Research and NASA. J. D. acknowledges support from the Alexander von Humboldt Foundation. M. E. and C. W. C. acknowledge partial support from NSF Grants No. 9802547 and No. 9803377.

- 
- [1] M. H. Anderson *et al.*, *Science* **269**, 198 (1995); K. B. Davis *et al.*, *Phys. Rev. Lett.* **75**, 3969 (1995); C. C. Bradley, C. A. Sackett, and R. G. Hulet, *Phys. Rev. Lett.* **78**, 985 (1997); see also C. C. Bradley *et al.*, *Phys. Rev. Lett.* **75**, 1687 (1995).  
 [2] M.-O. Mewes *et al.*, *Phys. Rev. Lett.* **78**, 582 (1997); E. W. Hagley *et al.*, *Science* **283**, 1706 (1999); I. Bloch, T. W. Hänsch, and T. Esslinger, *Phys. Rev. Lett.* **82**, 3008 (1999); B. P. Anderson and M. A. Kasevich, *Science* **282**, 1686 (1998).  
 [3] *Atom Interferometry*, edited by P. R. Berman (Academic Press, Cambridge, 1997).  
 [4] M. R. Andrews *et al.*, *Science* **275**, 637 (1997).  
 [5] J. Stenger *et al.*, *Phys. Rev. Lett.* **82**, 4569 (1999).  
 [6] M. Kozuma *et al.*, *Phys. Rev. Lett.* **82**, 871 (1999).  
 [7] E. W. Hagley *et al.*, *Phys. Rev. Lett.* **83**, 3112 (1999); M. Trippenbach *et al.*, *J. Phys. B* **33**, 47 (2000).

- [8] I. Bloch, T. W. Hänsch, and T. Esslinger, *Nature (London)* **403**, 166 (2000).  
 [9] The mean-field energy shift of the out-coupled wave packet in [5] can be used to infer the repulsion velocity. Here we measure the velocity directly.  
 [10] All uncertainties reported here are 1 standard deviation combined statistical and systematic uncertainties.  
 [11] F. Dalfovo *et al.*, *Rev. Mod. Phys.* **71**, 463 (1999).  
 [12] D. M. Giltner, R. W. McGowan, and S. A. Lee, *Phys. Rev. Lett.* **75**, 2638 (1995).  
 [13] Y. Torii *et al.*, *Phys. Rev. A* **61**, 041602(R) (2000).  
 [14] J. Denschlag *et al.*, *Science* **287**, 97 (2000).  
 [15] The condensate was imaged by first optically pumping the atoms to the  $F = 2$  ground state and then imaging the absorption of a probe beam on the  $F = 2 \rightarrow F' = 3$  transition. The pulse had a 5  $\mu$ s duration,  $\approx 170$  mW/cm<sup>2</sup> intensity, and was detuned 15 MHz from resonance.  
 [16] The momenta are not exactly  $p = 0$  and  $p = 2\hbar k$  because of repulsion effects that will be discussed.  
 [17] R. Trebino *et al.*, *Rev. Sci. Instrum.* **68**, 3277 (1997).  
 [18] The observation is consistent with the full predicted fringe contrast when we include the finite imaging resolution.  
 [19] We can treat the  $x$  direction independently of  $y$  and  $z$  when the wave function  $\psi = f e^{i\phi(x,y,z)}$  is separable, i.e.,  $\phi(x,y,z) = \varphi(x) + \eta(y,z)$ . Straight fringes imply this separability.  
 [20] Y. Castin and R. Dum, *Phys. Rev. Lett.* **77**, 5315 (1996).  
 [21] For  $T_0 = 6$  ms and an interference pattern with many fringes, we found that the coefficients of third and fourth order terms are smaller than  $1 \times 10^{-5} \mu\text{m}^{-3}$  and  $1 \times 10^{-7} \mu\text{m}^{-4}$ , respectively.  
 [22] In practice,  $C$  includes a random phase from mirror vibrations.  
 [23] We use  $\delta x = \frac{2\hbar k}{M}(T_2 - T_1) - x_\epsilon$  where  $\frac{2\hbar k}{M} = 5.9$  cm/s is the two photon recoil velocity of sodium and  $x_\epsilon$  is a small correction of the order  $\delta v T_1$  due to the repulsion of the wave packets. We include the correction in our data analysis in a self-consistent manner. The correction modifies  $\alpha$  insignificantly, but increases the final values of  $\delta v$  by  $\approx 0.05$  mm/s.  
 [24] V. M. Pérez-García *et al.*, *Phys. Rev. Lett.* **77**, 5320 (1996).  
 [25] In fact, after the first pulse the wave packets contract because the reduced mean-field energy can no longer support the wave packet size.  
 [26] We also correct the fringe spacings for the contraction of the wave packets between the final interferometer pulse and when the image is taken.  
 [27] We assume  $\delta v \ll \frac{\hbar k}{M}$ ,  $T\omega_x \ll 1$ , and harmonic motion in the trap.  
 [28] S. Burger *et al.*, *Phys. Rev. Lett.* **83**, 5198 (1999).  
 [29] M. R. Matthews *et al.*, *Phys. Rev. Lett.* **83**, 2498 (1999).  
 [30] K. W. Madison *et al.*, *Phys. Rev. Lett.* **84**, 806 (2000).  
 [31] A. D. Jackson, G. M. Kavoulakis, and C. J. Pethick, *Phys. Rev. A* **58**, 2417 (1998).

### 3.6 “A Bose-Einstein Condensate in an optical lattice”

J. Hecker Denschlag, J. E. Simsarian, H. Häffner, C. McKenzie, A. Browaeys, D. Cho, K. Helmerson, S. L. Rolston, and W. D. Phillips

J. Phys. B: At. Mol. Opt. Phys. **35**, 3095-3110 (2002)



## Chapter 4

# Controlling the interaction between atoms with Feshbach resonances

Feshbach resonances have become one of the most important tools to manipulate ultracold quantum gases and are largely responsible for the fast progress in this field in recent years. With the help of Feshbach resonances we can arbitrarily tune the interactions between atoms and can thus control their behavior. Feshbach resonances were first discussed in the context of nuclear physics [Fes58] and introduced into field of ultracold atoms in 1993 [Tie93]. After the first observation in 1998 [Ino98, Cou98, Rob98] they were used in range of experiments such as ultrahigh-resolution spectroscopy [Chi00], study of collapsing and exploding BECs [Don01], the creation of bright matter wave solitons [Kha02, Str02] and ultra cold molecules (see chapter 5). It also led to the production of new atomic [Cor00, Web03] and molecular [Joc03a, Gre03, Zwi03, Bou04] BECs and allowed for the controlled pairing in ultra-cold fermionic gases [Reg04, Zwi04, Chi04a].

In general, a Feshbach resonance is a scattering resonance and it occurs when a colliding pair of atoms is resonantly coupled to a molecular bound state (see Fig. 4.1). Depending on the parameters, the Feshbach resonance strongly influences the collision and changes the scattering length. A magnetically tunable Feshbach resonance is based on Zeeman shifting a bound molecular state into resonance with the scattering state. For an *optical* Feshbach resonance, as first predicted by Fedichev *et al.* [Fed96], the molecular level is coupled to the scattering state with a light field. This scheme not only works with a single photon transition but also with a Raman scheme (see Fig. 4.1) [Tha04]. Because of two-body losses due to photoassociation and consecutive decay of the molecule, the resonance curve for the optical

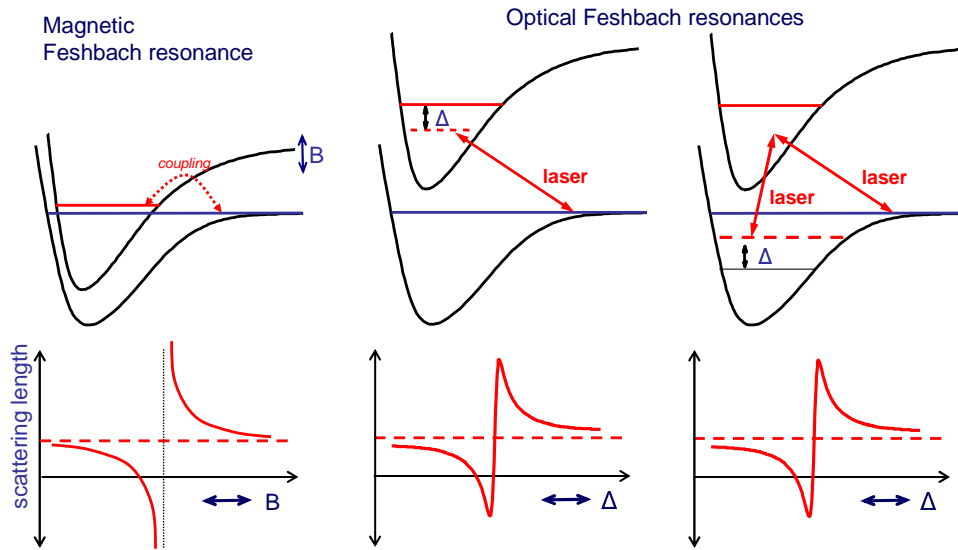


Figure 4.1: Magnetic and optical Feshbach resonances. By resonantly coupling a scattering state of two atoms to a bound molecular state the scattering length  $a$  changes. For an optical Feshbach resonance this coupling is provided by a strong light field in a photoassociation transition. (far right) Being a general concept, optical Feshbach resonances also appear in optical Raman transitions.

Feshbach resonance does not diverge in contrast to the magnetically tunable Feshbach resonance in Fig. 4.1.

In the following two sections we describe our experiments in which we have confirmed the existence of a particular magnetic Feshbach resonance in  ${}^6\text{Li}$  and optical Feshbach resonances in general.

## 4.1 Magnetically tunable Feshbach resonance in ${}^6\text{Li}$

As will become clear in the following chapters 5 and 6, the existence of the broad Feshbach resonance for  ${}^6\text{Li}$  is of central importance for recent experiments with Fermi gases. It appears in the collision channel of the two lowest spin states of  ${}^6\text{Li}$  and was predicted in 1998 by Houbiers *et al.* [Hou98]. Figure 4.2 shows the shape of this broad Feshbach resonance. In general the

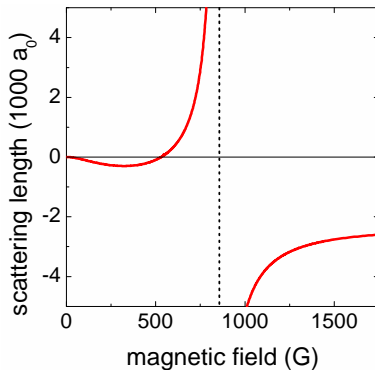


Figure 4.2: A broad Feshbach resonance  ${}^6\text{Li}$  appears in the collision channel of the two lowest spin states. It is located at 834 G and exhibits a zero crossing of the scattering length at about 530 G.

functional form of such a resonance can be conveniently approximated by

$$a = a_{bg} \left( 1 + \frac{\Delta_B}{B - B_{Res}} \right), \quad (4.1)$$

where  $a_{bg}$  is the background scattering length,  $B_{Res}$  is the resonance position and  $\Delta_B$  is the resonance width. In the case of  ${}^6\text{Li}$ , it turns out that  $a_{bg}$  is not constant at the position of the Feshbach resonance. This gives rise to a slightly changed expression for  $a$  [Bar04d].

In 2002 our group [Joc02] in parallel with other groups [Har02b, Die02, Bou03] was able to experimentally demonstrate the existence of this Feshbach resonance. Our approach was to study the elastic collision cross section  $\propto 4\pi a^2/(1 + k^2 a^2)$  in terms of evaporative loss as a function of the magnetic bias field. We were able to demonstrate the tunability of the interaction within the gas and also to precisely locate the zero crossing at 530(3) G which can be used to determine the position of the Feshbach resonance. The zero crossing was also observed by the Thomas group [Har02b]. Ketterle's group used inelastic loss spectroscopy to locate the Feshbach resonance [Die02]. However, as it turned out later, these losses were not centered on the resonance in contrast to Feshbach resonances in bosonic gases. Salomon's group measured the interaction energy from the expansion of a released Fermi gas to find the Feshbach resonance [Bou03]. This mean field energy could also be measured using radio-frequency (RF) spectroscopy [Reg03a, Gup03, Reg03] where the mean field interaction gives rise to a frequency shift of the spin flip resonance. We recently developed still another method to precisely determine the position of the Feshbach resonance. Using radio frequency we

precisely measured the transition frequency between various weakly bound molecular states in the vicinity of the Feshbach resonance. Together with a multichannel quantum scattering model all relevant scattering properties of  ${}^6\text{Li}$  as well as the position of the Feshbach resonance ( $834.1 \pm 0.15$  G) could be precisely determined [Bar04d].

## 4.2 Optical tuning of the scattering length

After their prediction in 1996 [Fed96, Boh97] optical Feshbach resonances have been first observed by Fatemi *et al.* [Fat00] in photoassociation spectroscopy in a thermal gas of sodium atoms. Fatemi *et al.* found that the photoassociation laser induced changes in the scattering wave function which was probed via photoionization. Our experiments with a  ${}^{87}\text{Rb}$  condensate demonstrated for the first time the tunability of the scattering length  $a$  with optical means [The04, Tha04]. By controlling the power and detuning of the optical laser light field we can change the atomic scattering length. With a power of  $500\text{W}/\text{cm}^2$  in our experiments we varied the scattering length in a range of  $\pm 100 a_0$  ( $1 a_0 = 1$  Bohr radius =  $0.529 \times 10^{-10}$  m). For comparison, the scattering length of the unperturbed atoms is  $100 a_0$ . The approximate mathematical expression for the scattering length is

$$a = a_{bg} \left( 1 + \frac{c (f - f_{Res})}{(f - f_{Res})^2 + (\Gamma_s/2)^2} \right). \quad (4.2)$$

Here,  $f$  denotes the laser frequency,  $f_{Res}$  is the resonance frequency for the photoassociation transition,  $c$  is a intensity dependent constant, and  $\Gamma_s$  is the spontaneous decay width of the excited molecular state. In the limit that  $\Gamma_s$  vanishes Eq. (4.1) and (4.2) become identical. A finite  $\Gamma_s$  prevents the scattering length from diverging on resonance (see Fig. 4.1) and is responsible for the unwanted loss of atoms due to spontaneous decay of photoassociated molecules. In principle, one can suppress these losses for a given change in scattering length by detuning far from the photoassociation resonance and using a high laser power. This is in complete analogy to optical dipole traps where powerful, far-detuned lasers are chosen to suppress spontaneous photon scattering. As recently pointed out by Julienne's group [Ciu05], some atomic species are more favorable for optical Feshbach tuning than others. Ultracold alkaline-earth-metal atoms, for example, have very narrow and strong molecular photoassociation lines. These lines are located close to the atomic intercombination  ${}^1S_0 - {}^3P_1$  transition and therefore exhibit a good Franck-Condon overlap. This is favorable for achieving large changes in the scattering length at small atomic losses. Compared to  ${}^{87}\text{Rb}$  the gain-loss

ratio for  $^{40}\text{Ca}$  is better by several orders of magnitude, raising interesting prospects for future application of optical Feshbach tuning. Besides changing the scattering length, optical Feshbach resonances can also be used to create ground state molecules [Koc05].



### **4.3 “Magnetic Field Control of Elastic Scattering in a Cold Gas of Fermionic Lithium Atoms”**

S. Jochim, M. Bartenstein, G. Hendl, J. Hecker Denschlag,  
R. Grimm, A. Mosk, and M. Weidemüller

Phys. Rev. Lett. **89**, 273202 (2002).



## Magnetic Field Control of Elastic Scattering in a Cold Gas of Fermionic Lithium Atoms

S. Jochim, M. Bartenstein, G. Hendl, J. Hecker Denschlag, and R. Grimm

*Institut für Experimentalphysik, Universität Innsbruck, Technikerstrasse 25, 6020 Innsbruck, Austria*

A. Mosk

*FOM instituut voor plasmafysica Rijnhuizen, P.O. Box 1207, 3430 BE Nieuwegein, The Netherlands*

M. Weidemüller

*Max-Planck-Institut für Kernphysik, Postfach 103980, 69029 Heidelberg, Germany*

(Received 24 July 2002; published 18 December 2002)

We study elastic collisions in an optically trapped spin mixture of fermionic lithium atoms in the presence of magnetic fields up to 1.5 kG by measuring evaporative loss. Our experiments confirm the expected magnetic tunability of the scattering length by showing the main features of elastic scattering according to recent calculations. We measure the zero crossing of the scattering length at 530(3) G which is associated with a predicted Feshbach resonance at  $\sim 850$  G. Beyond the resonance we observe the expected large cross section in the triplet scattering regime.

DOI: 10.1103/PhysRevLett.89.273202

PACS numbers: 34.50.-s, 05.30.Fk, 32.80.Pj, 39.25.+k

In an ultracold atomic gas, the  $s$ -wave scattering length characterizes the elastic interactions and has a profound effect on the physical behavior. The scattering length can be conveniently tuned by using a magnetic field when a Feshbach resonance is present. For bosonic atoms, such resonances have been observed [1–3], and they have found particular applications for attainment and manipulation of a Bose-Einstein condensate in  $^{85}\text{Rb}$  [4,5] and for the production of bright solitons in bosonic  $^7\text{Li}$  [6,7].

For fermionic gases, Feshbach resonances in  $s$ -wave scattering of atoms in different spin states are of great interest to experimentally explore the rich physics of paired fermionic gases [8–11]. For obtaining superfluidity in a Cooper-paired gas, magnetic tuning allows one to raise the critical temperature [8] from values far below the Fermi temperature into a region that seems accessible with current experimental methods. With resonantly tuned interactions the fermionic superfluid is predicted [9,10] to perform a crossover from a superfluid of weakly coupled Cooper pairs to a Bose-Einstein condensate of strongly coupled molecules. Feshbach tuning also offers a possible way to detect this molecular coupling through oscillations induced by magnetic-field transients [10] analogous to a recent observation with coupled bosonic atoms [5]. Experimental control of different pairing regimes thus represents an intriguing prospect of a fermionic gas with magnetically tuned interactions.

A narrow Feshbach resonance between two different spin states of fermionic  $^{40}\text{K}$  was recently observed by Loftus *et al.* [12]. The other fermionic species currently used in several experiments,  $^6\text{Li}$ , is predicted to show a Feshbach resonance with strong modifications of  $s$ -wave interactions in a very wide magnetic-field range [13–15]. At relatively small fields, this dependence was recently used by Granade *et al.* to obtain a sufficient scattering

cross section for the all-optical production of a degenerate Fermi gas of lithium [16].

In this Letter, we experimentally explore the magnetic tunability of elastic scattering in an optically trapped spin mixture of fermionic lithium atoms in high magnetic fields up to 1.5 kG. Our results verify the expected dependence of  $s$ -wave interactions in the whole magnetic-field range of interest [13–15]. As a particular feature associated with the predicted Feshbach resonance [13], we observe the zero crossing of the scattering length at a field of 530 G. The exact location of this feature is of great interest as a sensitive input parameter to better constrain the uncertainty in the molecular potentials for more accurate theoretical calculations of the scattering properties of  $^6\text{Li}$ . Our measurements of elastic collisions are based on evaporation out of an optical dipole trap.

The scattering properties in different spin mixtures of fermionic lithium atoms were theoretically investigated by Houbiers *et al.* [13], Kokkelmans *et al.* [14], and Venturi and Williams [15]. Magnetic tunability, of particular interest for Cooper pairing in a Fermi gas [8,9], was predicted for the stable combination of the two lowest states  $|1\rangle$  and  $|2\rangle$ ; at low magnetic field these states correspond to  $F = 1/2$ ,  $m_F = +1/2$ , and  $m_F = -1/2$ , respectively. Most prominently, a broad Feshbach resonance at  $\sim 850$  G is expected to mark the transition from the low-field scattering regime to the high-field region. As a precursor of the Feshbach resonance, the  $s$ -wave scattering length  $a$  crosses zero in the range between 500 and 550 G. Beyond the resonance, scattering in higher fields is dominated by the triplet potential with a very large and negative scattering length of  $-2200a_0$ , where  $a_0$  is the Bohr radius. The available theoretical data [13–15] show the same behavior for  $a(B)$  within some variations due to the limited knowledge of the

molecular interaction parameters. Figure 1(a) illustrates these predictions for the scattering length  $a(B)$  by a corresponding model curve that approximates the results of Refs. [13–15].

In a cold gas at finite temperature the cross section for elastic scattering of nonidentical particles is unitarity limited to a maximum value of  $\sigma_{\max} = 4\pi/k^2$ , where  $k = mv/(2\hbar)$  is the wave number corresponding to a relative velocity  $v$  and a reduced mass  $m/2$ . Taking into account the B-field dependent scattering length  $a(B)$  and the unitarity limit, the resulting B-field dependent cross section can be written as  $\sigma = 4\pi a^2/(1 + k^2 a^2)$ . For the considered  $|1\rangle - |2\rangle$  spin mixture of  ${}^6\text{Li}$  the expected behavior of the cross section is shown in Fig. 1(b) for the example of a wave number  $k = (300a_0)^{-1}$  close to our experimental conditions. Most notably, as a consequence of the unitarity limit in combination with the very large scattering length for high magnetic fields, the Feshbach resonance does not appear as a pronounced feature in the cross section. The zero crossing of the scattering length, however, leads to a vanishing scattering cross section and thus shows up as a manifestation of the resonance.

Our dipole trap [17] makes use of the enhancement of the laser intensity inside a linear optical resonator to create a large and deep trapping volume for lithium atoms. The power provided by a 2-W Nd:YAG laser (Innolight Mephisto-2000) at a wavelength of 1064 nm is enhanced by a factor of 120 to create a far red-detuned 1D optical lattice trap with an axial period of 532 nm and a transverse  $1/e$  radius of 115  $\mu\text{m}$ . The maximum trap depth is of the order of 1 mK. To vary the trap depth the resonator-internal power is servo-controlled by an acousto-optical modulator in the incident laser beam. From a standard magneto-optical trap (MOT) operated with diode lasers we typically transfer  $5 \times 10^5$   ${}^6\text{Li}$  atoms into roughly 1000 individual wells at a temperature of

$\sim 400$   $\mu\text{K}$ . The resulting peak density is  $\sim 1.5 \times 10^{11}$   $\text{cm}^{-3}$ . By extinguishing the repumping light of the MOT 1 ms before the main trapping light is turned off, all atoms are pumped into the two states  $|1\rangle$  and  $|2\rangle$  to create a 50-50 spin mixture [16].

The magnetic field is produced by a pair of water-cooled coils outside of the glass vacuum cell of the trap. At a maximum continuous operation current of 200 A the coils produce a magnetic field of 1.5 kG with a curvature of only 75 G/cm<sup>2</sup> along the symmetry axis; the corresponding power dissipation is 6 kW. The setup allows for a maximum ramp speed of 5 G/ms within the full range. The magnetic field is calibrated by radio-frequency induced transitions from  $|2\rangle$  to the state that at  $B = 0$  corresponds to  $F = 3/2$ ,  $m_F = +1/2$ . The latter is unstable against inelastic collisions with  $|2\rangle$  which leads to easily detectable loss. With a fit to the Breit-Rabi formula we obtain a calibration of the magnetic field to better than 1 G over the full range.

The basic idea of our measurements is to observe elastic collisions through evaporative loss at a variable magnetic field [18]. The method is particularly well suited for measuring the position of a resonance by locating the corresponding zero crossing of the scattering length. With this sensitive experimental input for theoretical calculations, as is readily available in our case [13–15], precise knowledge of the magnetic-field dependent scattering length can be obtained. Our dipole trap is loaded under conditions where the effective temperature  $T$  of a truncated Boltzmann distribution [19] is only slightly below the trap depth  $U$ . A strongly nonthermal distribution is thus created with a small truncation parameter  $\eta = U/k_B T \approx 2$ . The thermal relaxation resulting from elastic collisions then leads to rapid evaporative loss and cooling of the sample, i.e., an increase of  $\eta$ . The trap depth can be kept constant to study plain evaporation or, alternatively, ramped down to force the evaporation process.

In a series of plain evaporation experiments performed at a constant trap depth of 750  $\mu\text{K}$  we measure evaporative loss over the maximum accessible range of magnetic fields up to 1.5 kG. After a fixed holding time the remaining atoms are retrapped into the MOT and their number is measured via the fluorescence signal by a calibrated photodiode. The signal is recorded after holding times of 1 and 3 s corresponding to the time scale of evaporation. These holding times are short compared with the rest-gas limited lifetime of 30 s. Figure 2 shows the result of 1000 different measurements obtained in an acquisition time of 6 h. The data points are taken in a random sequence for 31 magnetic field values equally distributed over the full range. Data points for 1 and 3 s are recorded alternately. This way of data taking ensures that the signal is not influenced by residual long-term drifts of the experimental conditions.

The observed evaporation loss in Fig. 2 shows a pronounced dependence on the magnetic field, which we

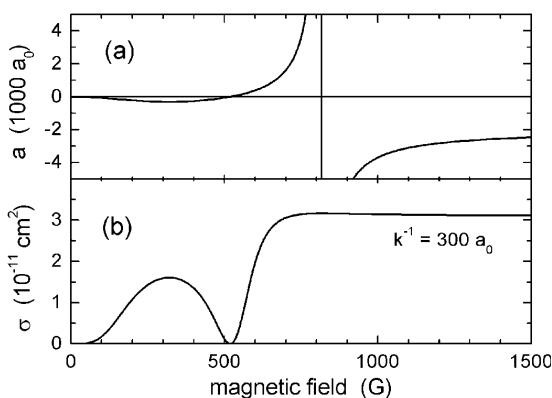


FIG. 1. (a) Model curve approximating the results of [13–15] for the  $s$ -wave scattering length of  ${}^6\text{Li}$  atoms in the two lowest spin states versus magnetic field. (b) Corresponding behavior of the scattering cross section at a finite collision energy with a relative wave number of  $k = (300a_0)^{-1}$ .

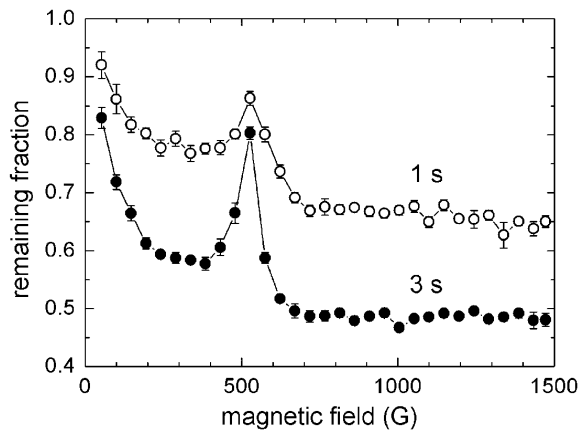


FIG. 2. Evaporative loss measurements over the full magnetic field range. The data points show the measured number of atoms remaining in the trap after 1 s ( $\circ$ ) and 3 s ( $\bullet$ ) of plain evaporation at a constant trap depth of  $750 \mu\text{K}$ .

compare with the expected cross section for elastic collisions ejecting atoms out of the trap. Figure 1(b) displays the cross section for  $k = (300a_0)^{-1}$ , which corresponds to a collision energy of about half the trap depth and thus to the relevant energies for evaporating collisions. After being very small at low magnetic fields, the observed loss increases for fields up to  $\sim 350$  G where the expected local maximum of evaporation shows up. The loss then decreases and disappears at about 530 G in agreement with the predicted zero crossing of the scattering length. Here the slight observed loss in the 1 s curve is explained by the finite ramp time of the magnetic field. In the 100 ms ramping time some evaporation does already take place. At 530 G the decrease of the trapped atom number between 1 and 3 s is fully explained by rest-gas losses without any further evaporation. For higher magnetic fields evaporative loss rapidly rises until it levels off at about 700 G. Up to the maximum attainable value of 1.5 kG high evaporation loss is observed. A slight decrease of the atom number for fields exceeding 1 kG occurs which we attribute to technical reasons; we observe an increasing noise for currents higher than  $\sim 130$  A in the error signal of the resonator lock. The relatively large and constant evaporative loss for fields exceeding 700 G is consistent with the predicted behavior of the cross section.

The evaporative cooling effect is confirmed by measuring the change of the truncation parameter  $\eta$  after 3 s of trapping at selected values of the magnetic field. For thermometry we turn off the magnetic field to avoid further elastic collisions and adiabatically lower the trap depth in a 1-s exponential ramp. The fraction of remaining atoms as a function of the relative depth then provides a good measure of  $\eta$ . At the zero crossing at 530 G we observe only a slight increase of  $\eta$  to a value of 2.3(3) which is explained by the unavoidable evaporation during

the magnetic-field ramps. At 340 G close to the local maximum of  $|a|$  we find an increase of  $\eta$  to 4.2(3) as a clear evidence of evaporative cooling. At 720 G, i.e., in the case of a large positive scattering length, a higher value of 5.5(4) is measured showing deeper evaporative cooling. Essentially the same  $\eta$  of 5.3(4) is obtained at  $B = 1290$  G where scattering takes place in the triplet-dominated regime with a very large negative scattering length.

We measure the minimum-loss feature in a closer range of magnetic fields to precisely determine the value of the magnetic field at which the zero crossing of scattering length occurs. The main data points in Fig. 3 are obtained with 500 individual measurements at a holding time of 3 s with the magnetic field randomly varied between 30 values in an interval between 370 and 670 G; the data shown in the inset are obtained with 1000 measurements in the very narrow range between 520 and 544 G. The results allow us to determine the B field for minimum evaporative loss, and thus the zero crossing of the scattering length to 530(3) G [20].

Forced evaporation measurements provide complementary data to plain evaporation and allow us to rule out a significant role of inelastic collisions. When the trap depth is ramped down, elastic collisions reduce trap loss in contrast to increased loss at constant trap depth. This can be understood by the spilling loss of energetic particles [19]: Without elastic collisions the most energetic particles are spilled out of the trap when its depth is reduced. With elastic collisions the evaporative cooling effect decreases the temperature and thus reduces the spilling loss.

In our forced evaporation measurements we reduce the trap depth in 10 s to 20% of its initial value in an exponential ramp and measure the number of remaining atoms; the results are displayed in Fig. 4. A minimum

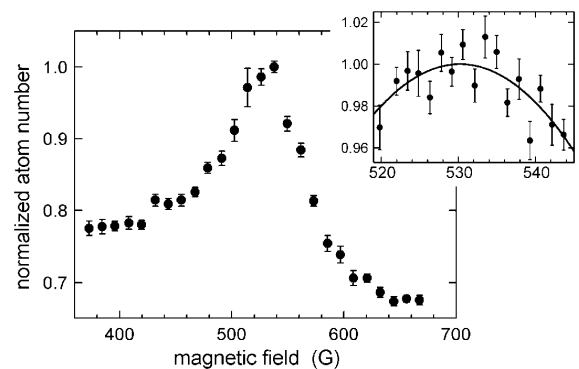


FIG. 3. Measurements on plain evaporation in magnetic fields close to the zero crossing of the scattering length under the same conditions as in Fig. 2 for a holding time of 3 s. Here the number of remaining atoms is normalized to the observed maximum value. The inset shows a series of measurements in a very narrow range around the maximum at 530(3) G together with a parabolic fit.

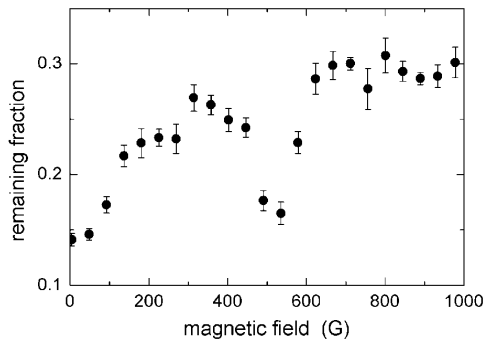


FIG. 4. Fraction of atoms remaining after forced evaporation versus applied magnetic field. The trap depth is ramped down exponentially in 10 s to 20% of the initial value.

number of atoms is now measured at 0 and 530 G instead of the maximum observed with constant trap depth. The largest number of atoms is observed in the high-field region above 650 G as expected for the large scattering cross section.

On a Feshbach resonance, enhanced inelastic loss can occur as a result of three-body collisions [1] or, if the system has internal energy, as a result of two-body decay [3]. For fermions, three-body processes are symmetry forbidden at ultralow energies when only  $s$ -wave collisions are involved. In a spin mixture at nonzero magnetic field, two-body decay is energetically possible (in our case with an energy release of  $k_B \times 3.5$  mK) but involves higher partial waves and relies on weak dipolar coupling. Consequently, inelastic loss can be expected to be weak in our experiments. Indeed, our data do not show any indication of inelastic loss even at the very center of the Feshbach resonance.

At much higher densities ( $\sim 10^{13}$  cm $^{-3}$ ) as compared to our conditions ( $\sim 10^{11}$  cm $^{-3}$ ), a recent experiment [21] has revealed inelastic loss with a maximum at 680 G. As our results support the predicted position of the  $s$ -wave resonance at  $\sim 850$  G, the explanation for the inelastic feature cannot be attributed to the Feshbach resonance in a simple way. The experiment [21] also provided evidence for a two-body nature of the underlying process with a rate constant of  $2 \times 10^{-12}$  cm $^3$ /s measured at  $\sim 20$   $\mu$ K. At a higher temperature of  $\sim 100$   $\mu$ K we derive an upper bound for the two-body rate constant of  $1 \times 10^{-12}$  cm $^3$ /s, whereas for a process involving higher partial waves one would expect the rate to increase with temperature. For three-body collisions our densities are too low to provide useful constraints. Obviously, inelastic loss in the fermionic spin mixture is an interesting problem that deserves more attention.

In conclusion, our measurements confirm the predicted magnetic tunability of the  $s$ -wave scattering length in a spin mixture of fermionic lithium atoms in the whole magnetic-field range of experimental interest. The ob-

served zero crossing of the scattering length at 530(3) G together with the large cross section observed for higher fields provides clear evidence of the predicted Feshbach resonance. Moreover, it enables more precise calculations of the  $^6\text{Li}$  scattering properties. The resonance itself is masked by unitarity-limited scattering and requires much deeper evaporative cooling for a direct observation. The fact that we do not see any significant effect of inelastic loss highlights the fact that the extremely large positive and negative scattering lengths attainable with fermionic lithium offer intriguing new possibilities for experiments on interacting Fermi gases.

We thank R.G. Hulet and H. Stoof for very useful discussions and V. Venturi for valuable input. Support by the Austrian Science Fund (FWF) within Project No. P15115 and SFB15 and by the Institut für Quanteninformation GesmbH is gratefully acknowledged.

Shortly before submission of the present Letter we learned about the measurements of the group of J.E. Thomas on the zero crossing of the scattering length which agree with our data.

- 
- [1] S. Inouye *et al.*, *Nature (London)* **392**, 151 (1998).
  - [2] P. Courteille *et al.*, *Phys. Rev. Lett.* **81**, 69 (1998).
  - [3] V. Vuletić, A. J. Kerman, C. Chin, and S. Chu, *Phys. Rev. Lett.* **82**, 1406 (1999).
  - [4] S. Cornish *et al.*, *Phys. Rev. Lett.* **85**, 1795 (2000).
  - [5] E. A. Donley, N. R. Claussen, S. T. Thompson, and C. E. Wieman, *Nature (London)* **417**, 529 (2002).
  - [6] L. Khaykovich *et al.*, *Science* **296**, 1290 (2002).
  - [7] K. Strecker, G. Partridge, A. Truscott, and R. Hulet, *Nature (London)* **417**, 150 (2002).
  - [8] H. T. C. Stoof, M. Houbiers, C. Sackett, and R. Hulet, *Phys. Rev. Lett.* **76**, 10 (1996).
  - [9] M. Holland, S. Kokkelmans, M. Chiofalo, and R. Walser, *Phys. Rev. Lett.* **87**, 120406 (2001).
  - [10] E. Timmermans, K. Furuya, P. W. Milonni, and A. K. Kerman, *Phys. Lett. A* **285**, 228 (2001).
  - [11] M. L. Chiofalo, S. J. J. M. F. Kokkelmans, J. L. Milstein, and M. J. Holland, *Phys. Rev. Lett.* **88**, 090402 (2002).
  - [12] T. Loftus *et al.*, *Phys. Rev. Lett.* **88**, 173201 (2002).
  - [13] M. Houbiers, H. T. C. Stoof, W. McAlexander, and R. Hulet, *Phys. Rev. A* **57**, R1497 (1998).
  - [14] S. Kokkelmans *et al.*, *Phys. Rev. A* **65**, 053617 (2002).
  - [15] V. Venturi and C. Williams (private communication).
  - [16] S. Granade, M. Gehm, K. O'Hara, and J. Thomas, *Phys. Rev. Lett.* **88**, 120405 (2002).
  - [17] A. Mosk *et al.*, *Opt. Lett.* **26**, 1837 (2001).
  - [18] C. Chin, V. Vuletić, A. J. Kerman, and S. Chu, *Phys. Rev. Lett.* **85**, 2717 (2000).
  - [19] O. J. Luiten, M. W. Reynolds, and J. T. M. Walraven, *Phys. Rev. A* **53**, 381 (1996).
  - [20] A finite collision energy  $E_C$  leads to a shift of  $+0.7G \times E_C/(k_B \times 100 \mu\text{K})$  [15], which for our data stays within the error.
  - [21] K. Dieckmann *et al.*, *cond-mat/0207046v2*.

#### 4.4 “Precise determination of ${}^6\text{Li}$ cold collision parameters by radiofrequency spectroscopy on weakly bound molecules”

M. Bartenstein, A. Altmeyer, S. Riedl, S. Jochim,  
C. Chin, J. Hecker Denschlag, R. Grimm, A. Simoni,  
E. Tiesinga, C. Williams, and P. Julienne

Phys. Rev. Lett. **94**, 103201 (2005)



## Precise Determination of ${}^6\text{Li}$ Cold Collision Parameters by Radio-Frequency Spectroscopy on Weakly Bound Molecules

M. Bartenstein,<sup>1</sup> A. Altmeyer,<sup>1</sup> S. Riedl,<sup>1</sup> R. Geursen,<sup>1</sup> S. Jochim,<sup>1</sup> C. Chin,<sup>1,\*</sup> J. Hecker Denschlag,<sup>1</sup> and R. Grimm<sup>1,2</sup>

<sup>1</sup>*Institut für Experimentalphysik, Universität Innsbruck, Technikerstraße 25, 6020 Innsbruck, Austria*

<sup>2</sup>*Institut für Quantenoptik und Quanteninformation, Österreichische Akademie der Wissenschaften, 6020 Innsbruck, Austria*

A. Simoni,<sup>†</sup> E. Tiesinga, C. J. Williams, and P. S. Julienne

*Atomic Physics Division, National Institute of Standards and Technology,*

*100 Bureau Drive Stop 8423, Gaithersburg, Maryland 20899, USA*

(Received 28 August 2004; published 18 March 2005)

We employ radio-frequency spectroscopy on weakly bound  ${}^6\text{Li}_2$  molecules to precisely determine the molecular binding energies and the energy splittings between molecular states for different magnetic fields. These measurements allow us to extract the interaction parameters of ultracold  ${}^6\text{Li}$  atoms based on a multichannel quantum scattering model. We determine the singlet and triplet scattering lengths to be  $a_s = 45.167(8)a_0$  and  $a_t = -2140(18)a_0$  ( $a_0 = 0.0529177$  nm), and the positions of the broad Feshbach resonances in the energetically lowest three  $s$ -wave scattering channels to be 83.41(15), 69.04(5), and 81.12(10) mT.

DOI: 10.1103/PhysRevLett.94.103201

PACS numbers: 34.50.-s, 05.30.Jp, 32.80.Pj, 67.40.Hf

Molecular level structure near a collision threshold uniquely determines the scattering properties of ultracold atoms. When a molecular state is tuned near the scattering threshold, the atomic scattering amplitude can be resonantly altered. Magnetically tuned Feshbach resonances [1] in ultracold fermionic gases have recently led to ground-breaking observations, including the condensation of molecules [2–6] and the studies of the crossover physics from a molecular Bose-Einstein condensate (BEC) to atomic Cooper pairs in the Bardeen-Cooper-Schrieffer state (BEC-BCS crossover) [5,7,8]. These studies are of general importance in physics as the ultracold Fermi gas provides a unique model system for other strongly interacting fermionic systems [9].

In spin mixtures of  ${}^6\text{Li}$  atoms, a broad Feshbach resonance in the energetically lowest  $s$ -wave channel [10] allows for precise interaction tuning. This, together with the extraordinary stability of the system against inelastic decay [2,11], makes  ${}^6\text{Li}$  the prime candidate for BEC-BCS crossover studies. A precise knowledge of the magnetic-field dependent scattering properties is crucial for a quantitative comparison of the experimental results with crossover theories. Of particular importance is the precise value of the magnetic field where the  $s$ -wave scattering diverges. At this unique point, the strongly interacting fermionic quantum gas is expected to exhibit universal properties [12]. Previous experiments explored the  ${}^6\text{Li}$  resonance by measuring inelastic decay [13], elastic collisions [14,15], and the interaction energy [16], but could locate the exact resonance point only to within a range between 80 and 85 mT.

An ultracold gas of weakly bound molecules is an excellent starting point to explore the molecular energy structure near threshold [17]. An improved knowledge on the exact  ${}^6\text{Li}$  resonance position was recently obtained in

an experiment that observed the controlled dissociation of weakly bound  ${}^6\text{Li}_2$  molecules induced by magnetic-field ramps [18]. These measurements provided a lower bound of 82.2 mT for the resonance position. Studies of systematic effects suggested an upper bound of 83.4 mT. Within this uncertainty range, however, we observe the physical behavior of the ultracold gas to exhibit a substantial dependence on the magnetic field [8]. In this Letter, we apply radio-frequency (rf) spectroscopy [17,19] on weakly bound molecules to precisely determine the interaction parameters of cold  ${}^6\text{Li}$  atoms. Together with a multichannel quantum scattering model, we obtain a full characterization of the two-body scattering properties, essential for BEC-BCS crossover physics.

The relevant atomic states are the lowest three sublevels in the  ${}^6\text{Li}$  ground state manifold, denoted by  $|1\rangle$ ,  $|2\rangle$ , and  $|3\rangle$ . Within the magnetic-field range investigated in this experiment, these levels form a triplet of states, essentially differing by the orientation of the nuclear spin ( $m_I = 1, 0, -1$ ). Figure 1 shows the energy level structure of the two scattering channels  $|1\rangle + |2\rangle$  and  $|1\rangle + |3\rangle$ , denoted by  $(1, 2)$  and  $(1, 3)$ , respectively. The broad Feshbach resonance occurs in the  $(1, 2)$  channel near 83 mT. When the magnetic field is tuned below the resonance, atoms in the  $(1, 2)$  channel can form weakly bound molecules [20]. For the  $(1, 3)$  channel, a similar Feshbach resonance [19] occurs near 69 mT.

Starting with molecules formed in the  $(1, 2)$  channel, we drive the rf transition to the  $(1, 3)$  channel at various magnetic-field values  $B$ . The rf excitation can dissociate a molecule into two free atoms (bound-free transition; see Fig. 1) [17] or, for  $B < 69$  mT, it can also drive the transition between the molecular states in the  $(1, 2)$  and  $(1, 3)$  channels (bound-bound transition). In both processes, the rf excitation results in loss of molecules in the

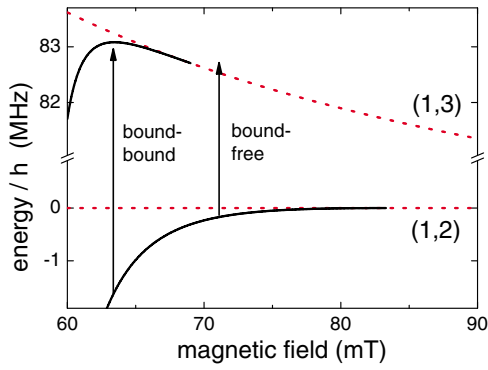


FIG. 1 (color online). Energy level structure near the  $\text{Li}_2$  dissociation threshold as a function of magnetic field  $B$ . The threshold energy of the (1, 3) scattering channel (upper dotted line) is plotted relative to the (1, 2) threshold (lower dotted line). In the (1, 2) channel, a molecular state (lower solid line) exists below the Feshbach resonance at  $\sim 83$  mT. In the (1, 3) channel, another molecular state (upper solid line) exists below the resonance at  $\sim 69$  mT. The bound-free and bound-bound transitions of molecules in the (1, 2) channel are illustrated by the arrows.

(1, 2) channel. This loss constitutes our experimental signal. We perform measurements at different magnetic fields for both the bound-free and the bound-bound transitions.

Our experimental procedure is similar to Ref. [8]. The optically trapped sample is cooled by forced evaporation at a magnetic field of 76.4 mT. With deep cooling we routinely produce a BEC of  $2 \times 10^5$  molecules [2], which at the lowest trap laser power of 3.8 mW has a peak density of  $4 \times 10^{12} \text{ cm}^{-3}$ . After evaporation we linearly ramp the field to a specific value between 66 and 72 mT in typically 200 ms. We then apply a single rf pulse for 200 ms with its frequency tuned close to the atomic transition  $|2\rangle$  to  $|3\rangle$ . Following the rf pulse, we apply state-selective absorption imaging, which is sensitive to free atoms in state  $|2\rangle$  and molecules in the (1, 2) channel.

To precisely determine the magnetic field, we employ rf spectroscopy on a “hot” thermal sample of  $2 \times 10^6$  atoms at a temperature  $T \approx 90 \mu\text{K}$  (about 6 times the Fermi temperature  $T_F$ ) with the highest trap laser power of 10.5 W. Under these conditions we do not observe any density-dependent frequency shifts, in agreement with [19]. The rf transition energy then corresponds to the internal energy difference  $hf_0$  between the states  $|2\rangle$  and  $|3\rangle$ , where  $h$  is Planck’s constant. This energy is magnetic-field dependent and the transition frequency is about 83 MHz in the magnetic-field range we study. The measured transition has a narrow linewidth of less than 1 kHz, and the center position can be determined to within a few hundred Hz. This high resolution allows us to calibrate our magnetic field to an accuracy of a few  $\mu\text{T}$  based on the Breit-Rabi formula and the  $^9\text{Li}$  parameters given in [21].

For bound-free transitions, the molecules in the (1, 2) channel make a transition to the (1, 3) scattering continuum. The excitation rate from a stationary molecule to an atomic scattering state with kinetic energy  $2E_k$  is deter-

mined by the Franck-Condon factor between the bound and free wave functions [22]. From energy conservation,  $2E_k$  is related to the rf transition energy  $hf$  by  $hf = hf_0 + E_b + 2E_k$ , where  $E_b$  is the binding energy of the molecules in the (1, 2) channel. The variation of the Franck-Condon factor with atomic kinetic energy leads to a broad and asymmetric dissociation line shape [22].

Rf dissociation spectra taken at 72.0 and 69.5 mT for a molecular BEC in a weak optical trap are shown in Fig. 2. An important feature of the spectra is the sharp rising edge on the low frequency side. This threshold corresponds to the dissociation of a molecule into two atoms with zero relative momentum. Therefore, the position of the edge relative to the atomic transition directly indicates the molecular binding energy.

We determine the dissociation threshold and thus the molecular binding energy by fitting the full line shape. The line shape function [22] depends on both the (1, 2) molecular binding energy  $E_b$  and the scattering length  $a_{13}$  in the (1, 3) channel. In the range of magnetic fields we investigate,  $a_{13}$  is much larger than the interaction range of the van der Waals potential of  $\sim 30a_0$ . The line shape function  $P(E)$  is then well approximated by [22]

$$P(E) \propto E^{-2}(E - E_b)^{1/2}(E - E_b + E')^{-1}, \quad (1)$$

where  $E = hf - hf_0$  and  $E' = \hbar^2/ma_{13}^2$ . From the fits to the experimental data [23], we determine the threshold positions, given in Table I. Together with the atomic transition frequencies, we conclude that the molecular binding energies are  $E_b = h \times 134(2)$  kHz at 72.013(4) mT and  $E_b = h \times 277(2)$  kHz at 69.483(4) mT.

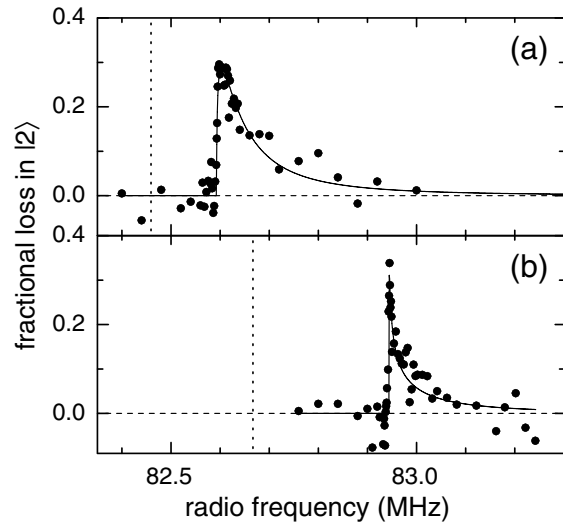


FIG. 2. Bound-free rf spectra at 72.013(4) mT (a) and 69.483(4) mT (b). Fractional loss in state  $|2\rangle$  is measured as a function of the radio frequency. The solid lines represent a fit based on Eq. (1). The atomic transition frequencies, which are measured independently, are indicated by the vertical dashed lines.

TABLE I. Comparison between our experimental and theoretical results. The magnetic field  $B$  is determined from the measured atomic transition frequency  $f_0$ . The molecular transition frequency  $f_{\text{mol}}$  refers to the resonance peak for bound-bound transitions (upper two rows) or the dissociation threshold (lower two rows). The values in parentheses indicate  $1\sigma$  uncertainties.

$B$ (mT)	$f_0$ (MHz)	$f_{\text{mol}}$ (MHz)	
		Experimental	Theory
66.1436(20)	82.968 08(20)	83.6645(3)	83.6640(10)
67.6090(30)	82.831 84(30)	83.2966(5)	83.2973(10)
69.4826(40)	82.666 86(30)	82.9438(20)	82.9419(13)
72.0131(40)	82.459 06(30)	82.5928(20)	82.5910(13)

For magnetic field  $B < 69$  mT, we can drive the rf transition between the (1, 2) and (1, 3) molecular states. Here, the resonance frequency is given by the energy difference of the two molecular states. To avoid possible systematic mean-field shifts at these lower magnetic fields [19], we prepare a thermal mixture of atoms and molecules with temperature  $T \approx T_F$  by a controlled heating method [8]. Rf spectroscopy is performed at 67.6 and 66.1 mT. The bound-bound transition signal at 66.1 mT is shown in Fig. 3. By fitting the narrow transition line with a Lorentzian profile, we determine the resonance frequency; see Table I. Notably, below the resonance in the (1, 3) channel at  $\sim 69$  mT, the bound-free transition is much weaker due to a Fano-type interference effect [22].

Because of the high precision of the measured transition frequencies, a careful analysis of systematic effects is necessary. Possible systematic shifts include differential light shifts of the two molecular states and density-dependent many-body shifts. In order to characterize these possible systematic errors, we experimentally investigate these shifts by varying the trap depth of the optical potential. In a deeper trap, both the differential light shifts and mean-field shifts are expected to increase. We repeat the

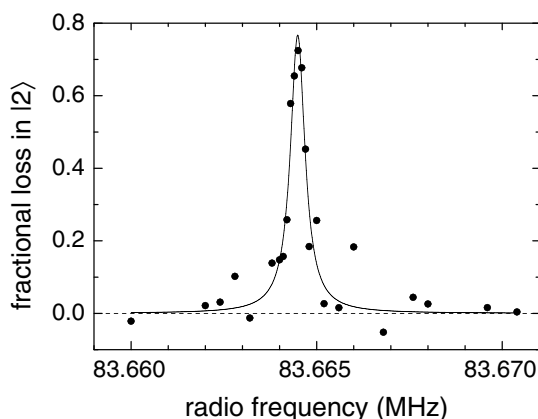


FIG. 3. Bound-bound rf spectrum at 66.144(2) mT. The fractional population loss in state  $|2\rangle$  shows a narrow resonance. We determine the center position to be 83.6645(3) MHz from a Lorentzian fit (solid line).

bound-free and bound-bound rf spectroscopy for different trap laser powers in a range between 3.8 and 310 mW. At a typical magnetic field of  $B = 69$  mT the peak number density of a molecular BEC is thereby varied between  $8 \times 10^{12} \text{ cm}^{-3}$  and  $5 \times 10^{13} \text{ cm}^{-3}$ . Within our statistical uncertainties we do not see any systematic density-dependent shifts.

Given the measured data summarized in Table I, it is possible to predict the location of the scattering resonances in the (1, 2), (1, 3), and (2, 3) channels if we have an accurate theoretical model of the collision. We use a standard multichannel model for the interaction of two  $^2\text{S}$  atoms with nuclear spin [24] to calculate the scattering lengths and bound state energies for these channels. It is necessary to include  $s$  waves only in the basis set, since we find that there is a negligible change within the experimental uncertainties if we also include higher partial waves in the basis set. The interaction potential model is the same as described in Ref. [14]. It uses a combination of Rydberg-Klein-Rees and *ab initio* potentials for the singlet ( $^1\Sigma_g^+$ ) and triplet ( $^3\Sigma_u^+$ ) states at short range and joins them smoothly onto long range potentials based on the exchange [25] and van der Waals dispersion energy [26], the lead term of which is  $C_6 = 1393.39(16) \text{ au}$  ( $1 \text{ au} = 9.57344 \times 10^{-26} \text{ J nm}^6$ ). As in Ref. [14], the singlet  $^1\Sigma_g^+$  and triplet  $^3\Sigma_u^+$  scattering lengths,  $a_s$  and  $a_t$ , respectively, are varied by making small variations to the inner wall of the potential. Once  $a_s$  and  $a_t$  are specified, all other scattering and bound state properties for all channels of two  $^6\text{Li}$  atoms are uniquely determined, including the positions of the resonances. Consequently, varying  $a_s$  and  $a_t$  to fit the binding energies and energy differences from rf spectroscopy determines the values of these two free parameters.

Fitting the data of the present experiment determines  $a_s = 45.167(8)a_0$  and  $a_t = -2140(18)a_0$ . The uncertainty includes both the uncertainty in the measured value of the magnetic field and the uncertainty in the rf measurements. Our scattering lengths agree within the uncertainties with previous determinations:  $a_s = 45.1591(16)a_0$  [18] and  $a_t = -2160(250)a_0$  [27]. Table I shows a comparison of the measured and best fit calculated energies. The calculated positions of the broad  $s$ -wave resonances for the (1, 2), (1, 3), and (2, 3) channels are 83.41(15), 69.04(5), and 81.12(10) mT, respectively.

Figure 4 shows the scattering lengths calculated for several different channels in the magnetic-field range of interest to BEC-BCS crossover experiments. We find that the formula  $a = a_b[1 + \Delta(B - B_0)^{-1}][1 + \alpha(B - B_0)]$  fits the calculated scattering lengths to better than 99% over the range of 60 to 120 mT. This expression includes the standard Feshbach resonance term [28] with the background scattering length  $a_b$ , resonance position  $B_0$ , and resonance width  $\Delta$ , and a leading-order correction parameterized by  $\alpha$ . The respective values for  $a_b$ ,  $B_0$ ,  $\Delta$ , and  $\alpha$  are  $-1405a_0$ , 83.4149 mT, 30.0 mT, and  $0.0040 \text{ mT}^{-1}$  for channel (1, 2),  $-1727a_0$ , 69.043 mT, 12.23 mT, and

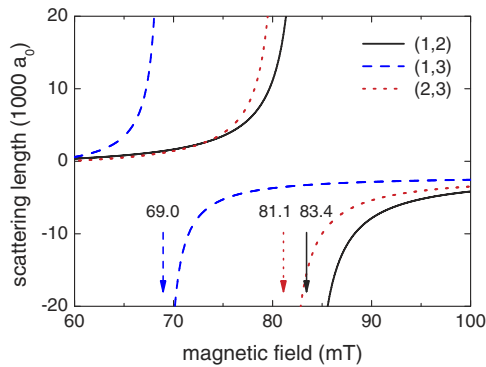


FIG. 4 (color online). Scattering lengths versus magnetic field from multichannel quantum scattering calculations for the (1, 2), (1, 3), and (2, 3) scattering channels. The arrows indicate the resonance positions.

$0.0020 \text{ mT}^{-1}$  for channel (1, 3), and  $-1490a_0$ ,  $81.122 \text{ mT}$ ,  $22.23 \text{ mT}$ , and  $0.00395 \text{ mT}^{-1}$  for channel (2, 3).

The (1, 3) channel molecular bound state can decay to the (1, 2) channel by a very weak spin-dipolar coupling. We have used the methods of Ref. [29] to calculate the two-body lifetime of the (1, 3) bound state due to predissociation to the (1, 2) channel and find that it is very long, greater than 10 s at 60.0 mT, increasing to 1000 s at 68.5 mT very close to resonance. However, (1, 3) molecules might be quenched by collisions with  $|2\rangle$  atoms or (1, 2) channel molecules, since with three different spin states involved in the collision, there would be no fermionic suppression of collision rates according to the mechanism of Ref. [11].

In conclusion, radio-frequency spectroscopy on ultracold, weakly bound molecules allowed us to precisely determine the molecular binding energies and the energy splittings between two molecular states for different magnetic fields. Based on the measured data and a multichannel quantum scattering model, we determine the scattering lengths as a function of magnetic field and the Feshbach resonance positions in the lowest three channels with unprecedented precision. With these data, we can fully characterize the interaction strength between particles in the BEC-BCS crossover regime for future experiments based on  $^6\text{Li}$  atoms.

We acknowledge support by the Austrian Science Fund (FWF) within SFB 15 and the Lise Meitner program and by the European Union. P.J. thanks the Office of Naval Research for partial support.

\*Present address: Department of Physics and the James Franck Institute, University of Chicago, Chicago, IL 60637, USA.

†Present address: UMR 6627 du CNRS, Lab. de Physique des Atomes, Lasers, Molécules et Surfaces, Université de Rennes, France.

- [1] E. Tiesinga, B. J. Verhaar, and H. T. C. Stoof, *Phys. Rev. A* **47**, 4114 (1993); S. Inouye *et al.*, *Nature (London)* **392**, 151 (1998).
- [2] S. Jochim *et al.*, *Science* **302**, 2101 (2003).
- [3] M. Greiner, C. A. Regal, and D. S. Jin, *Nature (London)* **426**, 537 (2003).
- [4] M. Zwierlein *et al.*, *Phys. Rev. Lett.* **91**, 250401 (2003).
- [5] T. Bourdel *et al.*, *Phys. Rev. Lett.* **93**, 050401 (2004).
- [6] R. G. Hulet, in Proceedings of the KITP Conference on Quantum Gases, Santa Barbara, CA, 2004 (unpublished).
- [7] M. Bartenstein *et al.*, *Phys. Rev. Lett.* **92**, 120401 (2004); C. A. Regal, M. Greiner, and D. S. Jin, *Phys. Rev. Lett.* **92**, 040403 (2004); M. W. Zwierlein *et al.*, *Phys. Rev. Lett.* **92**, 120403 (2004); J. Kinast *et al.*, *Phys. Rev. Lett.* **92**, 150402 (2004); M. Bartenstein *et al.*, *Phys. Rev. Lett.* **92**, 203201 (2004).
- [8] C. Chin *et al.*, *Science* **305**, 1128 (2004).
- [9] D. M. Eagles, *Phys. Rev.* **186**, 456 (1969); A. J. Leggett, in *Modern Trends in the Theory of Condensed Matter*, edited by A. Pekalski and R. Przystawa (Springer-Verlag, Berlin, 1980); P. Nozières and S. Schmitt-Rink, *J. Low Temp. Phys.* **59**, 195 (1985); Q. Chen, J. Stajic, S. Tan, and K. Levin, *cond-mat/0404274*.
- [10] M. Houbiers, H. T. C. Stoof, W. I. McAlexander, and R. G. Hulet, *Phys. Rev. A* **57**, R1497 (1998).
- [11] D. S. Petrov, C. Salomon, and G. V. Shlyapnikov, *Phys. Rev. Lett.* **93**, 090404 (2004).
- [12] H. Heiselberg, *Phys. Rev. A* **63**, 043606 (2001); T.-L. Ho, *Phys. Rev. Lett.* **92**, 090402 (2004).
- [13] K. Dieckmann *et al.*, *Phys. Rev. Lett.* **89**, 203201 (2002).
- [14] K. M. O'Hara *et al.*, *Phys. Rev. A* **66**, 041401(R) (2002).
- [15] S. Jochim *et al.*, *Phys. Rev. Lett.* **89**, 273202 (2002).
- [16] T. Bourdel *et al.*, *Phys. Rev. Lett.* **91**, 020402 (2003).
- [17] C. A. Regal, C. Ticknor, J. L. Bohn, and D. S. Jin, *Nature (London)* **424**, 47 (2003).
- [18] C. H. Schunck *et al.*, *cond-mat/0407373* [*Phys. Rev. A* (to be published)].
- [19] S. Gupta *et al.*, *Science* **300**, 1723 (2003).
- [20] J. Cubizolles *et al.* *Phys. Rev. Lett.* **91**, 240401 (2003); S. Jochim *et al.*, *Phys. Rev. Lett.* **91**, 240402 (2003).
- [21] J. Vanier and C. Audoin, *The Quantum Physics of Atomic Frequency Standards* (Adam Hilger Ltd., Bristol, 1989).
- [22] C. Chin and P. Julienne, *Phys. Rev. A* **71**, 012713 (2005).
- [23] We assume an exponential decay of the particle number and fit  $1 - e^{-\nu P(E)}$  to the loss signal, where  $\nu$  depends on the rf power. In principle, we can also determine interaction parameters from  $E'$ . However, our fits yield large uncertainties for  $E'$ .
- [24] H. T. C. Stoof, J. M. V. A. Koelman, and B. J. Verhaar, *Phys. Rev. B* **38**, 4688 (1988).
- [25] R. Côté, A. Dalgarno, and M. J. Jamieson, *Phys. Rev. A* **50**, 399 (1994).
- [26] Z.-C. Yan, J. F. Babb, A. Dalgarno, and G. W. F. Drake, *Phys. Rev. A* **54**, 2824 (1996).
- [27] E. R. I. Abraham, W. I. McAlexander, J. M. Gerton, R. G. Hulet, R. Côté, and A. Dalgarno, *Phys. Rev. A* **55**, R3299 (1997).
- [28] A. J. Moerdijk, B. J. Verhaar, and A. Axelsson, *Phys. Rev. A* **51**, 4852 (1995).
- [29] T. Köhler, E. Tiesinga, and P. S. Julienne, *Phys. Rev. Lett.* **94**, 020402 (2005).

## 4.5 “Tuning the scattering length with an optically induced Feshbach resonance”

M. Theis, G. Thalhammer, K. Winkler, M. Hellwig, G. Ruff, R. Grimm, and J. Hecker Denschlag

Phys. Rev. Lett. **93**, 123001 (2004)



## Tuning the Scattering Length with an Optically Induced Feshbach Resonance

M. Theis,<sup>1</sup> G. Thalhammer,<sup>1</sup> K. Winkler,<sup>1</sup> M. Hellwig,<sup>1</sup> G. Ruff,<sup>1,\*</sup> R. Grimm,<sup>1,2</sup> and J. Hecker Denschlag<sup>1</sup>

<sup>1</sup>*Institut für Experimentalphysik, Universität Innsbruck, Technikerstraße 25, 6020 Innsbruck, Austria*

<sup>2</sup>*Institut für Quantenoptik und Quanteninformation, Österreichische Akademie der Wissenschaften, 6020 Innsbruck, Austria*

(Received 21 April 2004; published 15 September 2004)

We demonstrate optical tuning of the scattering length in a Bose-Einstein condensate as predicted by Fedichev *et al.* [Phys. Rev. Lett. **77**, 2913 (1996)]. In our experiment, atoms in a <sup>87</sup>Rb condensate are exposed to laser light which is tuned close to the transition frequency to an excited molecular state. By controlling the power and detuning of the laser beam we can change the atomic scattering length over a wide range. In view of laser-driven atomic losses, we use Bragg spectroscopy as a fast method to measure the scattering length of the atoms.

DOI: 10.1103/PhysRevLett.93.123001

PACS numbers: 34.50.Rk, 03.75.Nt, 32.80.Pj, 34.20.Cf

The great progress in the field of ultracold quantum gases in recent years can be largely attributed to the existence of magnetically tunable Feshbach resonances [1]. Since their first experimental introduction into the field [2–4], they have been widely used to arbitrarily tune the interactions between atoms.

In general, a Feshbach resonance occurs when a colliding pair of atoms is resonantly coupled to a molecular bound state. A magnetically tunable Feshbach resonance is based on Zeeman shifting a bound molecular state into resonance with the scattering state. Alternative coupling schemes for inducing Feshbach resonances have been proposed but never experimentally applied to control atomic interactions. The use of radio frequency [5] and static electric fields [6] was suggested. Fedichev *et al.* [7] proposed optical coupling of the scattering state with the molecular state, which was theoretically analyzed further in [8,9]. This scheme, often referred to as “optical Feshbach resonance,” can be controlled via laser detuning and laser power.

Inducing Feshbach resonances with optical fields offers experimental advantages compared to magnetic fields. The intensity and detuning of optical fields can be rapidly changed. Furthermore, complex spatial intensity distributions can be easily produced which result in corresponding scattering length patterns across the sample. Optical transitions are always available, even when no magnetic Feshbach resonances exist. Recently, Fatemi *et al.* [10] observed optical Feshbach resonances in photoassociation spectroscopy. They used photoionization to probe optically induced changes in the scattering wave function. However, the direct influence of the optical Feshbach resonance on the atomic scattering properties was not studied.

In this Letter, we report a direct measurement of the atomic scattering length  $a$  in a BEC of <sup>87</sup>Rb  $|F = 1, m_F = -1\rangle$  as we cross an optical Feshbach resonance. With moderate laser intensities of about 500 W/cm<sup>2</sup>, we can change the scattering length over 1 order of magnitude from 10  $a_0$  to 190  $a_0$  ( $a_0 = 1$  Bohr radius).

To optically modify the scattering length, we use laser light tuned close to a photoassociation resonance which couples the continuum state of incoming free atoms to an excited molecular level (see inset in Fig. 1). This changes the wave function and consequently the scattering length of the scattering state. It also leads to atomic loss due to spontaneous decay via the molecular state. The resonant transition rate between the continuum state and the molecular state, which we denote  $\Gamma_{\text{stim}}$ , is proportional to the laser intensity. In our experiment,  $\Gamma_{\text{stim}}/2\pi$  is on the order of a few 10 kHz. This is 3 orders of magnitude less than the spontaneous decay rate  $\Gamma_{\text{spon}}$  from the excited molecular state. In [8], Bohn and Julienne give convenient expressions for the scattering length  $a$  and the inelastic collision rate coefficient  $K_{\text{inel}}$  which describes the photoassociation loss. For  $\Gamma_{\text{stim}} \ll \Gamma_{\text{spon}}$ , these expressions can

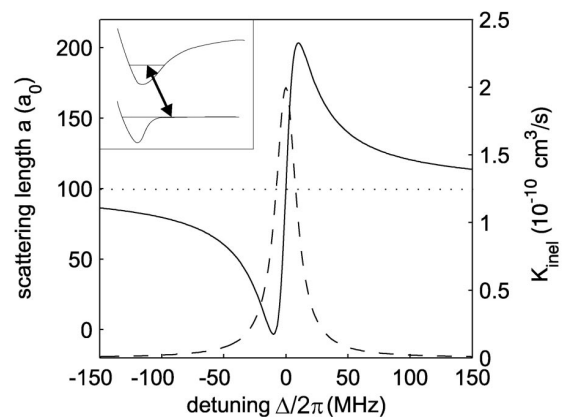


FIG. 1. Scattering length  $a$  (solid line) and inelastic collision rate coefficient  $K_{\text{inel}}$  (broken line) as a function of the laser detuning from the photoassociation resonance. The curves are based on Eqs. (1) and (2) for typical experimental parameters:  $\Gamma_{\text{stim}}/2\pi = 54\text{kHz}$ ,  $\Gamma_{\text{spon}}/2\pi = 20\text{MHz}$ ,  $k_i = 2.47 \times 10^5\text{m}^{-1}$ ,  $a_{\text{bg}} = 100a_0$  (dotted line). Inset: Scheme for optically coupling the scattering state with an excited molecular state.

be approximated and, for a condensate [11], read:

$$a = a_{\text{bg}} + \frac{1}{2k_i} \frac{\Gamma_{\text{stim}} \Delta}{\Delta^2 + (\Gamma_{\text{spon}}/2)^2} \quad (1)$$

$$K_{\text{inel}} = \frac{2\pi\hbar}{m} \frac{1}{k_i} \frac{\Gamma_{\text{stim}} \Gamma_{\text{spon}}}{\Delta^2 + (\Gamma_{\text{spon}}/2)^2} \quad (2)$$

where  $a_{\text{bg}}$  is the scattering length in the absence of light,  $\Delta$  is the detuning from the photoassociation line,  $m$  the atomic mass, and  $\hbar k_i$  the relative momentum of the collision. Figure 1 shows  $a$  and  $K_{\text{inel}}$  as functions of the detuning  $\Delta$  for typical experimental parameters. According to Eqs. (1) and (2), one should in general choose large detuning and strong coupling in order to maximize the change in scattering length while keeping the losses low.

Our experiments are carried out with an almost pure  $^{87}\text{Rb}$  condensate in the  $|F=1, m_F=-1\rangle$  spin state with typically  $1 \times 10^6$  atoms. The setup uses a magnetic transport scheme [12] to transfer atoms from a magneto-optical trap (MOT) chamber to a glass cell where the BEC is produced by rf-evaporation in a cigar shaped quadrupole and Ioffe configuration (QUIC) trap [13] with trap frequencies  $\omega_{\text{axial}}/2\pi = 15\text{Hz}$  and  $\omega_{\text{radial}}/2\pi = 150\text{Hz}$ . The intensity stabilized photoassociation laser beam ( $\approx 40\text{ mW}$ ) is derived from a Ti:Sa laser. It is aligned along the axial direction of the cigar shaped BEC and has a waist radius of  $76\ \mu\text{m}$ . Its linear polarization is perpendicular to the trapping magnetic bias field of 2 Gauss. In our experiments, we limit the maximum laser intensities to about  $500\text{ W/cm}^2$  because we observe the appearance of a growing component of thermal atoms for higher intensities. This effect is negligible for laser powers below  $500\text{ W/cm}^2$ .

In order to identify a suitable molecular level with strong coupling to the continuum state, we investigated molecular lines in the  $1_g$  and  $0_g^-$  potentials, which connect to the  $(S_{1/2} + P_{3/2})$  and  $(S_{1/2} + P_{1/2})$  asymptotes. We choose the excited state  $|0_g^-(\sim S_{1/2} + P_{3/2}), \nu=1, J=2\rangle$  which is located  $26.8\text{ cm}^{-1}$  below the  $D2$  line [14]. Figure 2 shows the corresponding photoassociation line together with the line for  $J=0$ . At a laser intensity of  $460\text{ W/cm}^2$ , the measured atom losses yield a peak inelastic collision rate  $K_{\text{inel}} = (2 \pm 1) \times 10^{-10}\text{ cm}^3/\text{s}$ , which is a factor of 5 weaker than  $K_{\text{inel}}$  in the example of [8]. Losses due to excitation of the  $D2$  line can be neglected. We observe a strong intensity dependent light shift of  $215\text{ MHz}/(\text{kW cm}^{-2})$  of the photoassociation line which might be mainly explained by coupling to a  $d$ -wave shape resonance [15].

Measuring the scattering length close to a photoassociation resonance requires a fast experimental method as atom losses restrict the observation time to below  $100\ \mu\text{s}$  in our experiments. Thus, the scattering length can neither be extracted from measurements of the collision rate

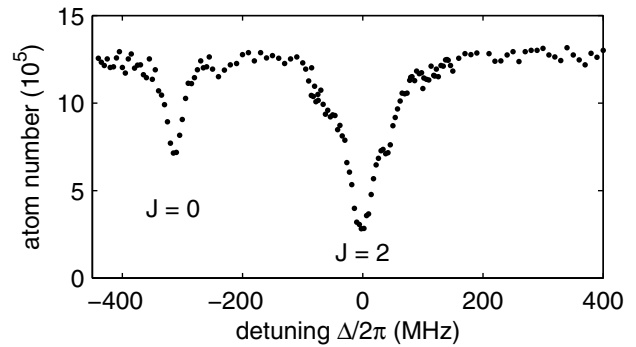


FIG. 2. Photoassociation spectrum of the excited molecular state used in the experiment. The two lines belong to the state  $|0_g^-(\sim S_{1/2} + P_{3/2}), \nu=1\rangle$  and have rotational quantum numbers  $J=0, 2$ , respectively. Shown is the remaining atom number after exposing a BEC to a  $70\ \mu\text{s}$  light pulse of  $460\text{ W/cm}^2$  intensity. The detuning is given relative to the  $J=2$  line. Each data point is an average of three measurements.

[4] nor from the mean-field energy in a condensate expansion [2], both of which require a few ms. Instead, we use Bragg spectroscopy [16] to determine the mean-field energy by imposing on the atoms a moving optical lattice composed of two counter-propagating laser beams with wave number  $k$  and an adjustable frequency difference  $\Delta f$ . The Bragg lattice transfers a momentum of  $2\hbar k$  to the atoms in a first order diffraction process. This is resonant when energy conservation is fulfilled, which for *noninteracting* atoms reads  $\hbar\Delta f_0 = (2\hbar k)^2/2m$ . For a condensate, however, the resonance frequency  $\Delta f_r$  is shifted by the mean-field energy. In the Thomas-Fermi approximation, this yields a value of

$$\Delta f_r = \Delta f_0 + \frac{8\hbar}{7m} n_0 a \quad (3)$$

where  $n_0$  denotes the atomic peak density [16]. Observing this shift of the Bragg resonance frequency therefore allows to measure the product of density and scattering length.

We derive the two Bragg beams from a laser which is  $1.4\text{ nm}$  blue detuned relative to the  $^{87}\text{Rb}$   $D2$  line. This determines  $\Delta f_0$  to be  $15.14\text{ kHz}$ . Two acousto-optical modulators are used to control the frequency difference  $\Delta f$  between the two counter-propagating beams. The beams have a diameter of  $\approx 900\ \mu\text{m}$  and are aligned along the radial trap axis in a horizontal direction. In our measurements, we apply a  $70\ \mu\text{s}$  square-pulse of Bragg light to the condensate. After  $12\text{ ms}$  of time of flight, when the momentum components of the condensate have spatially separated, we use absorption imaging to measure the portion of condensate atoms that have been diffracted. We always choose the intensity of the lattice such that about  $15\% - 20\%$  of the atoms are diffracted at resonance. Scanning  $\Delta f$  and determining the percentage

of diffracted atoms yields curves as shown in Fig. 3 from which we extract the resonance positions. Shining in a photoassociation laser pulse ( $70 \mu\text{s}$  square-pulse) at the same time as the Bragg pulse shifts the resonance position. This shift depends on the detuning  $\Delta$  from the molecular line (filled and open circles in Fig. 3).

For short illumination times  $T$  as in our experiment, the shape of the spectra fits well to the Fourier transform of the rectangular light pulse,  $\sin^2[\pi(\Delta f - \Delta f_r)T]/(\Delta f - \Delta f_r)^2$ , which we use to fit the data (see Fig. 3). Our measurements show that in spite of the Fourier-limited width of the Bragg resonance of 13 kHz (FWHM), we can resolve the peak position to better than  $\pm 100$  Hz.

When we invert the frequency difference of the Bragg laser beams and diffract atoms to a momentum state with  $-2\hbar k$  instead of  $+2\hbar k$ , we notice that the absolute value of the resonance frequency  $|\Delta f_r|$  changes. This can be explained by an initial condensate momentum of up to  $0.05 \hbar k$  which we find to slowly vary from day to day. This initial momentum is due to residual experimental imperfections like optical dipole forces of a slightly non-centered photoassociation beam. To eliminate this effect, we always measure  $\Delta f_r$  for  $+2\hbar k$  as well as for  $-2\hbar k$  and then take the difference.

Figure 4 shows the data we obtain from scanning the photoassociation laser over the optical resonance for a fixed laser intensity of  $460 \text{ W/cm}^2$ . The number of atoms in the condensate at the end of the laser pulse is plotted in Fig. 4(a) indicating the position of the molecular line. On resonance, about 90% of the atoms are lost after the  $70 \mu\text{s}$  of interaction time. Figure 4(b) shows the resonance frequency  $\Delta f_r$  for Bragg diffraction as a function of laser detuning  $\Delta$ . For large positive (and negative) detuning  $\Delta$ , the value of  $\Delta f_r$  agrees with

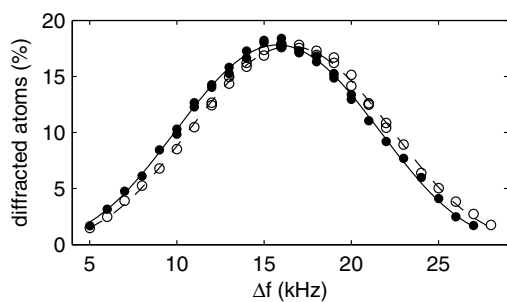


FIG. 3. Two Bragg resonance curves with an optically induced relative shift of 0.75 kHz. The percentage of the diffracted atoms is plotted against the frequency difference of the lattice beams. The two curves correspond to a detuning  $\Delta/2\pi = -47 \text{ MHz}$  (filled circles) and  $\Delta/2\pi = +47 \text{ MHz}$  (open circles) at a photoassociation laser intensity of  $460 \text{ W/cm}^2$ . The lines shown are fits to the data. For better comparison the right curve (open circles) has been scaled by a factor of 1.09 to the same height as the left one.

the 16.6 kHz expected from theory for the background scattering length  $a_{\text{bg}} = 100 a_0$  [17,18] and a BEC with  $\approx 8.2 \times 10^5$  atoms. As we tune across the molecular resonance, the measured resonance frequencies exhibit a distorted dispersive shape. Following Eq. (3), this is the result of the combination of two effects: first, the scattering length  $a$  varies with  $\Delta$  which alone should result in a dispersive line shape as in Fig. 1. Second, the atomic density  $n_0$  decreases due to photoassociation losses which would, if the scattering length was constant, result in a symmetrical dip for  $\Delta f_r$ . On the right-hand side of the resonance, these two effects nearly compensate each other whereas on the left-hand side, the effects add up to produce a prominent dip in  $\Delta f_r$ .

In order to extract the scattering length  $a$  from the measured frequencies one can, in a first approach, replace the dynamically changing density  $n_0$  in Eq. (3) by a time averaged value  $\langle n_0 \rangle_t$ . The average  $\langle n_0 \rangle_t$  can be derived from the rate equation for the local density  $\dot{n} = -2K_{\text{inel}}n^2$  [19] describing two-atom losses. This yields values for  $a$  which differ only marginally from the ones in Fig. 4(c). The data in Fig. 4(c) were obtained from a more

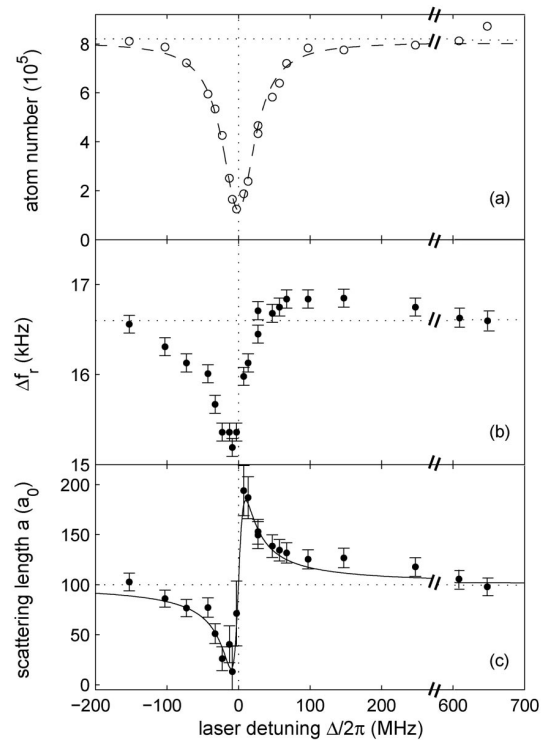


FIG. 4. Optical Feshbach resonance. In (a), the final atom number is plotted versus the detuning of the photoassociation laser (the dashed line is a Lorentz curve to guide the eye). The data in (b) display the measured Bragg resonance frequencies. In (c), the values for the scattering length obtained from the data in (a) and (b) are plotted. The continuous line is a fit of Eq. (1) to the data.

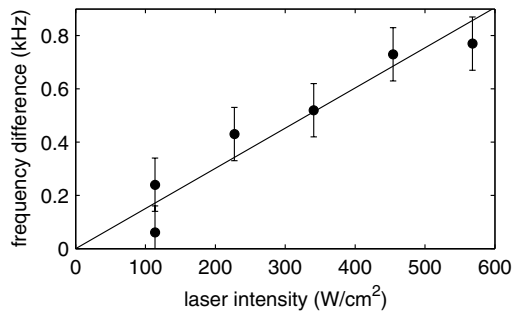


FIG. 5. Dependence of the optically induced mean-field shift on the laser intensity.

detailed examination which takes into account the full spatially resolved time evolution of the condensate density [20]. This includes the dynamical flattening of the condensate density profile caused by the rapid atom loss which is much faster than the trap frequencies [19]. Figure 4(c) shows that with a laser power of  $460 \text{ W/cm}^2$ , we can tune the scattering length over a range from  $10 a_0$  to  $190 a_0$ . A fit of Eq. (1) to these data for  $a$  yields a spontaneous decay width  $\Gamma_{\text{spont}}/2\pi$  of 20 MHz and a resonant inelastic collision rate coefficient  $K_{\text{inel}} = 1.7 \times 10^{-10} \text{ cm}^3/\text{s}$ . These values agree with those we obtain from atom loss measurements. Thus, our data consistently confirm the intrinsic relation between  $a$  and  $K_{\text{inel}}$  as expressed in Eqs. (1) and (2).

The measured width  $\Gamma_{\text{spont}}/2\pi$  of 20 MHz is larger than the expected molecular decay width of 12 MHz (corresponding to 2 times the atomic width). This might be explained by the line width of the Ti:Sa laser of about 4 MHz and a power broadening of the line due to different light shifts of unresolved molecular hyperfine states [18,19].

Figure 5 demonstrates the linear dependence of the scattering length  $a$  on the photoassociation laser intensity. For these measurements, we determine the Bragg resonance frequency for the detunings  $\Delta/2\pi \approx \pm 50 \text{ MHz}$  at various photoassociation laser intensities. This is slightly complicated by the light shift and broadening of the photoassociation line which lead to an uncertainty in  $\Delta/2\pi$  of  $\pm 10 \text{ MHz}$ . We keep the final atom number and density fixed by adjusting the pulse duration for each laser intensity. This ensures that only changes in  $a$  are reflected in the varying mean-field shift. In Fig. 5, we plot the frequency difference  $\Delta f(+50\text{MHz}) - \Delta f(-50\text{MHz})$  which increases our signal.

In conclusion, our experiments demonstrate the tunability of the scattering length in ultracold samples by optically coupling free atoms to a bound molecular state. Because of the exquisite control one has over laser fields,

we expect optical Feshbach resonances to be valuable when it comes to controlling atom-atom interactions in demanding applications. The inherent losses suggest the use of high laser intensities at large detuning and a good choice of the molecular state in order to optimize the ratio of change in scattering length and loss rate. Optical Feshbach tuning could be particularly useful to control atomic interactions in optical lattices which are discussed as potential future quantum information processors.

We thank Paul Julienne, Eite Tiesinga, John Bohn, Olivier Dulieu, Peter Fedichev, Andrea Micheli, and Helmut Ritsch for very helpful discussions. This work was supported by the Austrian Science Fund (FWF) within SFB 15 (project part 17) and by the European Union in the frame of the Cold Molecules TMR Network under Contract No. HPRN-CT-2002-00290.

---

\*Permanent address: Department of Physics, Bates College, Lewiston, ME 04240.

- [1] E. Tiesinga, B. J. Verhaar, and H. T. C. Stoof, *Phys. Rev. A* **47**, 4114 (1993).
- [2] S. Inouye *et al.*, *Nature (London)* **392**, 151 (1998).
- [3] Ph. Courteille *et al.*, *Phys. Rev. Lett.* **81**, 69 (1998).
- [4] J. L. Roberts *et al.*, *Phys. Rev. Lett.* **81**, 5109 (1998).
- [5] A. J. Moerdijk, B. J. Verhaar, and T. M. Nagtegaal, *Phys. Rev. A* **53**, 4343 (1996).
- [6] M. Marinescu and L. You, *Phys. Rev. Lett.* **81**, 4596 (1998).
- [7] P. Fedichev, Yu Kagan, G.V. Shlyapnikov, and J.T.M. Walraven, *Phys. Rev. Lett.* **77**, 2913 (1996).
- [8] J. Bohn and P.S. Julienne, *Phys. Rev. A* **56**, 1486 (1997).
- [9] V. Kokouline, J. Vala, and R. Kosloff, *J. Chem. Phys.* **114**, 3046 (2001).
- [10] F. K. Fatemi, K. M. Jones, and P. D. Lett, *Phys. Rev. Lett.* **85**, 4462 (2000).
- [11] For condensed atoms, the collision rate coefficient is only half of the coefficient for thermal atoms as all atoms share the same quantum state.
- [12] M. Greiner, I. Bloch, T.W. Hänsch, and T. Esslinger, *Phys. Rev. A* **63**, R031401 (2001).
- [13] T. Esslinger, I. Bloch, and T.W. Hänsch, *Phys. Rev. A* **58**, R2664 (1998).
- [14] A. Fioretti *et al.*, *Eur. Phys. J. D* **15**, 189 (2001).
- [15] A. Simoni, P.S. Julienne, E. Tiesinga, and C. J. Williams, *Phys. Rev. A* **66**, 063406 (2002).
- [16] J. Stenger *et al.*, *Phys. Rev. Lett.* **82**, 4569 (1999).
- [17] Eberhard Tiemann (private communication).
- [18] Paul Julienne and Eite Tiesinga (private communication).
- [19] C. McKenzie *et al.*, *Phys. Rev. Lett.* **88**, 120403 (2002).
- [20] This calculation is a simulation of the Rabi flopping between two levels corresponding to the condensate component at rest and the component with momentum  $2\hbar k$ . The changing density due to the loss is included by introducing a time dependent detuning.

## 4.6 “Inducing an optically induced Feshbach resonance via stimulated Raman coupling”

G. Thalhammer, M. Theis, K. Winkler, R. Grimm, and J. Hecker Denschlag

Phys. Rev. A **71**, 039902 (2005)



**Inducing an optical Feshbach resonance via stimulated Raman coupling**Gregor Thalhammer,<sup>1</sup> Matthias Theis,<sup>1</sup> Klaus Winkler,<sup>1</sup> Rudolf Grimm,<sup>1,2</sup> and Johannes Hecker Denschlag<sup>1</sup><sup>1</sup>*Institut für Experimentalphysik, Universität Innsbruck, Technikerstraße 25, 6020 Innsbruck, Austria*<sup>2</sup>*Institut für Quantenoptik und Quanteninformation, Österreichische Akademie der Wissenschaften, 6020 Innsbruck, Austria*

(Received 23 September 2004; published 8 March 2005; publisher error corrected 11 March 2005)

We demonstrate a method of inducing an optical Feshbach resonance based on a coherent free-bound stimulated Raman transition. In our experiment atoms in a <sup>87</sup>Rb Bose-Einstein condensate are exposed to two phase-locked Raman laser beams which couple pairs of colliding atoms to a molecular ground state. By controlling the power and relative detuning of the two laser beams, we can change the atomic scattering length considerably. The dependence of scattering length on these parameters is studied experimentally and modeled theoretically.

DOI: 10.1103/PhysRevA.71.033403

PACS number(s): 34.50.Rk, 32.80.Pj, 03.75.Nt, 34.20.Cf

**I. INTRODUCTION**

Feshbach resonances have become a central tool in the physics of ultracold quantum gases during the last years because they allow for a tuning of the interactions between atoms. Controlling interparticle interactions is a central key in many fields of modern physics and is especially relevant for future applications in quantum computation and exploring novel many-particle quantum effects. Beautiful experiments using magnetically tunable Feshbach resonances [1,2] have been performed, ranging from ultrahigh-resolution molecular spectroscopy [3] to the coherent coupling of atomic and molecular states [4] as well as the creation of bright matter wave solitons [5]. It also led to the production of new atomic [6] and molecular [7] Bose-Einstein condensates (BEC's) and allowed control of pairing in ultracold fermionic gases [8].

Recently we demonstrated how atom-atom interactions in a <sup>87</sup>Rb BEC can also be tuned with an optically induced Feshbach resonance [9] (see also [10]), a scheme which was originally proposed by Fedichev *et al.* [11,12]. Optically induced Feshbach resonances offer advantages over magnetically tuned Feshbach resonances since the intensity and detuning of optical fields can be rapidly changed. Furthermore, complex spatial intensity distributions can be easily produced and optical transitions are always available even when no magnetic Feshbach resonances exist. A disadvantage of optically induced Feshbach resonance is the inherent loss of atoms due to excitation and spontaneous decay of the molecular state [9]. Typical lifetimes for excited molecular states are on the order of 10 ns which corresponds to a linewidth of  $2\pi \times 16$  MHz. Evidently, coupling to molecular states with longer lifetime should improve the situation. Ground-state molecules are stable against radiative decay, and narrow transition linewidths on the order of kHz have been observed in two-photon Raman photoassociation [13,14]. This raises the question whether it is possible to create optical Feshbach resonances using stimulated Raman transitions and whether this scheme might be advantageous compared to the one-photon optical Feshbach resonance.

In this paper we indeed demonstrate that optical Feshbach resonances can be induced using a coherent two-color Ra-

man transition to a highly vibrationally excited molecular ground state in a <sup>87</sup>Rb BEC. In the experiment we show how the scattering length and loss rates can be tuned as a function of the intensity of the lasers and their detuning from molecular lines. We use Bragg spectroscopy [15] as a fast method to measure the scattering length in our sample [9]. To fit and analyze our data we use a model by Bohn and Julienne [16]. We find that using the Raman scheme for optically induced Feshbach resonances leads to similar results in tuning of the scattering length as for the single-photon Feshbach scheme. The Raman scheme does not lead to an improvement compared to the one-photon scheme because its atomic loss rate is not lower for a given change in scattering length. However, using a stimulated Raman transition does offer experimental advantages. To tune over the Feshbach resonance, the relative frequency of the two laser beams only has to be changed typically by several MHz which can be conveniently done using an acousto-optic modulator. This allows for very fast and precise control of the scattering length. On the other hand, working with a one-photon optical Feshbach resonance in the low-loss regime typically requires large detunings and scan ranges on the order of GHz. The Raman scheme relaxes the necessity for absolute frequency control of the lasers which can be tedious to maintain far away from atomic lines. Since off-resonant light fields in general lead to dipole forces acting on the atoms, a variation of the scattering length via optical tuning leads to a variation of the dipole forces on the atomic sample. This unwanted effect can be made negligible for the Raman scheme which tunes over resonance within a small frequency range.

The paper is organized as follows: We start in Sec. II by discussing the Raman scheme with a simple theoretical model. In Sec. III we describe in detail our experimental setup and the measurement method. In Sec. IV we discuss the experimental results which are compared with a theoretical model. The Appendix gives details of the model that is used to describe the data.

**II. RAMAN SCHEME FOR OPTICAL FESHBACH TUNING**

Before discussing optical Feshbach tuning based on a two-photon Raman transition, it is instructive to briefly recall

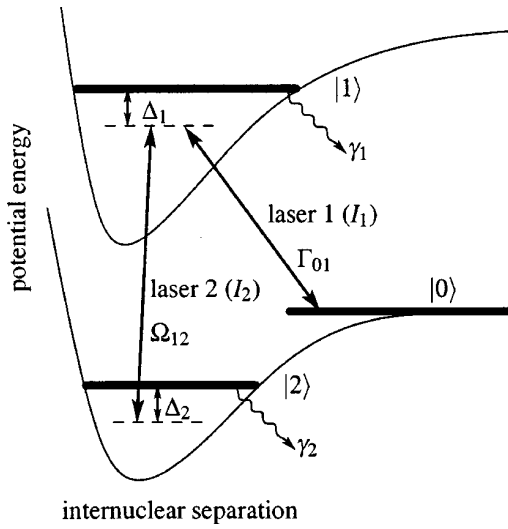


FIG. 1. Schematic diagram of the transitions used for optically coupling the collisional state  $|0\rangle$  to molecular states  $|1\rangle$  and  $|2\rangle$ .  $|1\rangle$  is electronically excited whereas  $|2\rangle$  is in the electronic ground state.  $\Delta_1$  and  $\Delta_2$  are defined to be positive for the shown configuration.

the one-photon scheme first [9,11,12]. This configuration uses a single laser beam tuned close to a transition from the scattering state of colliding atoms to a bound level in an excited molecular potential (states  $|0\rangle$  and  $|1\rangle$  in Fig. 1). Varying the detuning  $\Delta_1$  or the intensity  $I_1$  modifies the coupling and hence the scattering length. Atomic loss can occur through population of the electronically excited molecular state which has a decay width of  $\gamma_1$ .

Introducing a second laser as shown in Fig. 1 will now couple the collisional state  $|0\rangle$  to a bound level  $|2\rangle$  in the ground-state potential. As we will show, this allows for a tuning of the scattering length similar to the one-photon scheme. We now have, however, four parameters which can be used to influence the scattering length: the intensities  $I_1$  and  $I_2$  of lasers 1 and 2 and the detunings  $\Delta_1$  and  $\Delta_2$  as shown in Fig. 1.<sup>1</sup>

From [16] [Eqs. (4.8)–(4.11)] one can extract approximate expressions for the inelastic collision rate coefficient  $K_{\text{inel}}$  and the scattering length  $a$  in a Bose-Einstein condensate:<sup>2</sup>

$$K_{\text{inel}} = \frac{2\pi\hbar}{m} \frac{1}{k_i} \frac{\Gamma_{01}\gamma_1}{(\Delta_1 - \Omega_{12}^2/\Delta_2)^2 + (\gamma_1/2)^2}, \quad (1)$$

<sup>1</sup>As we observe a significant light shift of level  $|1\rangle$ , depending on the intensity  $I_1$  of laser 1 [9], we measure the detuning  $\Delta_1$  from the observed position of the one-photon line at a given intensity of laser 1. Note that  $\Delta_1$  is a one-photon detuning whereas  $\Delta_2$  is a two-photon detuning.

<sup>2</sup> $K_{\text{inel}}$  is reduced by a factor of 2 as compared to the case of thermal atoms. This is because in a BEC all atoms share the same quantum state.

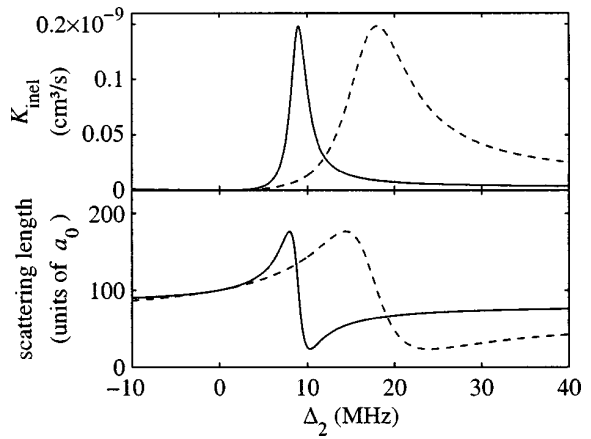


FIG. 2.  $K_{\text{inel}}$  and scattering length  $a$  according to Eqs. (1) and (2), plotted for two values of  $\Delta_1$ . Solid line:  $\Delta_1/2\pi=100$  MHz. Dashed line:  $\Delta_1/2\pi=50$  MHz. The other parameters are  $\Gamma_{01}/2\pi=50$  kHz,  $\Omega_{12}/2\pi=30$  MHz, and  $\gamma_1/2\pi=25$  MHz. The wave number  $k_i=2.5\times 10^5$  m<sup>-1</sup> corresponds to the finite size of the condensate wave function.  $a_0$  is the Bohr radius.

$$a = a_{\text{bg}} - \frac{1}{2k_i} \frac{\Gamma_{01}(\Delta_1 - \Omega_{12}^2/\Delta_2)}{(\Delta_1 - \Omega_{12}^2/\Delta_2)^2 + (\gamma_1/2)^2}. \quad (2)$$

Here  $\Gamma_{01}$  denotes the on-resonance stimulated transition rate from  $|0\rangle$  to  $|1\rangle$  which is proportional to  $I_1$ .  $\Omega_{12}$  is the Rabi frequency for the coupling of the states  $|1\rangle$  and  $|2\rangle$  and is proportional to  $\sqrt{I_2}$ .  $\hbar k_i$  is the relative momentum of the collision, where  $\hbar$  is Planck's constant divided by  $2\pi$ .  $a_{\text{bg}}$  is the background scattering length and  $m$  is the atomic mass.

Equations (1) and (2) neglect spontaneous decay from state  $|2\rangle$  ( $\gamma_2=0$ ) and assume  $\Gamma_{01}\ll\gamma_1$ . Setting  $\Omega_{12}=0$  yields the expressions for the one-photon Feshbach resonance as given in [9]. Equations (1) and (2) yield a Lorentzian and a corresponding dispersive line shape as a function of  $\Delta_1$ . In our experiments, however, we hold  $\Delta_1$  constant and scan  $\Delta_2$ . Figure 2 shows typical curves for  $K_{\text{inel}}$  and  $a$  for two detunings  $\Delta_1$ . The curves for  $K_{\text{inel}}$  are slightly asymmetric, but for  $\Delta_1\gg\Omega_{12}$  they can be well approximated by Lorentzians. This can be seen by expanding the denominator of Eq. (1) in terms of  $\Delta_2$  at the resonance position. A light shift displaces the position of the resonance to  $\Omega_{12}^2/\Delta_1$ . It is also interesting to note that the resonance width decreases with increasing detuning  $\Delta_1$  as  $\gamma_1(\Omega_{12}/\Delta_1)^2$ .

In a sense the two-photon Raman-Feshbach resonance can be coined in terms of a one-photon Feshbach scheme. The detuning  $\Delta_2$  effectively replaces the detuning  $\Delta_1$  of the one-photon Feshbach scheme.<sup>3</sup>

Since Eqs. (1) and (2) have exactly the same form as for the one-photon Feshbach resonance, it follows that, given a

<sup>3</sup>There is even a more direct way to understand the two-photon Feshbach resonance in terms of a one-photon Feshbach resonance. Laser 1 couples the collision state  $|0\rangle$  to a virtual level  $|2'\rangle$ , which is generated by laser 2 acting on level  $|2\rangle$ . The splitting between  $|2'\rangle$  and  $|1\rangle$  is given by  $\Delta_{2'}=\Delta_1-\Delta_2$ . Its linewidth is  $\gamma_1(\Omega_{12}/\Delta_{2'})^2$  and the transition rate  $\Gamma_{02'}=\Gamma_{01}(\Omega_{12}/\Delta_{2'})^2$ .

fixed free-bound transition rate  $\Gamma_{01}$ , the maximum tuning range of the scattering length for the two-photon case cannot be larger than in a one-photon scheme. Furthermore, given a fixed change in scattering length, the loss rate as determined by  $K_{\text{inel}}$  is not lower for the Raman scheme than for the one-photon scheme.

### III. EXPERIMENTAL SETUP AND METHODS

#### A. Production of BEC's

For the experiments we produce  $^{87}\text{Rb}$  BEC's of typically  $1.2 \times 10^6$  atoms in the spin state  $|F=1, m_F=-1\rangle$ . Our setup comprises a magnetic transfer line [17] to transport atoms from a magneto-optic trap (MOT) chamber to a glass cell where the BEC is produced and all experiments are carried out. In a first step about  $3 \times 10^9$  atoms are loaded within 4 s into a MOT directly from the background gas and are then cooled further to about 50  $\mu\text{K}$  in a molasses cooling phase. After optically pumping into the  $|F=1, m_F=-1\rangle$  state we load the atom cloud into a magnetic quadrupole trap with a gradient of 130 G/cm in the (strong) vertical direction. Within 1.4 s the atoms are then moved via a magnetic transfer line<sup>4</sup> over a distance of 48 cm including a 120° corner into a glass cell which is at a pressure below  $10^{-11}$  mbar. In this cell we finally load the cloud into a QUIC trap (a type of magnetic trap that incorporates the quadrupole and Ioffe configuration) [18], ending up with typically  $4 \times 10^8$  atoms at a temperature of about 250  $\mu\text{K}$ . All three coils of the QUIC trap are operated at a current of 40 A, dissipating 350 W. This results in trap frequencies of  $\omega_{\text{radial}}/2\pi=150$  Hz and  $\omega_{\text{axial}}/2\pi=15$  Hz at a magnetic bias field of 2 G. To achieve Bose-Einstein condensation we use forced radio-frequency evaporation for a period of 20 s. The stop frequency is chosen so that we end up with condensates with a thermal background of about 25% of noncondensed atoms. At this value we concurrently get the highest number of atoms in the condensate and good reproducibility. For our measurements we consider only the condensed atoms.

#### B. Raman lasers

To realize the Raman scheme shown in Fig. 1 we use the electronically excited molecular state  $|1\rangle=|0_g^-, \nu=1, J=2\rangle$  located  $26.8 \text{ cm}^{-1}$  below the  $(S_{1/2}+P_{3/2})$  dissociation asymptote [9,19]. About 290 MHz below the  $J=2$  line, there is another rotational level with  $J=0$ .<sup>5</sup> Although about 5 times weaker than the  $J=2$  line, its effect cannot be totally neglected in our experiment. We choose level  $|2\rangle$  to be the

<sup>4</sup>For our magnetic transport (similar to that described in [17]) 13 pairs of quadrupole coils are used. These transfer coils each have an inner diameter of 23.6 mm, an outer diameter of 65 mm, and a height of 5.7 mm and consist of 34 windings. They are arranged in two layers above and below the vacuum chamber with a separation of 50 mm. Peak currents of 75 A are necessary to maintain a vertical gradient of 130 G/cm during transfer.

<sup>5</sup>Due to different light shifts [9] for the  $J=0$  and  $J=2$  lines, their splitting is intensity dependent. The value of 290 MHz is valid for an intensity of 300 W/cm<sup>2</sup>.

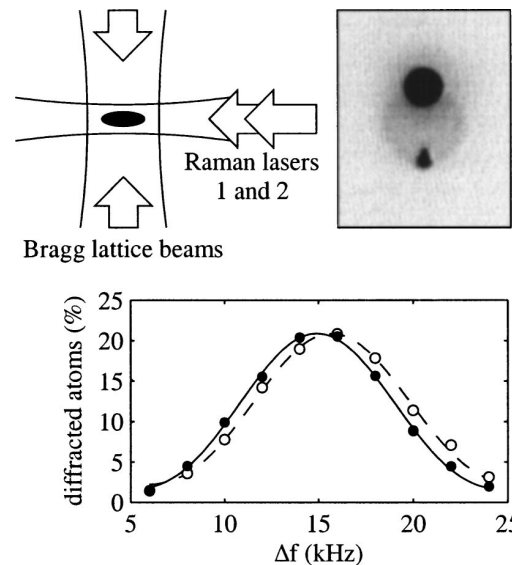


FIG. 3. Top left: experimental arrangement of the laser beams (top view). Top right: absorption image obtained after Bragg-diffracting a portion of the atoms to a state with a momentum of two photon recoils (lower atom cloud) and subsequent time of flight expansion. Bottom: Bragg resonance curves for two different relative detunings of the Raman lasers. The relative shift of 700 Hz is due to two different scattering lengths which are optically induced in the condensates. The atom numbers are the same for both curves. Shown is the percentage of diffracted atoms versus the frequency difference of the Bragg lattice beams. For better comparison we have scaled up the right curve by 10%.

second to last bound state in the ground-state potential. It has a binding energy of  $636 \text{ MHz} \times h$  [13] where  $h$  is Planck's constant.

The Raman laser beams are derived from a Ti:sapphire laser using an acousto-optical modulator at a center frequency of about 318 MHz in a double-pass configuration. This allows precise control of their relative frequency difference over several tens of MHz. Both Raman lasers propagate collinearly and are aligned along the weak axis of the magnetic trap (see Fig. 3). They have a  $1/e^2$  waist of 76  $\mu\text{m}$ , and their linear polarization is perpendicular to the magnetic bias field of the trap.

The Ti:sapphire laser is intensity stabilized and its frequency has a linewidth of about 3 MHz. In order to stabilize its frequency relative to the photoassociation lines, the laser is offset locked relative to the  $D_2$  line of atomic rubidium with the help of a scanning optical cavity. This yields an absolute frequency accuracy of better than 10 MHz. In all our experiments the Raman laser intensities were set to  $I_1=300 \text{ W/cm}^2$  and  $I_2=60 \text{ W/cm}^2$  at the location of the condensate, if not stated otherwise.

#### C. Bragg spectroscopy

To measure optically induced changes in the scattering length  $a$ , we use Bragg spectroscopy [9,15]. This method allows for a fast measurement on time scales below 100  $\mu\text{s}$  which is vital because of the rapid photoassociation losses

we experience in our experiments. A moving lattice composed of two counter propagating beams with wave number  $k$  and a frequency difference  $\Delta f$  is used to diffract some of the condensate atoms to a state with nonzero momentum. When energy and momentum conservation are fulfilled, the Bragg lattice resonantly transfers a momentum of two photon recoils  $2\hbar k$  in a first-order diffraction process. For the case of a homogeneous condensate of density  $n$ , the resonance energy for Bragg diffraction is given by the sum of transferred kinetic energy  $\hbar\Delta f_0 = (2\hbar k)^2/2m$  and the change in mean-field energy  $4\pi\hbar^2 na/m$ .<sup>6</sup> This corresponds to a frequency difference of the Bragg lasers of

$$\Delta f_r = \Delta f_0 + \frac{2\hbar}{m}na. \quad (3)$$

If the condensate is initially not at rest, the kinetic energy contribution  $\Delta f_0$  to the Bragg resonance frequency [Eq. (3)] contains an additional term  $2\hbar kp/m$ , where  $p$  is the initial atom momentum in the direction of the Bragg lattice. In our experiments we observe such a motional shift corresponding to condensate momentum of up to  $p=0.1\hbar k$ . This momentum can partly be attributed to optical dipole forces of Raman beams which are slightly noncentered on the condensate. Partly it can be attributed to a forced oscillation of the condensate in the magnetic trap at 150 Hz which coincides with the trapping frequency. Since this oscillation is driven by a higher harmonic of the line frequency (50 Hz), it is in phase with the line frequency and we are able to stabilize the initial condensate momentum by synchronizing the experiment to the line. A stable initial condensate momentum can then be determined and canceled out by measuring  $\Delta f_r$  alternately for Bragg diffraction to the  $+2\hbar k$  and  $-2\hbar k$  momentum components. After these measures we were left with a residual momentum noise level of up to  $p=0.01\hbar k$ .

In our setup the Bragg lattice beams are oriented along the horizontal direction perpendicular to the Raman laser beams (see Fig. 3) and have a width of  $\approx 0.9$  mm. We extract both beams from a single grating-stabilized diode laser and use two acousto-optical modulators to control the frequency difference. The laser is tuned 1.4 nm below the  $^{87}\text{Rb } D_2$  line which defines  $\Delta f_0$  in Eq. (3) to be 15.14 kHz. This frequency is much larger than the typical mean-field contribution,  $2\hbar na/m$ , which in our experiments was below 3 kHz.

We illuminate the trapped condensate for 100  $\mu\text{s}$  with the Bragg lattice light. After 12 ms of free expansion the diffracted atoms are spatially separated from the remaining atoms. Absorption imaging allows us to determine the diffraction efficiency. By adjusting the Bragg laser intensity (typically 1 mW) we keep the maximum diffraction efficiency between 15% and 20%. When we scan the frequency difference  $\Delta f$  and measure the fraction of Bragg-diffracted atoms we obtain curves as shown in Fig. 3 (bottom). These curves have a width of approximately 9 kHz as determined by the 100  $\mu\text{s}$  length of our Bragg pulses. The shape of the curves is given by the Fourier transform of our square light

pulses which we use to fit the data to obtain the resonance position  $\Delta f_r$  [9]. The shift between the two Bragg spectroscopy curves in Fig. 3 (bottom) is optically induced by shining in the Raman lasers at the same time as the Bragg lattice. For both curves the atom numbers are the same and  $\Delta_1 = 60$  MHz. Only the Raman detuning  $\Delta_2$  differs by 26 MHz. According to Eq. (3) this observed shift in Bragg resonance frequency is then due to a change in scattering length, induced by tuning  $\Delta_2$ . This demonstrates that we can tune the scattering length  $a$  with a Raman Feshbach resonance.

#### D. Determination of scattering length

We use Eq. (3) to determine the scattering length  $a$  from the measurements of the Bragg resonance frequency  $\Delta f_r$ . Equation (3), however, is derived for the case of a homogeneous condensate. Our trapped condensate, in contrast, which is subject to photoassociation losses, exhibits a time- and position-dependent density  $n$ . This can be taken into account by replacing the density  $n$  in Eq. (3) by an appropriate effective value  $\bar{n}$ .

A simple approach to estimate  $\bar{n}$  is to calculate the spatial and time average of the condensate density  $n$  over the duration of the Raman pulse length  $T$ . For this we use the rate equation for the local density  $\dot{n} = -2K_{\text{inel}}n^2$  for two-atom losses. The inelastic collision rate coefficient  $K_{\text{inel}}$  governing this process is obtained from measuring the atom number at the beginning and end of the light pulse. This procedure already yields good results which differ less than 10% from an improved approach which we use for our data analysis and which is explained in the following.

The improved approach consists of a full numerical simulation which describes Bragg diffraction in a dynamically and spatially resolved way. We divide the condensate into density classes and treat their time dependence individually. The Bragg diffraction process is identified as a Rabi oscillation between a coherent two level system—i.e., the BEC component at rest and the Bragg-diffracted component. The changing density of the condensate due to loss is reflected in a time-dependent resonance frequency [see Eq. (3)]. As a result of these calculations we obtain for each density class a Bragg resonance curve similar to the experimental ones shown in Fig. 3. Averaging over these resonance curves and determining the center position yields the simulated value for the Bragg resonance  $\Delta f_r$ . Using  $\Delta f_r = \Delta f_0 + 2\hbar\bar{n}a/m$  we can then determine the effective density  $\bar{n}$ .

## IV. RESULTS

### A. Raman scans

Figure 4 presents measurements where the detuning  $\Delta_1$  of laser 1 from the excited molecular state is set to  $\Delta_1/2\pi = 60$  MHz. The intensities of the Raman lasers 1 and 2 are 300 W/cm<sup>2</sup> and 60 W/cm<sup>2</sup>, respectively. Figure 4(a) shows the atom number after illuminating a condensate of initially  $1.4 \times 10^6$  atoms for 100  $\mu\text{s}$  with the Raman lasers. Scanning the Raman detuning  $\Delta_2$  we find a strong loss of atoms on resonance. As already expected from Eq. (1) the line shape is slightly asymmetric. Figure 4(b) shows the resonance fre-

<sup>6</sup>This is valid in the limit that only a small fraction of the condensate is diffracted.

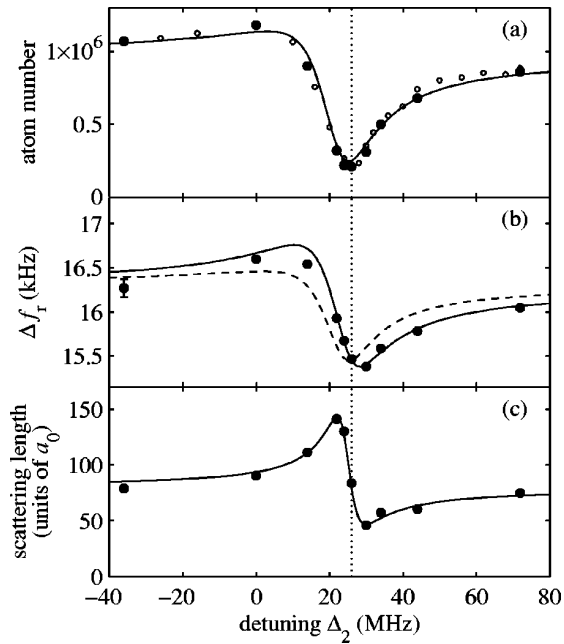


FIG. 4. Optical Feshbach resonance using a Raman scheme. (a) shows the measured atom number after the Raman pulse, (b) the measured Bragg resonance frequency, and (c) the scattering length, as determined from (a) and (b). In (a) the solid circles correspond to measurements where Bragg spectroscopy was used to determine the scattering length, while the small open circles stem from additional loss measurements without Bragg spectroscopy. From our measurements we estimate the uncertainty of the Bragg resonance frequency to be smaller than  $\pm 100$  Hz, as indicated by the error bar in (b). The solid lines in (a), (b), and (c) are from a model calculation (see the Appendix and text). The dashed line in (b) shows the expected signal if there was only loss in atom number but no change in scattering length (see also discussion in text). The vertical line indicates the location of maximal loss in (a) and helps to compare the relative positions of the three curves.

quency  $\Delta f_r$  as measured by Bragg spectroscopy. When we analyze the data in Figs. 4(a) and 4(b) with the improved procedure described in Sec. III D we obtain values for the scattering length which are shown in Fig. 4(c). The scattering length  $a$  shows a dispersive variation between  $50 a_0$  and  $140 a_0$  as we scan over the resonance. The dispersive scattering length curve is offset by about  $20 a_0$  from the background scattering length  $a_{bg} = 100 a_0$  for  $^{87}\text{Rb}$  in the  $|F=1, m_F=-1\rangle$  state [20–22]. This is due to the one-photon Feshbach tuning of laser 1, in agreement with our previous measurements [9].

We find that Eqs. (1) and (2) are not sufficient to describe these data properly, mainly because they neglect the decay rate  $\gamma_2$ . A more complete model (see the Appendix), also taking into account both the  $J=0$  and  $J=2$  rotational levels, was used for creating fit curves,<sup>7</sup> depicted as solid lines in Fig. 4. The fact that the data for atomic loss as well as for the scattering length  $a$  are both well described by the theoretical

<sup>7</sup>The resulting fit parameters are similar to those given in the Appendix.

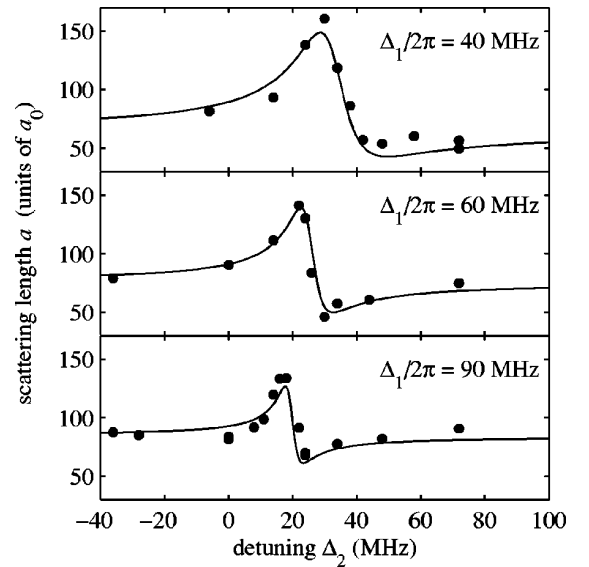


FIG. 5. Variation of the scattering length with Raman detuning for three various detunings  $\Delta_1$  from the excited molecular state. The solid line is a calculation (see the Appendix) which uses a single set of parameters for all curves.

curves is an intrinsic consistency check for our model and our data analysis.

The shape of the signal  $\Delta f_r$  in Fig. 4(b) is a combination of the effects of the varying scattering length  $a$  and the varying atom number [see Eq. (3)]. This is illustrated by the dashed and continuous lines in Fig. 4(b): The dashed line shows the expected signal if only the variations in atom number would occur and the scattering length stayed constant.<sup>8</sup> The solid line takes the variations in both atom number and scattering length into account. The deviation of the measured data points from the dashed line is due to an optical induced change of the scattering length.

## B. Dependence on detuning

We now investigate how detuning  $\Delta_1$  affects the scattering length  $a$ . Figure 5 shows a set of three curves showing the scattering length for detunings  $\Delta_1/2\pi = 40, 60,$  and  $90$  MHz.

The measurements clearly show that the position and width of the resonances depend on  $\Delta_1$ . The change in position can be mainly explained as light shifts of levels  $|1\rangle$  and  $|2\rangle$  due to laser 2. The decrease of the resonance width with increasing detuning  $\Delta_1$  follows directly our discussion in Sec. II. The solid lines are model calculations as described in detail in the Appendix. They are derived from a simultaneous fit to the data shown in Fig. 5 and a large number of atom loss measurements with different detunings (not shown). The set of fit parameters is listed in the Appendix. We also use this same set of parameters for the theoretical curves in Figs. 6 and 7.

<sup>8</sup>To account for the one-photon Feshbach tuning of laser 1, a value for the background scattering length  $a_{bg} = 80 a_0$  was used for the calculation.

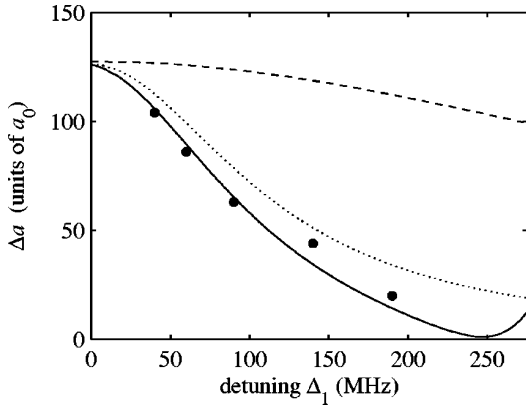


FIG. 6. Maximum variation in scattering length  $\Delta a = a_{\max} - a_{\min}$  versus one-photon detuning  $\Delta_1$ . Solid line: full model calculation (see the Appendix). Dotted line: three-level model (see Fig. 1), with  $\gamma_2/2\pi = 2$  MHz. Dashed line: three-level model, with  $\gamma_2/2\pi = 100$  kHz.

It is interesting to note from Fig. 5 that the amplitude of the dispersive scattering length signal decreases as  $\Delta_1$  becomes larger. This is not to be expected from the simple model Eqs. (1) and (2). To investigate this effect we have performed scans for atom loss and scattering length for several detunings  $\Delta_1$ . Figure 6 shows the maximum variation in scattering length,  $\Delta a = a_{\max} - a_{\min}$ , obtained for detunings  $\Delta_1$  ranging from 40 MHz to 200 MHz. Here,  $a_{\max}$  and  $a_{\min}$  are the maximal and minimal scattering length values for corresponding scan curves. Typical scan curves are shown in Fig. 5. Each data point in Fig. 6 was derived from a complete scan and corresponds to one day of data collection.

An analysis of our data using our theoretical model indicates that the decrease of  $\Delta a$  as a function of  $\Delta_1$  is a consequence of two effects.

(i) To properly model these measurements we have to assign to the molecular state  $|2\rangle$  in the ground-state potential

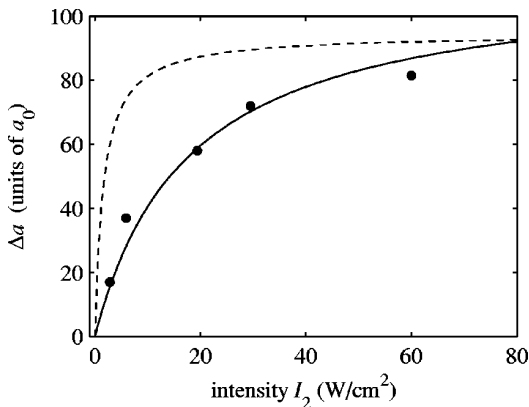


FIG. 7. Maximum variation in scattering length  $\Delta a = a_{\max} - a_{\min}$  versus  $I_2$ . For this data set  $I_1 = 300$  W/cm<sup>2</sup> and  $\Delta_1 = 60$  MHz. The solid line is a full model calculation (see the Appendix). The dashed line stems from the same model, but with  $\gamma_2/2\pi$  set to 100 kHz and is scaled by a factor of 0.84 for better comparison.

a non-negligible decay width  $\gamma_2/2\pi \approx 2$  MHz. For comparison, two calculations of a three-level model are plotted in Fig. 6. For small  $\gamma_2/2\pi = 100$  kHz (dashed line)  $\Delta a$  decreases only weakly. For  $\gamma_2/2\pi = 2$  MHz (dotted line) the theory fits the data much better. Such a large decay rate of a ground-state level is surprising. It seems too large to be explained purely by collisions. We find that the decay rate increases with the light intensity. At low light powers of a few W/cm<sup>2</sup> we have observed very narrow linewidths  $\gamma_2/2\pi$  on the order of a few kHz, similar to the values reported by [13,14]. The broadening of the molecular ground level could be due to coupling to excited molecular levels. We can exclude, however, from our experimental data that these levels are located within our experimental scanning range between the states  $|1\rangle$  and  $|3\rangle$ . This would lead to additional resonance features in the scattering length, absorption, and light shifts, which are inconsistent with our data. In contrast, our data indicate a relatively constant background loss rate of the ground level over the experimental scan range. This allows us to analyze the data successfully with our simple few-level model. Besides coupling to excited molecular states, we suspect that coupling to the  $d$ -wave shape resonance of the scattering channel also gives rise to a sizable contribution to the molecular decay rate. Because the  $d$ -wave shape resonance is located very close (a few MHz) to threshold, it is resonantly coupled to the molecular ground-state level via the Raman transition. To include the shape resonance is beyond the reach of our simple model and has to be investigated later.

(ii) The second reason for the decrease in  $\Delta a$  is a quantum interference effect involving both the  $J=2$  and  $J=0$  rotational levels as predicted by our model. At a detuning of  $\Delta_1/2\pi \approx 250$  MHz the interference effect leads to a complete disappearance of the optical Feshbach resonance. We observe this in a corresponding disappearance of the atom loss feature in our measurements (not shown). The interference effect alone—i.e., without a 2 MHz linewidth—is not sufficient to explain the experimental data in Fig. 6.

### C. Dependence on intensity

From the simple model Eq. (2) it is clear that the maximum variation in scattering length  $\Delta a$  is proportional to  $\Gamma_{01}$  and consequently scales linearly with the intensity  $I_1$  of laser 1. We have verified this dependence recently [9] for the case of a one-photon optical Feshbach resonance.

In contrast, the dependence of  $\Delta a$  on intensity  $I_2$  of laser 2 is not so trivial. According to the simple model, Eqs. (1) and (2), which neglects the decay rate  $\gamma_2$ , the maximum change  $\Delta a$  is independent of  $I_2$ . It is also clear, that for  $I_2 = 0$  we have  $\Delta a = 0$  since there is no dependence of scattering length on  $\Delta_2$  at all. This unphysical discontinuous behavior can be resolved if we introduce a finite decay rate  $\gamma_2 > 0$ . We then find that for increasing intensity  $I_2$ ,  $\Delta a$  rises monotonously from zero to a value where it saturates. We observe this general behavior in our measurements presented in Fig. 7. Our full model, as described in the Appendix, describes the measured data well if we set the decay rate to  $\gamma_2/2\pi = 2$  MHz (solid line). In contrast, the dashed line in Fig. 7 shows the calculation for the same model where  $\gamma_2$  is set to

$\gamma_2/2\pi=100$  kHz. Saturation then occurs at a much lower intensity  $I_2$  than for  $\gamma_2/2\pi=2$  MHz.

## V. CONCLUSION

Our experiments demonstrate the use of an optical Feshbach resonance for tuning of the scattering length via stimulated Raman coupling to a bound molecular state. Our results show that there is no advantage over a one-photon scheme when comparing tuning range and loss rate. However, for certain applications a Raman scheme is experimentally more favorable since it demands a lower tuning range of the lasers. Our presented theoretical model is in good agreement with our data and might be helpful when tailoring experimental parameters for a specific application. Furthermore, it gives insight into the process of creating stable ultracold molecules via two-photon photoassociation.

## ACKNOWLEDGMENTS

We appreciate the help of George Ruff and Michael Hellwig at an early stage of the experiment. We thank Paul Julienne, Eite Tiesinga, John Bohn, Olivier Dulieu, Peter Fedichev, Andrea Micheli, and Helmut Ritsch for valuable discussions. This work was supported by the Austrian Science Fund (FWF) within SFB 15 (project part 17) and the European Union in the frame of the Cold Molecules TMR Network under Contract No. HPRN-CT-2002-00290.

## APPENDIX: THEORETICAL MODEL AND FIT PARAMETERS

We use a theoretical model by Bohn and Julienne [16] to fit the data in Figs. 4–7. In the following we give a short summary of this model and present the procedure to calculate the scattering matrix  $S$ , the loss coefficient  $K_{\text{inel}}$ , and the scattering length  $a$ . The model has the advantage that it is concise and intuitive and it allows treatment of multilevel systems with several couplings between the levels. The numerical calculations involve simple manipulations of small matrices.

In Fig. 8 the level scheme for our two models involving four and six levels are shown. We first restrict our description to the four-level model as shown in the right part of Fig. 8. In this way our description stays compact and matrices are kept small. The extension to six or more levels follows the same scheme.

### Four-level model

Compared to Fig. 1 an additional excited level  $|3\rangle$  is added. This level corresponds to the rotational level  $J=0$  and lies 290 MHz below the  $J=2$  rotational level  $|1\rangle$  [9]. We work in the dressed atom picture and every level  $|i\rangle$  is attributed a detuning  $\Delta_i$  (see Fig. 8).  $\Delta_0$  is arbitrarily set to 0. The transition strengths from the continuum  $|0\rangle$  to levels  $|1\rangle$  and  $|3\rangle$  are described by stimulated rates  $\Gamma_{01}$  and  $\Gamma_{03}$  which are proportional to the intensity  $I_1$  of laser 1. The transitions between the bound levels  $|2\rangle$  and  $|1\rangle, |3\rangle$  are characterized by the Rabi frequencies  $\Omega_{12}$  and  $\Omega_{23}$ , respectively, which are

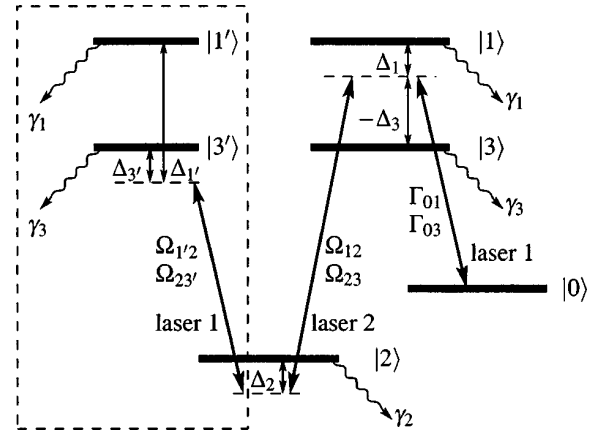


FIG. 8. Extended level scheme (compare to Fig. 1) for the four-level model (right-hand side) and its extension with six levels. State  $|3\rangle$  corresponds to the  $J=0$  level and lies 290 MHz below the  $J=2$  level  $|1\rangle$ . The four-level model is based on levels  $|0\rangle, |1\rangle, |2\rangle$ , and  $|3\rangle$ . The auxiliary levels  $|1'\rangle$  and  $|3'\rangle$  are introduced in the extended model to describe the coupling between  $|2\rangle$  and  $|1\rangle, |3\rangle$ , respectively, due to laser 1 (see text).

proportional to  $\sqrt{I_2}$ . Spontaneous decay from the bound levels leading to atomic losses is formally taken into account by introducing artificial levels  $|a_i\rangle$  for each level  $|i\rangle$  to which a transition at rate  $\gamma_i$  takes place (not shown in Fig. 8). All these couplings between different levels are summarized in the symmetric reaction matrix  $K$ . We arrange the level names in the order  $(0, a_1, a_2, a_3, 1, 2, 3)$  and use them as row and column indices. The nonzero matrix elements of the  $K$  matrix then read  $K_{01}=\sqrt{\Gamma_{01}}/2$ ,  $K_{03}=\sqrt{\Gamma_{03}}/2$ ,  $K_{ia_i}=\sqrt{\gamma_i}/2$ ,  $K_{12}=\Omega_{12}$ , and  $K_{23}=\Omega_{23}$ . Levels 0,  $a_1, a_2$ , and  $a_3$  are referred to as open channels, levels 1, 2, and 3 as closed channels. The reaction matrix  $K$  is partitioned into open and closed channel blocks,

$$K = \begin{pmatrix} \mathbf{0} & K^{\text{oc}} \\ K^{\text{co}} & K^{\text{cc}} \end{pmatrix}.$$

$K^{\text{oc}}$  reads in our case

$$K^{\text{oc}} = \begin{pmatrix} \sqrt{\Gamma_{01}}/2 & 0 & \sqrt{\Gamma_{03}}/2 \\ \sqrt{\gamma_1}/2 & 0 & 0 \\ 0 & \sqrt{\gamma_2}/2 & 0 \\ 0 & 0 & \sqrt{\gamma_3}/2 \end{pmatrix}.$$

$K^{\text{co}}$  is the transposed matrix of  $K^{\text{oc}}$  and

$$K^{\text{cc}} = \begin{pmatrix} 0 & \Omega_{12} & 0 \\ \Omega_{12} & 0 & \Omega_{23} \\ 0 & \Omega_{23} & 0 \end{pmatrix}.$$

From  $K$  the reduced  $K$  matrix

$$K^{\text{red}} = K^{\text{oc}}(D - K^{\text{cc}})^{-1}K^{\text{co}}$$

is calculated, eliminating the closed channels 1–3, where  $D$  denotes a diagonal matrix with diagonal elements

$(\Delta_1, \Delta_2, \Delta_3)$ . This determines the unitary  $4 \times 4$  scattering matrix  $S$ :

$$S = (\mathbf{1} + iK^{\text{red}})(\mathbf{1} - iK^{\text{red}})^{-1}.$$

From the matrix elements  $S_{ij}$  of  $S$  the trap loss coefficient  $K_{\text{inel}}$  is calculated by

$$K_{\text{inel}} = \frac{\pi\hbar}{\mu k_i} \sum_i |S_{0a_i}|^2 = \frac{\pi\hbar}{\mu k_i} (1 - |S_{00}|^2),$$

where  $\mu = m_{\text{Rb}}/2$  is the reduced Rb mass and  $\hbar k_i$  the relative momentum of the colliding atoms. The scattering length is obtained from  $S_{00}$  via

$$a = a_{\text{bg}} - \frac{1}{2k_i} \frac{\text{Im}(S_{00})}{\text{Re}(S_{00})},$$

where  $\text{Re}(S_{00})$  and  $\text{Im}(S_{00})$  denote the real and imaginary parts of  $S_{00}$ , respectively.

In the limit of small relative momentum  $\hbar k_i$  and small coupling strengths  $\Gamma_{0i} \ll \gamma_i$ ,  $K_{\text{inel}}$  and the light-induced change of the scattering length  $a - a_{\text{bg}}$  are independent of  $k_i$  because the  $\Gamma_{0i}$  are proportional to  $k_i$  (Wigner threshold regime) [16].

### Extension of the four-level model

The four-level model neglects that laser 1 (of which the intensity is typically 5 times greater than that of laser 2) also couples the levels  $|2\rangle$ - $|1\rangle$  and  $|2\rangle$ - $|3\rangle$ . However, this coupling should be taken into account since laser 1 is not far detuned from these transitions (see Fig. 8) due to the small binding energy of state  $|3\rangle$  ( $636 \text{ MHz} \times \hbar$ ) which is comparable to typical detunings  $\Delta_1$ . It mainly leads to broadening and light shifting of level  $|2\rangle$ . The additional coupling can approximately be taken care of by adding another two auxiliary levels  $|1'\rangle$  and  $|3'\rangle$  with detunings  $\Delta_{1'} = \Delta_1 + \Delta_2 + 2\pi \times 636 \text{ MHz}$  and  $\Delta_{3'} = \Delta_3 + \Delta_2 + 2\pi \times 636 \text{ MHz}$  as shown in Fig. 8. The coupling strengths  $\Omega_{1'2}$  and  $\Omega_{23'}$  are fixed by  $\Omega_{1'2} = \Omega_{12} \sqrt{I_1/I_2}$  and  $\Omega_{23'} = \Omega_{23} \sqrt{I_1/I_2}$ . Compared to the four-level model no new fit parameters are introduced. We can calculate  $K_{\text{inel}}$  and the scattering length  $a$  following the same recipe as for the four-level model, only with larger matrices. Fitting the data in Figs. 4–7 this extended model produced much better results than the four-level model. For completeness we give here the fit parameters which were used in the calculations in Figs. 5–7 ( $I_1 = 300 \text{ W/cm}^2$  and  $I_2 = 60 \text{ W/cm}^2$ ):  $\Gamma_{01}/2\pi = 42 \text{ kHz}$ ,  $\Gamma_{03}/2\pi = 8 \text{ kHz}$ ,  $\Omega_{12}/2\pi = 32 \text{ MHz}$ ,  $\Omega_{23}/2\pi = 12 \text{ MHz}$ ,  $\gamma_1/2\pi = 25 \text{ MHz}$ ,  $\gamma_3/2\pi = 22 \text{ MHz}$ , and  $\gamma_2/2\pi = 2 \text{ MHz}$ . We used  $k_i = 2.5 \times 10^{-5} \text{ m}^{-1}$ . Due to the limitations of our model, these fit parameters should not be mistaken as the true values of the corresponding physical quantities.

- 
- [1] E. Tiesinga, B. J. Verhaar, and H. T. C. Stoof, *Phys. Rev. A* **47**, 4114 (1993).
- [2] S. Inouye *et al.*, *Nature (London)* **392**, 151 (1998); Ph. Courteille, R. S. Freeland, D. J. Heinzen, F. A. van Abeelen, and B. J. Verhaar, *Phys. Rev. Lett.* **81**, 69 (1998); J. L. Roberts *et al.*, *ibid.* **81**, 5109 (1998).
- [3] C. Chin, V. Vuletic, A. J. Kerman, and S. Chu, *Phys. Rev. Lett.* **85**, 2717 (2000); A. Marte *et al.*, *ibid.* **89**, 283202 (2002).
- [4] E. A. Donley, N. R. Claussen, S. T. Thompson, and C. E. Wieman, *Nature (London)* **417**, 529 (2002).
- [5] L. Khaykovich *et al.*, *Science* **296**, 1290 (2002); K. E. Strecker, G. B. Partridge, A. G. Truscott, and R. G. Hulet, *Nature (London)* **417**, 150 (2002).
- [6] S. L. Cornish, N. R. Claussen, J. L. Roberts, E. A. Cornell, and C. E. Wieman, *Phys. Rev. Lett.* **85**, 1795 (2000); T. Weber, J. Herbig, M. Mark, H.-C. Nägerl, and R. Grimm, *Science* **299**, 232 (2003).
- [7] S. Jochim *et al.*, *Science* **302**, 2101 (2003); M. Greiner, C. A. Regal, and D. S. Jin, *Nature (London)* **426**, 537 (2003); M. Zwierlein *et al.*, *Phys. Rev. Lett.* **91**, 250401 (2003); T. Bourdel *et al.*, *ibid.* **93**, 050401 (2004).
- [8] C. A. Regal, M. Greiner, and D. S. Jin, *Phys. Rev. Lett.* **92**, 040403 (2004); M. W. Zwierlein *et al.*, *ibid.* **92**, 120403 (2004); C. Chin *et al.*, *Science* **305**, 1128 (2004).
- [9] M. Theis *et al.*, *Phys. Rev. Lett.* **93**, 123001 (2004).
- [10] F. K. Fatemi, K. M. Jones, and P. D. Lett, *Phys. Rev. Lett.* **85**, 4462 (2000).
- [11] P. O. Fedichev, Y. Kagan, G. V. Shlyapnikov, and J. T. M. Walraven, *Phys. Rev. Lett.* **77**, 2913 (1996).
- [12] J. L. Bohn and P. S. Julienne, *Phys. Rev. A* **56**, 1486 (1997).
- [13] R. Wynar, R. S. Freeland, D. J. Han, C. Ryu, and D. J. Heinzen, *Science* **287**, 1016 (2000).
- [14] T. Rom *et al.*, *Phys. Rev. Lett.* **93**, 073002 (2004); Ch. Lisdat, N. Vanhaecke, D. Comparat, and P. Pillet, *Eur. Phys. J. D* **21**, 299 (2002).
- [15] J. Stenger *et al.*, *Phys. Rev. Lett.* **82**, 4569 (1999).
- [16] J. L. Bohn and P. S. Julienne, *Phys. Rev. A* **60**, 414 (1999).
- [17] M. Greiner, I. Bloch, T. W. Hänsch, and T. Esslinger, *Phys. Rev. A* **63**, 031401 (2001).
- [18] T. Esslinger, I. Bloch, and T. W. Hänsch, *Phys. Rev. A* **58**, R2664 (1998).
- [19] A. Fioretti *et al.*, *Eur. Phys. J. D* **15**, 189 (2001).
- [20] E. Tiemann (private communication).
- [21] P. Julienne and E. Tiesinga (private communication).
- [22] P. S. Julienne, F. H. Mies, E. Tiesinga, and C. J. Williams, *Phys. Rev. Lett.* **78**, 1880 (1997).

# Chapter 5

## Converting atoms into ultracold molecules

With the success of the field of ultracold atomic gases came the quest for ultracold molecules (for a review see [Bah00, Mas01, Den04]). Molecules are interesting to work with, since in contrast to atoms, they exhibit vibrational and rotational degrees of freedom and thus offer potentially more possibilities for manipulation. One future goal is to gain full control over their quantum mechanical molecular state and to establish a *molecular* optics in the style of today's atom optics. Ultracold molecules will be useful for high precision spectroscopy and the search of a permanent electric dipole moment [Hud02]. Further, cold collisions between molecules can be studied. Controlling the association and dissociation of molecules could lead to a novel kind of coherent chemistry where quantum statistics and Bose-enhancement play an important role. As we will elaborate in chapter 6, binary molecules consisting of fermionic atoms are especially interesting to study due to their connection to high  $T_c$  superconductivity and Cooper pairing.

In contrast to atoms, laser cooling does not work for molecules in general due to the absence of closed optical transition schemes. For trapping and cooling molecules, buffer gas cooling in a magnetic trap [Wei98] and electrostatic deceleration and trapping [Bet99, Bet00] have been developed. Other methods, which recently have turned out to be particularly successful, synthesize the molecules from a gas of ultracold atoms. One method uses optical light fields to photoassociate a pair of atoms. A second method makes use of a Feshbach resonance to fuse atoms together either by slowly sweeping over the resonance or via three body recombination. The Feshbach resonance method has rapidly developed over the last two years and recently lead to the production of the first molecular BECs [Joc04, Gre03, Zwi03, Bou04]. In the following, recent experiments on the production of ultracold molecules

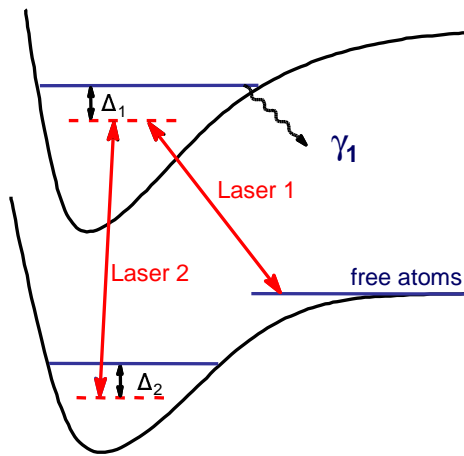


Figure 5.1: Ultracold molecules can be formed from an ultracold gas of atoms via photoassociation. With a one-photon transition (only laser 1), excited molecular states are formed with a short lifetime of typically a few ns. A two-color stimulated Raman transition can be used to create ground state molecules.

with Feshbach resonances and photoassociation will be discussed in detail.

## 5.1 Photoassociation

Photoassociation was first proposed in 1987 by Julienne *et al.* [Tho87, Ban95]. A scattering state of two atoms is optically excited in a free-bound transition to a molecular bound state (see Fig. 5.1). In the following years, a number of experimental groups around the world developed photoassociation into a spectroscopy tool to investigate molecular potentials and precisely locate their bound levels (for a review see [Wei99]). Photoassociation can be carried out in a one-color or a two-color scheme (see Fig. 5.1). In the one color scheme, excited molecules are formed which typically decay within a few ns of lifetime into free atom pairs or a range of different ground state molecules. In the two-color scheme ground state molecules in specific ro-vibrational states can be formed by using a stimulated Raman transition.

### One-color photoassociation

In 1998 the first detection of photoassociated molecules was reported [Fio98, Tak98, Nik99]. In these experiments, one-color photoassociation in a laser

cooled gas of alkali atoms produced molecules in an excited state which afterwards spontaneously decayed to molecular ground state levels. These ground state molecules were then detected via photoionization.

One main purpose of our one-color photoassociation experiment with a sodium condensate at NIST [McK02] was to investigate how fast a BEC of atoms can be converted into molecules. In a semi-classical theory that is commonly applied to collisions of laser-cooled atoms, the photoassociation time scale  $\tau$  is given by  $1/\tau = n\sigma v$ . Here,  $n$  is the density,  $v$  is the relative velocity of the atoms and  $\sigma$  is the reaction cross section which can be approximated by  $\pi R_c^2$  where  $R_c$  is the Condon radius. Interestingly, the maximum photoassociation rate from these considerations is several orders of magnitude slower than what we observed in our measurements where we could convert the BEC into molecules within a few  $\mu\text{s}$ . Beyond the semi-classical theory there is a unitary quantum limit for the conversion rate which we could not reach in our experiments due to the limitations of our laser intensity. This unitarity regime was later reached in measurements by Hulet's group when photoassociating a degenerate gas of  $^7\text{Li}$ . Their experimental findings agree well with the theoretical predictions [Pro03].

## Two-color photoassociation

Using a two-color photoassociation scheme (see Fig. 5.1) for the production of ultracold molecules has several interesting aspects. It allows for the production of stable *ground state* molecules in a specific quantum state with well-defined vibrational and rotational quantum numbers. The stimulated Raman transition also leads to a *coherent* coupling between atoms and molecules. This has given rise to quite a number of theoretical papers predicting Rabi flopping between an atomic BEC and a molecular BEC [Hei00], stimulated Raman adiabatic passage (STIRAP) for efficient conversion of an atomic BEC into a molecular BEC (for a selection of papers see [Mac04, Jul98, Var97, Dru02]) and superchemistry (see for example [Hei00, Moo02, Hop01]).

In 2000 Heinzen's group reported the production of  $\text{Rb}_2$  molecules out of an atomic Rb condensate using a free-bound stimulated optical Raman transition [Wyn00]. The presence of the molecules was inferred from the narrow kHz linewidth of the transition corresponding to molecular lifetimes on the order of 1 ms. Similar results were also observed in other groups afterwards, e.g. [Tol01, Rom04].

A recent experiment with a  $^{87}\text{Rb}$  BEC in our group [Win05] adds a new twist to this line of research. Using an experimental setup very similar to the one of D. Heinzen's group, we observe a narrow electromagnetically in-

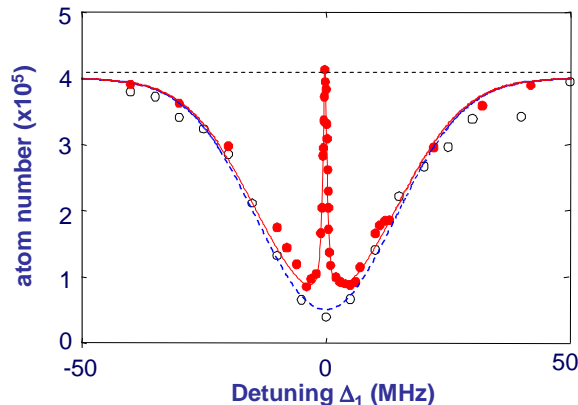


Figure 5.2: Observation of an atom-molecule dark state. Shown is a photoassociation line where laser 1 (see Fig. 5.1) is scanned over an the excited molecular state (dotted line, empty circles). In the presence of laser 2 which resonantly couples a molecular ground state level with the excited level, the photoassociation is dramatically reduced on resonance (full line, filled circles).

duced transparency (EIT) line in our photoassociation spectra (see Fig. 5.2). This line corresponds to a novel dark state <sup>1</sup>, a coherent superposition of the atomic BEC and a degenerate gas of Rb<sub>2</sub> ground state molecules. The superposition state decouples from the light field and leads to a striking suppression of photoassociation loss.

This dark state represents a very useful tool since from its mere observation we can directly conclude on 1) the presence of the molecules 2) the coherence between atoms and molecules, and 3) the quantum degeneracy of the molecular gas since it is coherently coupled to a BEC of atoms. From our measurements we can deduce that up to 100 Rb<sub>2</sub> molecules exist in our Rb condensate of about  $5 \times 10^5$  atoms. We find that our ground state molecules exhibit relatively short lifetimes due to laser induced decay. Currently, this puts practical constraints on efficient conversion of the atomic BEC into molecules. However, an increase of the number of molecules by several orders of magnitude should be possible by choosing better suited molecular states. With the dark resonance as an analysis tool, we will be able to conveniently optimize the conversion of atoms into molecules in the future.

---

<sup>1</sup>Dark states were first observed in atom spectroscopy [Ari76].

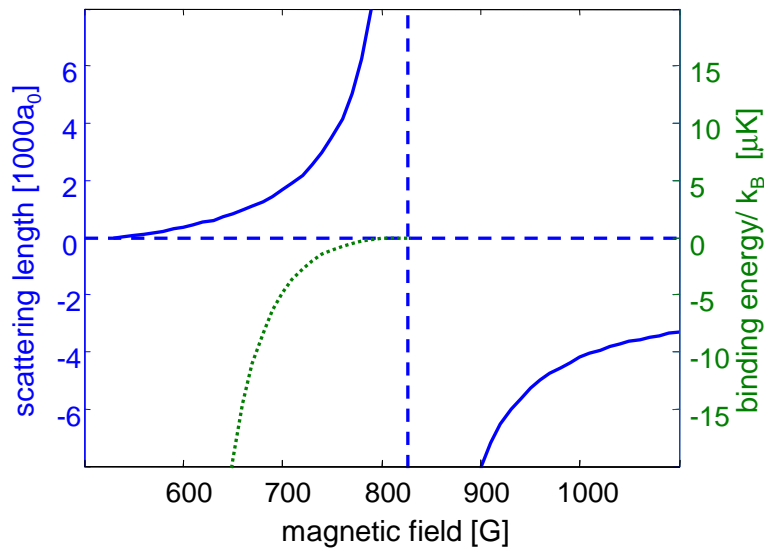


Figure 5.3: Scattering length (full line) and molecular binding energy for the weakly bound molecular state (dotted line) at the broad Feshbach resonance for fermionic  ${}^6\text{Li}$ . The binding energy vanishes quadratically as the resonance position (834 G) is approached. Above the resonance where the scattering length is negative, no weakly bound molecular state exists.

## 5.2 Producing molecules with Feshbach resonances

Using magnetically tunable Feshbach resonances for the production of molecules has proven to be very successful and already has led to a number of scientific breakthroughs. The generic feature behind this production method is the existence of a weakly bound molecular state on one side of the Feshbach resonance where the scattering length is positive (see Fig. 5.3). The binding energy of this molecular state vanishes quadratically as the Feshbach resonance position is approached. On the side with negative scattering length, no weakly bound state exists. Molecules are then produced either by sweeping over the resonance or by three-body recombination on the side of the Feshbach resonance with positive scattering length.

### Sweeping over the Feshbach resonance

The conversion of the atoms into molecules via sweeping can be qualitatively understood from Fig. 5.3. One starts with a degenerate gas of atoms in

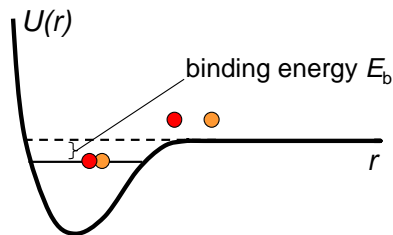


Figure 5.4: In three-body recombination close to the Feshbach resonance, the weakly bound molecular state is populated. In this process the binding energy  $E_b$  is released.

the quantum mechanical ground state on the side of the Feshbach resonance where the scattering length is negative. By adiabatically sweeping over the Feshbach resonance the quantum degenerate gas should stay energetically in the lowest state which, on the left hand side of the resonance, is clearly the molecular state. A more precise theoretical picture is given by Julienne *et al.* in [Jul04]. An early sweep experiment was performed in 2002 [Don02] with a  $^{85}\text{Rb}$  BEC where also coherences between atoms and molecules were observed. In the following year a wave of reports on molecule formation via sweeping were published from various groups. Molecules were produced in fermionic gases [Reg03, Str03, Cub03] and from bosonic BECs [Her03, Xu03, Dur04]. Recent studies [Hod05] show that the conversion efficiency is determined by the phase space density of the atomic cloud. Furthermore, in non-adiabatic sweeps the molecule conversion efficiency follows a Landau-Zener model.

### Three-body recombination

In our  $^6\text{Li}$  experiment we used three-body recombination in the vicinity of a Feshbach resonance to produce  $\text{Li}_2$  molecules [Joc03b]. This production method proved to be quite simple, efficient and robust and was also used by Ketterle's group [Zwi03]. In a collision of three atoms, two atoms in different spin states combine to form a molecule, whereas the third atom takes care of momentum and energy conservation. During this process the binding energy of the weakly bound molecule is released (see Fig. 5.4) and heats the sample. By tuning to the appropriate magnetic field, we chose this binding energy to be in the  $k_B \times \mu\text{K}$  range which corresponds roughly to the temperature of our atomic sample. Thus the release energy was comparatively small and could efficiently be removed by evaporative cooling.

The association process can also run backwards, dissociating a molecule

in a collision. Left alone for some time, the mix of atoms and molecules will establish a thermodynamic equilibrium which depends on the temperature and the the binding energy of the molecule [Chi04b]. The Boltzmann factor  $\exp(-E_b/k_bT)$  favors occupation of the molecular level, so that by constantly lowering the temperature the gas can be fully converted into molecules [Joc03a]. In order to clean our gas of molecules from the last remaining impurity atoms, we applied a Stern-Gerlach purification scheme [Joc03a]. A magnetic field gradient separated the atoms from the molecules due to their different magnetic momenta.

At the time of our experiments it came as a great surprise when we observed the very long lifetime of the  $\text{Li}_2$  molecules. Close to the Feshbach resonance the molecules lived for many seconds [Joc03a, Cub03, Str03]. This stood in strong contrast to previous experiments with molecules made from bosons where lifetimes were in the ms range for typical condensate densities of  $10^{14}/\text{cm}^2$ . Inelastic collisions between the boson-molecules lead to relaxation of the highly excited vibrational molecular state to lower vibrational states. The release of the corresponding energy induces particle loss. The puzzle for the stability of the ‘Fermi’-molecules was explained by Petrov *et al.* [Pet04] as a Pauli blocking effect. In order for the molecules to relax to lower vibrational states at least three fermionic constituents have to approach each other very closely in a collision. Since two of those atoms are identical in a two component gas, this collision is strongly suppressed.

The long lifetime of the Fermi-molecules finally cleared the road for the first BEC of molecules as discussed in chapter 6.



### 5.3 “Photoassociation of Sodium in a Bose-Einstein Condensate”

C. McKenzie, J. Hecker Denschlag, H. Häffner, A. Browaeys, L. E. E. de Araujo, F. K. Fatemi, K. M. Jones, J. E. Simsarian, D. Cho, A. Simoni, E. Tiesinga, P. S. Julienne, K. Helmerson, P. D. Lett, S. L. Rolston, and W. D. Phillips

Phys. Rev. Lett. **88**, 120403 (2002)



## Photoassociation of Sodium in a Bose-Einstein Condensate

C. McKenzie, J. Hecker Denschlag,\* H. Häffner,\* A. Browaeys, Luís E. E. de Araujo,† F. K. Fatemi,‡ K. M. Jones,§ J. E. Simsarian,|| D. Cho,¶ A. Simoni,\*\* E. Tiesinga, P. S. Julienne, K. Helmerson, P. D. Lett, S. L. Rolston, and W. D. Phillips

*National Institute of Standards and Technology, Gaithersburg, Maryland 20899*

(Received 27 November 2001; published 7 March 2002)

We form ultracold  $\text{Na}_2$  molecules by single-photon photoassociation of a Bose-Einstein condensate, measuring the photoassociation rate, linewidth, and light shift of the  $J = 1$ ,  $v = 135$  vibrational level of the  $A^1\Sigma_u^+$  molecular state. The photoassociation rate constant increases linearly with intensity, even where it is predicted that many-body effects might limit the rate. Our observations are in good agreement with a two-body theory having no free parameters.

DOI: 10.1103/PhysRevLett.88.120403

PACS numbers: 03.75.Fi, 33.20.Kf, 33.70.Jg, 34.20.Cf

Bose-Einstein condensates (BECs) of atomic gases [1,2] are versatile systems for the study of quantum behavior. Of particular interest are the suggestions for the coherent coupling of a BEC of atoms with a BEC of molecules [3–6] and the possibility of creating entangled atoms via coupling with molecular levels [7]. Photoassociation processes using stimulated Raman transitions have formed ground state molecules from ground state atoms in a BEC [8,9], but at very low rates. Here we explore the fundamental upper limits of molecule formation by making them at high rates using the elementary process of single-photon photoassociation.

In single-photon photoassociation, two atoms collide in the presence of a light field and form an excited state molecule. Photoassociative spectroscopy is used extensively to study collisions between laser-cooled atoms [10]. Photoassociation in a BEC presents quite a different regime: The collision energies are orders of magnitude lower than in a laser-cooled sample (the de Broglie wavelength is as big as the sample) and the densities are higher. This puts us in a regime where many-body effects may be important.

We concentrate on a particular photoassociation transition and measure the photoassociation spectra for various intensities and durations of the light pulse. From these, we determine the photoassociation rate, line shape, and the shift of the resonance. Finally, we examine various limits on the photoassociation rate.

Figure 1 shows the photoassociation process. The molecular level chosen for study is the  $J = 1$ ,  $v = 135$ , rotational-vibrational level of the  $A^1\Sigma_u^+$   $\text{Na}_2$  molecular state, excited from free atoms by a laser frequency of  $16913.37(2) \text{ cm}^{-1}$  [11]. We chose this level because its detuning from the  $D_1$  resonance is far enough ( $43 \text{ cm}^{-1}$ ) for atomic absorption to be negligible and because our experiments in a magneto-optical trap indicated a high photoassociation rate. The lifetime of our excited molecules is about 8.6 ns. The immediate decay of excited molecules into hot atoms or ground state molecules constitutes loss from the condensate. This loss is how we detect photoassociation.

We prepare an almost pure condensate of  $N \approx 4 \times 10^6$  sodium atoms in the  $|F = 1, m_F = -1\rangle$  ground state with a peak density of  $n_0 \approx 4 \times 10^{14} \text{ cm}^{-3}$ . The condensate is held in an anisotropic time-averaged orbiting potential (TOP) [12] magnetic trap with oscillation frequencies of  $\omega_x/\sqrt{2} = \omega_y = \sqrt{2} \omega_z = 2\pi \times 198 \text{ Hz}$  and corresponding Thomas-Fermi radii of  $\sqrt{2} r_x = r_y = r_z/\sqrt{2} = 15 \mu\text{m}$ .

To induce photoassociation, we illuminate the BEC with a Gaussian laser beam focused to  $120 \mu\text{m}$  FWHM at the condensate. The peak intensity is varied from 50 to  $1200 \text{ W cm}^{-2}$ . The polarization is linear and parallel with the rotation ( $z$ ) axis of the TOP trap bias field. The light is applied as a square pulse for between 10 and  $400 \mu\text{s}$  with rise and fall times less than  $0.5 \mu\text{s}$ .

The condensate number is measured using phase contrast imaging [13], taking two images before and two images after the photoassociation pulse to determine loss. The imaging occurs at 40 ms intervals using a  $100 \mu\text{s}$

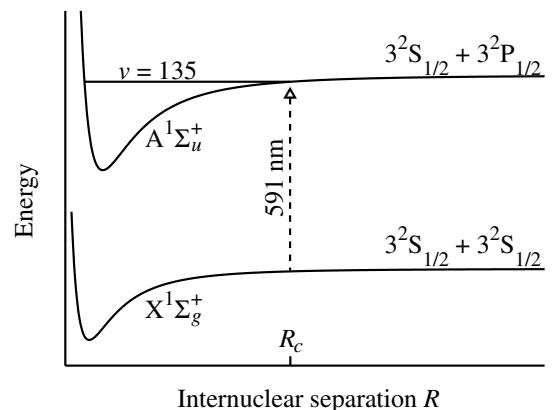


FIG. 1. The two-atom potentials for the ground state and the excited state used for photoassociation. The atoms are initially unbound and on the ground state asymptote and are excited into the  $J = 1$ ,  $v = 135$  level. From there they decay and are lost from the condensate.  $R_C = 2.0 \text{ nm}$  is the Condon radius, the internuclear separation where the energy of a resonant photon matches the difference between the potentials.

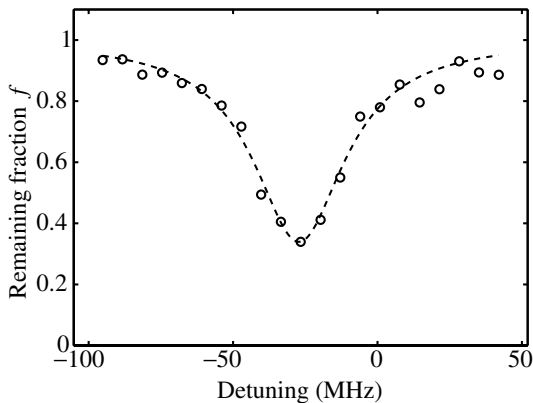


FIG. 2. A typical photoassociation loss spectrum. A  $140 \text{ W cm}^{-2}$  pulse was applied for  $100 \mu\text{s}$ . The dotted line is a fit to Eq. (2). The uncertainty in the frequency for each point is 5 MHz.

probe pulse from a laser tuned 1.78 GHz to the red of the  $3S_{1/2}, F = 1 \rightarrow 3P_{3/2}, F = 2$  transition. The imaging rate is limited by the readout time of our camera. The photoassociation pulse begins halfway between the second and the third images. We use multiple imaging pulses to improve statistics and to partially correct for small losses other than those due to the photoassociation pulse. These losses are typically 4% between images, most likely due to three-body losses and the imaging light. Once the number of atoms is extracted from the images [14], we calculate  $f$ , the fraction of atoms remaining after the photoassociation pulse.

Figure 2 shows a typical photoassociation spectrum. Each point represents a freshly prepared condensate. We use a Fabry-Perot etalon and a reference laser locked to an atomic Na line to measure differences in the photoassociation frequency with a precision of 5 MHz. The laser linewidth is  $<3$  MHz. All detunings quoted are relative to the center of the photoassociation line in the low intensity limit. For small trap loss, we expect the line to

$$f(\eta) = \frac{15}{2} \eta^{-5/2} \left\{ \eta^{1/2} + \frac{1}{3} \eta^{3/2} - (1 + \eta)^{1/2} \tanh^{-1} \left[ \sqrt{\eta/(1 + \eta)} \right] \right\}, \quad (2)$$

where  $\eta = K(I, \omega)n(0, \mathbf{0})t = K_m(I)n(0, \mathbf{0})t/(1 + \{2[\omega - \omega_0(I)]/\gamma(I)\}^2)$ . We use a three parameter fit of Eq. (2) to the spectra to extract the on-resonance rate constant  $K_m(I)$ , effective linewidth  $\gamma(I)$ , and central frequency  $\omega_0(I)$  (for example, the dotted line in Fig. 2). The fit is good. To further verify Eq. (2), we plot the measured  $1 - f$  as a function of pulse length for  $I = 140 \text{ W cm}^{-2}$  and  $\omega = \omega_0$ , along with a one parameter ( $K_m$ ) fit to the data (Fig. 3). The fitting uncertainties are indicated.

By fitting spectra obtained at various intensities, we measure  $K_m(I)$ ,  $\gamma(I)$ , and  $\omega_0(I)$ . Following [16] we calculate the unbroadened molecular linewidth of the chosen state to be  $\gamma_0/2\pi = 18.5$  MHz (nearly twice the atomic linewidth). This is in good agreement with the mea-

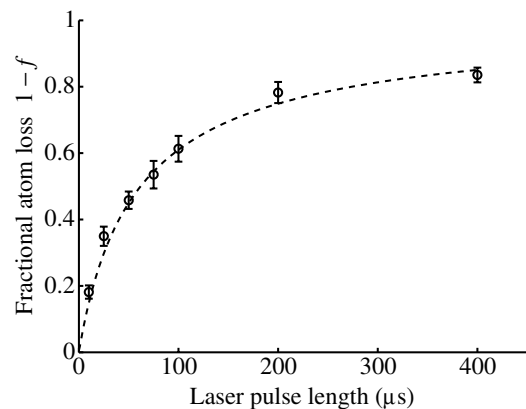


FIG. 3. The dependence of the maximum condensate loss on the photoassociation pulse length for  $I = 140 \text{ W cm}^{-2}$ ; the curve is a fit of Eq. (2).

be Lorentzian (in contrast to photoassociation lines in an uncondensed thermal sample where the kinetic energy distribution distorts the line shape [15]). For significant trap loss, as in Fig. 2, one must account for the change of the density profile during the photoassociation pulse.

The two-body photoassociation process changes the local atomic density as  $\dot{n}(t, \mathbf{r}) = -K(I, \omega)n^2(t, \mathbf{r})$ , where  $K(I, \omega)$  is the intensity and frequency dependent photoassociation rate constant. Because the characteristic time for the motion of the atoms, the trap oscillation period, is long compared to the photoassociation pulse, we can assume that the local density changes only due to photoassociation, and

$$n(t, \mathbf{r}) = \frac{n(0, \mathbf{r})}{1 + K(I, \omega)n(0, \mathbf{r})t}. \quad (1)$$

The density distribution flattens with time. Spatially integrating Eq. (1), assuming an initial, parabolic (Thomas-Fermi), density distribution and a uniform intensity  $I$ , leads to an expression for the fraction of atoms remaining in the condensate:

measured linewidth of 19.5(25) MHz in the low intensity limit, where it is independent of intensity. At higher intensities, we observe broadening with a maximum linewidth of 60 MHz at  $1 \text{ kW cm}^{-2}$ . Homogeneous power broadening is calculated to be 3 orders of magnitude too low to explain this width. It is, however, partially explained by differential light shifts of the unresolved molecular hyperfine states. These states are calculated to be split by less than 1 MHz at low intensities and about 30 MHz at our maximum intensity. Another possible contribution is the inhomogeneity of the photoassociation beam intensity combined with the large light shift (discussed below). Variations due to either local spatial inhomogeneity (e.g.,

interference fringes) or displacement of the cloud from the center of the Gaussian beam could account for the extra width. Assuming these inhomogeneous broadening mechanisms do not change the area of the line (verified by a simulation), we take the on-resonance photoassociation rate constant to be  $K_0(I) = K_m(I)\gamma(I)/\gamma(I \rightarrow 0)$ .

Figure 4 shows corrected and uncorrected rate constants as a function of intensity (for various pulse lengths). The error bars are the fitting uncertainties. Once we correct for the inhomogeneous broadening we get a linear dependence on intensity with a slope of  $dK_0/dI = 3.5(2)(10) \times 10^{-10} \text{ (cm}^3 \text{ s}^{-1})/(\text{kW cm}^{-2})$ . The uncertainties are due, respectively, to fitting and to the combined uncertainties in the measurement of the intensity and density. For intensities above  $1.2 \text{ kW cm}^{-2}$ , which we could achieve only by more tightly focusing the photoassociation laser, atomic dipole forces significantly perturb the condensate, thwarting meaningful measurements. A coupled-channels, two-body scattering calculation with no adjustable parameters [17] yields a photoassociation rate constant of  $dK_0/dI = 4.1 \times 10^{-10} \text{ (cm}^3 \text{ s}^{-1})/(\text{kW cm}^{-2})$  for our range of intensities. This includes a factor of 2 decrease relative to a noncondensed gas and agrees well with our experimental result.

We study the photoassociation light shift, previously observed in a noncondensed gas [18], in a set of experiments where the total fluence (intensity  $\times$  pulse length) of the pulse was kept constant, to maintain the depth of the photoassociation dip in an easily observable regime. The results are shown in Fig. 5. The measured light shift is  $-164(35) \text{ MHz}/(\text{kW}/\text{cm}^2)$ , which leads at high intensity to a shift large compared to the linewidth. The principal contribution to the uncertainty is the intensity calibration. During preparation of this work, we became aware of similar results in lithium [19].

While the strength of the photoassociation resonance is dominated by  $s$ -wave scattering, the dominant contribution to the light shift is due to a  $d$ -wave shape reso-

nance. A theoretical calculation of the light shifts using Eq. (3.7) of Ref. [20], including the effect of the  $d$ -wave shape resonance embedded in the continuum, gives an average value of  $-130 \text{ MHz}/(\text{kW}/\text{cm}^2)$  with a spread of  $\pm 13 \text{ MHz}/(\text{kW}/\text{cm}^2)$  due to the hyperfine structure.

We now consider the upper limit to the photoassociation rate constant  $K_0$  [this implies a lower limit on the photoassociation time  $\tau = (K_0 n)^{-1}$ ]. If one uses a semiclassical theory that is commonly applied to collisions of laser-cooled atoms [21], then  $K = \sigma v = \pi R_C^2 P v$ , where  $R_C$  is the Condon radius (see Fig. 1), and  $P$  is the probability of a photoassociative transition with a maximum value of 1. If we take the relative velocity  $v$  of the atoms to be  $\hbar/(2mr_y) = 0.6 \text{ mm s}^{-1}$ , where  $m$  is the atomic mass, then the maximum photoassociation rate constant is 4 orders of magnitude lower than our highest measured value. This reveals the inadequacy of a semiclassical approach, which fails to take into account threshold laws [10].

Quantum theories for the photoassociation rate constant can be compared by expressing  $K$  as  $K = (\hbar/m)L$ , where  $L$  is a characteristic length. Two-body  $s$ -wave scattering theory for a BEC gives  $L_s = |S(k)|^2/k$ , where  $\hbar k$  is the relative collision momentum and  $S(k)$  is the  $S$ -matrix element for atom loss via photoassociation. References [20,22] show that, on resonance,

$$L_s(I) = \frac{4\gamma_0\Gamma(k, I)/k}{[\gamma_0 + \Gamma(k, I)]^2}, \quad (3)$$

where  $\hbar\Gamma(k, I) = 2\pi|\langle e|\hbar\Omega|k\rangle|^2$  is the Fermi-golden-rule stimulated-decay width of the excited molecular state  $|e\rangle$  due to the optical coupling  $\hbar\Omega \propto \sqrt{I}$  with the colliding atoms. Since  $\Gamma \propto k$  as  $k \rightarrow 0$ , and  $\Gamma/\gamma_0 < 0.001$  in our range of power and collision energy,  $L_s$  is independent of  $k$ .  $L_s$  is linear in  $I$  for our experimental conditions, and  $dL_s/dI$  is calculated to be  $24 \text{ nm}/(\text{kW}/\text{cm}^2)$ . This gives the above-quoted rate constant in good agreement with the experiment. In our power range,  $L_s$  can be significantly

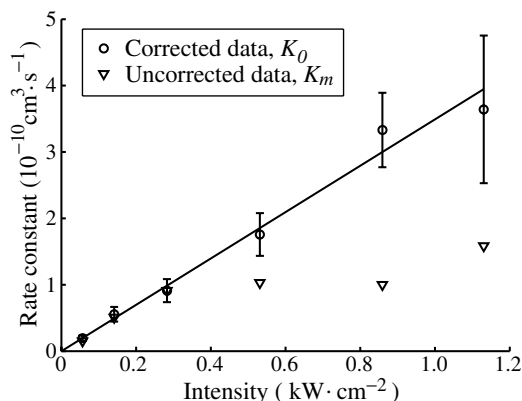


FIG. 4. Resonant photoassociation rate constant as a function of intensity. The corrected data has been adjusted to account for the inhomogeneous broadening.

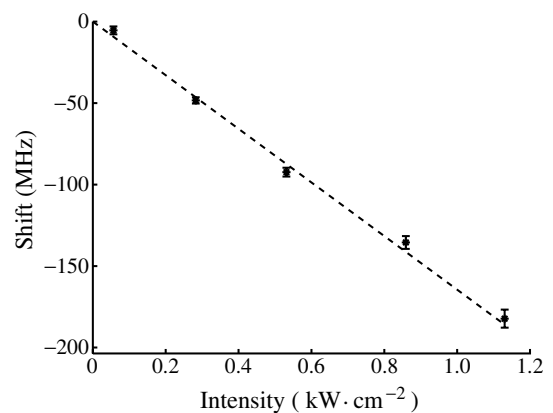


FIG. 5. The light shift of the resonance as a function of laser intensity.

larger than the Condon point for the transition, 2.0 nm. Note that Eq. (3) shows that  $L_s(I)$  will saturate with increasing  $I$  and decrease for sufficiently large  $I$ .

The upper limit to the two-body quantum  $K_0$  is the unitarity limit where  $|S|^2 = 1$  so  $L_u = 1/k = \lambda/2\pi$ , where  $\lambda$  is the de Broglie wavelength. Since  $\lambda$  is on the order of the BEC size  $L_s/L_u \ll 1$ , thus our experiment is well below the unitarity constraint.

Recent many-body theoretical work [3,23,24] has suggested an upper limit to  $K_0$  in a BEC of  $K_0 \sim \frac{\hbar}{m}L_J$ , where  $L_J = \frac{n^{-1/3}}{2\pi}$  and  $n^{-1/3}$  is the mean distance between particles. One might question if two-body scattering methods are applicable at densities where  $L_s$  becomes larger than  $L_J$ . At our maximum density  $L_J = 22$  nm, so  $L_s/L_J \approx 1$  at our highest intensities. Nevertheless, the linearity of  $K_0(I)$  (Fig. 4) shows that, with our experimental uncertainty, we have no evidence for the failure of two-body theory.

Larger values of  $L_s/L_J$  might be accessible by a modification to our experimental design. We can use the atomic dipole force (which currently limits our ability to use high intensities) to our advantage by trapping the atoms with the photoassociation laser. Without changing the atomic dipole forces, the laser can be suddenly brought from far off molecular resonance to on molecular resonance to induce photoassociation. Difficulties due to the molecular light shift might be reduced by finding a transition with a smaller light shift.

In conclusion, we have measured the single-photon photoassociation in a BEC, in good agreement with two-body theory. This agreement represents a confirmation of the factor-of-two reduction for a two-body inelastic process in a BEC. The characteristic time for photoassociation is as short as 5  $\mu$ s, much shorter than the 100  $\mu$ s to traverse the mean distance between atoms, another demonstration of the extreme quantum nature of the collisions. Our largest rate is still much smaller than the unitarity limit, but is on the order of a limit suggested on the basis of many-body effects; however, we have yet to see the effects of this limit.

We acknowledge funding support from the U.S. Office of Naval Research and NASA. J. H. D. and H. H. acknowledge funding from the Alexander von Humboldt foundation. A. B. was partially supported by DGA (France).

\*Institut für Experimentalphysik, Universität Innsbruck, Technikerstrasse 25, A-6020 Innsbruck, Austria.

†The Institute of Optics, University of Rochester, Rochester, NY 14627.

‡Naval Research Laboratory, Washington, D.C. 20375.

§Department of Physics, Williams College, Williamstown, MA 01267.

||Bell Laboratories, Lucent Technologies, Holmdel, NJ 07733.

¶Department of Physics, Korea University, 5-1 Ka Anamdong, Sungbuk-ku, Seoul 136-701, Korea.

\*\*INFN and LENS, Università di Firenze, Largo E. Fermi 2, I-50125, Firenze, Italy.

- [1] M. H. Anderson, J. R. Ensher, M. R. Matthews, C. E. Wieman, and E. A. Cornell, *Science* **269**, 198 (1995).
- [2] K. B. Davis, M.-O. Mewes, M. R. Andrews, N. J. van Druten, D. S. Durfee, D. M. Kurn, and W. Ketterle, *Phys. Rev. Lett.* **75**, 3969 (1995).
- [3] M. Kořtrun, M. Mackie, R. Côté, and J. Javanainen, *Phys. Rev. A* **62**, 063616 (2000).
- [4] D. J. Heinzen, R. Wynar, P. D. Drummond, and K. V. Kheruntsyan, *Phys. Rev. Lett.* **84**, 5029 (2000).
- [5] E. Timmermans, P. Tommasini, R. Côté, M. Hussein, and A. Kerman, *Phys. Rev. Lett.* **83**, 2691 (1999).
- [6] P. S. Julienne, K. Burnett, Y. B. Band, and W. C. Stwalley, *Phys. Rev. A* **58**, R797 (1998).
- [7] K. Helmerson and L. You, *Phys. Rev. Lett.* **87**, 170402 (2001).
- [8] R. Wynar, R. S. Freeland, D. J. Han, C. Ryu, and D. J. Heinzen, *Science* **287**, 1016 (2000).
- [9] J. M. Gerton, D. Strelak, I. Prodan, and R. G. Hulet, *Nature (London)* **408**, 692 (2000).
- [10] J. Weiner, V. S. Bagnato, S. Zilio, and P. S. Julienne, *Rev. Mod. Phys.* **71**, 1 (1999).
- [11] Unless otherwise stated, all uncertainties reported here are one standard deviation combined systematic and statistical uncertainties.
- [12] M. Kozuma, L. Deng, E. W. Hagley, J. Wen, R. Lutwak, K. Helmerson, S. L. Rolston, and W. D. Phillips, *Phys. Rev. Lett.* **82**, 871 (1999).
- [13] M. R. Andrews, M.-O. Mewes, N. J. van Druten, D. S. Durfee, D. M. Kurn, and W. Ketterle, *Science* **273**, 84 (1996).
- [14] Because we are in a regime where the phase shift of the light passing through the BEC is large (up to several radians), the extracted density is a multivalued function of the phase contrast signal. We assume a Thomas-Fermi distribution for the atoms to resolve this ambiguity.
- [15] K. M. Jones, P. D. Lett, E. Tiesinga, and P. S. Julienne, *Phys. Rev. A* **61**, 012501 (2000).
- [16] M. Movre and G. Pichler, *J. Phys. B* **13**, 697 (1980).
- [17] C. Samuelis, E. Tiesinga, T. Laue, M. Elbs, H. Knöckel, and E. Tiemann, *Phys. Rev. A* **63**, 012710 (2001).
- [18] K. M. Jones, S. Maleki, L. P. Ratliff, and P. D. Lett, *J. Phys. B* **30**, 289 (1997).
- [19] J. M. Gerton, B. J. Frew, and R. G. Hulet, *Phys. Rev. A* **64**, 053410 (2001).
- [20] J. L. Bohn and P. S. Julienne, *Phys. Rev. A* **60**, 414 (1999).
- [21] A. Gallagher and D. E. Pritchard, *Phys. Rev. Lett.* **63**, 957 (1989).
- [22] J. L. Bohn and P. S. Julienne, *Phys. Rev. A* **54**, R4637 (1996).
- [23] J. Javanainen and M. Mackie, cond-mat/0108349, 2001.
- [24] J. Javanainen (private communication).

## 5.4 “Atom-molecule dark states in a Bose-Einstein condensate”

K. Winkler, G. Thalhammer, M. Theis, H. Ritsch, R. Grimm,  
and J. Hecker Denschlag

cond-mat/0505732, submitted for publication



# Atom-molecule dark states in a Bose-Einstein condensate

K. Winkler,<sup>1</sup> G. Thalhammer,<sup>1</sup> M. Theis,<sup>1</sup> H. Ritsch,<sup>2</sup> R. Grimm,<sup>1,3</sup> and J. Hecker Denschlag<sup>1</sup>

<sup>1</sup>*Institut für Experimentalphysik, Universität Innsbruck, 6020 Innsbruck, Austria*

<sup>2</sup>*Institut für Theoretische Physik, Universität Innsbruck, 6020 Innsbruck, Austria*

<sup>3</sup>*Institut für Quantenoptik und Quanteninformation,  
Österreichische Akademie der Wissenschaften, 6020 Innsbruck, Austria*

(Dated: May 30, 2005)

We have created a dark quantum superposition state of a Rb Bose-Einstein condensate (BEC) and a degenerate gas of Rb<sub>2</sub> ground state molecules in a specific ro-vibrational state using two-color photoassociation. As a signature for the decoupling of this coherent atom-molecule gas from the light field we observe a striking suppression of photoassociation loss. In our experiment the maximal molecule population in the dark state is limited to about 100 Rb<sub>2</sub> molecules due to laser induced decay. The experimental findings can be well described by a simple three mode model.

PACS numbers: 34.50.Rk, 32.80.Pj, 03.75.Nt, 42.50.Gy

The phenomenon of coherent dark states is well known in quantum optics and is based on a superposition of long-lived system eigenstates which decouples from the light field. Since their discovery [1] dark states have found numerous applications. Prominent examples are electromagnetically induced transparency and lasing without inversion [2], sub-recoil laser cooling [3], and ultra-sensitive magnetometers [4]. A particular application is the coherent transfer of population between two long-lived states by a stimulated Raman adiabatic passage (STIRAP) [5].

In the emerging field of ultracold molecules, the conversion of atomic into molecular BECs is a central issue. A series of recent experiments on the creation of molecular quantum gases rely on the application of Feshbach resonances [6]. This coupling mechanism, however, is restricted to the creation of molecules in the highest ro-vibrational level and is only practicable for a limited number of systems. As a more general method a stimulated optical Raman transition can directly produce deeply bound molecules as demonstrated a few years ago [7, 8]. STIRAP was proposed as a promising way for a fast, efficient and robust process to convert a BEC of atoms into a molecular condensate [9–14]. The central prerequisite for this kind of STIRAP is a dark superposition state of a BEC of atoms and a BEC of molecules.

In this Letter, we report the observation of such a collective multi-particle dark state in which atoms in a BEC are pairwise coupled coherently to ground state molecules. This dark atom-molecule BEC shows up in a striking suppression of photoassociative loss, as illustrated by the spectra in Fig. 1. In one-color photoassociation, the excitation of a molecular transition produces a resonant loss feature that reflects the optical transition linewidth, see Fig. 1(a). The presence of a second laser field coupling the electronically excited molecular state to a long-lived ground-state level can drastically reduce this loss, as shown in Fig. 1(b) and (c). In (b), for example, we observe a striking loss suppression by about a factor of 70 on resonance.

Already the mere observation of an atom-molecule dark resonance in a BEC proves that a coherent, quan-

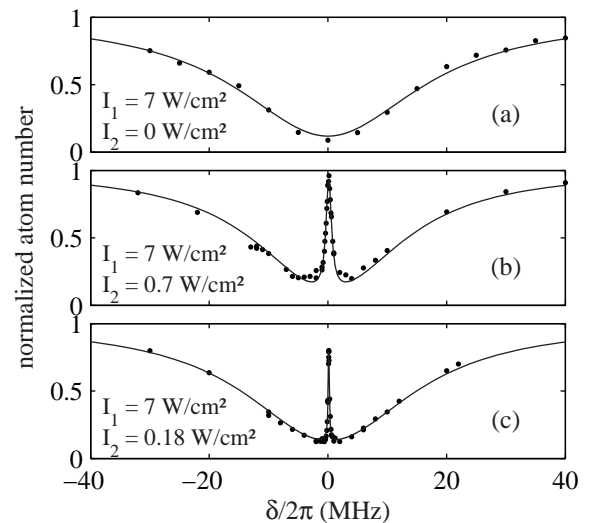


FIG. 1: Dark resonances in two-color photoassociation. (a) Atomic loss signal in one-color photoassociation as a function of the laser detuning from the electronically excited molecular line. (b), (c) When we apply a second laser (fixed frequency) which resonantly ( $\Delta = 0$ ) couples the excited molecular state to a long lived molecular ground state, the losses are strongly suppressed at  $\delta = 0$ . Depending on the intensity of laser 2, this dark resonance can get very narrow. The atom life time on the dark resonance in (b) is 140 ms whereas in (a) atoms have an initial decay time of about 2 ms. Intensities of laser 1 ( $I_1$ ) and 2 ( $I_2$ ) are as indicated.

tum degenerate gas of molecules has been formed. This follows from the facts that 1) the dark state is by definition a coherent superposition of atoms and molecules and 2) the atomic BEC is a coherent matter-wave. In this fully coherent situation, the molecular fraction itself must be quantum degenerate with a phase-space density corresponding to the number of molecules. The very narrow resonance lines indicate the high resolution of our measurements and the potential sensitivity of the dark state as an analysis tool. Using a BEC allows direct inter-

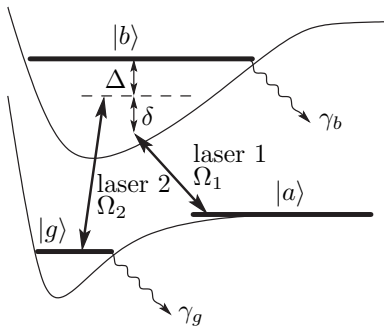


FIG. 2: Level scheme.  $\Delta$  and  $\delta$  denote the detunings.  $\Omega_1$  and  $\Omega_2$  are the Rabi frequencies. The excited molecular state  $|b\rangle$  spontaneously decays with a rate  $\gamma_b$  to levels outside this scheme. The molecular state  $|g\rangle$  is attributed a decay rate  $\gamma_g$  which phenomenologically takes into account losses through inelastic collisions and laser induced dissociation, e.g. when laser 1 couples  $|g\rangle$  to the unstable state  $|b\rangle$ . In all our measurements laser 1 is scanned (varying  $\delta$ ) while laser 2 is held fixed at a particular detuning  $\Delta$ .

pretation and clear understanding of our data without ambiguity. Thermal averaging of signal features plays no role in contrast to previous measurements in thermal gases [8, 15, 16].

The starting point of our measurements is a BEC of  $4 \times 10^5$   $^{87}\text{Rb}$  atoms in the spin state  $|F=1, m_F=-1\rangle$  [17]. In the level scheme of Fig. 2 the atomic BEC state is represented by  $|a\rangle$ . Laser 1 couples this state to the excited molecular state  $|b\rangle$ . Laser 2 couples  $|b\rangle$  to the molecular ground state  $|g\rangle$ . We choose level  $|b\rangle$  to be the electronically excited molecular state  $|0_g^-, \nu=1, J=2\rangle$  located  $26.8\text{ cm}^{-1}$  below the  $S_{1/2} + P_{3/2}$  dissociation asymptote [17]. For level  $|g\rangle$  we choose the second to last bound state in the ground state potential. It has a binding energy of  $E_b/h = 636\text{ MHz}$  [7].  $|a\rangle$ ,  $|b\rangle$  and  $|g\rangle$  form the lambda-system for the atom-molecule dark states.

We illuminate the trapped condensate for typically 10 ms with two phase-locked laser beams in a Raman configuration as shown in Fig. 2. Both laser beams are derived either from a single diode laser or, for higher optical powers, from a Ti:Sapphire laser. The frequency difference between the two beams is created with an acousto-optical modulator at a center frequency of about 320 MHz in a double-pass configuration. This allows precise control of the beams' relative frequency difference over several tens of MHz. Both beams propagate collinearly and are aligned along the weak axis of the trap. They have a waist of about  $100\ \mu\text{m}$ , and their linear polarization is perpendicular to the magnetic bias field of the trap. The diode laser and the Ti:Sapphire laser both have line widths of less than 1 MHz. They are offset locked relative to the  $D_2$ -line of atomic rubidium with the help of a scanning optical cavity. This yields an absolute frequency stability of better than 10 MHz.

We are able to describe all our spectra with a relatively

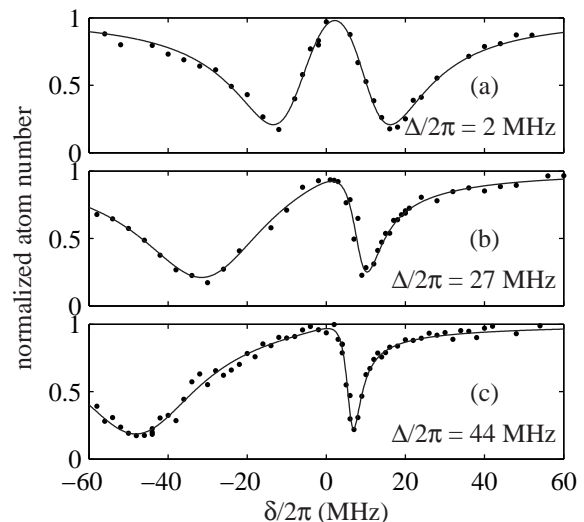


FIG. 3: Two-color photoassociation spectra for various detunings  $\Delta$  at a large intensity  $I_2 = 20\text{ W/cm}^2$ . Here  $I_1 = 80\text{ W/cm}^2$ . The solid lines are fit curves based on our theoretical model.

simple three mode model. Although the atom-molecule dark states are intrinsically complicated and entangled, in a first approximation the atoms and molecules can be represented as coherent matter fields [9–14]. Using the notation of M. Mackie *et al.* [11] we obtain a set of differential equations for the normalized field amplitudes  $a$ ,  $b$ , and  $g$  of the BEC state, the excited molecular and ground state, respectively:

$$\begin{aligned} i\dot{a} &= -\Omega_1 a^* b, \\ i\dot{b} &= [(\Delta + \delta) - i\gamma_b/2] b - \frac{1}{2}(\Omega_1 a a + \Omega_2 g), \\ i\dot{g} &= (\delta - i\gamma_g/2) g - \frac{1}{2}\Omega_2 b. \end{aligned} \quad (1)$$

We refer to  $\Omega_1$  as the free-bound Rabi frequency (see Fig. 2). It scales with intensity  $I_1$  of laser 1 and initial atom density  $\rho$  as  $\Omega_1 \propto \sqrt{I_1} \sqrt{\rho}$ . The bound-bound Rabi frequency  $\Omega_2 \propto \sqrt{I_2}$  only depends on the intensity  $I_2$  of laser 2. The detunings  $\Delta$  and  $\delta$  are defined as depicted in Fig. 2.  $\gamma_b$  and  $\gamma_g$  denote the effective decay rates of state  $|b\rangle$  and  $|g\rangle$  (for details see Fig. 2).  $|a|^2$ ,  $|b|^2$ , and  $|g|^2$  give the ratio between the respective atom (molecule) number and the initial atom number. In the absence of losses, i.e.  $\gamma_b = \gamma_g = 0$ , particle numbers are conserved globally,  $|a|^2 + 2|b|^2 + 2|g|^2 = 1$ . Unlike the previous theoretical treatments [9–14] where the decay rate  $\gamma_g$  was basically neglected, we find that  $\gamma_g$  is relatively large and intensity dependent,  $\gamma_g = \gamma_g(I_1)$ . In our simple model we do not include atomic continuum states other than the BEC state. We neglect inhomogeneity effects due to the trapping potentials and finite size laser beams. Energy shifts caused by the mean-field interaction of atoms and molecules are small and neglected.

In order to determine the parameters of our model and to check it for consistency, we performed measure-

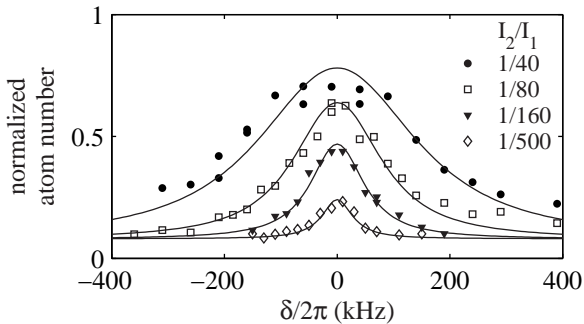


FIG. 4: Dark resonances (blow-up of the central part of Fig. 1 (c) and similar curves) for different intensity ratios  $I_2/I_1$  (see legend) at a fixed intensity  $I_1 = 7 \text{ W/cm}^2$ . The solid curves are calculations based on our theoretical model.  $\Delta = 0$ .

ments in a broad parameter range of intensities and detunings. Fits to the photoassociation curves determine all unknown parameters of the system such as  $\Omega_1$ ,  $\Omega_2$ ,  $\gamma_b$  and  $\gamma_g$ . Figure 3 shows photoassociation spectra for a relatively high laser power  $I_2 = 20 \text{ W/cm}^2$  and various detunings  $\Delta$ . For a small detuning  $\Delta$  (Fig. 3 (a)) the dark resonance line from Fig. 1 has broadened considerably. This spectrum can also be viewed as two absorption lines resulting from a strong Autler-Townes splitting which was also observed in thermal gases [8, 16]. From the 30 MHz separating the two resonance dips, the magnitude of the Rabi frequency  $\Omega_2$  can be directly determined. For a larger detuning  $\Delta$ , the resulting spectrum becomes asymmetric and turns into a narrow and a broad dip, see Fig. 3 (b) and (c). The narrow loss feature is related to the two-photon Raman transition while the broad dip is due to the one-photon transition  $|a\rangle \rightarrow |b\rangle$ . Note that similar to Fig. 1, losses are suppressed at  $\delta = 0$ .

Figure 4 shows the dark resonances in the low power limit where  $I_1$  is held constant and  $I_2$  is lowered in 4 steps. The dark state transforms more and more into a grey state, because losses become more dominant due to a nonzero decay rate  $\gamma_g$ . The height of the dark resonance decreases when the pumping rate  $\Omega_2^2/\gamma_b$  comes in the range of the decay rate of the molecular ground state  $\gamma_g$ . This allows for a convenient determination of  $\gamma_g$ . From Fig. 4 it is also clear that the width of the dark resonance decreases with  $\Omega_2$ . For  $\Omega_2 \ll \gamma_b$  the width is given by  $\Omega_2^2/\gamma_b + \gamma_g$ , corresponding to power broadening and the effective ground state relaxation. The following set of parameters describes all our measurements quite accurately and was used in particular for the calculated solid lines in Fig. 4:  $\Omega_1/(\sqrt{I_1}\sqrt{\rho/\rho_0}) = 2\pi \times 8 \text{ kHz}/(\text{W cm}^{-2})^{1/2}$  at a peak density of  $\rho_0 = 2 \times 10^{-14} \text{ cm}^{-3}$ ,  $\Omega_2/\sqrt{I_2} = 2\pi \times 7 \text{ MHz}/(\text{W cm}^{-2})^{1/2}$ , and  $\gamma_b = 2\pi \times 13 \text{ MHz}$ . We find that the decay rate  $\gamma_g$  of the ground state molecular level increases with the intensity  $I_1$  of laser 1 as shown in Fig. 5. A dependence of  $\gamma_g$  on  $I_2$  was negligible in our experiments where typ-

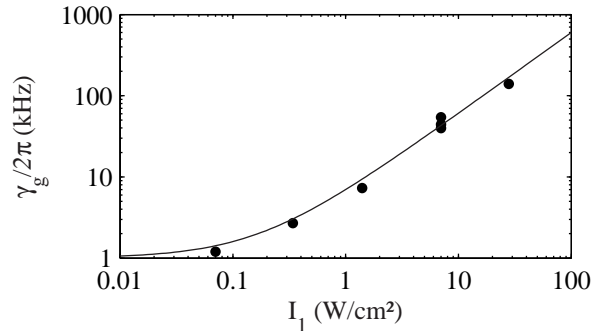


FIG. 5: Dependence of the decay rate  $\gamma_g$  of the ground state molecules on the laser intensity  $I_1$ , measured with an intensity ratio  $I_2/I_1 = 1/40$ . The solid curve is given by  $\gamma_g = 2\pi \times 6 \text{ kHz}/(\text{W cm}^{-2})I_1 + 2\pi \times 1 \text{ kHz}$ .

ically  $I_2/I_1 \sim 1/5 \dots 1/500$ . We model the behavior of  $\gamma_g$  as  $\gamma_g = 2\pi \times 6 \text{ kHz}/(\text{W cm}^{-2})I_1 + \gamma_{\text{bg}}$ , the sum of a light-induced decay rate proportional to  $I_1$  and background decay rate  $\gamma_{\text{bg}}$  due to inelastic collisions in the absence of light. From measurements at low intensities we can estimate an upper value for the background decay rate of about  $\gamma_{\text{bg}} \approx 2\pi \times 1 \text{ kHz}$  for  $\rho_0 = 2 \times 10^{14} \text{ cm}^{-3}$ . This value for  $\gamma_{\text{bg}}$  is consistent with previous experimental results for  $^{87}\text{Rb}$  at similar atom densities [7]. The increase of  $\gamma_g$  with  $I_1$  is due to several imperfections which break the ideal 3-level lambda system. Laser 1 also couples the molecular ground state  $|g\rangle$  to the short-lived excited molecular state  $|b\rangle$ , which leads to an incoherent loss of the molecules due to spontaneous decay. Due to the rather small frequency difference ( $\approx 2\pi \times 636 \text{ MHz}$ ) of the two Raman lasers and the strong bound-bound transition, this cannot be neglected. In addition, only 290 MHz below level  $|b\rangle$  exists another excited molecular state  $|0_g^-, \nu = 1, J = 0\rangle$  which represents an additional loss channel [17]. These two contributions explain about one third of our observed losses. Furthermore, losses can also stem from a photodissociation transition which couples ground state molecules directly to the continuum above the  $S_{1/2} + P_{1/2}$  dissociation asymptote.

Having determined the parameters we can use model (1) to calculate the fraction of ground state molecules  $|g\rangle^2$ . For the measurements presented in Fig. 4 we have a peak molecular fraction of  $2 \times 10^{-4}$  corresponding to about 100 molecules (at  $\delta = 0$  and  $I_2/I_1 = 1/500$ ). For comparison, for  $I_2/I_1 = 1/40$  the molecule number is only about 25 at  $\delta = 0$ . It is interesting to note how few molecules are needed to stabilize almost a million atoms against photoassociation. This large asymmetry of the particle numbers reflects the different coupling strengths of the free-bound and bound-bound transitions. Naturally the question arises how the experimental parameters should be chosen to optimize the number of molecules. This is non-trivial due to the finite decay rate  $\gamma_g$ . With model (1) we have numerically mapped out molecule numbers as a function of time, detuning and laser

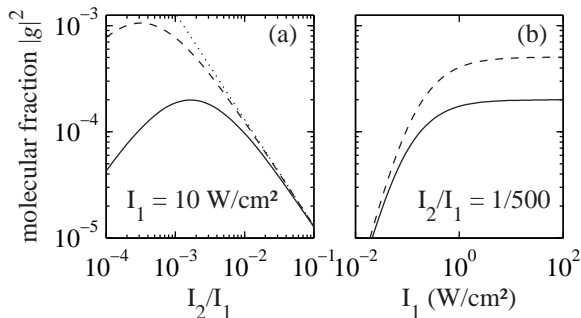


FIG. 6: (a) Maximum molecular fraction as function of the intensity ratio  $I_2/I_1$  at a fixed intensity  $I_1 = 10 \text{ W/cm}^2$  and (b) as a function of intensity  $I_1$  at a fixed intensity ratio  $I_2/I_1 = 1/500$ . The solid lines show the molecule fraction for the measured decay rate  $\gamma_g = 2\pi \times 6 \text{ kHz}/(\text{W cm}^{-2})I_1 + \gamma_{\text{bg}}$ . The dashed lines show the molecule fraction assuming a lower decay rate  $\gamma_g = 2\pi \times 1 \text{ kHz}/(\text{W cm}^{-2})I_1 + \gamma_{\text{bg}}$ . The dotted line corresponds to  $\gamma_g = 0$ . The calculations are based on Eqs. (1) with  $\Delta = 0$ .

intensities, starting out with a pure atomic BEC and simply switching on the lasers. In general within a few  $\mu\text{s}$  of evolution, the dark state is formed. This involves only negligible losses of atoms since the dark state is very close to our initial BEC state. The maximum number of molecules of every evolution is then determined. We find that we can optimize the molecular production by working at  $\Delta = 0$  although other values for  $\Delta$  can be used. For  $\Delta = 0$  the maximum number of molecules correspond to  $\delta = 0$ , hence both lasers are on resonance. Figure 6 shows the molecular fraction as a function of the laser intensities. In Fig. 6(a), as  $I_2/I_1$  is lowered from high values, the molecule fraction initially grows and follows a straight dotted line which coincides with the ideal route for STIRAP. Following this route would lead to a full

conversion of atoms into molecules in the absence of loss  $\gamma_g$ . This can be seen from Eqs. (1) when setting  $\dot{b} = 0$  and  $b = 0$  such that  $|g|^2 = \Omega_1^2/\Omega_2^2|a|^4$ . For finite  $\gamma_g$ , however, the molecular fraction curve rolls over for some value of  $I_2/I_1$ , when the molecule loss rate is larger than its production rate. A smaller  $\gamma_g$  would lead to a larger number of molecules (dashed line). The finite  $\gamma_g$  in our experiments leads to a maximum molecule number at  $I_2/I_1 \sim 1/500$ , a ratio which we also used in our measurements (see Fig. 4, open diamonds). For this optimum value the dependence of the molecular fraction on  $I_1$  is shown in Fig. 6(b). Here it becomes clear that the laser intensities have to be kept above a certain threshold so that losses are not dominated by the background decay rate  $\gamma_{\text{bg}}$  of the molecular state.

To summarize, we have created a novel multi-particle dark state where an optical Raman transition coherently couples an atomic Rb BEC of about  $4 \times 10^5$  atoms to a quantum degenerate gas of up to 100 Rb<sub>2</sub> ground state molecules. Our investigations can be extended in a straight forward manner to create and study BECs of arbitrarily deeply bound molecules and coherent atom/molecule mixtures. The dark resonance has proven itself as a useful tool to analyze the atom-molecule system and to optimize the optical conversion of atomic to molecular BECs. An increase of the number of molecules by several orders of magnitude should be possible by choosing better suited ground and excited molecular states for the free-bound Raman transition.

We appreciate the help of George Ruff and Michael Hellwig at an early stage of the experiment. We thank Paul Julienne, Eite Tiesinga, Peter Drummond and Karen Kheruntsyan for valuable discussions. This work was supported by the Austrian Science Fund (FWF) within SFB 15 (project parts 12 and 17) and the European Union in the frame of the Cold Molecules TMR Network under contract No. HPRN-CT-2002-00290.

- 
- [1] E. Arimondo and G. Orriols, *Lett. Nuovo Cim.* **17**, 333 (1976).
  - [2] For a review see S.E. Harris, *Physics Today* **50**, 36 (1997).
  - [3] A. Aspect *et al.*, *Phys. Rev. Lett.* **61**, 826 (1988).
  - [4] M. Stähler *et al.*, *Opt. Lett.* **27**, 1472 (2002).
  - [5] K. Bergmann, H. Theuer, and B.W. Shore, *Rev. Mod. Phys.* **70**, 1003 (1998).
  - [6] For a review D. Kleppner, *Phys. Today* **57**, 12 (2004).
  - [7] R. Wynar, R.S. Freeland, D.J. Han, C. Ryu, and D.J. Heinzen, *Science* **287**, 1016 (2000).
  - [8] B. Laburthe Tolra, C. Drag, and P. Pillet, *Phys. Rev. A* **64**, 061401 (2001).
  - [9] A. Vardi, D. Abrashkevich, E. Frishman, and M. Shapiro, *J. Chem. Phys.* **107**, 6166 (1997); A. Vardi, V.A. Yurovsky, and J.R. Anglin, *Phys. Rev. A* **64**, 063611 (2001).
  - [10] P.S. Julienne, K. Burnett, Y.B. Band, and W.C. Stwalley, *Phys. Rev. A* **58**, R797 (1998).
  - [11] J. Javanainen and M. Mackie, *Phys. Rev. A* **58**, R789 (1998); M. Mackie, A. Collin, and J. Javanainen, *Phys. Rev. A* **71**, 017601 (2005).
  - [12] J.J. Hope, M.K. Olsen, and L.I. Plimak, *Phys. Rev. A* **63**, 043603 (2001).
  - [13] P. D. Drummond, K.V. Kheruntsyan, D.J. Heinzen, and R.H. Wynar, *Phys. Rev. A* **65**, 063619 (2002); P.D. Drummond, K.V. Kheruntsyan, D.J. Heinzen, and R.H. Wynar, *Phys. Rev. A* **71**, 017602 (2005).
  - [14] B. Damski *et al.*, *Phys. Rev. Lett.* **90**, 110401 (2003).
  - [15] C. Lisdat, N. Vanhaecke, D. Comparat, and P. Pillet, *Eur. Phys. J. D* **21**, 299 (2002).
  - [16] U. Schlöder, T. Deuschle, C. Silber, and C. Zimmermann, *Phys. Rev. A* **68**, 051403 (2003).
  - [17] For details see G. Thalhammer *et al.*, *Phys. Rev. A* **73**, 033403 (2005).

## 5.5 “Pure Gas of Optically Trapped Molecules Created from Fermionic Atoms”

S. Jochim, M. Bartenstein, A. Altmeyer, G. Hendl, C. Chin,  
J. Hecker Denschlag, and R. Grimm

Phys. Rev. Lett. **91**, 240402 (2003)



## Chapter 6

# Bose-Einstein condensation of molecules and the BEC-BCS crossover

Properties of quantum degenerate gases are largely determined by quantum statistics. At low enough temperatures bosons form a BEC and fermions form a Fermi sea. An interesting situation arises when a gas of particles changes its quantum statistics, i.e. fermionic particles become bosons or vice versa. This happens, for example, when we combine two fermionic atoms to form a composite boson. However, depending on the strength of their bonding, these fermion pairs (or composite bosons) can still have strong fermionic characteristics. In the strong coupling limit the fermion pair is a bosonic molecule which can undergo Bose-Einstein condensation. In the weak coupling limit the coupled atoms are Cooper pairs in a degenerate Fermi gas and lead to BCS superfluidity [Bar57], (see also chapter 2). These Cooper pairs are delocalized in the sense that the distance between the paired atoms can be larger than the mean particle distance in the Fermi gas. It should be possible to continuously go over from the regime of BEC superfluidity to BCS superfluidity by controlling the coupling between the fermions. This is called the BEC-BCS crossover. The BEC-BCS crossover has been the subject of great theoretical interest for more than three decades [Eag69, Leg80, Noz85, Hol01, Oha02, Sta04]. For an overview see [Che04]. Using ultracold degenerate fermionic quantum gases and Feshbach resonances it is now possible for the first time to experimentally access and study this regime since with the Feshbach resonance we can control the interaction and coupling of the fermionic atoms. Figure 6.1 illustrates how this works.

On the left hand side of the Feshbach resonance where the scattering length is positive, a weakly bound molecular state exists (see also Fig. 5.3).

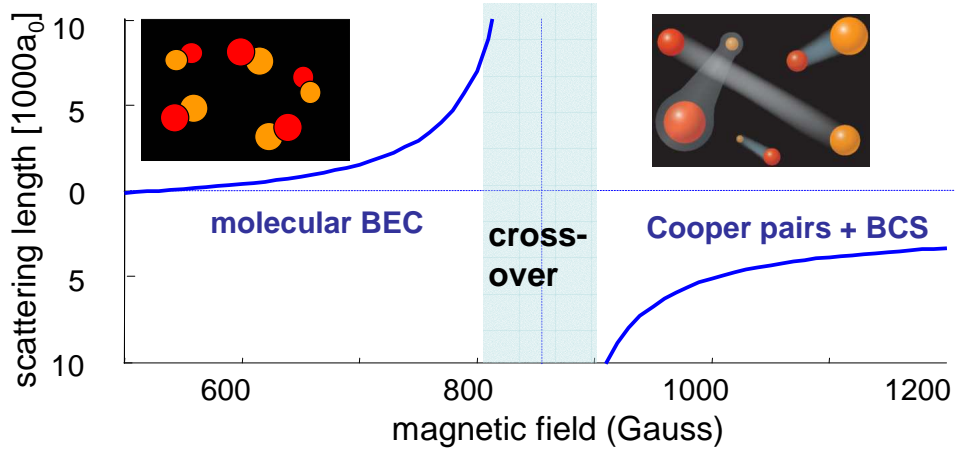


Figure 6.1: BEC-BCS crossover. By controlling the coupling in pairs of fermions with a Feshbach resonance we can continuously go over from a tight coupling regime (molecules) to a weak coupling regime (Cooper pairs). For low enough temperatures this corresponds to a continuous change from BEC superfluidity to BCS superfluidity, called the BEC-BCS crossover. The shaded area where the scattering length diverges, marks an interesting universal regime where the interaction between the particles is unitarity limited.

The binding energy of these molecules is tunable via the magnetic field strength. For low magnetic fields we are in the strongly coupled regime where the molecules behave as pure bosons and can form a BEC. On the side of the Feshbach resonance with negative scattering length, no such weakly bound molecular state exists and we will have a degenerate Fermi gas with attractive interactions. For low enough temperatures the fermionic atoms should pair up similar to Cooper pairs and form a superfluid. The interaction between the atoms is proportional to the scattering length  $|a|$  and can be tuned with the magnetic field. In the typical BCS regime the interactions between the fermions are very weak, i.e.  $k_F|a| \ll 1$ . In this regime the critical temperature  $T_c$  for Cooper pairing and superfluidity is very low, i.e. a small fraction of the Fermi temperature  $T_c \propto T_F \exp\left(-\frac{\pi}{2k_F|a|}\right)$  (see also Eq. 2.15).

With typical Fermi temperatures on the order of  $\mu\text{K}$  in our experiments, fermionic superfluidity in the BCS limit is then very hard to achieve, since it would require temperatures in the pK range. What helps dramatically, however, is that close to the Feshbach resonance the Fermi gas is strongly interacting, i.e. the scattering length  $a$  becomes very large. This raises  $T_c$  to a large fraction of  $T_F$  ( $\approx 0.2 T_F$ ) and brings it right into the range where

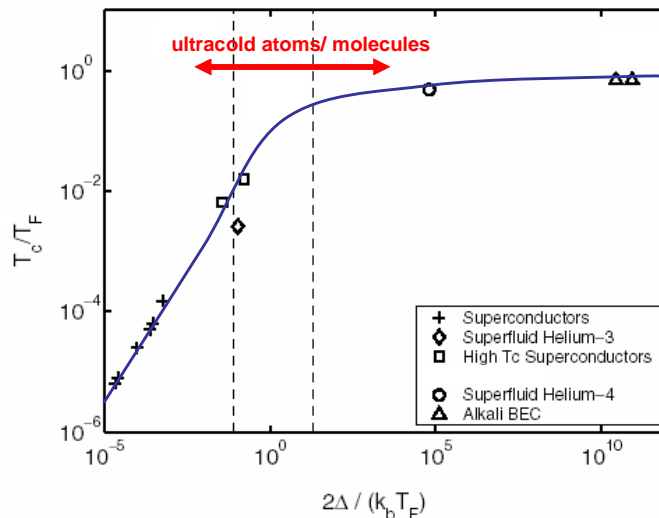


Figure 6.2: Overview of superfluidity in different Fermi pair coupling regimes. For strong coupling (here given in terms of the energy gap  $\Delta$ , we are in the BEC regime and the critical temperature  $T_c$  is around the Fermi temperature  $T_F$ . For weak coupling, as for example in typical superconductors,  $T_c$  is a small fraction of  $T_F$ . In the regime of resonance superfluidity (the range between the dashed lines) where we have a strongly interacting Fermi gas,  $T_c \approx T_F$ . This figure is adapted from [Hol01].

it becomes accessible in current experiments. This regime has been theoretically studied and is termed *resonance superfluidity* [Hol01, Oha02, Sta04]. Figure 6.2 gives an overview over the superfluid regimes in various physical systems.  $T_c/T_F$  strongly depends on the coupling strength of the Fermi pair. It should be pointed out that pairing of fermions and superfluidity plays an important role in several fields of physics beyond the standard systems of superconductors (normal and high- $T_c$ ) and superfluid Helium 3. Two such fields are, for example, astronomy and nuclear physics where we deal with degenerate Fermi gases in neutron stars and nuclei, respectively.

Studying the Fermi gas right on the Feshbach resonance is interesting from another point of view. Here the scattering length diverges (see Fig. 6.1) and as a consequence the interaction between the particles becomes unitarity limited by the finite Fermi momentum  $k_F$  (see also section 2.1.3). The scattering length then completely drops out of the physical description and is not relevant anymore. We are entering a universal regime where the behavior of the gas becomes independent of the particularities of the atomic interaction properties. A number of theoretical predictions for the behav-

ior of these gases, regarding mechanical stability, collective excitations and thermodynamics (see for example [Hei01, Ho04, Geh03b]) have been brought forth recently and can now be tested experimentally.

In the following two sections we first describe the experimental realization of Bose-Einstein condensation of molecules and fermionic pairs. Afterwards we discuss several experiments which investigate the BEC-BCS crossover with several methods, studying the size, collective oscillations and the pairing gap of the Fermi gas <sup>1</sup>. For these crossover experiments we used the molecular BEC as a convenient starting point.

## 6.1 Bose-Einstein condensation of Fermi pairs: molecules and Cooper pairs

### Molecular BEC

In 2003, our group and that of D. Jin simultaneously produced the world's first molecular BECs [Joc03a, Gre03]. These condensates consisted of the dimeric molecules  $\text{Li}_2$  and  $\text{K}_2$  for our and Jin's group, respectively. Several weeks later this was followed by reports of molecular condensation of  $\text{Li}_2$  from the groups of W. Ketterle [Zwi03] and C. Salomon [Bou04]. The condensate in our experiment contained more than  $10^5$   $\text{Li}_2$  molecules and was produced starting out with a laser cooled spin mixture of  $^6\text{Li}$  in an optical dipole trap (see previous chapter 5). During only 2 seconds of a single forced evaporation ramp, molecules were formed from three-body recombination near a Feshbach resonance and brought to condensation. The forced evaporative cooling was very efficient due to high trapping frequencies in the optical dipole trap and large elastic scattering cross sections close to the Feshbach resonance. Here we could conveniently follow the work of the Thomas group [Gra02] (for theoretical ground work see also [Lui96]), who had previously used this method to create a degenerate Fermi gas.

It is the long lifetime of many seconds of the molecules which was essential for the success of molecular condensation. As discussed already in chapter 5, the long lifetime is the result of a Pauli suppression effect in inelastic collisions.

In our original paper [Joc03a] we inferred the presence of the condensate from two facts. First, a measurement of the phase space density of our molecular gas clearly showed quantum degeneracy. Second, our molecular gas must have been in thermal equilibrium due to its long lifetime of many seconds.

---

<sup>1</sup>Recently R. Hulet's group has demonstrated another interesting method to investigate the cross over using an optical transition [Par05].

Furthermore we found clear signatures for superfluidity of the molecular gas 1) by measuring a characteristic frequency of a collective oscillation mode and 2) by observing mean field effects which are in general only present for degenerate quantum gases. A few weeks later, after upgrading our imaging system, we could also observe an in-situ bimodal density distribution during condensation [Bar04c] which is commonly regarded as a smoking gun for the BEC phase transition. We currently produce almost pure BECs ( $> 90\%$ ) of about  $2 \times 10^5$   $\text{Li}_2$  molecules at temperatures of a few 10 nK with typical lifetimes reaching 40 s.

The molecular BEC is a convenient starting point for the BEC-BCS crossover experiments. Reaching low temperatures through evaporative cooling tends to be easier on the BEC side than on the BCS side where Pauli blocking slows down evaporation. Further, measuring temperatures on the BEC side is simpler because the thermal cloud is much better separated from the degenerate gas than on the BCS side.

### Pair condensation

Only a couple of months after the first BEC of molecules D. Jin's group and W. Ketterle's group made interesting experiments which were interpreted as a condensation of fermionic atom pairs [Reg04, Zwi04]. Starting out with an ultracold degenerate Fermi gas on the BCS side, the Fermi gas was quickly swept across the Feshbach resonance onto the BEC side and imaged. There, for low enough temperatures, the appearance of a molecular BEC was observed. The high fraction of molecules on the BEC side led to the conclusion that preformed pairs of fermions must have already existed on the BCS side. Furthermore, since the sweep time was much too short for condensation to take place, these Fermi pairs also had to be condensed already on the BCS side.

In a separate line of experiments we could support these interpretations. Using radio-frequency spectroscopy <sup>2</sup> we were able to measure the binding energy of the fermion pairs on the BCS side as a function of temperature, density and atomic interaction strength [Chi04a]. The binding energy between the fermionic atoms can be understood in terms of a pairing gap as it is known from superconductivity.

Calculations of the group around P. Törmä agreed qualitatively and quantitatively with our experimental findings [Kin04b]. Their model predicted that at temperatures just below the Fermi temperature preformed Fermi pairs should appear which is also what we observed in the experiment. At

---

<sup>2</sup>Details of the radio-frequency spectroscopy method will be explained in the next section.

temperatures around  $0.2 T_F$ , superfluidity in the core of our gas should set in. Finally, at our lowest temperatures of around  $0.05 T_F$  a large fraction of the fermionic gas should be superfluid. Indeed, our experiment showed that at this temperature all fermions in the gas had paired up. In a beautiful experiment Zwierlein *et al.* very recently demonstrated superfluidity on the BCS side by creating vortices in the Fermi gas [Zwi05].

## 6.2 Probing the BEC-BCS crossover

Starting with a basically pure condensate of  ${}^6\text{Li}_2$  molecules held in a far detuned optical dipole trap, we explored the BEC-BCS crossover by simply sweeping the magnetic field across the Feshbach resonance. While doing so, we used various methods to investigate our system of ultracold fermions and pairs of fermions.

### Adiabatic crossing

In a first experiment we performed in-situ imaging of the trapped degenerate gas during the crossover [Bar04c]. We found that the gas density was well described by a Thomas-Fermi distribution. Calculations by Strinati *et al.* showed very good agreement with our experimental data [Per04].

By slowly ramping the magnetic field across the Feshbach resonance in an adiabatic way (time scale  $\approx 1$  s), the molecular BEC was converted into a strongly interacting degenerate Fermi gas. By slowly ramping back over the Feshbach resonance, this Fermi gas was fully reconverted into a molecular BEC. No additional losses of atoms nor any heating could be observed. This demonstrates the reversibility and adiabaticity of the crossover and consequently also conservation of entropy. Isentropic behavior is very useful because it allows us to conveniently estimate the temperature of the Fermi gas on the BCS side from a temperature measurement on the BEC side [Car04]. As a result, our high condensate fraction of  $>90\%$  corresponds to an extremely low temperature of  $k_B T < 0.04 E_F$  in the non-interacting Fermi gas limit. For such low temperatures, superfluidity has been predicted on the BCS side close to the Feshbach resonance [Hol01] and was experimentally confirmed recently [Zwi05].

Studying the size of our trapped gas we observed a smooth change of the cloud size during crossover. The cloud size increased monotonously with the magnetic field until it levelled off on the BCS side <sup>3</sup>. The increase of

---

<sup>3</sup>The cloud size was rescaled in order to compensate for unwanted changes in the trapping potential.

the cloud size can be partially understood as a response to the increasing repulsive interaction between the particles on the BEC side and partially due to the conversion into a degenerate Fermi gas which is governed by the Pauli principle. Although it is as predicted, the smoothness of the crossover is still somewhat surprising since on-resonance the effective interaction of the gas changes abruptly from strongly repulsive to strongly attractive. Related measurements on the crossover were carried out in the group of C. Salomon in Paris [Bou04] where the anisotropy and the release energy of the cloud was studied. Again, a smooth and monotone behavior was observed.

Directly on the Feshbach resonance where the scattering length diverges, the universal behavior of the gas has been studied experimentally by various groups [Bar04c, Bou04, Har02a].

### Collective excitations

Our collective excitation experiments were motivated by Sandro Stringari who predicted an interesting behavior across the BEC-BCS crossover [Str04]. Already with atomic BECs, the study of collective excitations has proven to be an important tool to characterize the properties of these superfluid gases and to gain insight into their behavior (see for example [Jin97, Mew96, Che02, Str96]). Collective excitations can be quite sensitive to interaction effects, and their frequencies can in general be measured with high accuracy. The subject of collective excitations is a large field with many theoretical and experimental groups having contributed over the years. For the lack of space we cannot go into detailed discussions here and merely give an overview. For introductory literature we refer to [Pit03, Pet02, Dal99a, GO99, Bar04a]. With respect to collective oscillations one distinguishes between compressional modes and surface modes which can be characterized by angular momentum and radial quantum numbers. Different modes have different sensitivities on properties of the trapped gas, its equation of state as well as the trapping potential. Depending on the state of a gas, two different asymptotic regimes can be realized: the collisional/ hydrodynamic and collisionless regime. In general, these different regimes result in different collective excitation responses, which can be used to identify the state of the gas.

We performed our experiments [Bar04b] in a cigar shaped dipole trap where we excited two different oscillation modes, a slow axial quadrupole mode and a fast radial monopole (breathing) mode. We studied the change in frequencies and damping of these modes in the crossover as we passed through several regimes: BEC limit, strongly interacting BEC, unitary limit and strongly interacting Fermi gas. In brief, our measurements on the *axial* quadrupole mode agree well with the theoretical predictions. Close to

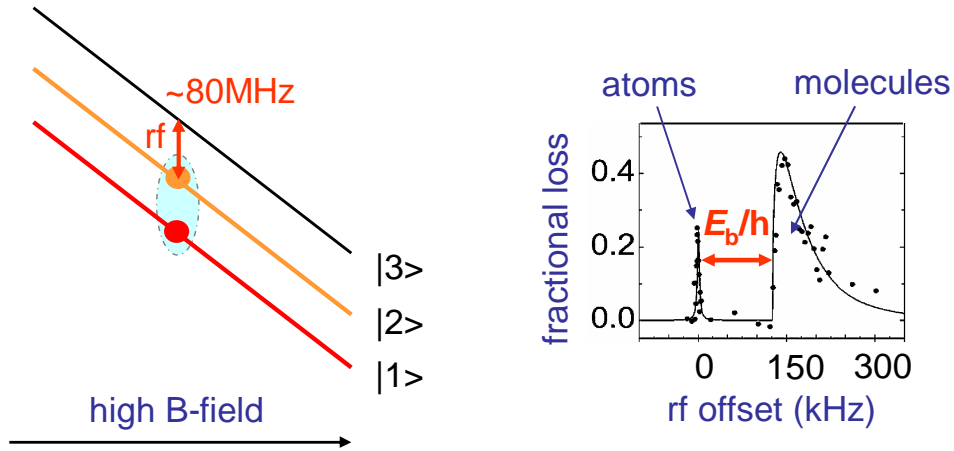


Figure 6.3: Radio-frequency (rf) spectroscopy. (left) We use rf of about 80 MHz to flip the spin from state  $|2\rangle$  to state  $|3\rangle$ . In our gas of atoms the induced loss in state  $|2\rangle$  gives rise to a narrow absorption line (right). If state  $|2\rangle$  is bound in a molecule, then in order to flip the spin, both the molecule has to be broken up and the spin is to be flipped. This requires additional energy and thus produces a second absorption line at higher frequencies. The distance between the two lines corresponds to the binding energy  $E_b$  of the molecule.

resonance very low damping is observed which gives strong evidence for superfluidity. For the *radial* breathing mode the frequency shifts are in general larger than predicted. Especially on resonance our data do not agree with the calculations for the universal regime [Str04, Hei04, Hu04, Man05]. Apart from these quantitative differences, we also discovered a striking and unexpected feature in our measurements. An abrupt change of the oscillation frequency appeared on the BCS side which was accompanied by strong damping. We currently interpret this as a sudden transition from a superfluid to a collisionless phase.

Parallel to our work, the group of J. Thomas studied extensively the radial breathing mode in the crossover region [Kin04a, Kin04c, Kin05]. Qualitatively, their results are similar to ours. Quantitatively there are some discrepancies. In general they observe smaller frequency shifts compared to our measurements. Further, on resonance in the unitary limit their data agree with the theoretical predictions in contrast to ours. The reason for this different behavior is not yet fully understood and needs to be investigated further.

## Measuring the binding energy of Fermi pairs

Rf spectroscopy was first introduced by the groups of D. Jin and W. Ketterle as a powerful and sensitive tool to measure interaction effects of the Fermi gas near the Feshbach resonance [Reg03a, Gup03] and to measure the binding energy of the molecules on the BEC side of the Feshbach resonance [Reg03]. We have extended the rf spectroscopy method to measure the binding energy of fermion pairs across the whole crossover [Chi04a]. Figure 6.3 illustrates the scheme. In brief, driving a spin flip of the nuclear spin in our atomic  ${}^6\text{Li}$  gas we can measure accurately the energy it takes to do so. For free atoms this energy is given precisely by the well known Breit-Rabi formula [Bar04a]. If the atoms, on the other hand, are bound in a molecule or some kind of Cooper pair, then flipping the spin takes some additional energy which corresponds to the binding energy.

We found that far away from the Feshbach resonance on the BEC side, the measured binding energy of the molecules is well described by conventional two-body physics. As we approach the Feshbach resonance the binding energy increasingly deviates from this theory. Further, we observed an increasing dependence of the binding energy on the gas density, which demonstrates the setting in of many-body effects. As we approach the Feshbach resonance the two-body bound state continuously goes over into a Cooper pair kind of bound state which is stabilized by the degenerate Fermi gas around it. Right on resonance and on the BCS side, where no molecules can exist according to two-body theory, we still observe bound states which correspond the pairs of fermions.

There is still a lot we can learn in the future about the properties of the Fermi pairs with the help of rf spectroscopy. The shape of the rf-peak of the Fermi pair, for example, contains information on the pair size. By studying how the rf-signals depend on temperature and density of the degenerate Fermi gas, scaling effects can be studied which are especially interesting in view of existing theoretical predictions in the universal regime [Hei01, Ho04].



## 6.3 “Bose-Einstein Condensation of Molecules”

S. Jochim, M. Bartenstein, A. Altmeyer, G. Hendl, S. Riedl, C. Chin, J. Hecker Denschlag, and R. Grimm

Science **302**, 2101-2103 (2003)

# Bose-Einstein Condensation of Molecules

S. Jochim,<sup>1</sup> M. Bartenstein,<sup>1</sup> A. Altmeyer,<sup>1</sup> G. Hendl,<sup>1</sup> S. Riedl,<sup>1</sup>  
C. Chin,<sup>1</sup> J. Hecker Denschlag,<sup>1</sup> R. Grimm<sup>1,2\*</sup>

We report on the Bose-Einstein condensation of more than  $10^5$   $\text{Li}_2$  molecules in an optical trap starting from a spin mixture of fermionic lithium atoms. During forced evaporative cooling, the molecules are formed by three-body recombination near a Feshbach resonance and finally condense in a long-lived thermal equilibrium state. We measured the characteristic frequency of a collective excitation mode and demonstrated the magnetic field–dependent mean field by controlled condensate spilling.

Since the first experiments on Bose-Einstein condensation (BEC) in ultracold atomic gases in 1995 (1–3), atoms of eight chemical elements have been condensed. BEC of more complex objects such as molecules or Cooper-paired atoms will open up many new avenues of research because they offer new degrees of freedom. An intriguing example is the fundamental change in quantum statistics when paired fermions form composite bosons. Recent experiments have demonstrated the formation of molecules in ultracold atomic gases of bosons (4–9) and fermions (10–13). Experiments starting with atomic BEC show the creation of molecular clouds at the threshold to quantum degeneracy (7) or clearly in that regime (9), but not in a thermal equilibrium state. In most of these experiments, weakly bound dimers are produced via magnetically tuned Feshbach resonances (14). Such a scattering resonance occurs when a free colliding atom pair energetically coincides with a bound molecular state. On the side of the resonance where the energy of the molecular level is below the dissociation limit, a weakly bound dimer state exists. The experiments indicate an important difference between weakly bound dimers composed of bosonic and of fermionic atoms. Dimers of bosons show a quick decay via inelastic atom-molecule or molecule-molecule collisions (9), so that quantum-degenerate molecular clouds can only be created in a transient regime. In contrast, the dimers of fermions exhibit a remarkable stability (11–13, 15). Such molecular gases have been observed with lifetimes far longer than the time scales for elastic collisions and thermalization. This fact has been explained by a fermionic suppression of vibrational quenching in molecule collisions (16). Their stability allows us to use bosonic mole-

cules composed of fermionic atoms to achieve molecular BEC in thermal equilibrium.

Our experiment is based on evaporative cooling of an optically trapped mixture of fermionic  ${}^6\text{Li}$  atoms in the two lowest spin states (11–13, 17–21). During the cooling process, a large number of bosonic dimers are formed by three-body recombination and finally condense into a molecular BEC. The spin mixture exhibits a broad Feshbach resonance at a magnetic field of about 850 G (18, 19, 22, 23), which leads to a pronounced magnetic field dependence of the scattering length  $a$  (Fig. 1) that characterizes the  $s$ -wave interactions. Dimers in a single weakly bound state can be formed in the range of large positive  $a$  with a binding energy of  $\hbar^2/(ma^2)$ , where  $\hbar$  is Planck's constant  $h$  divided by  $2\pi$  and  $m$  is the mass of a  ${}^6\text{Li}$  atom. This has been observed in magnetic field–dependent loss features (24) and changes in the interaction energy of the gas (21). Two recent experiments have directly demonstrated the presence of these molecules and investigated some of their properties (12, 13). For negative scattering length, no weakly bound dimer state exists. For negative scattering length, where a weakly bound dimer state does not exist, the  ${}^6\text{Li}$  gas exhibits a remarkable stability against collisional decay, and deeply degenerate Fermi gases have been created (20).

Our optical dipole trap is realized with a single Gaussian laser beam at a wavelength of 1030 nm, which is focused to a waist of 23  $\mu\text{m}$ . At the full power of  $P_0 = 10.5$  W, the radial and axial oscillation frequencies are  $\Omega_r/2\pi = 14.5$  kHz and  $\Omega_z/2\pi = 140$  Hz, respectively, and the atom trap is  $U_0 \approx k_B \times 800$   $\mu\text{K}$  deep ( $k_B$  denotes Boltzmann's constant). When the power  $P$  is reduced to a relative value  $p = P/P_0$ , the optical trap frequencies follow  $p^{1/2}\Omega_i$  ( $i = r, z$ ) and the trap depth for the atoms is  $U_{\text{at}} = pU_0$ . Our magnetic field  $B$  used for Feshbach tuning exhibits a curvature that gives rise to an additional contribution to the trapping potential. For the tight radial confinement of the optical trap, this effect is negligibly small. For the weak axis, however, a magnetic trap-

ping effect becomes important with decreasing  $p$ . Taking this into account, the axial trap frequency is given by  $\omega_z = \sqrt{p\Omega_z^2 + \omega_m^2}$ . Here  $\omega_m/2\pi = 24.5$  Hz  $\times \sqrt{B/\text{kG}}$  is the magnetic contribution, which is precisely known for our coils. For weak traps with  $p \ll 0.03$  ( $U_{\text{at}}/k_B \ll 25$   $\mu\text{K}$ ), the magnetic contribution dominates, and the axial confinement is harmonic with a corresponding frequency known on the percent level. In this regime, the mean trap frequency is given by  $\bar{\omega} = (p\Omega_r^2\omega_m)^{1/3}$ . For the weakly bound  ${}^6\text{Li}$  dimers, all external forces are twice the ones on the individual atoms. Thus, the molecular trap is two times deeper than the atom trap ( $U_{\text{mol}} = 2U_{\text{at}}$ ), and the trap frequencies are identical. Gravity is compensated for by a magnetic field gradient of 1.1 G/cm.

We start the evaporation process with  $\sim 1.5 \times 10^6$  atoms at a temperature of  $\sim 80$   $\mu\text{K}$ , a peak number density of  $\sim 10^{14}$   $\text{cm}^{-3}$ , and a peak phase-space density of  $\sim 5 \times 10^{-3}$ . The mean elastic collision rate is as high as  $\sim 5 \times 10^4$   $\text{s}^{-1}$ . These excellent starting conditions are obtained by a two-stage loading process. The atoms are loaded into the dipole trap from another deep, large-volume standing wave trap (25), which itself is loaded from a magneto-optical trap. Forced evaporative cooling is then performed by reducing the trap power (17, 20). We use a simple exponential ramp with a relative power  $p(t) = \exp(-t/\tau)$ , where the time constant  $\tau = 0.23$  s is experimentally optimized. A feedback system allows us to precisely control the laser power to levels well below  $p = 10^{-4}$ .

BEC of weakly bound molecules occurs when we perform evaporative cooling at a large positive scattering length of  $a \approx +3500a_0$ , where  $a_0$  is Bohr's radius. In this case, the evaporation process shows a strikingly different behavior in comparison with the corresponding situation at large negative scattering length, where no dimers can be produced.

First we discuss the creation of a degenerate Fermi gas without the possibility of molecule formation at a magnetic field of 1176 G, where  $a \approx -3500a_0$  (23). Here the evaporation pro-

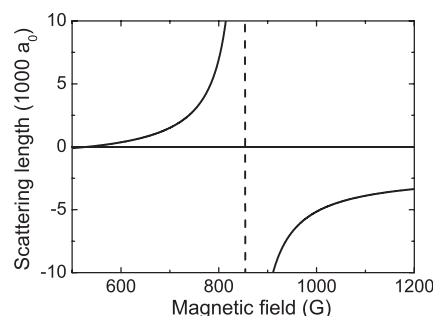


Fig. 1. Feshbach resonance at  $\sim 850$  G in a mixture of the two lowest spin states of  ${}^6\text{Li}$  (18). The  $s$ -wave scattering length  $a$  is plotted as a function of the magnetic field  $B$ .

<sup>1</sup>Institut für Experimentalphysik, Universität Innsbruck, Technikerstraße 25, 6020 Innsbruck, Austria.  
<sup>2</sup>Institut für Quantenoptik und Quanteninformation, Österreichische Akademie der Wissenschaften, 6020 Innsbruck, Austria.

\*To whom correspondence should be addressed. E-mail: rudolf.grimm@uibk.ac.at

## REPORTS

ceeds in a very similar way as that described in (17, 20). The measured atom number  $N$  (26) first follows a scaling law  $N/N_0 = p^\alpha$  (27), with  $\alpha \approx 0.25$ . In this regime, the temperature of the gas is typically a factor of 10 below the trap depth (27), and the elastic collision rate stays well above  $10^4 \text{ s}^{-1}$ . The crossover to Fermi degeneracy, where the thermal energy  $k_B T$  reaches the Fermi energy  $E_F = \hbar \bar{\omega} (3N)^{1/3}$ , takes place at  $p \approx 0.05$  ( $U_{\text{at}}/k_B \approx 40 \text{ } \mu\text{K}$ ). By further decreasing  $p$ , the trap depth  $U_{\text{at}} \propto p$  decreases faster than the Fermi energy  $E_F \propto p^{1/3}$ . A threshold occurs when  $E_F$  reaches  $U_{\text{at}}$  and the trap is filled up to the "rim." Further decrease of  $p$  then leads to a spilling of atoms out of the trap and thus to a rapid decrease of  $N$  with  $p$ . Our data (Fig. 2) clearly show this spilling effect for  $p < 1 \times 10^{-3}$  ( $U_{\text{at}}/k_B < 800 \text{ nK}$ ). Modeling the spilling curves provides us with an upper bound of  $k_B T < 0.2E_F$  for the temperature in terms of the Fermi energy. In the regime of a completely filled shallow trap, the number of atoms in the two-component spin mixture is given by two times the number of quantum states in the trap. A numerical calculation, shown in Fig. 2, confirms this interpretation of our data.

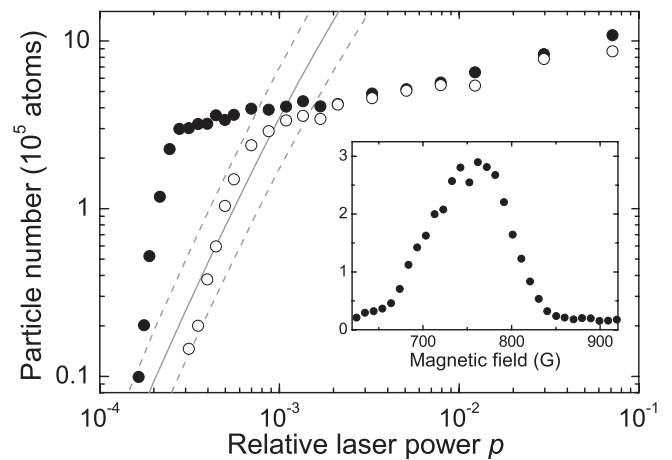
The same evaporation procedure is performed at a magnetic field of 764 G, where the scattering length  $a \approx +3500a_0$  (23) has essentially the same magnitude but opposite sign. Here the weakly bound dimers have a binding energy of  $\sim 2 \text{ } \mu\text{K}$ , and their formation has been observed in several experiments (12, 13, 21). In order to detect the molecules, we dissociate them and measure the number of resulting atoms (26). For this purpose, we abruptly turn on the full trap power, which strongly heats the sample and leads to collisional dissociation. In order to ensure that we dissociate all molecules, we also apply a magnetic field ramp across the Feshbach resonance (13). The number of atoms measured after the dissociation process thus yields the number of free atoms together with atoms having formed molecules.

Below  $p = 1 \times 10^{-3}$  the measured atom numbers (solid circles in Fig. 2) show a striking difference in comparison with the case of the degenerate Fermi gas. Down to a power level of  $p = 3 \times 10^{-4}$  ( $U_{\text{mol}}/k_B \approx 480 \text{ nK}$ ), the trap holds almost all particles and contains up to 20 times more atoms than would be possible for fermions. Hence, the trapped sample can no longer be an atomic Fermi gas. The trap is filled with bosonic molecules in the weakly bound state (28). The lifetime of the molecular ensemble, for which we measure about 20 s at a fixed trap depth of  $U_{\text{mol}}/k_B \approx 560 \text{ nK}$ , exceeds the time scale of elastic collisions ( $\sim 100 \text{ } \mu\text{s}$ ) by several orders of magnitude. This highlights the fact that the molecular cloud exists in a thermal equilibrium state.

The formation of molecules during the evaporative cooling process can be understood

in terms of a chemical atom-molecule equilibrium (29, 30). Exothermal three-body recombination processes compete with dissociation by endothermal two-body processes. When the gas is cooled down, the equilibrium shifts to an increasing fraction of molecules. Because atom-atom, atom-molecule, and molecule-molecule collisions have comparable cross sections near the resonance (16), evaporation continues at about the same speed. In the final stage of cooling, all relevant energies, such as the thermal energy  $k_B T$  and the trap depths  $U_{\text{at}}$  and  $U_{\text{mol}}$ , are far below the binding energy  $\hbar^2/(ma^2)$ , so that in chemical equilibrium one is left with an essentially pure sample of molecules. The fact that the binding energy of  $\sim 2 \text{ } \mu\text{K}$  at our optimized magnetic field of 764 G is a few times larger than the final trap depth (inset, Fig. 1) fits well into this picture.

The observation that a large number of  $N_{\text{mol}} \approx 1.5 \times 10^5$  molecules is confined in our very shallow, only 480 nK deep trap under thermal equilibrium conditions already shows that a molecular BEC is formed. The trap offers about 10 times more quantum states for dimers as compared to the case of atoms discussed before (31). Because we observe a factor of  $\sim 20$  more particles than for the degenerate atomic Fermi gas, the molecular gas is necessarily quantum degenerate. Because of the high elastic collision rates, which stay well above  $10^3 \text{ s}^{-1}$  even for very shallow traps, the sample is also thermalized. The temperature then is a small fraction of the trap depth. According to standard evaporation theory (27), we can typically assume  $T \approx 0.1 U_{\text{mol}}/k_B \approx 50 \text{ nK}$ . This is well below the critical temperature for BEC, for



which we calculate  $T_C = \hbar \bar{\omega} k_B^{-1} (N_{\text{mol}}/1.202)^{1/3} = 280 \text{ nK}$ . Because the condensate fraction is given by  $1 - (T/T_C)^3$ , these arguments show that the molecular BEC must be almost pure.

To investigate the molecular condensate, we have studied a characteristic collective excitation mode (32, 33). For a cigar-shaped sample in the Thomas-Fermi limit, well fulfilled in our experiment, such a quadrupolar mode is expected at a frequency of  $\sqrt{5/2} \omega_z = 2\pi \times 33.8 \text{ Hz}$ . We perform our measurement at  $p = 3.5 \times 10^{-4}$  ( $U_{\text{mol}}/k_B \approx 560 \text{ nK}$ ) with a trapped sample of  $\sim 10^5$  molecules. We apply a sinusoidal modulation to the magnetic field with an amplitude of 3.5 G to modulate the molecular scattering length  $a_m \propto a$  (16) with a relative amplitude of about 5%. After 2 s of continuous excitation, we measure the remaining number of particles in the trap. The resonance manifests itself in a sharp dip in the number of particles (Fig. 3). The observed resonance frequency of 33.6 Hz is in remarkable agreement with the expectation. We point out that a noncondensed gas deep in the hydrodynamic regime would show a similar frequency of 33.2 Hz (34), but thermalization in our shallow trap excludes this scenario (35). The measured collective excitation frequency rules out a gas in the collisionless regime, which would show its resonant loss at  $2\omega_z = 2\pi \times 42.8 \text{ Hz}$ , and thus again confirms the thermalization of the sample. The observed narrow resonance width of  $\sim 1 \text{ Hz}$  shows a very low damping rate and is consistent with an almost pure BEC (33, 36).

An essential property of a BEC is its mean field potential  $U_{\text{MF}} = 4\pi n a_m \hbar^2/(2m)$  resulting

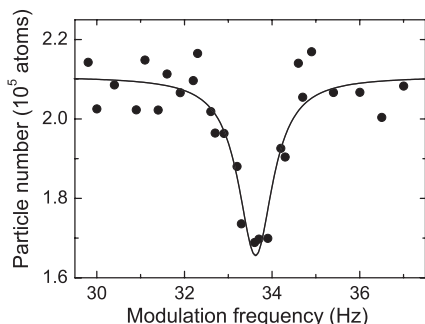


**Fig. 3.** Resonance of a collective excitation mode at  $\sqrt{5/2} \omega_z$ . The oscillation is excited by magnetic modulation of the molecular BEC mean field. The solid curve shows a Lorentzian fit to the data.

from  $s$ -wave interactions; here  $n$  denotes the molecular density. For our molecular BEC with large positive  $a_m$ , the mean field is repulsive and thus stabilizes the BEC against collapse and decay. In a trap of finite depth, however, the mean field repulsion limits the maximum number of trappable molecules. When the chemical potential  $\mu$  reaches the trap depth, a similar spilling effect is expected as we see for the Fermi gas, but for weaker traps. The decrease of our molecular signal (Fig. 2) below  $p = 3 \times 10^{-4}$  ( $U_{\text{mol}}/k_B \approx 480$  nK) may be explained by such a spilling effect.

We used spilling in a controlled way to demonstrate the mean field of the molecular BEC and to investigate its dependence on the magnetic field. After producing the BEC at a magnetic field of  $B_1 = 772$  G and  $p = 3.5 \times 10^{-4}$  ( $U_{\text{mol}}/k_B \approx 560$  nK), we adiabatically tilt the vertical trapping potential by application of a magnetic field gradient  $B'$  that is smoothly ramped up within 50 ms. The number of remaining particles as a function of the applied field gradient (Fig. 4) shows the loss of molecules resulting from the reduced trap depth. When the magnetic field is kept at the evaporation field of  $B_1 = 772$  G, where  $a = 4100a_0$  (23), even very weak gradients lead to loss (open circles in Fig. 4). This indicates that the chemical potential is close to the potential depth, so that the trap is full. The chemical potential can be lowered by reducing the scattering length. For this purpose, we ramp the magnetic field to a smaller value. A spilling curve taken at  $B_2 = 731$  G, where  $a = 2200a_0$  (23), indeed shows a markedly different behavior (solid circles in Fig. 4). Here small gradients do not lead to any loss and the curve thus shows a flat top. For gradients  $|B'|$  exceeding 0.65 G/cm, molecules get spilled until everything is lost at  $|B'| = 1.3$  G/cm. The sharp onset of the spilling confirms the essentially pure nature of the BEC.

A comparison of the two spilling curves in Fig. 4 provides us with information on the ratio of the scattering lengths  $a_m$  at the two magnetic fields  $B_1$  and  $B_2$ . In the spilling region above  $|B'| = 0.65$  G/cm, the trap is full in both cases,

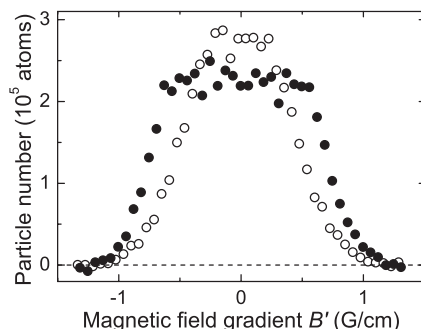


**Fig. 4.** Controlled spilling of the BEC by application of a magnetic field gradient  $B'$ . This variable gradient is applied in addition to the constant gradient of 1.1 G/cm that we use for gravity compensation. The data are taken at the two different magnetic fields  $B_1 = 772$  G (open circles) and  $B_2 = 731$  G (solid circles), where the mean field of the BEC is different by a factor of  $\sim 2$ .

and the trapped particle number is inversely proportional to  $a_m$ . Comparing the two spilling curves in that region, we obtain a scattering length ratio of  $a_m(B_1)/a_m(B_2) = 2.4(2)$ . This factor is indeed close to the factor of 1.9 (23) expected from the proportionality of atomic and molecular scattering lengths  $a_m \propto a$  (16) and the dependence of  $a$  shown in Fig. 1. This observation demonstrates the mean field of the molecular BEC together with its magnetic tunability.

The ability to control interactions in a Bose condensed ensemble of paired fermionic atoms has many exciting prospects (37, 38). It opens up unique ways to cool a fermionic gas far below the Fermi temperature (39) and to study different regimes of superfluidity (40–43). The experimental exploration of the strongly interacting crossover regime between a BEC-like and a Cooper-paired phase is a particular challenge and promises more insight into the physical mechanisms underlying superconductivity.

#### References and Notes

- M. Anderson, J. Ensher, M. Matthews, C. Wieman, E. Cornell, *Science* **269**, 198 (1995).
- K. Davis *et al.*, *Phys. Rev. Lett.* **75**, 3969 (1995).
- C. Bradley, C. Sackett, J. Tollett, R. Hulet, *Phys. Rev. Lett.* **75**, 1687 (1995).
- R. Wynar, R. S. Freeland, D. J. Han, C. Ryu, D. J. Heinzen, *Science* **287**, 1016 (2000).
- E. A. Donley, N. R. Claussen, S. T. Thompson, C. E. Wieman, *Nature* **417**, 529 (2002).
- C. Chin, A. J. Kerman, V. Vuletić, S. Chu, *Phys. Rev. Lett.* **90**, 033201 (2003).
- J. Herbig *et al.*, *Science* **301**, 1510 (2003); published online 21 August 2003 (10.1126/science.1088876).
- S. Dürr, T. Volz, A. Marte, G. Rempe, preprint available at <http://arxiv.org/abs/cond-mat/0307440>.
- K. Xu, *et al.* preprint available at <http://arxiv.org/abs/cond-mat/0310027>.
- C. A. Regal, C. Ticknor, J. L. Bohn, D. S. Jin, *Nature* **424**, 47 (2003).
- K. E. Strecker, G. B. Partridge, R. G. Hulet, *Phys. Rev. Lett.* **91**, 080406 (2003).
- J. Cubizolles, T. Bourdel, S. J. J. M. F. Kokkelmans, G. V. Shlyapnikov, C. Salomon, preprint available at <http://arxiv.org/abs/cond-mat/0308018>.

- S. Jochim *et al.*, *Phys. Rev. Lett.*, in press (preprint available at <http://arxiv.org/abs/cond-mat/0308095>).
- S. Inouye *et al.*, *Nature* **392**, 151 (1998).
- C. A. Regal, M. Greiner, D. S. Jin, preprint available at <http://arxiv.org/abs/cond-mat/0308606>.
- D. S. Petrov, C. Salomon, G. V. Shlyapnikov, preprint available at <http://arxiv.org/abs/cond-mat/0309010>.
- S. Granade, M. E. Gehm, K. M. O'Hara, J. E. Thomas, *Phys. Rev. Lett.* **88**, 120405 (2002).
- K. M. O'Hara *et al.*, *Phys. Rev. A* **66**, 041401 (2002).
- S. Jochim *et al.*, *Phys. Rev. Lett.* **89**, 273202 (2002).
- K. M. O'Hara, S. L. Hemmer, M. E. Gehm, S. R. Granade, J. E. Thomas, *Science* **298**, 2179 (2002); published online 7 November 2002 (10.1126/science.1079107).
- T. Bourdel *et al.*, *Phys. Rev. Lett.* **91**, 020402 (2003).
- M. Houbiers, H. T. C. Stoof, W. McAlexander, R. Hulet, *Phys. Rev. A* **57**, R1497 (1998).
- The position of the Feshbach resonance is known to within a few tens of Gauss. All numbers given for the scattering lengths and binding energies are subject to a corresponding systematic error.
- K. Dieckmann *et al.*, *Phys. Rev. Lett.* **89**, 203201 (2002).
- A. Mosk *et al.*, *Opt. Lett.* **26**, 1837 (2001).
- We measure the atom number via fluorescence detection after recapture into a magneto-optical trap. In order to avoid molecule formation and loss when the Feshbach tuning field is ramped down before detection, we heat the sample by abruptly turning on the full laser power of the optical dipole trap. At low phase-space densities, the thermal gas is not affected by the downward Feshbach ramp (13).
- K. M. O'Hara, M. E. Gehm, S. R. Granade, J. E. Thomas, *Phys. Rev. A* **64**, 051403 (2001).
- We know that only the weakly bound state is populated, because the release of binding energy in a three-body process would otherwise lead to immediate trap loss. Moreover, our dissociation-based detection is sensitive only to molecules in this state.
- C. Chin, R. Grimm, preprint available at <http://arxiv.org/abs/cond-mat/0309078>.
- S. J. J. M. F. Kokkelmans, G. V. Shlyapnikov, C. Salomon, preprint available at <http://arxiv.org/abs/cond-mat/0308384>.
- For the harmonically approximated trap with same frequencies and twice the depth, the molecules have eight times more quantum states than the atoms. The lower  $\omega_z$  at 764 G as compared to 1176 G gives another factor of 1.24.
- S. Stringari, *Phys. Rev. Lett.* **77**, 2360 (1996).
- D. M. Stamper-Kurn, H.-J. Miesner, S. Inouye, M. R. Andrews, W. Ketterle, *Phys. Rev. Lett.* **81**, 500 (1998).
- D. Guéry-Odelin, F. Zambelli, J. Dalibard, S. Stringari, *Phys. Rev. A* **60**, 4851 (1999).
- A noncondensed ensemble in the hydrodynamic regime, where the elastic collision rate exceeds all other time scales, would rapidly cool down by evaporation to temperatures far below the trap depth and thus form a BEC.
- D. S. Jin, M. R. Matthews, J. R. Ensher, C. E. Wieman, E. A. Cornell, *Phys. Rev. Lett.* **78**, 764 (1997).
- L. Pitaevskii, S. Stringari, *Science* **298**, 2144 (2002).
- A. Cho, *Science* **301**, 750 (2003).
- L. D. Carr, G. V. Shlyapnikov, Y. Castin, preprint available at <http://arxiv.org/abs/cond-mat/0308306>.
- H. T. C. Stoof, M. Houbiers, C. Sackett, R. Hulet, *Phys. Rev. Lett.* **76**, 10 (1996).
- M. Holland, S. J. J. M. F. Kokkelmans, M. L. Chiofalo, R. Walsler, *Phys. Rev. Lett.* **87**, 120406 (2001).
- E. Timmermans, K. Furuya, P. W. Milonni, A. K. Kerman, *Phys. Lett. A* **285**, 228 (2001).
- Y. Ohashi, A. Griffin, *Phys. Rev. Lett.* **89**, 130402 (2002).
- We thank P. Zoller for very useful discussions and for stimulating the measurement of the collective excitation frequency. We acknowledge support by the Austrian Science Fund (FWF) within Spezialforschungsbereich 15 (project part 15) and by the European Union through the Cold Molecules Training and Mobility of Researchers Network under contract no. HPRN-CT-2002-00290. C.C. is a Lise-Meitner fellow of the FWF.

3 November 2003; accepted 11 November 2003  
Published online 13 November 2003;  
10.1126/science.1093280

Include this information when citing this paper.

## 6.4 “Observation of the pairing gap in a strongly interacting Fermi gas”

C. Chin, M. Bartenstein, A. Altmeyer, S. Riedl, S. Jochim,  
J. Hecker Denschlag, and R. Grimm

Science **305**, 1128-1130 (2004)

16. A. vanOtterlo *et al.*, *Phys. Rev. B* **52**, 16176 (1995).
17. G. Schmid, S. Todo, M. Troyer, A. Dornreich, *Phys. Rev. Lett.* **88**, 167208 (2002).
18. A. Görlitz, *Phys. Rev. Lett.* **87**, 130402 (2001).
19. M. Greiner, I. Bloch, O. Mandel, T. W. Hänsch, T. Esslinger, *Appl. Phys. B* **73**, 769 (2001).
20. M. T. DePue, C. McCormick, S. L. Winoto, S. Oliver, D. S. Weiss, *Phys. Rev. Lett.* **82**, 2262 (1999).
21. B. L. Tolra *et al.*, *Phys. Rev. Lett.* **92**, 190401 (2004).
22. H. Moritz, T. Söferle, M. Köhl, T. Esslinger, *Phys. Rev. Lett.* **91**, 250402 (2003).
23. T. Söferle, H. Moritz, C. Schori, M. Köhl, T. Esslinger, *Phys. Rev. Lett.* **92**, 130403 (2004).
24. B. Paredes *et al.*, *Nature* **429**, 277 (2004).
25. V. Dunjko, V. Lorent, M. Olshanii, *Phys. Rev. Lett.* **86**, 5413 (2001).
26. M. Greiner, O. Mandel, T. Esslinger, T. W. Hänsch, I. Bloch, *Nature* **415**, 39 (2002).
27. T. Kinoshita, T. Wenger, D. S. Weiss, in preparation.
28. D. J. Han, M. T. DePue, D. S. Weiss, *Phys. Rev. A* **63**, 023405 (2001).
29. M. T. DePue, S. L. Winoto, D. J. Han, D. S. Weiss, *Opt. Commun.* **180**, 73 (2000).
30. S. L. Winoto, M. T. DePue, N. E. Bramall, D. S. Weiss, *Phys. Rev. A*, **59**, R19 (1999).
31. We thank M. Olshanii, K. Gibble, and J. Banavar for

useful discussions and V. Dunjko for providing us with the exact 1D Bose gas theory curves. This work was supported by the NSF grant no. PHY-0137477.

**Supporting Online Material**

www.sciencemag.org/cgi/content/full/1100700/DC1  
SOM Text  
Table S1

25 May 2004; accepted 20 July 2004

Published online 29 July 2004;

10.1126/science.1100700

Include this information when citing this paper.

# Observation of the Pairing Gap in a Strongly Interacting Fermi Gas

C. Chin,<sup>1</sup> M. Bartenstein,<sup>1</sup> A. Altmeyer,<sup>1</sup> S. Riedl,<sup>1</sup> S. Jochim,<sup>1</sup>  
J. Hecker Denschlag,<sup>1</sup> R. Grimm<sup>1,2\*</sup>

We studied fermionic pairing in an ultracold two-component gas of <sup>6</sup>Li atoms by observing an energy gap in the radio-frequency excitation spectra. With control of the two-body interactions through a Feshbach resonance, we demonstrated the dependence of the pairing gap on coupling strength, temperature, and Fermi energy. The appearance of an energy gap with moderate evaporative cooling suggests that our full evaporation brought the strongly interacting system deep into a superfluid state.

The spectroscopic observation of a pairing gap in the 1950s marked an important experimental breakthrough in research on superconductivity (1). The gap measurements provided a key to investigating the paired nature of the particles responsible for the frictionless current in metals at very low temperatures. The ground-breaking Bardeen-Cooper-Schrieffer (BCS) theory, developed at about the same time, showed that two electrons in the degenerate Fermi sea can be coupled by an effectively attractive interaction and will form a delocalized, composite particle with bosonic character. BCS theory predicted that the gap in the low-temperature limit is proportional to the critical temperature  $T_c$  for the phase transition, in agreement with the experimental measurements. In general, the physics of superconductivity and superfluidity go far beyond the weak-coupling limit of BCS theory. In the limit of strong coupling, paired fermions form localized bosons, and the system can undergo Bose-Einstein condensation (BEC). The BCS limit and the BEC limit are connected by a smooth BCS-BEC crossover, which has been a subject of great theoretical interest for more than three decades (2–5). The formation of pairs generally represents a key ingredient of superfluidity in fermionic sys-

tems, and the gap energy is a central quantity to characterize the pairing regime.

The rapid progress in experiments with ultracold degenerate Fermi gases (6) has opened up a unique testing ground to study phenomena related to pairing and superfluidity at densities typically a billion times below the ones in usual condensed-matter systems. In cold-atom experiments, magnetically tuned scattering resonances (Feshbach resonances) serve as a powerful tool to control the two-body coupling strength in the gas (7). On the basis of such a resonance, a strongly interacting degenerate Fermi gas was recently realized (8). A major breakthrough then followed, with the creation of Bose-Einstein condensates of molecular dimers composed of fermionic atoms (9–13), which corresponds to the realization of a BEC-type superfluid in the strong coupling limit. By variation of the coupling strength, subsequent experiments (12, 14–18) began to explore the crossover to a BCS-type system. This BEC-BCS crossover is closely linked to the predicted “resonance superfluidity” (19–22) and a “universal” behavior of a Fermi gas with resonant interactions (23, 24). The observation of the condensation of atom pairs (15, 16) and measurements of collective oscillations (17, 18) support the expected superfluidity at presently attainable temperatures in Fermi gases with resonant interactions.

We prepared our ultracold gas of fermionic <sup>6</sup>Li atoms in a balanced spin-mixture of the two lowest sub-states |1> and |2> of the electronic 1s<sup>2</sup> 2s ground state, employing methods of laser

cooling and trapping and subsequent evaporative cooling (9). A magnetic field  $B$  in the range between 650 to 950 G was applied for Feshbach tuning through a broad resonance centered at the field  $B_0 \approx 830$  G. In this high-field range, the three lowest atomic levels form a triplet of states |1>, |2>, and |3>, essentially differing by the orientation of the nuclear spin ( $m_I = 1, 0, -1$ , where  $m_I$  is the nuclear magnetic quantum number). In the resonance region with  $B < B_0$ , the s-wave scattering length  $a$  for collisions between atoms in states |1> and |2> is positive. Here, two-body physics supports a weakly bound molecular state with a binding energy  $E_b = \hbar^2/(ma^2)$ , where  $\hbar$  is Planck’s constant  $h$  divided by  $2\pi$  and  $m$  is the atomic mass. Molecules formed in this state can undergo BEC (9–13). At  $B = B_0$ , the two-body interaction is resonant ( $a \rightarrow \pm\infty$ ), corresponding to a vanishing binding energy of the molecular state. Beyond the resonance ( $B > B_0$ ), the scattering length is negative ( $a < 0$ ), which leads to an effective attraction. Here, two-body physics does not support a weakly bound molecular level, and pairing can only occur because of many-body effects.

Our experimental approach (9, 14) facilitated preparation of the quantum gas in various regimes with controlled temperature, Fermi energy, and interaction strength. We performed evaporative cooling under conditions (25) in which an essentially pure molecular Bose-Einstein condensate containing  $N = 4 \times 10^5$  paired atoms could be created as a starting point for the experiments. The final laser power of the evaporation ramp allowed us to vary the temperature  $T$ . The Fermi energy  $E_F$  (Fermi temperature  $T_F = E_F/k_B$ , with Boltzmann’s constant  $k_B$ ) was controlled by a recompression of the gas, which we performed by increasing the trap laser power after the cooling process (25). We then varied the interaction strength by slowly changing the magnetic field to the desired final value. The adiabatic changes applied to the gas after evaporative cooling proceeded with conserved entropy (14). Lacking a reliable method to determine the temperature  $T$  of a deeply degenerate, strongly interacting Fermi gas in a direct way, we characterized the system by the temperature  $T'$  measured after an isentropic conversion into the BEC limit (25). For

<sup>1</sup>Institut für Experimentalphysik, Universität Innsbruck, Technikerstraße 25, 6020 Innsbruck, Austria.

<sup>2</sup>Institut für Quantenoptik und Quanteninformation, Österreichische Akademie der Wissenschaften, 6020 Innsbruck, Austria.

\*To whom correspondence should be addressed. E-mail: rudolf.grimm@uibk.ac.at

a deeply degenerate Fermi gas, the true temperature  $T$  is substantially below our observable  $T'$  (25, 26), but a general theory for this relation is not yet available.

Radio-frequency (RF) spectroscopy has been introduced as a powerful tool to study interaction effects in ultracold Fermi gases (27–29). Molecular binding energies have been measured for  $^{40}\text{K}$  atoms (29), for which the potential of the method to observe fermionic pairing gap energies has also been pointed out. RF spectroscopy has been applied to  $^6\text{Li}$  atoms to study interaction effects up to magnetic fields of 750 G (28). One important observation was the absence of mean-field shifts in the strongly interacting regime. This effect can be attributed to the fact that, in the relevant magnetic-field range, all s-wave scattering processes between  $^6\text{Li}$  atoms in the states  $|1\rangle$ ,  $|2\rangle$ , and  $|3\rangle$  are simultaneously unitarity-limited. This property of  $^6\text{Li}$  is very favorable for RF spectroscopy because it suppresses shifts and broadening by mean-field effects.

We drove RF transitions from state  $|2\rangle$  to the empty state  $|3\rangle$  at  $\sim 80$  MHz and monitored the loss of atoms in state  $|2\rangle$  after weak excitation by a 1-s RF pulse, using state-selective absorption imaging (14). Our experiment was optimized to obtain a resolution of  $\sim 100$  Hz, corresponding to an intrinsic sensitivity to interaction effects on the scale of  $\sim 5$  nK, which is more than two orders of magnitude below the typical Fermi temperatures.

We recorded RF spectra for different degrees of cooling and in various coupling regimes (Fig. 1). We realized the molecular regime at  $B = 720$  G ( $a = +120$  nm). For the resonance region, we examined two different magnetic fields, because the precise resonance location  $B_0$  is not exactly known. Our two values  $B = 822$  G (16) and 837 G (13, 18) may be considered as lower and upper bounds for  $B_0$ . We also studied the regime beyond the resonance with a large negative scattering length at  $B = 875$  G ( $a \approx -600$  nm). Spectra taken in a “hot” thermal sample at  $T \approx 6T_F$  (where  $T_F = 15$   $\mu\text{K}$ ) show the narrow atomic  $|2\rangle \rightarrow |3\rangle$  transition line (Fig. 1, top) and serve as a frequency reference. We present our spectra as a function of the RF offset with respect to the bare atomic transition frequency.

Spectral signatures of pairing have been theoretically considered (30–34). A clear signature of the pairing process is the emergence of a double-peak structure in the spectral response as a result of the coexistence of unpaired and paired atoms. The pair-related peak is located at a higher frequency than the unpaired-atoms signal, because energy is required for pair breaking. For understanding of the spectra, both the homogeneous line shape of the pair signal (31, 33) and the inhomogeneous line broadening due to the density distribution in the harmonic trap need to be taken into account

(34). As an effect of inhomogeneity, fermionic pairing due to many-body effects takes place predominantly in the central high-density region of the trap, and unpaired atoms mostly populate the outer region of the trap where the density is low (34–36). The spectral component corresponding to the pairs thus shows a large inhomogeneous broadening in addition to the homogeneous width of the pair-breaking signal. For the unpaired atoms, the homogeneous line is narrow and the effects of inhomogeneity and mean-field shifts are negligible. These arguments explain why the RF spectra in general show a relatively sharp peak for the unpaired atoms together with a broader peak attributed to the pairs.

We observed clear double-peak structures already at  $T'/T_F = 0.5$ , which we obtained with moderate evaporative cooling down to a laser power of  $P = 200$  mW (Fig. 1, middle,  $T_F = 3.4$   $\mu\text{K}$ ). In the molecular regime  $B = 720$  G, the sharp atomic peak was well separated from the broad dissociation signal (29), which showed a molecular binding energy of  $E_b = h \times 130$  kHz  $= k_B \times 6.2$   $\mu\text{K}$ . For  $B \rightarrow B_0$ , the peaks began to overlap. In the resonance region [822 G and 837 G (Fig. 1)], we still observed a relatively narrow atomic peak at the original position together with a pair signal. For magnetic fields beyond the resonance, we could resolve the double-peak structure for fields up to  $\sim 900$  G.

For  $T'/T_F < 0.2$ , realized with a deep evaporative cooling ramp down to an optical

trap power of  $P = 3.8$  mW, we observed the disappearance of the narrow atomic peak in the RF spectra (Fig. 1, bottom,  $T_F = 1.2$   $\mu\text{K}$ ). This shows that essentially all atoms were paired. In the BEC limit (720 G), the dissociation line shape is identical to the one observed in the trap at higher temperature and Fermi energy. Here the localized pairs are molecules with a size much smaller than the mean interparticle spacing, and the dissociation signal is independent of the density. In the resonance region [822 G and 837 G (Fig. 1)], the pairing signal shows a clear dependence on density (Fermi energy), which becomes even more pronounced beyond the resonance (875 G). We attribute this to the fact that the size of the pairs becomes comparable to or larger than the interparticle spacing. In addition, the narrow width of the pair signal in this regime (Fig. 1, bottom,  $B = 875$  G) indicates a pair localization in momentum space to well below the Fermi momentum  $\hbar k_F = \sqrt{2mE_F}$  and thus a pair size exceeding the interparticle spacing.

To quantitatively investigate the crossover from the two-body molecular regime to the fermionic many-body regime, we measured the pairing energy in a range between 720 and 905 G. The measurements were performed after deep evaporative cooling ( $T'/T_F < 0.2$ ) for two different Fermi temperatures,  $T_F = 1.2$   $\mu\text{K}$  and  $T_F = 3.6$   $\mu\text{K}$  (Fig. 2). As an effective pairing gap, we defined  $\Delta\nu$  as the frequency difference between the pair-signal maximum and the bare atomic resonance. In the BEC limit, the effective

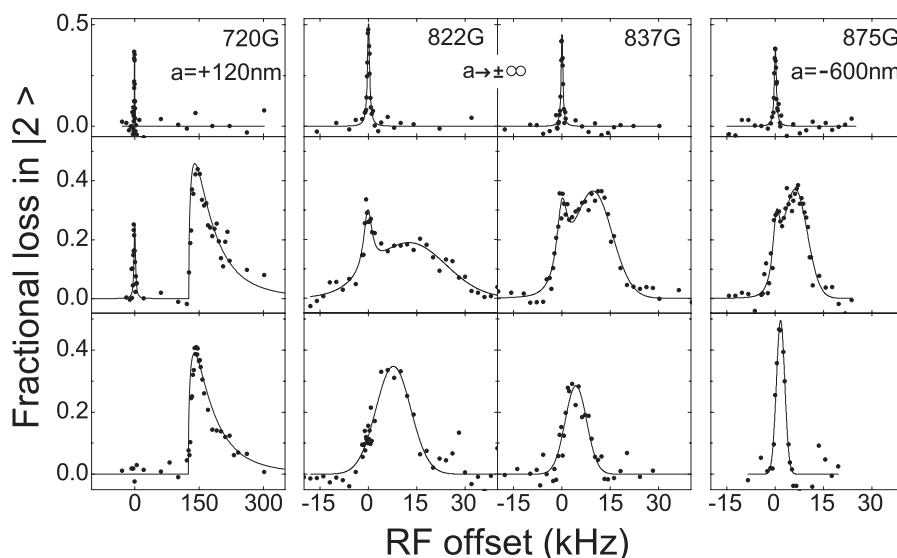


**Fig. 1.** RF spectra for various magnetic fields and different degrees of evaporative cooling. The RF offset ( $k_B \times 1$   $\mu\text{K} \equiv h \times 20.8$  kHz) is given relative to the atomic transition  $|2\rangle \rightarrow |3\rangle$ . The molecular limit is realized for  $B = 720$  G (first column). The resonance regime is studied for  $B = 822$  G and  $B = 837$  G (second and third columns). The data at 875 G (fourth column) explore the crossover on the BCS side. Top row, signals of unpaired atoms at  $T' \approx 6T_F$  ( $T_F = 15$   $\mu\text{K}$ ); middle row, signals for a mixture of unpaired and paired atoms at  $T' = 0.5T_F$  ( $T_F = 3.4$   $\mu\text{K}$ ); bottom row, signals for paired atoms at  $T' < 0.2T_F$  ( $T_F = 1.2$   $\mu\text{K}$ ). The true temperature  $T$  of the atomic Fermi gas is below the temperature  $T'$ , which we measured in the BEC limit. The solid lines are introduced to guide the eye.

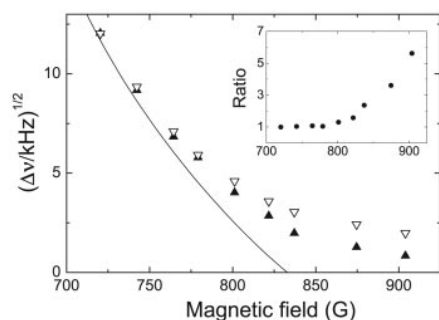


**Fig. 2.** Measurements of the effective pairing gap  $\Delta\nu$  as a function of the magnetic field  $B$  for deep evaporative cooling and two different Fermi temperatures,  $T_F = 1.2 \mu\text{K}$  (solid symbols) and  $3.6 \mu\text{K}$  (open symbols). The solid line shows  $\Delta\nu$  for the low-density limit, where it is essentially given by the molecular binding energy (25). Inset: The ratio of the effective pairing gaps measured at the two different Fermi energies.

tive pairing gap  $\Delta\nu$  simply reflects the molecular binding energy  $E_b$  (Fig. 2, solid line) (25). With an increasing magnetic field, in the BEC-BCS crossover,  $\Delta\nu$  shows an increasing deviation from this low-density molecular limit and smoothly evolves into a density-dependent many-body regime where  $h\Delta\nu < E_F$ .

A comparison of the pairing energies at the two different Fermi energies (Fig. 2, inset) provides further insight into the nature of the pairs. In the BEC limit,  $\Delta\nu$  is solely determined by  $E_b$  and thus does not depend on  $E_F$ . In the universal regime on resonance,  $E_F$  is the only energy scale, and we indeed observed the effective pairing gap  $\Delta\nu$  to increase linearly with the Fermi energy. We found a corresponding relation  $h\Delta\nu \approx 0.2 E_F$ . Beyond the resonance, where the system is expected to change from a resonant to a BCS-type behavior,  $\Delta\nu$  was found to depend more strongly on the Fermi energy and the observed gap ratio further increased. We interpret this in terms of the increasing BCS character of pairing, for which an exponential dependence  $h\Delta\nu/E_F \propto \exp(-\pi/2k_F|a|)$  is expected.

In a further series of measurements (Fig. 3), we applied a controlled heating method to study the temperature dependence of the gap in a way that allowed us to keep all other parameters constant. After production of a pure molecular Bose-Einstein condensate ( $T' < 0.2T_F$ ) in the usual way, we adiabatically changed the conditions to  $B = 837 \text{ G}$  and  $T_F = 1.2 \mu\text{K}$ . We then increased the trap laser power by a factor of nine ( $T_F$  increased to  $2.5 \mu\text{K}$ ), using exponential ramps of different durations. For fast ramps, this recompression was nonadiabatic and increased the entropy. By variation of the ramp time, we explored a range from our lowest temperatures up to  $T'/T_F = 0.8$ . The emergence of the gap with decreasing temperature is clearly visible in the RF spectra (Fig. 3). The marked increase of  $\Delta\nu$  for decreasing temperature is

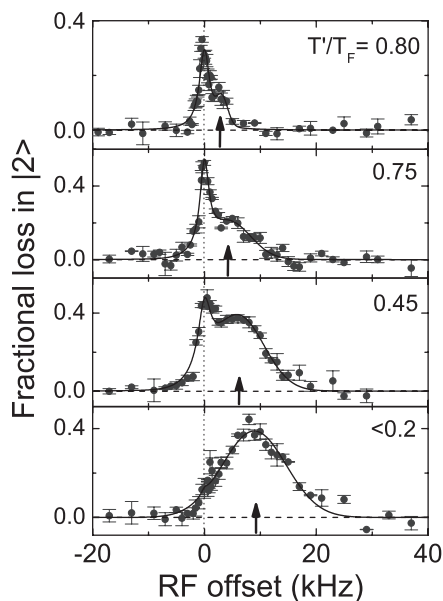


**Fig. 3.** RF spectra measured at  $B = 837 \text{ G}$  and  $T_F = 2.5 \mu\text{K}$  for different temperatures  $T'$  adjusted by controlled heating. The solid lines are fits to guide the eye, using a Lorentzian curve for the atom peak and a Gaussian curve for the pair signal. The vertical dotted line marks the atomic transition, and the arrows indicate the effective pairing gap  $\Delta\nu$ .

in good agreement with theoretical expectations for the pairing gap energy (5).

The conditions of our experiment were theoretically analyzed for the case of resonant two-body interaction (34). The calculated RF spectra are in agreement with our experimental results and demonstrate how a double-peak structure emerges as the gas is cooled below  $T'/T_F \approx 0.5$  and how the atomic peak disappears with further decreasing temperature. In particular, the work clarifies the role of the “pseudo-gap” regime (5, 22), in which pairs are formed before superfluidity is reached. According to the calculated spectra, the atomic peak disappears at temperatures well below the critical temperature for the phase-transition to a superfluid. A recent theoretical study of the BCS-BEC crossover at finite temperature (36) predicted the phase-transition to a superfluid to occur at a temperature that on resonance is only  $\sim 30\%$  below the point where pair formation sets in.

We have observed fermionic pairing already after moderate evaporative cooling. With much deeper cooling applied, the unpaired atom signal disappeared from our spectra. This observation shows that pairing takes place even in the outer region of the trapped gas where the density and the local Fermi energy are low. Our results thus strongly suggest that a resonance superfluid is formed in the central region of the trap (34). Together with the observations of resonance condensation of fermionic pairs (15, 16) and weak damping of collective excitations (17,

18), our observation of the pairing gap provides a strong case for superfluidity in experiments on resonantly interacting Fermi gases.

**References and Notes**

1. M. Tinkham, *Introduction to Superconductivity* (McGraw-Hill, New York, ed. 2, 1996).
2. D. M. Eagles, *Phys. Rev.* **186**, 456 (1969).
3. A. J. Leggett, in *Modern Trends in the Theory of Condensed Matter*, A. Pekalski, R. Przystawa, Eds. (Springer-Verlag, Berlin, 1980), pp. 13–27.
4. P. Nozières, S. Schmitt-Rink, *J. Low Temp. Phys.* **59**, 195 (1985).
5. Q. Chen, J. Stajic, S. Tan, K. Levin, in preparation (available at <http://arxiv.org/abs/cond-mat/0404274>).
6. A. Cho, *Science* **301**, 750 (2003).
7. S. Inouye et al., *Nature* **392**, 151 (1998).
8. K. M. O'Hara, S. L. Hemmer, M. E. Gehm, S. R. Granade, J. E. Thomas, *Science* **298**, 2179 (2002); published online 7 Nov 2002 (10.1126/science.1079107).
9. S. Jochim et al., *Science* **302**, 2101 (2003); published online 13 November 2003 (10.1126/science.1093280).
10. M. Greiner, C. A. Regal, D. S. Jin, *Nature* **426**, 537 (2003).
11. M. W. Zwierlein et al., *Phys. Rev. Lett.* **91**, 250401 (2003).
12. T. Bourdel et al., *Phys. Rev. Lett.* **93**, 050401 (2004).
13. R. Hulet, paper presented at the Kauli Institute for Theoretical Physics Conference on Quantum Gases, Santa Barbara, CA, 10 to 14 May 2004.
14. M. Bartenstein et al., *Phys. Rev. Lett.* **92**, 120401 (2004).
15. C. A. Regal, M. Greiner, D. S. Jin, *Phys. Rev. Lett.* **92**, 040403 (2004).
16. M. W. Zwierlein et al., *Phys. Rev. Lett.* **92**, 120403 (2004).
17. J. Kinast, S. L. Hemmer, M. E. Gehm, A. Turlapov, J. E. Thomas, *Phys. Rev. Lett.* **92**, 150402 (2004).
18. M. Bartenstein et al., *Phys. Rev. Lett.* **92**, 203201 (2004).
19. M. Holland, S. J. J. M. F. Kokkelmans, M. L. Chiofalo, R. Walser, *Phys. Rev. Lett.* **87**, 120406 (2001).
20. E. Timmermans, K. Furuya, P. W. Milonni, A. K. Kerman, *Phys. Lett. A* **285**, 228 (2001).
21. Y. Ohashi, A. Griffin, *Phys. Rev. Lett.* **89**, 130402 (2002).
22. J. Stajic et al., *Phys. Rev. A* **69**, 063610 (2004).
23. H. Heiselberg, *Phys. Rev. A* **63**, 043606 (2001).
24. T.-L. Ho, *Phys. Rev. Lett.* **92**, 090402 (2004).
25. Materials and methods are available as supporting material on Science Online.
26. L. D. Carr, G. V. Shlyapnikov, Y. Castin, *Phys. Rev. Lett.* **92**, 150404 (2004).
27. C. Regal, D. Jin, *Phys. Rev. Lett.* **90**, 230404 (2003).
28. S. Gupta et al., *Science* **300**, 1723 (2003); published online 8 May 2003 (10.1126/science.1085335).
29. C. A. Regal, C. Ticknor, J. L. Bohn, D. S. Jin, *Nature* **424**, 47 (2003).
30. P. Törmä, P. Zoller, *Phys. Rev. Lett.* **85**, 487 (2000).
31. J. Kinnunen, M. Rodríguez, P. Törmä, *Phys. Rev. Lett.* **92**, 230403 (2004).
32. H. P. Büchler, P. Zoller, W. Zwerger, in preparation (available at <http://arxiv.org/abs/cond-mat/0404116>).
33. R. B. Diener, T.-L. Ho, in preparation (available at <http://arxiv.org/abs/cond-mat/0405174>).
34. J. Kinnunen, M. Rodríguez, P. Törmä, *Science* **305**, 1131; published online 22 July 2004 (10.1126/science.1100782).
35. A. Bulgac, in preparation (available at <http://arxiv.org/abs/cond-mat/0309358>).
36. A. Perali, P. Pieri, L. Pisani, G. C. Strinati, *Phys. Rev. Lett.* **92**, 220404 (2004).
37. We thank P. Törmä for a stimulating exchange of results and very useful discussions and W. Zwerger and H. P. Büchler for many stimulating discussions. Supported by the Austrian Science Fund (FWF) within special researchbereich 15 (project part 15) and by the European Union in the frame of the Cold Molecules Training and Mobility of Researchers Network under contract no. HPRN-CT-2002-00290. C.C. is a Lise-Meitner research fellow of the FWF.

**Supporting Online Material**

[www.sciencemag.org/cgi/content/full/1100818/DC1](http://www.sciencemag.org/cgi/content/full/1100818/DC1)  
Materials and Methods  
References and Notes

27 May 2004; accepted 13 July 2004  
Published online 22 July 2004;  
10.1126/science.1100818

Include this information when citing this paper.

## 6.5 “Crossover from a Molecular Bose-Einstein Condensate to a Degenerate Fermi Gas”

M. Bartenstein, A. Altmeyer, S. Riedl, S. Jochim, C. Chin,  
J. Hecker Denschlag, and R. Grimm

Phys. Rev. Lett. **92**, 120401 (2004)



## 6.6 “Collective excitations of a degenerate gas at the BEC-BCS crossover”

M. Bartenstein, A. Altmeyer, S. Riedl, S. Jochim, C. Chin,  
J. Hecker Denschlag, and R. Grimm

Phys. Rev. Lett. **92**, 203201 (2004)



## Collective Excitations of a Degenerate Gas at the BEC-BCS Crossover

M. Bartenstein,<sup>1</sup> A. Altmeyer,<sup>1</sup> S. Riedl,<sup>1</sup> S. Jochim,<sup>1</sup> C. Chin,<sup>1</sup> J. Hecker Denschlag,<sup>1</sup> and R. Grimm<sup>1,2</sup>

<sup>1</sup>*Institut für Experimentalphysik, Universität Innsbruck, Technikerstraße 25, 6020 Innsbruck, Austria*

<sup>2</sup>*Institut für Quantenoptik und Quanteninformation, Österreichische Akademie der Wissenschaften, 6020 Innsbruck, Austria*

(Received 29 March 2004; published 19 May 2004)

We study collective excitation modes of a fermionic gas of  ${}^6\text{Li}$  atoms in the BEC-BCS crossover regime. While measurements of the axial compression mode in the cigar-shaped trap close to a Feshbach resonance confirm theoretical expectations, the radial compression mode shows surprising features. In the strongly interacting molecular BEC regime, we observe a negative frequency shift with increasing coupling strength. In the regime of a strongly interacting Fermi gas, an abrupt change in the collective excitation frequency occurs, which may be a signature for a transition from a superfluid to a collisionless phase.

DOI: 10.1103/PhysRevLett.92.203201

PACS numbers: 34.50.-s, 05.30.Fk, 32.80.Pj, 39.25.+k

The crossover from a Bose-Einstein condensate (BEC) to a Bardeen-Cooper-Schrieffer (BCS) superfluid has for decades attracted considerable attention in many-body theory [1]. Bose-Einstein condensates of molecules formed by fermionic atoms of  ${}^6\text{Li}$  and  ${}^{40}\text{K}$  [2–5] provide a unique system to experimentally explore this BEC-BCS crossover. In such ultracold gases magnetically tuned scattering resonances, known as Feshbach resonances, allow one to control and vary the interaction strength over a very broad range. Recent experiments have entered the crossover regime and yield results on the interaction strength by measuring the cloud size [6] and expansion energy [5]. Moreover, two experiments [7,8] have demonstrated the condensed nature of fermionic atom pairs in the crossover regime.

Important questions are related to superfluidity in the crossover regime [9]. When a molecular BEC is converted into an ultracold Fermi gas [6], one can expect ultralow temperatures and superfluidity to extend far into the Fermi gas regime [10]. Detection tools to probe superfluidity in this regime are therefore requested. The investigation of collective excitation modes [11] is well established as a powerful method to gain insight into the physical behavior of ultracold quantum gases in different regimes of Bose [12] and Fermi gases [13]. A recent paper [14] points out an interesting dependence of the collective frequencies in the BEC-BCS crossover of a superfluid Fermi gas. Superfluidity implies a hydrodynamic behavior which can cause substantial changes in the excitation spectrum and in general very low damping rates. However, in the crossover regime the strong interaction between the particles also results in hydrodynamic behavior in the normal, nonsuperfluid phase. Therefore the interpretation of collective modes in the BEC-BCS crossover in terms of superfluidity is not straightforward and needs careful investigation to identify the different regimes.

In this Letter, we report on measurements of fundamental collective excitation modes in the BEC-BCS crossover for various coupling strengths in the low-

temperature limit. In Ref. [2], we have already presented a first measurement of the collective excitation of a molecular BEC in the limit of strong coupling. As described previously [2,6], we work with a spin mixture of  ${}^6\text{Li}$  atoms in the two lowest internal states. For exploring different interaction regimes, we use a broad Feshbach resonance, the position of which we determined to 837(5) G [15]. The different interaction regimes can be characterized by the coupling parameter  $1/(k_F a)$ , where  $a$  represents the atom-atom scattering length and  $k_F$  is the Fermi wave number. Well below the Feshbach resonance ( $B < 700$  G), we can realize the molecular BEC regime with  $1/(k_F a) \gg 1$ . On resonance, we obtain the unitarity-limited regime of a universal fermionic quantum gas with  $1/(k_F a) = 0$  [16]. An interacting Fermi gas of atoms is realized beyond the resonance where  $1/(k_F a) < 0$ .

The starting point of our experiments is a cigar-shaped molecular BEC produced by evaporative cooling in an optical dipole trap in the same way as described in Ref. [6]. Radially the sample is confined by a 35-mW laser beam (wavelength 1030 nm) focused to a waist of  $25\ \mu\text{m}$ . The radial vibration frequency is  $\omega_r \approx 2\pi \times 750$  Hz. The axial vibration frequency is  $\omega_z = 2\pi \times (601B/\text{kG} + 11)^{1/2}$  Hz, where the predominant contribution stems from magnetic confinement caused by the curvature of the Feshbach tuning field  $B$ , and a very small additional contribution arises from the weak axial optical trapping force.

For exploring collective excitations in the BEC-BCS crossover regime, we ramp the magnetic field from the evaporation field of 764 G, where the molecular BEC is formed, to fields between 676 and 1250 G within 1 s. In previous work [6], we have shown that the conversion to an atomic Fermi gas proceeds in an adiabatic and reversible way, i.e., without increase of entropy. From the condensate fraction in the BEC limit, for which we measure more than 90% [6], we can give upper bounds for the temperature in both the BEC limit and the non-interacting Fermi gas limit of  $T < 0.46T_{\text{BEC}}$  and  $T < 0.03T_F$  [10], respectively. Here  $T_{\text{BEC}}$  ( $T_F$ ) denotes the

critical temperature (Fermi temperature). With a total number of atoms  $N \approx 4 \times 10^5$  (free atoms and atoms bound to molecules) and a geometrically averaged trap frequency at 837 G of  $\bar{\omega} = (\omega_r^2 \omega_z)^{1/3} \approx 2\pi \times 230$  Hz, we calculate a Fermi energy  $E_F = \hbar^2 k_F^2 / 2m = \hbar \bar{\omega} (3N)^{1/3} = k_B \times 1.2 \mu\text{K}$  for a noninteracting cloud, where  $m$  is the mass of an atom and  $k_B$  is Boltzmann's constant.

To excite the *axial* compression mode at a given magnetic field, we increase the optical confinement in a 10-ms time interval by a factor of 1.5. The laser power is varied slow enough for the radial motion to follow adiabatically, but fast enough to induce axial oscillations. The relative amplitude of the resulting axial oscillation is kept small, typically  $\sim 10\%$ . We observe the oscillation by *in situ* imaging of the cloud [6] after a variable hold time  $t$  at constant trap parameters. To determine the collective oscillation frequency  $\Omega_z$  and the damping rate  $\Gamma_z$ , we fit a damped harmonic oscillation  $z(t) = z_0 + A_z \exp(-\Gamma_z t) \times \sin(\Omega_z t + \phi_z)$  to the observed time evolution of the cloud size, where  $z_0$ ,  $A_z$ , and  $\phi_z$  are additional fit parameters.

The measured oscillation frequencies and damping rates are shown in Fig. 1. The data are normalized to the axial trap frequency  $\omega_z$ , as determined by excitation of the axial sloshing mode. We point out that the axial confinement is harmonic because of the dominant magnetic trapping, and we can measure  $\omega_z$  with a  $10^{-3}$  precision. In the BEC limit, the measured collective fre-

quencies are in agreement with the expected  $\Omega_z/\omega_z = \sqrt{5/2} = 1.581$  [11,17]. With increasing magnetic field, we observe a decrease in the collective excitation frequency until a minimum is reached at about 900 G, i.e., in the regime of a strongly interacting Fermi gas where  $1/(k_F a) \approx -0.5$ . With further increasing magnetic field and decreasing interaction strength, we then observe a gradual increase of the collective frequency toward  $\Omega_z/\omega_z = 2$ . The latter value is expected for a collisionless degenerate Fermi gas, where the elastic collision rate is strongly reduced by Pauli blocking. Because of the large damping rates in the transition regime between hydrodynamic and collisionless behavior, the excitation frequencies cannot be determined with high accuracy. The observed axial damping is consistent with a gradual transition between these two regimes [18].

The insets of Fig. 1 show a zoom-in of the data for the resonance region between 750 and 900 G. The collective frequency that we measure on resonance exhibits the small 2% down-shift expected for the unitarity limit ( $\Omega_z/\omega_z = \sqrt{12/5} = 1.549$ ) [14]. For the damping rate, we observe a clear minimum at a magnetic field of 815(10) G, which is close to the resonance position. It is interesting to note that this damping minimum coincides with the recent observation of a maximum fraction of condensed fermionic atom pairs in Ref. [18]. For the minimum damping rate, we obtain the very low value of  $\Gamma_z/\omega_z \approx 0.0015$ , which corresponds to a  $1/e$  damping time of  $\sim 5$  s.

To excite the *radial* compression mode, we reduce the optical confinement for  $50 \mu\text{s}$ , which is short compared with the radial oscillation period of 1.3 ms. In this short interval the cloud slightly expands radially, and then begins to oscillate when the trap is switched back to the initial laser power. The relative oscillation amplitude is  $\sim 10\%$ . To detect the radial oscillation, we turn off the trapping laser after various delay times  $t$  and measure the radial size  $r(t)$  after 1.5 ms of expansion. The measured radial size  $r(t)$  reflects the oscillating release energy. From the corresponding experimental data, we extract the excitation frequency  $\Omega_r$  and damping  $\Gamma_r$  by fitting the radial cloud size to  $r(t) = r_0 + A_r \exp(-\Gamma_r t) \sin(\Omega_r t + \phi_r)$ , where  $r_0$ ,  $A_r$ , and  $\phi_r$  are additional fit parameters. Typical radial oscillation curves are shown in Fig. 2.

The magnetic-field dependence of the radial excitation frequency  $\Omega_r$  and the damping rate  $\Gamma_r$  is shown in Fig. 3. Here we normalize the data to the trap frequency  $\omega_r$ , which we obtain by measuring the radial sloshing mode at the given magnetic field [19]. This normalization suppresses anharmonicity effects in the measured compression mode frequency to below 3% [21]. For low magnetic fields, the measured frequency ratio approaches the BEC limit [11,22] ( $\Omega_r/\omega_r = 2$ ). With increasing magnetic field, i.e., increasing interaction strength, we observe a large down-shift of the frequency. On resonance ( $B = 837$  G), we observe  $\Omega_r/\omega_r = 1.62(2)$ . Above resonance, i.e., with the gas entering the strongly interacting Fermi

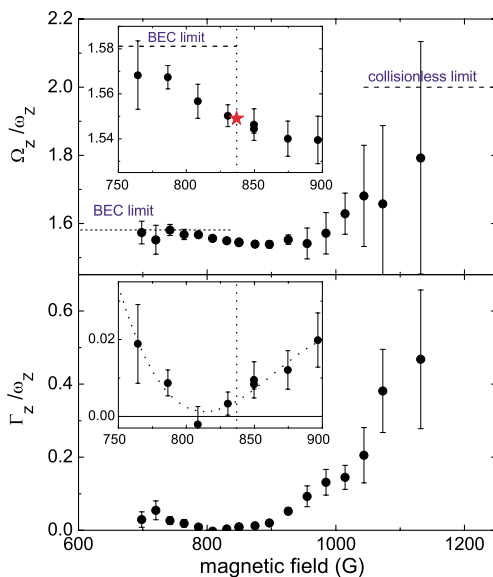


FIG. 1 (color online). Measured frequency  $\Omega_z$  and damping rate  $\Gamma_z$  of the axial compression mode, normalized to the trap frequency  $\omega_z$ . In the upper graph, the dashed lines indicate the BEC limit of  $\Omega_z/\omega_z = \sqrt{5/2}$  and the collisionless Fermi gas limit with  $\Omega_z/\omega_z = 2$ . The insets show the data in the resonance region. Here the vertical dotted line indicates the resonance position at 837(5) G. The star marks the theoretical prediction of  $\Omega_z/\omega_z = \sqrt{12/5}$  in the unitarity limit. In the lower inset, the dotted line is a third-order polynomial fit to the data.

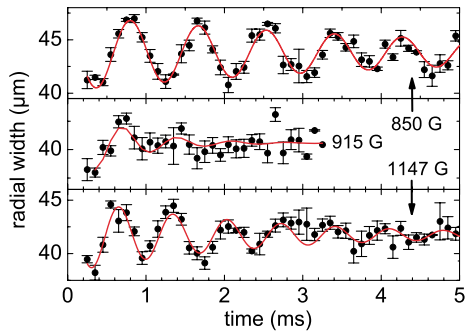


FIG. 2 (color online). Oscillations of the radial compression mode at different magnetic fields in the strongly interacting Fermi gas regime. The solid lines show fits by damped harmonic oscillations.

gas regime, the oscillation frequency further decreases until a maximum shift of almost 30% [ $\Omega_r/\omega_r = 1.42(5)$ ] is reached at  $B = 890$  G. With further increasing magnetic field, i.e., decreasing interaction strength, an abrupt change to  $\Omega_r/\omega_r \approx 2$  is observed. For  $B > 920$  G our data are consistent with a Fermi gas in the collisionless regime. The damping of the radial compression mode is small in the BEC limit and reaches a minimum close to the unitarity regime. At  $B = 910$  G, where the abrupt change occurs, we observe very strong damping (see also middle trace in Fig. 2).

We have performed further experiments to check our data on the radial compression mode for systematic effects. We have repeated the measurements after recompressing the trap to 9 times higher trap laser power

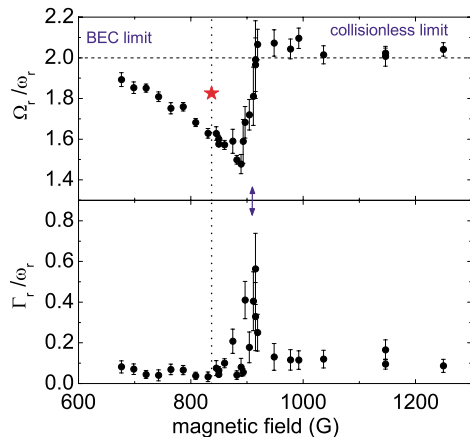


FIG. 3 (color online). Measured frequency  $\Omega_r$  and damping rate  $\Gamma_r$  of the radial compression mode, normalized to the trap frequency (sloshing mode frequency)  $\omega_r$ . In the upper graph, the dashed line indicates  $\Omega_r/\omega_r = 2$ , which corresponds to both the BEC limit and the collisionless Fermi gas limit. The vertical dotted line marks the resonance position at 837(5) G. The star indicates the theoretical expectation of  $\Omega_r/\omega_r = \sqrt{10/3}$  in the unitarity limit. A striking change in the excitation frequency occurs at  $\sim 910$  G (arrow) and is accompanied by anomalously strong damping.

( $\omega_r \approx 2.4$  kHz). The corresponding data confirm all our observations in the shallower trap. In particular, the negative frequency shift and the sudden change in the collective frequency show up in essentially the same way. The recompressed trap also allows us to eliminate a small residual anharmonicity shift from our measurement of the collective frequency at 837 G, and we obtain  $\Omega_r/\omega_r = 1.67(3)$  for the harmonic trap limit. We have also checked that the frequency of the compression mode in the resonance region does not depend on the way we prepare the ultracold gas. Direct evaporation at a fixed magnetic field, without starting from a molecular BEC, leads to the same collective frequency. Preliminary measurements at higher temperatures, however, show a trend towards smaller frequency shifts in the radial compression mode and to smoother changes of the collective frequency.

Our measurements on the radial compression mode show *three surprises*. The corresponding features, which we discuss in the following, cannot be explained on the basis of available theoretical models and suggest new physics in the BEC-BCS crossover regime.

*Surprise one.*—For a strongly interacting BEC, Ref. [23] has predicted up-shifts of the collective frequencies with increasing coupling strength based on beyond mean-field theory corrections [24]. Applying these predictions to a molecular BEC in the crossover regime, the collective excitation frequencies should follow  $\delta\Omega_i/\Omega_i = c_i\sqrt{n_m a_m^3}$  ( $i = z, r$ ), where  $n_m$  is the peak molecular number density and  $a_m = 0.6a$  [25] is the molecule-molecule scattering length. For our highly elongated trap geometry, the numerical factors are  $c_r = 5c_z = 0.727$ . In contrast to these expectations, we observe a strong frequency down-shift in the radial direction. Using the above formula to fit the first four data points, we obtain a negative coefficient of  $c_r = -1.2(3)$ . For the axial oscillation we obtain  $c_z = -0.04(5)$ . Note that a substantial down-shift in radial direction is observed even at the low magnetic field of 676 G where the molecular gas parameter is relatively small ( $n_m a_m^3 = 0.001$ ). Apparently, the beyond mean-field theory of a BEC is not adequate to describe the transition from a molecular BEC to a strongly interacting gas in the BEC-BCS crossover.

*Surprise two.*—The universal character of the strongly interacting quantum gas on resonance suggests a simple equation of state for which one expects  $\Omega_z/\omega_z = \sqrt{12/5} = 1.549$  and  $\Omega_r/\omega_r = \sqrt{10/3} = 1.826$  for the collective excitation frequencies [14]. While our measurements confirm the predicted axial frequency, we obtain a different frequency in the radial direction of  $\Omega_r/\omega_r = 1.67(3)$ .

*Surprise three.*—The abrupt change of the excitation frequency and the large damping rate are not expected in a normal degenerate Fermi gas, where the collective excitation frequency is expected to vary smoothly from the hydrodynamic regime to the collisionless one. Furthermore, for the damping rate of the radial mode in the

transition regime, a maximum value of  $\Gamma_r/\omega_r = 0.09$  is calculated in Ref. [18]. Our measured damping rate of  $\Gamma_r/\omega_r \approx 0.5$  is clearly inconsistent with this prediction for the normal (nonsuperfluid) hydrodynamic regime. However, both the sudden change of the collective frequency and a strong damping are expected for a transition from the superfluid to the normal phase [26].

In conclusion, our experiments demonstrate that the collective modes of a degenerate gas in the BEC-BCS crossover region show a pronounced dependence on the coupling strength and thus provide valuable information on the physical behavior of the system. For the axial compression mode, the frequency shift observed in the unitarity limit confirms theoretical expectations. However, the radial compression mode reveals a surprising behavior. In the strongly interacting BEC regime, the observed frequency shifts have an opposite sign as compared to expectations from beyond mean-field theory and the frequency shift on resonance is even larger than expected. The most striking feature is an abrupt change of the radial collective frequency in the regime of a strongly attractive Fermi gas where  $1/(k_F a) \approx -0.5$ . The transition is accompanied by very strong damping. The observation supports an interpretation in terms of a transition from a hydrodynamic to a collisionless phase. A superfluid scenario for the hydrodynamic case seems plausible in view of current theories on resonance superfluidity [9] and the very low temperatures provided by the molecular BEC [10]. A definite answer, however, to the sensitive question of superfluidity requires further careful investigations, e.g., on the temperature dependence of the phase transition.

We warmly thank S. Stringari for stimulating this work and for many useful discussions. We also thank W. Zwerger and M. Baranov for very useful discussions. We acknowledge support by the Austrian Science Fund (FWF) within SFB 15 (project part 15) and by the European Union in the frame of the Cold Molecules TMR Network under Contract No. HPRN-CT-2002-00290. C. C. thanks the FWF for financial support.

*Note added.*—A recent paper by John Thomas' group [27] reports on measurements of the radial compression mode in the resonance region, which show much weaker frequency shifts than we observe. This apparent discrepancy needs further investigation.

- 
- [1] A. J. Leggett, in *Modern Trends in the Theory of Condensed Matter*, edited by A. Pekalski and R. Przystawa (Springer-Verlag, Berlin, 1980); P. Nozières and S. Schmitt-Rink, *J. Low Temp. Phys.* **59**, 195 (1985); E. Timmermans, K. Furuya, P. W. Milonni, and A. K. Kerman, *Phys. Lett. A* **285**, 228 (2001); J. N. Milstein, S. J. J. M. F. Kokkelmans, and M. J. Holland, *Phys. Rev. A* **66**, 043604 (2002); Y. Ohashi and A. Griffin, *Phys. Rev.*

- Let.* **89**, 130402 (2002); R. Combescot, *Phys. Rev. Lett.* **91**, 120401 (2003); A. Perali, P. Pieri, and G. C. Strinati, *Phys. Rev. A* **68**, 031601(R) (2003); J. Stajic *et al.*, *cond-mat/0309329*.
- [2] S. Jochim *et al.*, *Science* **302**, 2101 (2003).
- [3] M. Greiner, C. A. Regal, and D. S. Jin, *Nature (London)* **426**, 537 (2003).
- [4] M. W. Zwierlein *et al.*, *Phys. Rev. Lett.* **91**, 250401 (2003).
- [5] T. Bourdel *et al.*, *cond-mat/0403091*.
- [6] M. Bartenstein *et al.*, *Phys. Rev. Lett.* **92**, 120401 (2004).
- [7] C. A. Regal, M. Greiner, and D. S. Jin, *Phys. Rev. Lett.* **92**, 040403 (2004).
- [8] M. W. Zwierlein *et al.*, *Phys. Rev. Lett.* **92**, 120403 (2004).
- [9] M. Holland *et al.*, *Phys. Rev. Lett.* **87**, 120406 (2001).
- [10] L. D. Carr, G. V. Shlyapnikov, and Y. Castin, *Phys. Rev. Lett.* **92**, 150404 (2004).
- [11] S. Stringari, *Phys. Rev. Lett.* **77**, 2360 (1996).
- [12] L. Pitaevski and S. Stringari, *Bose-Einstein Condensation* (Clarendon, Oxford, 2003), and references therein.
- [13] G. M. Bruun and C. W. Clark, *Phys. Rev. Lett.* **83**, 5415 (1999); G. M. Bruun and B. R. Mottelson, *Phys. Rev. Lett.* **87**, 270403 (2001); A. Minguzzi and M. P. Tosi, *Phys. Rev. A* **63**, 023609 (2001).
- [14] S. Stringari, *Europhys. Lett.* **65**, 749 (2004).
- [15] We determined the resonance position by measuring the molecular binding energy using radio-frequency spectroscopy as introduced in C. A. Regal, C. Ticknor, J. L. Bohn, and D. S. Jin, *Nature (London)* **424**, 47 (2003).
- [16] H. Heiselberg, *Phys. Rev. A* **63**, 043606 (2001).
- [17] M.-O. Mewes *et al.*, *Phys. Rev. Lett.* **77**, 988 (1996).
- [18] L. Vichi, *J. Low Temp. Phys.* **121**, 177 (2000).
- [19] We excite the radial sloshing mode by pulsed application of a vertical magnetic gradient. With increasing magnetic field and, thus, increasing radial cloud size, the anharmonicity of the Gaussian-shaped radial potential leads to a decrease of the sloshing mode frequency. For  $\omega_r/2\pi$ , we observe a corresponding decrease from 765 Hz at 676 G to 710 Hz at magnetic fields above 1.2 kG; at 837 G we obtain 740 Hz. Our measurements of the sloshing mode frequency agree well with an expected scaling of the lowest-order anharmonicity correction with the squared cloud size [20].
- [20] S. Stringari (private communication).
- [21] The anharmonicity corrections to frequencies of both the compression mode ( $\Omega_r$ ) and the sloshing mode ( $\omega_r$ ) scale in the same way with the increasing cloud size with a slightly larger prefactor for the compression mode [20]. Our normalization  $\Omega_r/\omega_r$  reduces the anharmonicity effect by typically a factor of 5.
- [22] F. Chevy *et al.*, *Phys. Rev. Lett.* **88**, 250402 (2002).
- [23] L. Pitaevski and S. Stringari, *Phys. Rev. Lett.* **81**, 4541 (1998).
- [24] T. D. Lee, K. W. Huang, and C. N. Yang, *Phys. Rev.* **106**, 1135 (1957).
- [25] D. S. Petrov, C. Salomon, and G. V. Shlyapnikov, *cond-mat/0309010*.
- [26] M. A. Baranov and D. S. Petrov, *Phys. Rev. A* **62**, 041601 (2000).
- [27] J. Kinast *et al.*, *Phys. Rev. Lett.* **92**, 150402 (2004).

# Chapter 7

## Summary and Outlook

Controlling ultracold gases on the quantum level has now become reality through the work of many theoretical and experimental groups around the world. In this compilation I have presented a number of experiments where my collaborators and I have contributed to this development. We have learned to control bosonic as well as fermionic atoms with respect to their internal and external degrees of freedom. We can bring ensembles of atoms, be it a BEC or a degenerate Fermi gas, into their quantum mechanical ground state. Phase imprinting makes it possible to shape the BEC wavefunction, and we were able to create solitons, non-linear waves. Using Bragg diffraction we built various atom interferometers which could be used to map out the phase distribution on a condensate. Loading a BEC into an optical lattice we enter the realm of solid state physics. We demonstrated how to populate particular Bloch states and how to coherently transfer population between the bands. By accelerating the lattice we observed generalized Bloch-oscillations, and an accelerator for BEC was constructed. We have learned to control the interaction between atoms via magnetically and optically tunable Feshbach resonances. Using these Feshbach resonances or photoassociation we were able to produce excited and ground state molecules in well defined quantum states. Further, we managed to produce the first molecular BEC starting from a Fermi gas of atoms. Controlling the coupling of these fermionic atoms with the help of a Feshbach resonance, we could explore the BEC-BCS crossover and an interesting universal regime. Studying collective oscillations and performing radio-frequency spectroscopy we could investigate these regimes and found evidence for pairing of fermions and superfluidity in a degenerate Fermi gas.

In spite of all the recent developments and exciting achievements, the field of ultracold atoms is not coming to a halt but appears to progress faster. One reason for this is that research with ultracold atoms is not confined any longer

to the field of quantum optics. It contributes already actively to several disciplines like statistical physics, condensed matter physics, solid state physics, plasma physics, many-body physics, ultra-cold chemistry, physics of chaos, metrology, non-linear physics phenomena and quantum information processing. The high degree of control on the quantum level and the versatility of the cold atom technology allows us to build ‘toy’ model systems to investigate physics problems from all different physics branches. For example, cold atoms can be used as a testing ground for fundamental theories or as quantum simulators for complex physical model systems. Finally, combining the cold atom know-how with the developed technologies of other fields of physics could help to solve physics problems for which we long to have deeper understanding.

# Bibliography

- [Abo01] J. R. Abo-Shaeer, C. Raman, J. M. Vogels, and W. Ketterle, *Observation of Vortex Lattices in Bose-Einstein Condensates*, *Science* **292**, 476 (2001).
- [Ada94] C. S. Adams, M. Sigel, J. Mlynek, *Atom Optics*, *Phys. Rep.* **240**, 143 (1994).
- [And95] M. H. Anderson, J. R. Ensher, M. R. Matthews, C. E. Wieman, and E. A. Cornell, *Observation of Bose-Einstein Condensation in a Dilute Atomic Vapor*, *Science* **269**, 198 (1995).
- [And96] M. R. Andrews, M.-O. Mewes, N. J. van Druten, D. S. Durfee, D. M. Kurn, and W. Ketterle, *Direct, Nondestructive Observation of a Bose Condensate*, *Science* **273**, 84 (1996).
- [And98] B. P. Anderson and M. A. Kasevich, *Macroscopic Quantum Interference from Atomic Tunnel Arrays*, *Science* **282**, 1686 (1998).
- [Ank05] Th. Anker, M. Albiez, R. Gati, S. Hunsmann, B. Eiermann, A. Trombettoni, and M. K. Oberthaler, *Nonlinear Self-Trapping of Matter Waves in Periodic Potentials*, *Phys. Rev. Lett.* **94**, 020403 (2005).
- [Ari76] E. Arimondo and G. Orriols, *Nonabsorbing atomic coherences by coherent two-photon transitions in a three-level optical pumping*, *Lett. Nuovo Cim.* **17**, 333 (1976).
- [Ash70] A. Ashkin, *Acceleration and Trapping of Particles by Radiation Pressure*, *Phys. Rev. Lett.* **24**, 156 (1970).
- [Bah00] J. T. Bahns, P. L. Gould and W. C. Stwalley, *Formation of Cold ( $T = 1K$ ) Molecules*, *Adv. At. Mol. Opt. Phys.* **42**, 171-224 (2000).
- [Ban95] Y. B. Band and P. S. Julienne, *Ultracold-molecule production by laser-cooled atom photoassociation*, *Phys. Rev. A* **51**, R4317 (1995).

- [Bar57] J. Bardeen, L. N. Cooper, and J. R. Schrieffer, *Theory of Superconductivity*, Phys. Rev. **108**, 1175 (1957).
- [Bar01] M. D. Barrett, J. A. Sauer, and M. S. Chapman, *All-Optical Formation of an Atomic Bose-Einstein Condensate*, Phys. Rev. Lett. **87**, 010404 (2001).
- [Bar04a] M. Bartenstein, *From Molecules to Cooper Pairs: Experiments in the BEC-BCS Crossover*, Ph.D. thesis, Universität Innsbruck (2005).
- [Bar04b] M. Bartenstein, A. Altmeyer, S. Riedl, S. Jochim, C. Chin, J. Hecker Denschlag, and R. Grimm, *Collective excitations of a degenerate gas at the BEC-BCS crossover*, Phys. Rev. Lett. **92**, 203201 (2004).
- [Bar04c] M. Bartenstein, A. Altmeyer, S. Riedl, S. Jochim, C. Chin, J. Hecker Denschlag, and R. Grimm, *Crossover from a Molecular Bose-Einstein Condensate to a Degenerate Fermi Gas*, Phys. Rev. Lett. **92**, 120401 (2004).
- [Bar04d] M. Bartenstein, A. Altmeyer, S. Riedl, R. G. S. Jochim, C. Chin, J. Hecker Denschlag, R. Grimm, A. Simoni, E. Tiesinga, C. Williams, and P. Julienne, *Precise determination of  $^6\text{Li}$  cold collision parameters by radiofrequency spectroscopy on weakly bound molecules*, Phys. Rev. Lett. **94**, 103201 (2005).
- [Ber87] T. Bergeman, G. Erez, and H. Metcalf, *Magnetostatic trapping fields for neutral atoms*, Phys. Rev. A **35**, 1535 (1987).
- [Ber97] P. R. Berman, Ed., *Atom interferometry* (Academic Press, Cambridge, 1997).
- [Ber00] S. Bernet, R. Abfalterer, C. Keller, M. K. Oberthaler, J. Schmiedmayer and A. Zeilinger, *Matter waves in time-modulated complex light potentials*, Phys. Rev. A **62**, 023606 (2000).
- [Bet99] H. L. Bethlem, G. Berden, and G. Meijer, *Decelerating neutral dipolar molecules*, Phys. Rev. Lett. **83**, 1558 (1999).
- [Bet00] H. L. Bethlem, G. Berden, F. M. H. Crompvoets, R. T. Jongma, A. J. A. van Rooij, and G. Meijer, *Electrostatic trapping of ammonia molecules*, Nature **406**, 491 (2000).
- [Boh97] J. Bohn and P. S. Julienne, *Prospects for influencing scattering lengths with far-off-resonant light*, Phys. Rev. A **56**, 1486 (1997).

- [Bos24] S. N. Bose, *Plancks Gesetz und Lichtquantenhypothese*, Z. Phys. **26**, 178 (1924).
- [Bou03] T. Bourdel, J. Cubizolles, L. Khaykovich, K. M. F. Magalhães, S. J. J. M. F. Kokkelmans, G. V. Shlyapnikov, and C. Salomon, *Measurement of the Interaction Energy near a Feshbach Resonance in a  $^6\text{Li}$  Fermi Gas*, Phys. Rev. Lett. **91**, 020402 (2003).
- [Bou04] T. Bourdel, L. Khaykovich, J. Cubizolles, J. Zhang, F. Chevy, M. Teichmann, L. Tarruell, S. J. J. M. F. Kokkelmans, and C. Salomon, *Experimental Study of the BEC-BCS Crossover Region in Lithium 6*, Phys. Rev. Lett. **93**, 050401 (2004).
- [Bra95] C. C. Bradley, C. A. Sackett, J. J. Tollett, and R. G. Hulet, *Evidence of Bose-Einstein Condensation in an Atomic Gas with Attractive Interactions*, Phys. Rev. Lett. **75**, 1687 (1995), *ibid.* **79**, 1170 (1997).
- [Bri00] H.-J. Briegel, T. Calarco, D. Jaksch, J.I. Cirac and P. Zoller, *Quantum computing with neutral atoms*, Journal of Modern Optics **47**, 415 (2000).
- [Bur99] S. Burger, K. Bongs, S. Dettmer, W. Ertmer, K. Sengstock, A. Sanpera, G. V. Shlyapnikov, and M. Lewenstein, *Dark Solitons in Bose-Einstein Condensates*, Phys. Rev. Lett. **83**, 5198 (1999).
- [Cal03] T. Calarco, U. Dorner, P. S. Julienne, C. J. Williams, and P. Zoller, *Quantum computations with atoms in optical lattices: Marker qubits and molecular interactions*, Phys. Rev. A **70**, 012306 (2004).
- [Car03] J. Carlson, S.-Y. Chang, V. R. Pandharipande, and K. E. Schmidt, *Superfluid Fermi Gases with Large Scattering Length*, Phys. Rev. Lett. **91**, 050401 (2003).
- [Car04] L. D. Carr, G. Shlyapnikov, and Y. Castin, *Achieving a BCS Transition in an Atomic Fermi Gas*, Phys. Rev. Lett. **92**, 150404 (2004).
- [Cat04] F. Cataliotti, S. Burger, C. Fort, P. Maddaloni, F. Minardi, A. Trombettoni, A. Smerzi, and M. Inguscio, *Josephson Junction arrays with Bose-Einstein Condensates*, Science **293**, 843 (2001).
- [Che02] F. Chevy, V. Bretin, P. Rosenbusch, K. W. Madison, and J. Dalibard, *Transverse Breathing Mode of an Elongated Bose-Einstein Condensate*, Phys. Rev. Lett. **88**, 250402 (2002).

- [Che04] Q. Chen, J. Stajic, S. Tan, and K. Levin, *BCS-BEC Crossover: From High Temperature Superconductors to Ultracold Superfluids*, cond-mat/0404274 (2004).
- [Che05] C. Cherubini, F. Federici, S. Succi, and M. P. Tosi *Excised acoustic black holes: the scattering problem in the time domain*, gr-qc/0504048 (2005).
- [Chi00] C. Chin, V. Vuletic, A. J. Kerman, and S. Chu, *High Resolution Feshbach Spectroscopy of Cesium*, Phys. Rev. Lett. **85**, 2717 (2000).
- [Chi04a] C. Chin, M. Bartenstein, A. Altmeyer, S. Riedl, S. Jochim, J. Hecker Denschlag, and R. Grimm, *Observation of the pairing gap in a strongly interacting Fermi gas*, Science **305**, 1128 (2004).
- [Chi04b] C. Chin and R. Grimm, *Thermal equilibrium and efficient evaporation of an ultracold atom-molecule mixture*, Phys. Rev. A **69**, 033612 (2004).
- [Chu86] S. Chu, J. E. Bjorkholm, A. Ashkin, and A. Cable, *Experimental Observation of Optically Trapped Atoms*, Phys. Rev. Lett. **57**, 314 (1986).
- [Chu98] S. Chu, *Nobel Lecture: The manipulation of neutral particles*, **70**, 685 (1998).
- [Ciu05] R. Ciurylo, E. Tiesinga, and P. S. Julienne, *Optical tuning of the scattering length of cold alkaline-earth-metal atoms*, Phys. Rev. A **71**, 030701 (2005).
- [Coh98] C. Cohen-Tannoudij, *Nobel Lecture: Manipulating atoms with photons*, Rev. Mod. Phys. **70**, 707 (1998).
- [Cor00] S. L. Cornish, N. R. Claussen, J. L. Roberts, E. A. Cornell, and C. E. Wieman, *Stable  $^{85}\text{Rb}$  Bose-Einstein Condensates with Widely Tunable Interactions*, Phys. Rev. Lett. **85**, 1795 (2000).
- [Cou98] Ph. Courteille, R. S. Freeland, and D. J. Heinzen, *Observation of a Feshbach Resonance in Cold Atom Scattering*, Phys. Rev. Lett. **81**, 69 (1998).
- [Cri04] M. Cristiani, O. Morsch, N. Malossi, M. Jona-Lasinio, M. Anderlini, E. Courtade, and E. Arimondo, *Instabilities of a Bose-Einstein condensate in a periodic potential: an experimental investigation*, Optics Express **12**, 4 (2004).

- [Cub03] J. Cubizolles, T. Bourdel, S. Kokkelmans, G. Shlyapnikov, and C. Salomon, *Production of Long-Lived Ultracold  $Li_2$  Molecules from a Fermi Gas*, Phys. Rev. Lett. **91**, 240401 (2003).
- [Dah96] M. Ben Dahan, E. Peik, J. Reichel, Y. Castin and C. Salomon, *Bloch Oscillations of Atoms in an Optical Potential*, Phys. Rev. Lett. **76**, 4508 (1996).
- [Dal99a] F. Dalfovo, S. Giorgini, L. P. Pitaevskii, and S. Stringari, *Theory of Bose-Einstein condensation in trapped gases*, Rev. Mod. Phys. **71**, 463 (1999).
- [Dal99b] J. Dalibard, *Collisional dynamics of ultra-cold atomic gases*, in: M. Inguscio, S. Stringari, and C. E. Wieman (Eds.), *Proceedings of the International School of Physics - Enrico Fermi*, 321, IOS Press, 1999.
- [Dav95] K. B. Davis, M.-O. Mewes, M. R. Andrews, N. J. van Druten, D. S. Durfee, D. M. Kurn, and W. Ketterle, *Bose-Einstein Condensation in a Gas of Sodium Atoms*, Phys. Rev. Lett. **75**, 3969 (1995).
- [DeM99a] B. DeMarco, J. L. Bohn, J. P. Burke, Jr., M. Holland, and D. S. Jin, *Measurement of  $p$ -Wave Threshold Law Using Evaporatively Cooled Fermionic Atoms*, Phys. Rev. Lett. **82**, 4208 (1999).
- [DeM99b] B. DeMarco and D. S. Jin, *Onset of Fermi Degeneracy in a Trapped Atomic Gas*, Science **285**, 1703 (1999).
- [Den99] L. Deng, E. W. Hagley, J. Denschlag, J. E. Simsarian, C. W. Clark, M. A. Edwards, K. Helmerson, S. L. Rolston, W. D. Phillips, *Temporal, Matter-Wave Dispersion Talbot Effect*, Phys. Rev. Lett. **83**, 5407 (1999).
- [Deng99b] L. Deng, E. W. Hagley, J. Wen, M. Trippenbach, Y. Band, P. S. Julienne, J. E. Simsarian, K. Helmerson, S. L. Rolston and W. D. Phillips, *Four-wave mixing with matter waves*, Nature **398**, 218 (1999).
- [Den00] J. Denschlag, J. E. Simsarian, D. L. Feder, C. W. Clark, L. A. Collins, J. Cubizolles, L. Deng, E. W. Hagley, K. Helmerson, W. P. Reinhardt, S. L. Rolston, B. I. Schneider, and W. D. Phillips, *Generating Solitons by Phase Engineering of a Bose-Einstein Condensate*, Science **287**, 97 (2000).
- [Den02] J. Hecker Denschlag, J. E. Simsarian, H. Häffner, C. McKenzie, A. Browaeys, D. Cho, K. Helmerson, S. L. Rolston, and W. D. Phillips, *A Bose-Einstein Condensate in an optical lattice*, J. Phys. B: At. Mol. Opt. Phys. **35**, 3095 (2002).

- [Den04] J. Hecker Denschlag, H.-C. Nägerl, and R. Grimm, *Moleküle am absoluten Nullpunkt*, Physik Journal **3**, 33 (2004).
- [Dho02] K. Dholakia, G. Spalding and M. MacDonald, *Optical Tweezers: the next generation*, Physics World **15**, 31 (2002).
- [Die02] K. Dieckmann, C. A. Stan, S. Gupta, Z. Hadzibabic, C. H. Schunck, and W. Ketterle, *Decay of an Ultracold Fermionic Lithium Gas near a Feshbach Resonance*, Phys. Rev. Lett. **89**, 203201 (2002).
- [Dob99] L. Dobrek, M. Gajda, M. Lewenstein, K. Sengstock, G. Birkl, and W. Ertmer, *Optical generation of vortices in trapped Bose-Einstein condensates*, Phys. Rev. A **60**, R3381 (1999).
- [Don01] E. A. Donley, N. R. Claussen, S. L. Cornish, J. L. Roberts, E. A. Cornell, and C. E. Wieman, *Dynamics of collapsing and exploding Bose-Einstein condensates*, Nature **412**, 295 (2001).
- [Don02] E. A. Donley, N. R. Claussen, S. T. Thompson, and C. E. Wieman, *Atom-molecule coherence in a Bose-Einstein condensate*, Nature **417**, 529 (2002).
- [Dru02] P. D. Drummond, K. V. Kheruntsyan, D. J. Heinzen, and R. H. Wynar, *Stimulated Raman adiabatic passage from an atomic to a molecular Bose-Einstein condensate*, Phys. Rev. A **65**, 063619 (2002).
- [Dur04] S. Dürr, A. Volz, T. Marte, and G. Rempe, *Observation of Molecules Produced from a Bose-Einstein Condensate*, Phys. Rev. Lett. **92**, 020406 (2004).
- [Eag69] D. M. Eagles, *Possible Pairing without Superconductivity at Low Carrier Concentrations in Bulk and Thin-Film Superconducting Semiconductors*, Phys. Rev. **186**, 456 (1969).
- [Eie04] B. Eiermann, Th. Anker, M. Albiez, M. Taglieber, P. Treutlein, K.-P. Marzlin, and M. K. Oberthaler, *Bright Bose-Einstein Gap Solitons of Atoms with Repulsive Interaction*, Phys. Rev. Lett. **92**, 230401 (2004).
- [Ein25] A. Einstein, *Sitzungsberichte der Preussischen Akademie der Wissenschaften, Physikalisch-mathematische Klasse* (1924) p. 261; (1925) p. 3.
- [Ess98] T. Esslinger, I. Bloch, and T. W. Hänsch, *Bose-Einstein condensation in a quadrupole-Ioffe-configuration trap*, Phys. Rev. A **58**, R2664 (1998).

- [Fal04] L. Fallani, L. De Sarlo, J. Lye, M. Modugno, R. Saers, C. Fort, M. Inguscio, *Observation of dynamical instability for a Bose-Einstein condensate in a moving 1D optical lattice*, Phys. Rev. Lett. **93**, 140406 (2004).
- [Fat00] F. K. Fatemi, K. M. Jones, and P. D. Lett, *Observation of Optically Induced Feshbach Resonances in Collisions of Cold Atoms*, Phys. Rev. Lett. **85**, 4462 (2000).
- [Fed96] P. Fedichev, Yu Kagan, G. V. Shlyapnikov, and J. T. M. Walraven, *Influence of Nearly Resonant Light on the Scattering Length in Low-Temperature Atomic Gases*, Phys. Rev. Lett. **77**, 2913 (1996).
- [Fed03] Petr O. Fedichev and Uwe R. Fischer, *Gibbons-Hawking Effect in the Sonic de Sitter Space-Time of an Expanding Bose-Einstein-Condensed Gas*, Phys. Rev. Lett. **91**, 240407 (2003).
- [Fes58] H. Feshbach, *A Unified Theory of Nuclear Reactions*, Ann. Phys. **5**, 337 (1958).
- [Fio98] A. Fioretti, D. Comparat, A. Crubellier, O. Dulieu, F. Masnou-Seeuws, and P. Pillet, *Formation of cold Cs<sub>2</sub> Molecules through Photoassociation*, Phys. Rev. Lett. **80**, 4402 (1998).
- [For03] C. Fort, F. Cataliotti, L. Fallani, F. Ferlaino, P. Maddaloni, and M. Inguscio, *Collective excitations of a trapped Bose-Einstein condensate in the presence of a 1D optical lattice*, Phys. Rev. Lett. **90**, 140405 (2003).
- [Geh03b] M. E. Gehm, S. L. Hemmer, S. R. Granade, K. M. O'Hara, and J. E. Thomas, *Mechanical stability of a strongly interacting Fermi gas of atoms*, Phys. Rev. A **68**, 011401(R) (2003).
- [Gib93] K. Gibble and S. Chu, *Laser-cooled Cs frequency standard and a measurement of the frequency shift due to ultracold collisions*, Phys. Rev. Lett. **70**, 1771 (1993).
- [GO99] D. Guéry-Odelin, F. Zambelli, J. Dalibard, and S. Stringari, *Collective oscillations of a classical gas confined in harmonic traps*, Phys. Rev. A **60**, 4851 (1999).
- [Gou86] P. L. Gould, G. A. Ruff, and D. E. Pritchard, *Diffraction of atoms by light: The near-resonant Kapitza-Dirac effect*, Phys. Rev. Lett. **56**, 827-830 (1986).

- [Gra02] S. R. Granade, M. E. Gehm, K. M. O'Hara, and J. E. Thomas, *All-Optical Production of a Degenerate Fermi Gas*, Phys. Rev. Lett. **88**, 120405 (2002).
- [Gre02] M. Greiner, O. Mandel, T. Esslinger, T. W. Hänsch, and I. Bloch, *Quantum phase transition from a superfluid to a Mott insulator in a gas of ultracold atoms*, Nature **415**, 39 (2002).
- [Gre03] M. Greiner, C. A. Regal, and D. S. Jin, *Emergence of a molecular Bose-Einstein condensate from a Fermi gas*, Nature **426**, 540 (2003).
- [Gri96] A. Griffin, *Conserving and gapless approximations for an inhomogeneous Bose gas at finite temperatures*, Phys. Rev. B **53**, 9341 (1996).
- [Gri00] R. Grimm, and M. Weidemüller, *Optical Dipole Traps for Neutral Atoms*, Adv. At. Mol. Opt. Phys. **42**, 95 (2000).
- [Gup03] S. Gupta, Z. Hadzibabic, M. W. Zwierlein, C. A. Stan, K. Dieckmann, C. H. Schunck, E. G. M. van Kempen, B. J. Verhaar, and W. Ketterle, *RF Spectroscopy of Ultracold Fermions*, Science **300**, 1723 (2003).
- [Gus97] T.L. Gustavson, P. Bouyer, and M.A. Kasevich, *Precision Rotation Measurements with an Atom Interferometer Gyroscope*, Phys. Rev. Lett. **78**, 2046 (1997).
- [Had02] Z. Hadzibabic, C. A. Stan, K. Dieckmann, S. Gupta, M. W. Zwierlein, A. Görlitz, and W. Ketterle, *Two species mixture of quantum degenerate Bose and Fermi gases*, Phys. Rev. Lett. **88**, 160401 (2002).
- [Hän75] T. W. Hänsch and A. L. Schawlow, *Cooling of gases by laser radiation*, Optics Comm. **13**, 68 (1975).
- [Har01] K. M. O'Hara, M. E. Gehm, S. R. Granade, and J. E. Thomas, *Scaling laws for evaporative cooling in time-dependent optical traps*, Phys. Rev. A **64**, 051403 (2001).
- [Har02a] K. M. O'Hara, S. L. Hemmer, M. E. Gehm, S. R. Granade, and J. E. Thomas, *Observation of a Strongly Interacting Degenerate Fermi Gas of Atoms*, Science **298**, 2179 (2002).
- [Har02b] K. M. O'Hara, S. L. Hemmer, S. R. Granade, M. E. Gehm, J. E. Thomas, V. Venturi, E. Tiesinga, and C. J. Williams, *Measurement of the zero crossing in a Feshbach resonance of fermionic  ${}^6\text{Li}$* , Phys. Rev. A **66**, 041401(R) (2002).

- [Hei00] D. J. Heinzen, R. Wynar, P. D. Drummond, and K. V. Kheruntsyan, *Superchemistry: Dynamics of Coupled Atomic and Molecular Bose-Einstein Condensates*, Phys. Rev. Lett. **84**, 5029 (2000).
- [Hei01] H. Heiselberg, *Fermi systems with long scattering lengths*, Phys. Rev. A **63**, 043606 (2001).
- [Hei04] H. Heiselberg, *Collective Modes of Trapped Gases at the BEC-BCS Crossover*, Phys. Rev. Lett. **93**, 040402 (2004).
- [Her03] J. Herbig, T. Kraemer, M. Mark, T. Weber, C. Chin, H.-C. Nägerl, and R. Grimm, *Preparation of a Pure Molecular Quantum Gas*, Science **301**, 1510 (2003).
- [Hes85] H. Hess, Bull. Am. Phys. Soc. **30**, 854 (1985).
- [Hes86] H. Hess, *Evaporative cooling of magnetically trapped and compressed spin-polarized hydrogen*, Phys. Rev. B **34** 3476 (1986).
- [Ho04] T.-L. Ho, *Universal Thermodynamics of Degenerate Quantum Gases in the Unitarity Limit*, Phys. Rev. Lett. **92**, 090402 (2004).
- [Hod05] E. Hodby, S. T. Thompson, C. A. Regal, M. Greiner, A. C. Wilson, D. S. Jin, E. A. Cornell, and C. E. Wieman, *Production Efficiency of Ultracold Feshbach Molecules in Bosonic and Fermionic Systems*, Phys. Rev. Lett. **94**, 120402 (2005).
- [Hol01] M. Holland, S. J. J. M. F. Kokkelmans, M. L. Chiofalo, and R. Walser, *Resonance Superfluidity in a Quantum Degenerate Fermi Gas*, Phys. Rev. Lett. **87**, 120406 (2001).
- [Hop01] J. J. Hope and M. K. Olsen, *Quantum Superchemistry: Dynamical Quantum Effects in Coupled Atomic and Molecular Bose-Einstein Condensates*, Phys. Rev. Lett. **86**, 3220 (2001).
- [Hou98] M. Houbiers, H. T. C. Stoof, W. McAlexander, and R. Hulet, *Elastic and inelastic collisions of  $^6\text{Li}$  atoms in magnetic and optical traps*, Phys. Rev. A **57**, R1497 (1998).
- [Hu04] H. Hu, A. Minguzzi, X.-J. Liu, and M. P. Tosi, *Collective Modes and Ballistic Expansion of a Fermi Gas in the BCS-BEC Crossover*, Phys. Rev. Lett. **93**, 190403 (2004).
- [Hua63] K. Huang, *Statistical Mechanics*, Wiley, New York (1963).

- [Hud02] J. J. Hudson, B. E. Sauer, M. R. Tarbutt, and E. A. Hinds, *Measurement of the Electron Electric Dipole Moment Using YbF Molecules*, Phys. Rev. Lett. **89**, 023003 (2002).
- [Ino98] S. Inouye, M. Andrews, J. Stenger, H.-J. Miesner, S. Stamper-Kurn, and W. Ketterle, *Observation of Feshbach resonances in a Bose-Einstein Condensate*, Nature **392**, 151 (1998).
- [Ino99] S. Inouye, T. Pfau, S. Gupta, A. P. Chikkatur, A. Görlitz, D. E. Pritchard, and W. Ketterle, *Observation of phase-coherent amplification of atomic matter waves*, Nature **402**, 641 (1999).
- [Ino01] S. Inouye, S. Gupta, T. Rosenband, A. P. Chikkatur, A. Görlitz, T. L. Gustavson, A. E. Leanhardt, D.E. Pritchard, and W. Ketterle, *Observation of vortex phase singularities in Bose-Einstein condensates*, Phys. Rev. Lett. **87**, 080402 (2001).
- [Jak98] D. Jaksch, C. Bruder, J. I. Cirac, C. W. Gardiner, and P. Zoller, *Cold Bosonic Atoms in Optical Lattices*, Phys. Rev. Lett. **81**, 3108 (1998).
- [Jak99] D. Jaksch, H.-J. Briegel, J.I. Cirac, C.W. Gardiner, and P. Zoller, *Entanglement of atoms via cold controlled collisions*, Phys. Rev. Lett. **82**, 1975 (1999).
- [Jak02] D. Jaksch, V. Venturi, J. I. Cirac, C. J. Williams, and P. Zoller, *Creation of a Molecular Condensate by Dynamically Melting a Mott Insulator*, Phys. Rev. Lett. **89**, 040402 (2002).
- [Jes96] P. S. Jessen and I. H. Deutsch, *Optical lattices*, Adv. Atom. Mol. Opt. Phys. **37**, 95 (1996).
- [Jin97] D. S. Jin, M. R. Matthews, J. R. Ensher, C. E. Wieman, and E. A. Cornell, *Temperature-Dependent Damping and Frequency Shifts in Collective Excitations of a Dilute Bose-Einstein Condensate*, Phys. Rev. Lett. **78**, 764 (1997).
- [Joc02] S. Jochim, M. Bartenstein, G. Hendl, J. Hecker Denschlag, R. Grimm, A. Mosk, and M. Weidemüller, *Magnetic Field Control of Elastic Scattering in a Cold Gas of Fermionic Lithium Atoms*, Phys. Rev. Lett. **89**, 273202 (2002).
- [Joc03a] S. Jochim, M. Bartenstein, A. Altmeyer, G. Hendl, S. Riedl, C. Chin, J. Hecker Denschlag, and R. Grimm, *Bose-Einstein Condensation of Molecules*, Science **302**, 2101 (2003).

- [Joc03b] S. Jochim, M. Bartenstein, A. Altmeyer, G. Hendl, C. Chin, J. Hecker Denschlag, and R. Grimm, *Pure Gas of Optically Trapped Molecules Created from Fermionic Atoms*, Phys. Rev. Lett. **91**, 240402 (2003).
- [Joc04] S. Jochim, *Bose-Einstein condensation of molecules*, Ph.D. thesis, Universität Innsbruck (2004).
- [Jon03] M. Jona-Lasinio, O. Morsch, M. Cristiani, N. Malossi, J. H. Müller, E. Courtade, M. Anderlini, and E. Arimondo, *Asymmetric Landau-Zener Tunneling in a Periodic Potential*, Phys. Rev. Lett. **91**, 230406 (2003).
- [JOSA] Special issue on *Laser cooling of matter*, J. Opt. Soc. Am. B **20**, Vol. 5, 883-1145 (2003).
- [Jul92] P. Julienne, A. Smith, and K. Burnett, *Theory of collisions between lasercooled Atoms*, Advances in Atomic, Molecular, and Optical Physics **30**, 141 (1992).
- [Jul98] P. S. Julienne, K. Burnett, Y. B. Band, and W. C. Stwalley, *Stimulated Raman molecule production in Bose-Einstein condensates*, Phys. Rev. A **58**, R797 (1998).
- [Jul04] P. S. Julienne, E. Tiesinga, T. Köhler, *Making cold molecules by time-dependent Feshbach resonances*, J. Mod. Optics Volume **51**, 1787 (2004).
- [Kat03] H. Katori, M. Takamoto, V.G. Pal'chikov, and V.D. Ovsiannikov, *Ultrastable Optical Clock with Neutral Atoms in an Engineered Light Shift Trap*, Phys. Rev. Lett. **91**, 173005 (2003).
- [Ket96] W. Ketterle and N. J. van Druten, *Evaporative Cooling of trapped atoms*, Adv. Atom. Mol. Phys. **37**, 181 (1996).
- [Ket99] W. Ketterle, D. S. Durfee, and D. M. Stamper-Kurn, *Making, probing and understanding Bose-Einstein condensates*, in: M. Inguscio, S. Stringari, and C. E. Wieman (Eds.), Proceedings of the International School of Physics - Enrico Fermi, 67, IOS Press, 1999.
- [Kha02] L. Khaykovich, F. Schreck, G. Ferrari, T. Bourdel, J. Cubizolles, L. D. Carr, Y. Castin, and C. Salomon, *Formation of a Matter-Wave Bright Soliton*, Science **296**, 1290 (2002).
- [Kil99] T. C. Killian, S. Kulin, S. D. Bergeson, L. A. Orozco, C. Orzel, and S. L. Rolston, *Creation of an Ultracold Neutral Plasma*, Phys. Rev. Lett. **83**, 4776 (1999).

- [Kin04a] J. Kinast, S. L. Hemmer, M. E. Gehm, A. Turlapov, and J. E. Thomas, *Evidence for Superfluidity in a Resonantly Interacting Fermi Gas*, Phys. Rev. Lett. **92**, 150402 (2004).
- [Kin04b] J. Kinnunen, M. Rodriguez, and P. Törmä, *Pairing gap and in-gap excitations in trapped fermionic superfluids*, Science **305**, 1131 (2004).
- [Kin04c] J. Kinast, A. Turlapov, and J. E. Thomas, *Breakdown of hydrodynamics in the radial breathing mode of a strongly interacting Fermi gas*, Phys. Rev. A **70**, 051401 (2004).
- [Kin05] J. Kinast, A. Turlapov, and J. E. Thomas, *Damping of a Unitary Fermi Gas*, Phys. Rev. Lett. **94**, 170404 (2005).
- [Kin04] T. Kinoshita, T.R. Wenger, and D. S. Weiss, *Observation of a one-dimensional Tonks-Girardeau gas*, Science **305**, 1125 (2004).
- [Koc05] C.P. Koch, F. Masnou-Seeuws, and R. Kosloff, *Creating Ground State Molecules with Optical Feshbach Resonances in Tight Traps*, Phys. Rev. Lett. **94**, 193001 (2005).
- [Koz99] M. Kozuma, L. Deng, E. W. Hagley, J. Wen, R. Lutwak, K. Helmer-son, S. L. Rolston, and W. D. Phillips, *Coherent Splitting of Bose-Einstein Condensed Atoms with Optically Induced Bragg Diffraction*, Phys. Rev. Lett. **82**, 871 (1999).
- [Kun97] S. Kunze, K. Dieckmann, and G. Rempe, *Diffraction of Atoms from a Measurement Induced Grating*, Phys. Rev. Lett. **78**, 2041 (1997).
- [Leg80] A. J. Leggett, *Diatomic Molecules and Cooper Pairs*, in: A. Pekalski and R. Przystawa (Eds.), *Modern Trends in the Theory of Condensed Matter*, 13-27, Springer-Verlag, Berlin, 1980.
- [Lui96] O. J. Luiten, M. W. Reynolds, and J. T. M. Walraven, *Kinetic theory of the evaporative cooling of a trapped gas*, Phys. Rev. A **53**, 381 (1996).
- [Mac04] M. Mackie, K. Härkönen, A. Collin, K. Suominen, and J. Javanainen, *Improved efficiency of stimulated Raman adiabatic passage in photoassociation of a Bose-Einstein condensate*, Phys. Rev. A **70**, 013614 (2004) and references therein.
- [Mad00] K. W. Madison, F. Chevy, W. Wohlleben, and J. Dalibard, *Vortex formation in a stirred Bose-Einstein condensate*, Phys. Rev. Lett. **84**, 806 (2000).

- [Man03] O. Mandel, M. Greiner, A. Widera, T. Rom, T. W. Hänsch, and I. Bloch, *Controlled collisions for multi-particle entanglement of optically trapped atoms*, Nature **425**, 937 (2003).
- [Man03a] O. Mandel, M. Greiner, A. Widera, T. Rom, T. W. Hänsch, and I. Bloch, *Coherent transport of neutral atoms in spin-dependent optical lattice potentials*, Phys. Rev. Lett. **91**, 010407 (2003).
- [Man05] N. Manini and L. Salasnich, *Bulk and Collective Properties of a Dilute Fermi Gas in the BCS-BEC Crossover*, Phys. Rev. A **71**, 033625 (2005).
- [Mar88] P. J. Martin, B. G. Oldaker, A. M. Miklich, and D. E. Pritchard, *Bragg scattering of atoms from a standing light wave*, Phys. Rev. Lett. **60**, 515 (1988).
- [Mas01] F. Masnou-Seeuws and P. Pillet, *Formation of ultracold molecules ( $T_j 200$  mK) via photoassociation in a gas of laser-cooled atoms*, Adv. At. Mol. Opt. Phys. **47**, 53-127, (2001).
- [McK02] C. McKenzie, J. Hecker Denschlag, H. Häffner, A. Browaeys, L. E. E. de Araujo, F. K. Fatemi, K. M. Jones, J. E. Simsarian, D. Cho, A. Simoni, E. Tiesinga, P. S. Julienne, K. Helmerson, P. D. Lett, S. L. Rolston, and W. D. Phillips, *Photoassociation of Sodium in a Bose-Einstein Condensate*, Phys. Rev. Lett. **88**, 120403 (2002).
- [Met99] H. J. Metcalf and P. van der Straaten, *Laser Cooling and Trapping* Springer, New York, 1999.
- [Mew96] M.-O. Mewes, M. R. Andrews, N. J. van Druten, D. M. Kurn, D. S. Durfee, C. G. Townsend, and W. Ketterle, *Collective Excitations of a Bose-Einstein Condensate in a Magnetic Trap*, Phys. Rev. Lett. **77**, 988 (1996).
- [Moo02] M. G. Moore and A. Vardi, *Bose-Enhanced Chemistry: Amplification of Selectivity in the Dissociation of Molecular Bose-Einstein Condensates*, Phys. Rev. Lett. **88**, 160402 (2002).
- [Mor01] O. Morsch, J. H. Müller, M. Cristiani, D. Ciampini, and E. Arimondo, *Bloch Oscillations and Mean-Field Effects of Bose-Einstein Condensates in 1D Optical Lattices*, Phys. Rev. Lett. **87**, 140402, (2001).
- [Mor03] H. Moritz, T. Stöferle, M. Köhl, and T. Esslinger, *Exciting collective oscillations in a trapped 1D gas*, Phys. Rev. Lett. **91**, 250402 (2003).

- [Nik99] A. N. Nikolov, E. E. Eyler, X. T. Wang, J. Li, H. Wang, W. C. Stwalley, and P. L. Gould, *Observation of Ultracold Ground-State Potassium Molecules*, Phys. Rev. Lett. **82**, 703 (1999).
- [Noz85] P. Nozières and S. Schmitt-Rink, J. Low Temp. Phys. **59**, 195 (1985).
- [Oha02] Y. Ohashi and A. Griffin, *BCS-BEC Crossover in a Gas of Fermi Atoms with a Feshbach Resonance*, Phys. Rev. Lett. **89**, 130402 (2002).
- [Par04] B. Paredes, A. Widera, V. Murg, O. Mandel, S. Flling, I. Cirac, G. V. Shlyapnikov, T.W. Hnsch, and I. Bloch, *Tonks-Girardeau gas of ultracold atoms in an optical lattice* Nature **430** (2004).
- [Par05] G. B. Partridge, K. E. Strecker, R. I. Kamar, M. W. Jack, and R. G. Hulet, *Molecular Probe of Pairing in the BEC-BCS Crossover*, cond-mat/0505353.
- [Pei03] S. Peil, J. V. Porto, B. Laburthe Tolra, J. M. Obrecht, B. E. King, M. Subbotin, S. L. Rolston, and W. D. Phillips, *Patterned loading of a Bose-Einstein condensate into an optical lattice*, Phys. Rev. A **67**, 051603 (2003).
- [Per04] A. Perali, P. Pieri, and G. C. Strinati, *Quantitative Comparison between Theoretical Predictions and Experimental Results for the BCS-BEC Crossover*, Phys. Rev. Lett. **93**, 100404 (2004).
- [Pet95] W. Petrich, M. H. Anderson, J. R. Ensher, and E. A. Cornell, *Tightly confining magnetic trap for evaporative cooling of neutral atoms*, Phys. Rev. Lett. **74**, 3352 (1995).
- [Pet02] C. J. Pethick and H. Smith, *Bose-Einstein Condensation in Dilute Gases*, Cambridge University Press, Cambridge (2002).
- [Pet04] D. Petrov, C. Salomon, and G. Shlyapnikov, *Weakly bound dimers of fermionic atoms*, Phys. Rev. Lett. **93**, 090404 (2004).
- [Phi98] W. D. Phillips, *Nobel Lecture: Laser cooling and trapping of neutral atoms*, Rev. Mod. Phys. **70**, 721 (1998).
- [Pit03] L. Pitaevskii and S. Stringari, *Bose-Einstein Condensation*, Oxford University Press, 2003.
- [Pro03] I. D. Prodan, M. Pichler, M. Junker, R. G. Hulet, and J. L. Bohn, *Intensity Dependence of Photoassociation in a Quantum Degenerate Atomic Gas*, Phys. Rev. Lett. **91**, 080402 (2003).

- [Pez04] L. Pezz, L. Pitaevskii, A. Smerzi, S. Stringari, G. Modugno, E. De Mirandes, F. Ferlaino, H. Ott, G. Roati, and M. Inguscio, *Insulating behavior of a trapped ideal Fermi gas*, Phys. Rev. Lett. **93**, 120401 (2004).
- [Raa87] E. Raab, M. Prentiss, A. Cable, S. Chu, and D. Pritchard, *Trapping of neutral Sodium atoms with Radiation pressure*, Phys. Rev. Lett. **59**, 2631 (1987).
- [Reg03] C. A. Regal, C. Ticknor, J. L. Bohn, and D. S. Jin, *Creation of ultracold molecules from a Fermi gas of atoms*, Nature **424**, 47 (2003).
- [Reg03a] C. A. Regal and D. S. Jin, *Measurement of Positive and Negative Scattering Lengths in a Fermi Gas of Atoms*, Phys. Rev. Lett. **90**, 230404 (2003).
- [Reg04] C. A. Regal, M. Greiner, and D. S. Jin, *Observation of Resonance Condensation of Fermionic Atom Pairs*, Phys. Rev. Lett. **92**, 040403 (2004).
- [Roa02] G. Roati, F. Riboli, G. Modugno, and M. Inguscio, *Fermi-Bose quantum degenerate  $^{40}\text{K}$  -  $^{87}\text{Rb}$  mixture with attractive interaction*, Phys. Rev. Lett. **89**, 150403 (2002).
- [Rob98] J. L. Roberts, N. R. Claussen, J. P. Burke, Jr., C. H. Greene, E. A. Cornell, and C. E. Wieman, *Resonant Magnetic Field Control of Elastic Scattering in Cold  $^{85}\text{Rb}$* , Phys. Rev. Lett. **81**, 5109 (1998).
- [Rom04] T. Rom, T. Best, O. Mandel, A. Widera, M. Greiner, and T. W. Hänsch, and I. Bloch, *State Selective Production of Molecules in Optical Lattices*, Phys. Rev. Lett. **93**, 073002 (2004).
- [Sch01] F. Schreck, L. Khaykovich, K. L. Corwin, G. Ferrari, T. Bourdel, J. Cubizolles, and C. Salomon, *Quasipure Bose-Einstein Condensate Immersed in a Fermi Sea*, Phys. Rev. Lett. **87**, 080403 (2001).
- [Sch04] C. Schori, T. Stöferle, H. Moritz, M. Köhl, and T. Esslinger, *Excitations of a Superfluid in a 3D Optical Lattice*, Phys. Rev. Lett. **93**, 240402 (2004).
- [Sco04] R.G. Scott, A.M. Martin, S. Bujkiewicz, T.M. Fromhold, N. Malossi, O. Morsch, M. Cristiani, and E. Arimondo, *Transport and Disruption of Bose-Einstein Condensates in Optical-Lattices*, Phys. Rev. A **69**, 033605(2004).

- [Sen95] K. Sengstock and W. Ertmer, *Laser Manipulation of Atoms*, Advances in Atomic, Molecular and Optical Physics **35**, 1-45 (1995).
- [Sim00] J. E. Simsarian, J. Denschlag, C. W. Clark, L. Deng, M. A. Edwards, E. W. Hagley, K. Helmerson, S. L. Rolston, and W. D. Phillips, *Imaging the Phase of an evolving Bose-Einstein Condensate wavefunction*, Phys. Rev. Lett **85**, 2040 (2000).
- [Sna98] M. J. Snadden, J. M. McGuirk, P. Bouyer, K. G. Haritos, and M. A. Kasevich, *Measurement of the Earth's Gravity Gradient with an Atom Interferometer-Based Gravity Gradiometer*, Phys. Rev. Lett. **81**, 971 (1998).
- [Sta04] J. Stajic, J. N. Milstein, Q. Chen, M. L. Chiofalo, M. J. Holland, and K. Levin, *Nature of superfluidity in ultracold Fermi gases near Feshbach resonances*, Phys. Rev. A **69**, 063610 (2004).
- [Ste99] J. Stenger, S. Inouye, A. P. Chikkatur, D. M. Stamper-Kurn, D. E. Pritchard, and W. Ketterle, *Bragg Spectroscopy of a Bose-Einstein Condensate*, Phys. Rev. Lett. **82**, 4569 (1999).
- [Str96] S. Stringari, *Collective Excitations of a Trapped Bose-Condensed Gas*, Phys. Rev. Lett. **77**, 2360 (1996).
- [Str02] K. E. Strecker, G. B. Partridge, A. G. Truscott, and R. G. Hulet, *Formation and propagation of matter-wave soliton trains*, Nature **417**, 150 (2002).
- [Str03] K. E. Strecker, G. B. Partridge, and R. G. Hulet, *Conversion of an Atomic Fermi Gas to a Long-Lived Molecular Bose Gas*, Phys. Rev. Lett. **91**, 080406 (2003).
- [Str04] S. Stringari, *Collective oscillations of a trapped Fermi gas near a Feshbach Resonance*, Europhys. Lett. **65**, 749 (2004).
- [Tak98] T. Takekoshi, B. M. Patterson, and R. J. Knize, *Observation of optically trapped cold cesium molecules*, Phys. Rev. Lett. **81**, 5105 (1998).
- [Tha04] G. Thalhammer, M. Theis, K. Winkler, R. Grimm, and J. Hecker Denschlag, *Inducing an optically induced Feshbach resonance via stimulated Raman coupling*, Phys. Rev. A **71**, 039902 (2005).
- [The04] M. Theis, G. Thalhammer, K. Winkler, M. Hellwig, G. Ruff, R. Grimm, and J. Hecker Denschlag, *Tuning the scattering length with an optically induced Feshbach resonance*, Phys. Rev. Lett. **93**, 123001 (2004).

- [The05] M. Theis, *Optical Feshbach resonances in a Bose-Einstein condensate*, Ph.D. thesis, Universität Innsbruck (2005).
- [Tho87] H. R. Thorsheim, J. Weiner, and P. S. Julienne, *Laser-induced photoassociation of ultracold sodium atoms*, Phys. Rev. Lett. **58**, 2420 (1987).
- [Tie93] E. Tiesinga, B. J. Verhaar, and H. T. C. Stoof, *Threshold and resonance phenomena in ultracold ground-state collisions*, Phys. Rev. A **47**, 4114 (1993).
- [Tin96] M. Tinkham, *Introduction to superconductivity*, McGraw-Hill, New York, ed. 2. (1969).
- [Tol01] B. Laburthe Tolra, C. Drag, and P. Pillet, *Observation of cold state-selected cesium molecules formed by stimulated Raman photoassociation*, Phys. Rev. A **64**, 061401 (2001).
- [Tre97] R. Trebino, K. W. DeLong, D. N. Fittinghoff, J. N. Sweetser, M. A. Krumbügel, B. A. Richman, and D. J. Kane, *Measuring ultrashort laser pulses in the time-frequency domain using frequency-resolved optical gating*, Rev. Sci. Instrum. **68**, 3277 (1997).
- [Tru01] A. G. Truscott, K. E. Strecker, W. I. McAlexander, G. B. Partridge, and R. G. Hulet, *Observation of Fermi Pressure in a Gas of Trapped Atoms*, Science **291**, 2570 (2001).
- [Var97] A. Vardi, D. Abrashkevich, E. Frishman, and M. Shapiro, *Theory of radiative recombination with strong laser pulses and the formation of ultracold molecules via stimulated photo-recombination of cold atoms*, J. Chem. Phys. **107**, 6166 (1997).
- [Web03] T. Weber, J. Herbig, M. Mark, H.-C. Nägerl, and R. Grimm, *Bose-Einstein Condensation of Cesium*, Science **299**, 232 (2003).
- [Wei98] J. D. Weinstein, R. deCarvalho, T. Guillet, B. Friedrich, and J. M. Doyle, *Magnetic trapping of calcium monohydride molecules at millikelvin temperatures*, Nature **395**, 148 (1998).
- [Wei99] J. Weiner, V. S. Bagnato, S. Zilio, and P. S. Julienne, *Experiments and theory in cold and ultracold collisions*, Rev. Mod. Phys. **71**, 1 (1999).
- [Win05] K. Winkler, G. Thalhammer, M. Theis, H. Ritsch, R. Grimm, and J. Hecker Denschlag, *Atom-molecule dark states in a Bose-Einstein condensate*, to be published, cond-mat/0505732 (2005).

- [Wyn00] R. Wynar, R. S. Freeland, D. J. Han, C. Ryu, and D. J. Heinzen, *Molecules in a Bose Einstein condensate*, Science **287**, 1016 (2000).
- [Xu03] K. Xu, T. Mukaiyama, J. R. Abo-Shaeer, J. K. Chin, D. E. Miller, and W. Ketterle, *Formation of Quantum-Degenerate Sodium Molecules*, Phys. Rev. Lett. **91**, 210402 (2003).
- [Zwi03] M. W. Zwierlein, C. A. Stan, C. H. Schunck, S. M. F. Raupach, S. Gupta, Z. Hadzibabic, and W. Ketterle, *Observation of Bose-Einstein Condensation of Molecules*, Phys. Rev. Lett. **91**, 250401 (2003).
- [Zwi04] M. Zwierlein, C. A. Stan, C. H. Schunck, S. M. F. Raupach, A. J. Kerman, and W. Ketterle, *Condensation of Pairs of Fermionic Atoms near a Feshbach Resonance*, Phys. Rev. Lett. **92**, 120403 (2004).
- [Zwi05] M.W. Zwierlein, J.R. Abo-Shaeer, A. Schirotzek, C.H. Schunck, and W. Ketterle, *Vortices and superfluidity in a strongly interacting Fermi gas*, cond-mat/0505635.

# Acknowledgements

I feel very fortunate to have worked together with so many wonderful and inspiring people in recent years without whom none of this work would have been possible. The creative work atmosphere in our groups as well as the necessary resources were the basis for successful research and lots of fun.

I would like to thank Rudi Grimm for his support in every respect. He is a great mentor in scientific as well as non-scientific issues. Thanks to Rudi's help, financial resources were also never a problem. Furthermore I enjoyed that he granted me lots of freedom for pursuing my own research work.

I am also very thankful to my former bosses at NIST: Bill Phillips, Steve Rolston, Kris Helmerson, and Paul Lett. Being a postdoc at NIST was a wonderful experience for me. Not only was I able to work in such a stimulating environment, but I could also fully focus on physics without other obligations.

In Innsbruck, excellent work was done by our students and postdocs. The fermionic lithium experiments were driven by Selim Jochim, Markus Bartenstein, Alexander Altmeyer, Stefan Riedl, Reece Geurson and Cheng Chin with whom I had so many interesting discussions. You guys turned an underdog into a world class experiment. Thank you so much! For the rubidium BEC experiment, Matthias Theis, Gregor Thalhammer, Klaus Winkler and Michael Hellwig did a great job setting up the experiment and doing measurements. Many, many thanks to you all. I also want to acknowledge the valuable help of George Ruff, Ina Kinski, Stefan Schmid and Florian Lang who were there as visitors or who have just started their research projects.

I would like to thank my colleagues Hanns-Christoph Nägerl and Florian Schreck, as well as all the students in the three cesium projects and the new fermion mixture project for their team spirit, enthusiasm and the good times we had together.

Many thanks go to the laser cooling group at NIST, with whom the first part of the work was carried out and in particular to Jesse Simsarian and Fredrik Fatemi.

Many more people in Innsbruck have contributed to making it such an

exciting place for physics. I would like to thank especially Rainer Blatt, Peter Zoller, Wilhelm Zwerger, Helmut Ritsch, Ferdinand Schmidt-Kaler, Jürgen Eschner, Christoph Becher, Hartmut Häffner, Timo Körber, Christian Roos, Wolfgang Hänsel and all the other members of the physics institutes for their support.

Outside Innsbruck we have numerous collaborators which deserve a big thank you, in particular I would like to mention Paul Julienne and Eite Tiesinga.

For their support in technical and administrative issues I would like to acknowledge Christine Götsch-Obmascher, Anneliese Werner, Patrizia Moser, Karin Köhle, Toni Schönherr, Stefan Haslwanter, Joseph Dummer, Helmut Jordan, Martin Hellbert, Konrad Damhofer, and Manuel Kluibenschädel.

My dearest thanks go to my beloved wife Nancy and my family for always being there for me. Nancy, I hope that my habilitation will help that soon we find a place where we both can work and live together. I dedicate this work to you!